

Heavy minerals in the palaeo and modern Orange River and offshore southern Namibia

Albertina Ndahafifwa Nakashole

Submitted in accordance with the requirements for the degree of Doctor of Philosophy

The University of Leeds
School of Earth and Environment

November 2017

Declaration of Authorship

Chapter 4 of the thesis has been published to *Sedimentary Geology* journal 364 (2018) 103-120.

A.N. Nakashole; D.M., Hodgson; R.J., Chapman; D.J., Morgan and R.J., Jacob. Long-term controls on continental-scale bedrock river terrace deposition from integrated clast and heavy mineral assemblage analysis: an example from the lower Orange River, Namibia.

A.N. Nakashole – main author involved in manuscript writing as well as clast assemblage and heavy mineral assemblage data collection.

D.M., Hodgson – in depth review of manuscript

R.J., Chapman – in depth review of manuscript

D.J., Morgan – involved in the discussion of manuscript

R.J., Jacob – review of manuscript and also provided clast assemblage data

Acknowledgements

First, I am grateful to my supervisors Rob Chapman, Dave Hodgson, Dan Morgan and Jürgen Jacob for their support, encouragement and most importantly for their time.

I am thankful to Godfrey Ngaisiue and Richard Gray for their support with all aspects of the project. Lahja Ndjalo has been of huge help during the duration of the study. I am grateful to her for helping with sampling logistics and provision of data. Thank you for running the show on the south end of the Atlantic.

I would like to thank my family for their moral support, encouragement and for providing a listening ear. My friends have been a source of support throughout this journey.

I am grateful to Bronwill De Bryun and Hillbert Boyce for helping with collection of most of the Atlantic 1 samples. My colleagues at NAMDEB (Maggy Mufenda, Ileni Mbangula and Hester Hourie) and Debeers Marine Namibia (Tanja Kubirske, Ndaindila Namhindo, Claus Jendrissek, Onemus Shithigona) are thanked for support with sample logistics as well as provision of information. To Gottfried Grobbelaar thank you for your support with field work and the cheese sandwiches toasted on coals. Martin Shiimi is thanked for helping me acquire seismic data. The NAMDEB and Debeers Marine Namibia security teams are thanked for their support during sample collection.

The majority of Orange River samples used for this study were provided by Jürgen Jacob. I am forever thankful to him. My gratitude goes to the NAMDEB and Debeers Marine survey teams for providing GPS sample data. I am grateful to Matt Grimshaw for answering my never ending ArcGIS questions.

I am thankful to the Human Resource team at Debeers Marine Namibia (Rondine Jacobs, Hilda Kambala and Bianca Kruse) for logistical support.

Abstract

Linking the erosional record of drainage basins with the depositional record of sedimentary basins is a major challenge in geosciences. Thick diamondiferous gravel terrace deposits along the lower Orange River and their coeval downstream offshore deposits provide a rare opportunity for understating source-to-sink relationships. Two distinct gravel terrace deposits are recognised, based on clast and heavy mineral assemblage analysis at Boom, Lorelei, Sendelingsdrif, Daberas, Auchas Major, Auchas Lower and Arrisdrif, referred to as the Proto and Meso Orange River deposits. These are compared to offshore sample sites.

The Proto Orange River deposits are coarser and characterised by a dominance of Karoo Supergroup shale and sandstone clasts whereas the younger Meso Orange River gravels exhibit a banded iron formation dominance. Differences in clast assemblage between the Proto and Meso deposits are ascribed to a more powerful river system during Proto-Orange River time, driven by a changing drainage basin geomorphology, rather than reworking of older deposits or changes in clast provenance. This is accompanied by an increase in local bedrock sources, including amphibole-epidote in the heavy mineral assemblages. The fluvial and marine gravels have similar detrital heavy mineral assemblage derived from the Namaqua Metamorphic Complex and Gariiep Belt. Offshore, the eastern regions show a higher amphibole-epidote content similar to that of the Meso Orange River gravel. Therefore, offshore amphibole-epidote distribution is a function of the relative amount of Namaqua Metamorphic Complex derived sediments and also decay of these two minerals over time and is neither a function of northward longshore drift nor geomorphology of the seabed or sea level.

Diamond indicator minerals derived from kimberlites do not persist into the heavy mineral assemblage of the study area. In Atlantic 1, a weak positive correlation of coarse magnetite with diamond grade for gravels that are closer to the Orange River mouth could be explained by their hydrodynamic similarities.

Table of Contents

Acknowledgements.....	iii
Abstract.....	iv
Chapter 1 Introduction	1
1.1 Project Overview and Rationale	1
1.2 Novelty of the study	6
1.3 Aims and Objectives.....	6
1.4 Research Questions.....	7
1.5 Thesis Structure	10
Chapter 2 Geology of the Namibian West Coast Placer	12
2.1 Introduction.....	12
2.2 Regional Geological Setting	16
2.3 Source of Diamonds.....	18
2.4 Eocene gravel	20
2.5 Lower Orange River gravel terraces.....	21
2.6 Marine gravel beaches	21
2.6.1 Raised beaches	25
2.6.2 Back barrier, front barrier and lagoon deposits	25
2.6.3 Shallow Marine Atlantic 1 gravels	29
2.7 Deflation deposits.....	29
2.8 Significance and application of heavy mineral analysis to the reconstruction of palaeo-environments.....	32
Chapter 3 Analytical Procedures.....	35
3.1 Previous Work.....	35
3.2 Clast Analysis.....	36
3.3 Determination of heavy mineral proportions	37
3.3.1 Sample Collection	37
3.3.2 Sieving	40
3.3.3 Bulk Sediment Geochemistry.....	40
3.3.4 Gravity Settling Table.....	44
3.3.5 Grain counting using polarizing microscope Stereo Zoom microscope.....	50
3.3.6 Mineral Identification on SEM and Mineral Surface Texture Analysis.....	52

3.3.7	Mineral Composition	54
Chapter 4	Long-term controls on continental-scale bedrock river terrace deposition from integrated clast and heavy mineral assemblage analysis: an example from the lower Orange River ..	58
4.1	Introduction.....	58
4.2	Geological Setting and Geomorphology	61
4.2.1	Geological Setting	61
4.2.2	Geomorphology.....	62
4.3	Results	64
4.3.1	Gravel Characterisation	64
4.3.2	Heavy Mineral Assemblages of the Proto and Meso Orange River gravels	74
4.3.3	Distinction of the Proto and Meso Orange River deposits on basis of clast and heavy mineral assemblage	77
4.4	Discussion	82
4.4.1	Controls on clast assemblage differences.....	82
4.4.2	Controls on mineralogy of heavy mineral assemblages	85
4.4.3	Implications for river terrace deposits analysis	87
4.5	Conclusions.....	91
Chapter 5	The relationship between bathymetry, geomorphology and the distribution of heavy minerals	92
5.1	Introduction.....	92
5.2	Geological Setting	94
5.2.1	Cretaceous unit.....	94
5.2.2	Eocene unit	95
5.2.3	Miocene unit.....	95
5.2.4	Pleistocene unit.....	95
5.3	Sea Level Changes in Southern Africa.....	97
5.4	Oceanographic Setting	99
5.5	Seabed Morphology and Bathymetry	101
5.5.1	Bathymetry and landforms	101
5.5.2	Southeast Domain.....	101
5.5.3	Northeast Domain	102
5.5.4	Northwest Domain.....	102
5.5.5	Southwest Domain	104
5.6	Heavy Mineral Assemblages	110

5.7	Mineral Grain Size Distribution	111
5.8	Discussion	117
5.8.1	Sea Bed Geomorphology	122
5.8.2	Effect of Sea Water Chemistry	127
5.8.3	Effect of Sea Currents	129
5.8.4	Effect of Sea Level	130
5.9	Conclusions	132
Chapter 6 Correlation of Orange River and Atlantic 1 gravel deposits using heavy mineral assemblage.....		133
6.1	Introduction.....	133
6.2	Heavy mineral assemblage	136
6.3	Geochemical composition of bulk samples.....	146
6.4	Mineral surface textures	151
6.4.1	Orange River samples	151
6.4.2	Atlantic 1 samples	152
6.4.3	Comparison of Orange River and Atlantic 1 samples using mineral surface textures	152
6.5	Mineral composition.....	162
6.5.1	Garnet	163
6.5.2	Epidote	163
6.5.3	Magnetite	164
6.6	Relationship between heavy mineral distribution and diamond grade in Atlantic 1	164
6.6.1	Diamond grade.....	165
6.6.2	Correlation of heavy mineral concentration with diamond grade	165
6.7	Discussion	166
6.7.1	Integration of bulk geochemistry and heavy mineral assemblage.....	166
6.7.2	Controls on variations of mineral surface textures	176
6.7.3	Controls on mineralogy of heavy mineral assemblage	179
6.7.4	Controls on the relationship between heavy mineral assemblage and diamond grade	185
6.8	Conclusions	186

Chapter 7 Discussion	189
7.1 What factors control heavy mineral and clast assemblages in gravel terrace deposits of continental-scale bedrock rivers, and do terraces of different ages have distinct assemblages?	189
7.2 How can heavy mineral assemblages be used to characterise seabed marine gravels on passive continental margins?	197
7.2.1 Sediment supply.....	200
7.2.2 Effect of Sea Level.....	201
7.2.3 Effect of Sea Currents.....	201
7.2.4 Post Depositional Processes.....	202
7.3 How can onshore and offshore heavy mineral assemblages be correlated?	205
7.4 How can a better understanding of long-term relationships between river catchment dynamics and offshore sedimentation patterns be used to improve predictions and reduce uncertainties in exploration for offshore diamondiferous deposits in Atlantic 1?	213
Chapter 8 Conclusions and Future Work.....	216
8.1 Conclusions.....	216
8.2 Future Work.....	219
References	221
Appendix A: Heavy Mineral Assemblage Data	254
Appendix B: Bulk Sediment geochemistry data	262
Appendix C: Mineral Composition Data	268

List of Tables

Table 3.1 Total number of clasts analysed per size fraction for Orange River samples, this study.....	37
Table 3.2 Manufacturers recommended operating parameters for the Mineral Processing Table.	46
Table 3.3 Orange River samples analysed for repeat grain counting.	51
Table 3.4 Total number of mineral grains identified on the SEM for Orange River samples.	55
Table 3.5 Total number of mineral grains identified on the SEM for Atlantic 1 samples.....	55
Table 3.6 Number of garnet, magnetite and epidote grains from selected Orange River samples analysed for composition with the JEOL JXA8230 electron microprobe.	56
Table 3.7 Number of garnet, magnetite and epidote grains from selected Atlantic samples analysed for composition with the JEOL JXA8230 electron microprobe.	57
Table 4.1 Mineralogy of the Namaqua Metamorphic Complex and Gariep Belt rocks.	66
Table 4.2 Relative chemical stability of heavy minerals, from Morton and Hallsworth (2007).	78
Table 6.1 Common major and minor elements that make up the heavy minerals of the river and marine samples.....	149
Table 6.2 Comparison of surface textures between Proto Orange River gravels, Meso Orange River gravels and Atlantic 1 gravels.	162
Table 6.3 Diamond grade and stone size for Atlantic samples. Panel size is 625 m ²	171

List of Figures

- Figure 1.1. Intrinsic and extrinsic factors that can control sediment distribution from continents to oceans. Modified from Romans and Graham (2013). 4
- Figure 1.2. Orange River and Atlantic 1 study area. Red symbols represent sample locations. Onshore elevation data from Jarvis et al. (2008) 5
- Figure 2.1. Distribution of gravel terrace deposits (grey colour) along the lower Orange River. Deposits analysed in this study are marked in bold. Modified from Jacob et al. (1999). 14
- Figure 2.2 Distribution of clastic marine gravel and wind deflation lag deposits along the Namibian coast. Modified from Spaggiari et al. (2006). 15
- Figure 2.3. Geology of southern Africa. Adapted from Jacob (2005). 17
- Figure 2.4. Elevation terrain of southern Africa. Note the elevated central plateau. Adapted from Jacob (2005). 18
- Figure 2.5 (A) Basal Eocene marine succession overlain by a thick aeolian layer, Buntfeldschuh. The sequence is capped by ferricrete. Thickness for aeolian sandstone and ferricrete from Bluck et al. (2007) and Miller (2008), respectively. (B) Clay matrix of the marine gravel. Honey-yellow pebbles are chalcedony. For scale camera lens is 52 mm in diameter. 23
- Figure 2.6 (A) In situ fluvial sandstone bedrock, Mining Area 1 about 10 km north of Orange River mouth. (B) Post mining view of East Cliff where the F-Beach was stacked. The broken white line represents the top surface of F-Beach..... 24
- Figure 2.7 (A) A series of east-west orientated bedrock gullies, exposed after mining. The average depth and width of the gullies at this location is 1.8 m and 2.1 m, respectively. (B) A 2.3 m wide gully exposed after mining. Pictures taken looking west, Mining Area 1. 26
- Figure 2.8 (A) Clastic coarse barrier beach gravel with series of repeating sequences (highlighted by broken white line) that terminates in blinding fabric gravel. (B) Close up of blinding fabric gravel, position X in Picture A. Pictures taken looking northeast..... 27
- Figure 2.9 (A) Clay rip-up clast in front barrier beach gravels. Camera lens cover for scale. (B) Back barrier beach deposits with alternating sand and poorly consolidated gravel layers. Note bioturbation in sand layers (white circles). 28
- Figure 2.10 Chalcedony (honey-yellow) and agate pebbles in (A) insitu Eocene gravel and (B) deflation deposit at Buntfeldschuh. For scale camera lens is 52 mm in diameter..... 30
- Figure 2.11 (A) Deflation lag of vein quartz after the country rock has been completely weathered, Chameis, Sperrgebiet. (B) Wind formed flutes on dolomite rock

surface. Northward wind direction is denoted by arrows. Picture B taken looking north. For scale camera lens is 52 mm in diameter.	31
Figure 3.1 Flow sheet of gravel processing on the MV Mafuta mining vessel. Sample collection point indicated by arrow.	39
Figure 3.2. Comparison of Fe content between first and repeat XRF analyses, Orange River samples.	41
Figure 3.3 Comparison of Mn content between first and repeat XRF analyses, Orange River samples.	42
Figure 3.4 Comparison of Ca content between first and repeat XRF analyses, Atlantic 1 samples.	43
Figure 3.5 Comparison of Mn content between first and repeat XRF analyses, Atlantic 1 samples.	44
Figure 3.6 Laboratory Mineral separator. A = water inlet (light blue), B = spray pipe (dark blue), C = sample feed point, D = tailings outlet, E = tailings pipe (green), F = sedimentation tank (white).	47
Figure 3.7 (A) Heavy minerals concentrate (dark) and light minerals during processing after separation on the gravity table of 0.5-1 mm size fraction of Auchas Lower Meso sample. (B). Close up view of Picture A bottom.	48
Figure 3.8 Heavy minerals concentrate (dark) and light minerals after separation on the gravity table of 0.5-1 mm size fraction of Auchas Outlet Meso Trench sample. Close up view of Picture A bottom.	49
Figure 3.9 Comparison between first and repeat heavy mineral assemblage for Proto Orange River samples. Size fractions are (A) 0.5-1 mm and (B) 0.25-0.50 mm. The error bars indicate deviation from the average value.	53
Figure 3.10 Comparison between first and repeat heavy mineral assemblage for Meso Orange River samples. Size fractions are (A) 0.5-1 mm and (B) 0.25-0.50 mm. The error bars indicate deviation from the average value.	54
Figure 4.1 (A) Study area with distribution of gravel terrace deposits (orange colour) along the lower Orange River. Deposits analysed in this study are marked in bold. (B) Proto Orange River and Meso Orange River profiles relative to the modern Orange River profile. Figures A and B modified from Jacob et al. (1999) and Jacob (2005), respectively.	60
Figure 4.2 Simplified geology of the lower Orange River. Locations of Sendelingsdrif, Daberas, Auchas and Arrisdrif deposits are indicated for reference. Namibia GIS-based data obtained from the Geological Survey of Namibia. South African data after de Villiers and Sohng (1959).	62
Figure 4.3 (A) Representative photograph of the thick Proto Orange River terrace deposit at Sendelingsdrif deposit. Photograph taken looking east. (B) and (C)	

Photograph of deep scours cut into bedrock below the bedrock strath level at Auchas deposit. Note the smooth walls of the scours formed by abrasion. . 67

Figure 4.4 Imbricated clasts (marked by white lines) (A) and coarse cross bedding (B) as seen in Proto Orange River unit and above Meso Orange River unit, respectively. (C) Meso Orange River gravel. 68

Figure 4.5 Agate (A), Karoo sedimentary rocks (B) and BIF (C) clasts that comprise the exotic clast suite of the Orange River derived gravels. (D) Fresh non-weathered feldspar clasts from Proto Orange River gravel, Daberas deposit. 69

Figure 4.6 Key clasts of the Orange River gravel terrace deposits and their respective provenances. Namaqua MC denotes Namaqua Metamorphic Complex. Modified from Jacob (2005). 70

Figure 4.7 Clast assemblage of Proto and Meso Orange River gravels for size fractions (A) 16-25 mm, (B) 8-16 mm and (C) 3-8 mm. Data from Jacob (2005). Sample locations are indicated in Figure 4.1A. 73

Figure 4.8 Clast roundness of the Proto and Meso Orange River gravels. Modern Orange River data is included for comparison. Data from Jacob (2005). 74

Figure 4.9 Heavy mineral assemblage of Proto and Meso Orange River deposits for size fractions (A) 1-2 mm, (B) 0.5-1 mm (C) and 0.25-0.50 mm. Sample locations are indicated in Figure 4.1A. 76

Figure 4.10 Variation in the proportions of amphibole and epidote proportions between the Proto and Meso Orange River deposits for size fractions (A) 1-2 mm, (B) 0.5-1 mm and (C) 0.25-0.50 mm. 77

Figure 4.11 Downstream change in amphibole-epidote/magnetite ratio from Boom to Arrisdrif for the Proto Orange River gravel (orange symbols) and Meso Orange River gravel (black symbols). (A) 1-2 mm, (B) 0.5-1 mm and (C) 0.25-0.50 mm. Meso Orange River samples with anomalous amphibole-epidote/magnetite ratios are for the Upper Meso units. 79

Figure 4.12 Clast assemblage and heavy mineral assemblage variations between Proto Orange River and Meso Orange River gravel. Heavy mineral assemblage data is from 0.5-1 mm size fraction whereas clast assemblage data is for (A) 16-25 mm, (B) 8-16 mm and (C) 3-8 mm. 80

Figure 4.13 Comparison of Namaqua Metamorphic Complex clasts and amphibole-epidote content. (A) 1-2 mm, (B) 0.5-1 mm (C) and 0.25-0.50 mm. 81

Figure 4.14 (A) Garnet compositions in MgO versus FeO from the Namaqua Metamorphic Complex (Humphreys and Van Bever Donker, 1990; Cornell et al., 1992; Diener et al., 2013; Bial et al., 2015) and Gariep Belt garnets (Diener et al., 2017). (B) Data for Proto and Meso Orange River garnets. (C) MgO

versus FeO from the Namaqua Metamorphic Complex and Gariep Belt (D) Data for Proto and Meso Orange River garnets.....	82
Figure 4.15 Clast and heavy mineral assemblage of the Proto Orange River and Meso Orange River deposits and the respective controls affecting the differences.	90
Figure 5.1. Location map of Atlantic 1 with respect to the lower Orange River. Onshore elevation after Jarvis et al. (2008).	93
Figure 5.2 (A) Stratigraphy of Atlantic 1 geology. (B) Representative cross section of sedimentary geology of Atlantic 1. Both figures modified from Mubita et al. (2015).	96
Figure 5.3 Sea levels associated with shoreline movements in southern Africa between the Cretaceous period and Quaternary. Outcrop localities on which the interpretation are based are denoted by letters; AB – Agulhas Bank, B- Birbury, E- east coast, N – Namibia, S – south coast, W – west coast, Z – Zululand. Modified from Siesser and Dingle (1981).	98
Figure 5.4 Bathymetry domains of the Atlantic 1 region. Red symbols denotes sample locations. The brown solid line represent the approximate last sea level low stand (-120 m isobath). Numbers 1, 2, 3, 4 and 5 indicate the location of the bathymetry sections shown in Figures 5.4, 5.5, 5.6, 5.8 and 5.9, respectively.	103
Figure 5.5 Representative bathymetry of the Southeast Domain. Location of the area shown is denoted by 1 in Figure 5.3. Red dots indicate sample positions.	104
Figure 5.6 Representative sea bed morphology of the Southeast Domain as seen from the bathymetry and associated seismic data. The location of the area shown is denoted as 2 in Figure 5.3. Sample positions (red dots) indicated on the bathymetry map in (A) are denoted on the seismic section in (B) by the black arrow. Black line in Figure A marks the position of the seismic section.	105
Figure 5.7 Shallow broad depression bordered in the west by a ridge, Region N, Northeast Domain. Location of the area shown is denoted by 3 in Figure 5.3. Black line in Figure A marks the position of the seismic section.	106
Figure 5.8 Coast parallel and coast perpendicular linear features (red lines) in the Northwest Domain. Red symbols denotes sample locations. The brown solid line represent the approximate last sea level low stand (-120 m isobath). Refer to Figure 5.1 for regional reference.....	107
Figure 5.9 Coast parallel erosional features in Region V, Northwest Domain. Location of the area shown is denoted by 4 in Figure 5.3. Black lines in Figure A labelled X and Y indicate positions of seismic sections for Figure B and Figure C, respectively. Arrows in Figures B and C indicate sample locations denoted by red circles in Figure A.	108

Figure 5.10 Coast parallel features in the Region W, Northwest Domain. Location of the area shown is denoted by 5 in Figure 5.3. Black line in Figure A marks the position of the seismic section in Figure B.	109
Figure 5.11 Coast perpendicular gullies in the bedrock of raised beach gravels exposed after mining. Photographs taken looking west.	112
Figure 5.12 Heavy mineral assemblage of Region K. Figures A, B, C represent size fractions 1-2 mm, 0.5-1 mm and 0.25-0.50 mm, respectively.	113
Figure 5.13 Heavy mineral assemblage of Region N. Figures A, B and C represent size fractions 1-2 mm, 0.5-1 mm and 0.25-0.50 mm, respectively.	114
Figure 5.14. Heavy mineral assemblage of Region V. Figures A, B, C represent size fractions 1-2 mm, 0.5-1 mm and 0.25-0.50 mm, respectively.	115
Figure 5.15. Heavy mineral assemblage of Region W. Figures A, B, C represent size fractions 1-2 mm, 0.5-1 mm and 0.25-0.50 mm, respectively. No heavy mineral was recovered in sample W-S4 in the 1-2 mm size fraction.	116
Figure 5.16 Spatial distribution of heavy mineral assemblage in Atlantic 1. Figures A, B and C represent 1-2 mm, 0.5-1 mm and 0.25-0.50 mm, respectively.	118
Figure 5.17 Difference in magnetite content between Regions K, N, V and M. Figures A and B represent size fractions 0.5-1 mm and 0.25-0.50 mm, respectively.	119
Figure 5.18 (A) SEM image of clinopyroxene (light grey) with plagioclase (dark grey) and titanomagnetite (white) intergrowth. Figures B, C and D show EDS spectrums of clinopyroxene, plagioclase and titanomagnetite, respectively. The y-axis in Figures B, C and D represent peak count intensity.	120
Figure 5.19 Compositional difference between biogenic apatite (A) and authigenic apatite (B). The y-axis in Figures A and B represent peak count intensity.	121
Figure 5.20 Comparison between samples that are located inside and samples that are located outside linear depressions from the same region, Region V. Data for 0.25-0.50 mm size fraction.	123
Figure 5.21 Comparison of Atlantic 1 garnets with Namaqua Metamorphic Complex and Gariep Belt garnets. Data for Namaqua Metamorphic Complex garnets from Humphreys and Van Bever Donker (1990), Cornell et al. (1992), Diener et al. (2013) and Bial et al. (2015) whereas Gariep Belt garnet data after Diener et al. (2017).	124
Figure 5.22 Comparison of (A) magnetite, (B) garnet, (C) amphibole-epidote and (D) ilmenite grain size between the Atlantic 1 regions.	125
Figure 5.23 Variation of sand coarseness among the Atlantic 1 regions.	126
Figure 6.1 Orange River and Atlantic 1 study area. Red symbols represent sample locations. Onshore elevation data from Jarvis et al. (2008).	135

Figure 6.2 Heavy mineral assemblage of Proto Orange River and Atlantic 1 deposits. Figures A, B, C represent size fractions 1-2 mm, 0.5-1 mm and 0.25-0.50 mm, respectively. Due to absence of apatite in the river samples, apatite data is excluded from this plot for ease of comparison..... 138

Figure 6.3 Heavy mineral assemblage of Meso Orange River and Atlantic 1 deposits. Figures A, B, C represent size fractions 1-2 mm, 0.5-1 mm and 0.25-0.50 mm, respectively. Due to absence of apatite in the river samples, apatite data is excluded from this plot for ease of comparison..... 139

Figure 6.4 Comparison of garnet and magnetite content between the river and marine deposits. Figures A, B, C represent size fractions 1-2 mm, 0.5-1 mm and 0.25-0.50 mm, respectively. 140

Figure 6.5 Comparison of garnet, magnetite and ilmenite content between the river and marine deposits. Figures A, B, C represent size fractions 1-2 mm, 0.5-1 mm and 0.25-0.50 mm, respectively. 141

Figure 6.6 Spatial variation of heavy mineral assemblage in the Proto Orange River deposits (A) and Atlantic 1 samples (B, C and D). Heavy mineral data for the Proto Orange River deposits is for 1-2 mm whereas data for Atlantic 1 deposits in B, C and D is for 1-2 mm, 0.5-1 mm and 0.25-0.50 mm size fractions, respectively. Due to absence of apatite in the river samples, apatite data is excluded from this plot for ease of comparison. Elevation data for Orange River area from Jarvis et al. (2008)..... 142

Figure 6.7 Spatial variation of heavy mineral assemblage in the Proto Orange River deposits (A) and Atlantic 1 samples (B, C and D). Heavy mineral data for the Proto Orange River deposits is for 0.5-1 mm whereas data for Atlantic 1 deposits in B, C and D is for 1-2 mm, 0.5-1 mm and 0.25-0.50 mm size fractions, respectively. Due to absence of apatite in the river samples, apatite data is excluded from this plot for ease of comparison. Topography data for Orange River area from (Jarvis et al., 2008)..... 143

Figure 6.8 Spatial variation of heavy mineral assemblage in the Meso Orange River deposits (A) and Atlantic 1 samples (B, C and D). Heavy mineral data for the Meso Orange River deposits is for 1-2 mm whereas data for Atlantic 1 deposits in B, C and D is for 1-2 mm, 0.5-1 mm and 0.25-0.50 mm size fractions, respectively. Due to absence of apatite in the river samples, apatite data is excluded from this plot for ease of comparison. Topography data for Orange River area from Jarvis et al. (2008)..... 144

Figure 6.9 Spatial variation of heavy mineral assemblage for the Meso Orange River deposits (A) and Atlantic 1 samples (B, C and D). Heavy mineral data for the Meso Orange River deposits is for 0.5-1 mm whereas data for Atlantic 1 deposits in B, C and D is 1-2 mm, 0.5-1 mm and 0.25-0.50 mm size fractions, respectively. Due to absence of apatite of apatite in the rive samples, apatite

data is excluded from this plot for ease of comparison. Topography data for Orange River area from (Jarvis et al., 2008).....	145
Figure 6.10 Comparison of two modern Orange River samples with Atlantic 1 gravels. Figures A, B, C represent size fractions 1-2 mm, 0.5-1 mm and 0.25-0.50 mm, respectively.....	148
Figure 6.11. Comparison of bulk sample composition between Proto Orange River samples, Meso Orange River samples and Atlantic 1 samples for 0.25-0.50 mm size fraction. Anomalous sample K-S3 from Region K (Fe = 385, 860 ppm) is excluded from Figures A, C, D and E.....	149
Figure 6.12 Covariation of bulk sample composition and heavy mineral assemblage in Proto Orange River samples, Meso Orange River samples and Atlantic 1 samples for 0.25-0.5 mm size fraction.	150
Figure 6.13 Garnet: (A) Conchoidal fractures, Proto Orange River gravel, Auchas Major Deposit. Note the few etch pits (arrows) on the fractured surface. (B) Etch pits superimposed on conchoidally fractured surface (white rectangle), Proto gravel, Arrisdrif Deposit. (C) Large euhedral pits, Proto Orange River gravel, Boom Deposit. (D) Close up view of area inside white square in Picture C.	153
Figure 6.14 Garnet: (A) Euhedral etch pits (arrows), Meso Orange River Boom Deposit. (B) Cobbled structure and etch pits (arrows) on conchoidally fractured surface, Proto Orange River Sendelingsdrif Deposit. (C) Cobbled structure and euhedral etch pits (white square) Proto Orange River gravel, Auchas Major Deposit. (D) Close up of euhedral etch pits inside white square in Picture C.	154
Figure 6.15 Epidote: (A) Extensive chemical etching. (B) Close up view of white boxed area in Picture A. (C) Etch pits on epidote from Meso Orange River gravel. (D) Close up view of Picture C. Both grains from Meso Orange River gravel, Sendelingsdrif Deposit.	155
Figure 6.16 Epidote: Saw tooth terminations on epidote from Meso Orange River gravel, Arrisdrif Deposit.....	156
Figure 6.17 Magnetite: (A) Large fractured dissolution pit (white square), Meso Orange River gravel, Sendelingsdrif Deposit. (B). Close up of dissolution pit in Picture A. (C) Conchoidal fracture (white square) on magnetite, Proto Orange River gravel, Sendelingsdrif Deposit. (D) Honeycomb dissolution texture (white arrows), Proto Orange River gravel, Arrisdrif Deposit.....	157
Figure 6.18 Garnet: Conchoidal fractures on garnets from Region K (A and B) and Region V (C). Picture D shows small dissolution pits (arrows), Region N. Imbricate wedge marks on garnet, Region W (E and F).	158
Figure 6.19 Epidote: Large dissolution pit (A and B). Irregular dissolution pits on a rounded epidote (C and D). All grains from Region V.....	159

Figure 6.20 Epidote: Saw tooth terminations (arrows in A) from Region K (A and B) and Region V (C and D).....	160
Figure 6.21 Magnetite: Irregular dissolution pits, Region N.	161
Figure 6.22 (A) Garnet compositions in MgO versus FeO from the Namaqua Metamorphic Complex (Humphreys and Van Bever Donker, 1990; Cornell et al., 1992; Diener et al., 2013; Bial et al., 2015) and Gariep Belt garnets (Diener et al., 2017). (B) Data for Proto and Meso Orange River and Atlantic 1 garnets. (C) MgO versus FeO from the Namaqua Metamorphic Complex and Gariep Belt. (D) Data for Proto and Meso Orange River and Atlantic 1 garnets. ...	168
Figure 6.23 Epidote composition from Proto Orange River deposits (n = 20), Meso Orange River deposits (n = 20) and Atlantic 1 deposits (n = 32).	169
Figure 6.24 Magnetite composition from Proto Orange River deposits, Meso Orange River deposits and Atlantic 1 deposits.	170
Figure 6.25 Variation of diamond grade (A) and stone size (B) in Region K, Region N, Region V and Region W.....	172
Figure 6.26 Covariation of diamond stone size and grade in Atlantic 1.	173
Figure 6.27 Variation of diamond grade and stone size with magnetite proportions for the Atlantic 1 gravels.....	174
Figure 6.28 Comparison of diamond grade and stone with garnet (A, B, C, D), amphibole-epidote (E) and ilmenite (F) proportions for the Atlantic 1 gravels.	175
Figure 6.29 Comparison of relative density of Atlantic 1 heavy minerals and diamonds. Numbers in brackets are density values. No values are plotted on the x-axis.	176
Figure 7.1 Generalised diagram of sedimentary system profile between continents (source) and oceans (sink). Modified from Romans and Graham (2013). .	192
Figure 7.2 Clast assemblage (inset) and heavy mineral assemblage of Proto and Meso Orange River deposits. Size fractions are 3-25 mm and 0.25-0.50 mm for clast and heavy mineral assemblage data, respectively. Clast assemblage data for Proto and Meso Orange River gravels represent average of sampled deposits. Clast assemblage and elevation data after Jacob (2005) and Jarvis et al. (2008), respectively.	196
Figure 7.3 Synthesis on major changes in clast and heavy mineral assemblage of the Orange River deposits, and the interpreted controls. Yellow, brown and green arrows point in the direction of increase.....	197
Figure 7.4 Heavy mineral proportion trends in Atlantic 1 for 0.25-0.50 mm size fraction.	203

Figure 7.5 Offshore Orange River profile constructed from bathymetry data across Region L to Region T (Course A), Region M to Region U (Course B) and Region N to Region V (Course C)..... 208

Figure 7.6 Longitudinal profile of the Proto Orange River and Meso Orange River. Onshore river profiles constructed using data from Jacob (2005). Offshore river profile constructed from bathymetry data across Region L to Region T (Course A), Region M to Region U (Course B) and Region N to Region V (Course C). 209

Figure 7.7 Depositional sequence of Orange River and Atlantic 1 gravel deposits. 212

Chapter 1 Introduction

1.1 Project Overview and Rationale

The flux of sediment and carbon from continents to oceans over different timescales and physiographic configuration remains poorly constrained. Therefore, linking the erosional record of onshore drainage basins with the depositional record of offshore sedimentary basins is a major challenge in earth sciences (e.g., Allen, 2008; Romans and Graham, 2013; Clift et al., 2014; Romans et al., 2016). The depositional record of terrace deposits within bedrock rivers form a crucial link between areas of degradation (drainage basins) and aggradation (sedimentary basins), and therefore have the potential to improve our understanding on the timing and character of river systems during sediment transfer from the continents (source) to oceans (sink) (Pazzaglia and Gardner, 1993; Aalto et al., 2008; Marsaglia et al., 2010; Kuehl et al., 2016). Gravel terrace deposits of continental-scale rivers provide both a fragmented record of drainage basin evolution, and a means to predict and unravel the depositional record of quasi-contemporaneous marine sediments. The timing of fluvial terraces deposition of continental-scale bedrock rivers has been correlated to tectonic uplift (e.g., Lewis et al., 2017) and climate (e.g., Bridgland and Westaway, 2008; Counts et al., 2015) (Fig. 1.1). However, these environmental signals (tectonic uplift and climate) may propagate through the source-to-sink system as they are subjected to modification during transport, in the sediment transfer zone or post sediment deposition. In rare cases, the volume of sediments produced onshore may balance the volume of sediments deposited in the offshore (Covault et al., 2011) but such cases require rapid transfer of sediments and a short transport distance (Romans et al., 2016). Over longer timescales and distances the sediment supply signal is 'shredded' (Allen, 2008; Jerolmack and Paola, 2010; Romans et al., 2016). On continental shelves, sediments are subject to the effect of relative sea level change, ocean currents, waves, fluvial and aeolian processes

as well as post deposition modification that may alter the volume and composition of the sediments delivered by rivers to the coast (Fig. 1.1). Also, sediments may be bypassed to the deep sea by gravity flows (e.g., Covault and Fildani, 2014). Understanding the erosional record of continental-scale rivers may help constrain the stratigraphic record of continental shelf sediments. The diamondiferous fluvial gravel terrace deposits along the lower Orange River and the coeval offshore gravel deposits, southern Namibia, provide a rare opportunity to study the propagation of signal transfer from source to sink (Fig. 1.2) due to the well constrained onshore depositional record. The Orange River deposits have been constrained in terms of the incision and aggradation history of the Orange River as deduced from detailed and extensive clast assemblage study of Jacob (2005). Jacob (2005) classified the Orange River deposits into older Proto Orange River deposits and younger Meso Orange River deposits on the basis of their upstream catchment area-derived exotic clast assemblage, bedrock strath level and palaeo-river course. These studies were designed to establish the timing of influx of diamonds into the fluvial and marine environments, as these deposits have underpinned major mining operations for over a hundred years. Currently, the extraction of diamonds from the marine licence area (Atlantic 1) is a major source of diamonds. However, the understanding of the nature and origins of the marine gravels is limited, because there is no available data defining the clast assemblages of the Atlantic 1 gravel deposits. Therefore the distribution and depositional sequence of the Atlantic 1 gravels is poorly understood.

Analysis of the clast lithology of fluvial deposits has been used as a tool for unravelling landscape evolution (Bridgland and Westaway, 2008). The provenance signal carried by clasts may be altered through mechanical degradation during transport or chemical degradation post deposition. An alternative is the use of heavy minerals, because they are chemically more resistant (Hassan, 1976; Morton, 1984, 1991; Goodbred et al., 2014). However, the two techniques are rarely integrated despite their respective limitations. For the first time, clast assemblage and heavy mineral assemblage of the Proto and Meso Orange River gravel deposits are integrated to characterise the lower Orange River deposits. The integrated clast and heavy mineral assemblage of the river deposits is applied to the offshore gravels to understand the distribution

and timing of the deposition of the Atlantic 1 marine gravels in response to the evolving depositional and erosional phases of the Orange River.

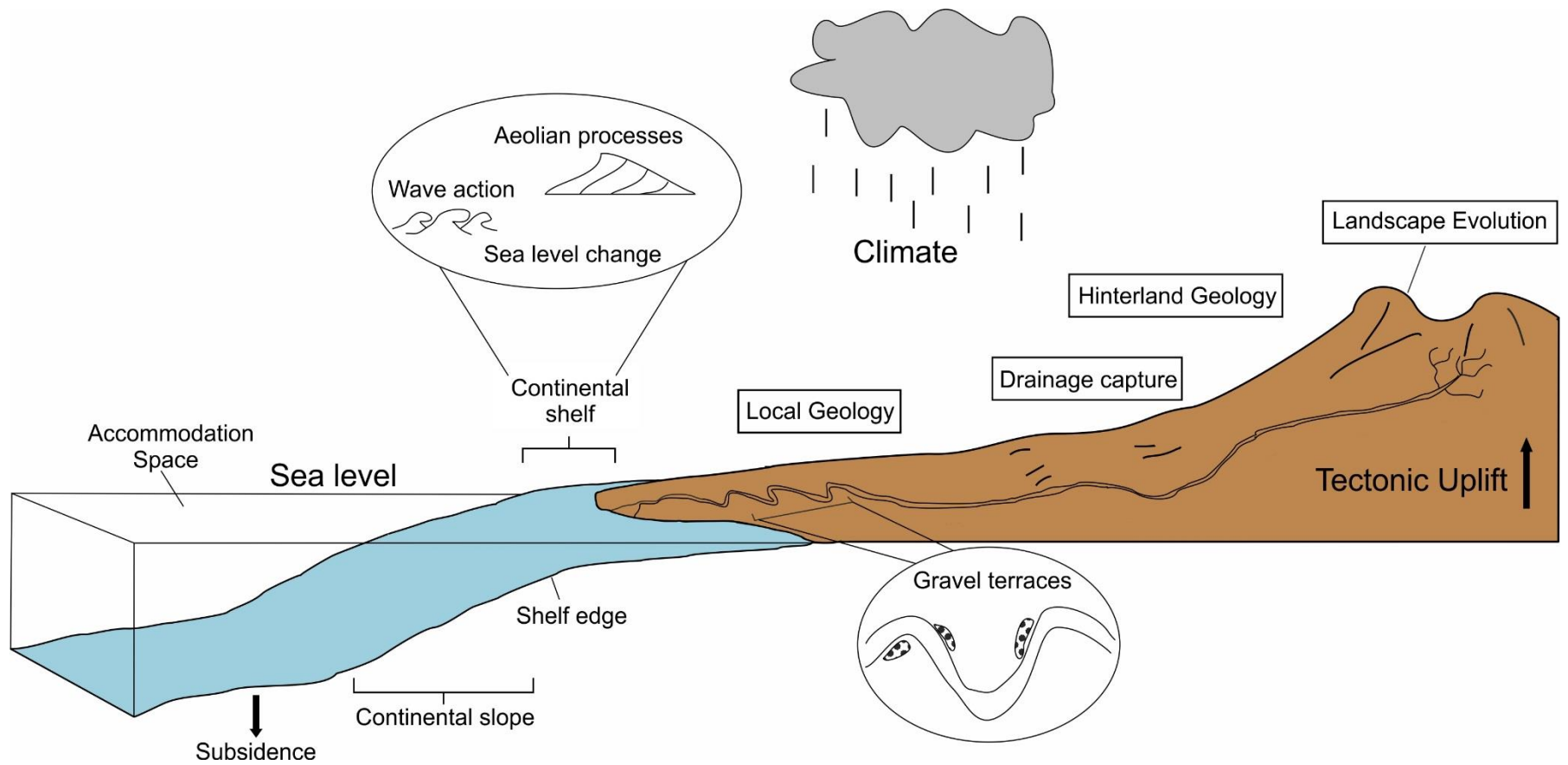


Figure 1.1. Intrinsic and extrinsic factors that can control sediment distribution from continents to oceans. Modified from Romans and Graham (2013).

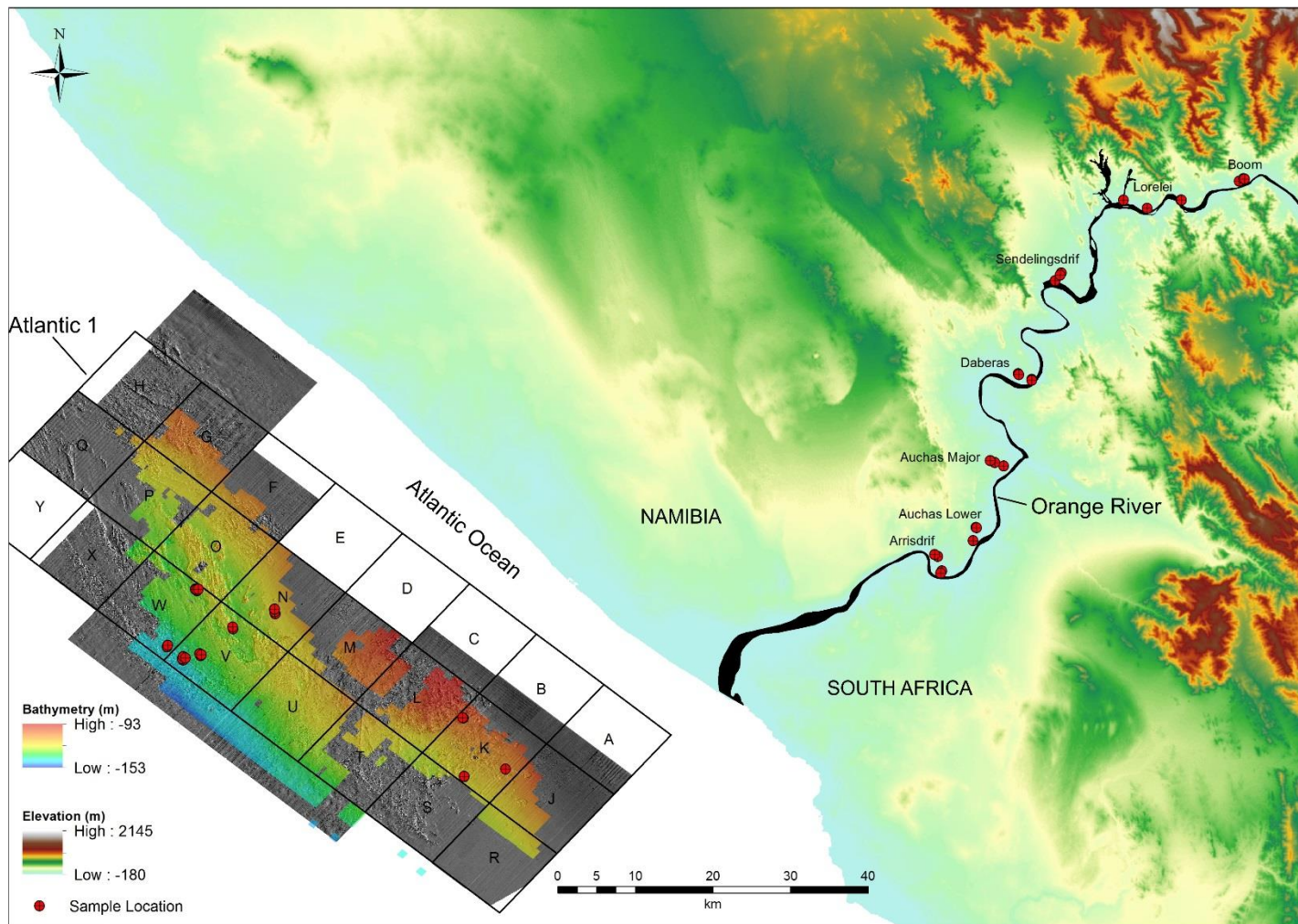


Figure 1.2. Orange River and Atlantic 1 study area. Red symbols represent sample locations. Onshore elevation data from Jarvis et al. (2008)

1.2 Novelty of the study

Although understanding the flux of sediment from continents to oceans remains a grand challenge of the earth sciences, advances will require integrated and novel approaches to better constrain systems. An important component of these source-to-sink studies when applied to deep time configuration is an understanding of the hinterland source area. Most provenance studies and palaeogeographic reconstructions of drainage basins and sedimentary basins have often employed the use of clast assemblages or heavy minerals independently (Gibbard, 1979; Dowdeswell et al., 1985; Bridgland, 1999; Mikesell et al., 2010; Uddin et al 2007; Morton et al, 2011). In particular, the use of heavy mineral analysis is typically only applied to the basinal deposits, rather than both fluvial and marine deposits to make provenance links and to infer temporal relationships. In this study, for the first time the Orange River and Atlantic 1 gravels are characterised using heavy minerals. No study has previously used any data from the offshore deposits. In addition this study will be the first to integrate both clast and heavy mineral assemblage data to investigate the evolution of onshore-offshore facies relationships. The novel integrated clast and heavy mineral assemblage approach, with onshore and offshore deposits, can be applied to other linked systems around the planet in order to unravel evolution history of continental scale bedrock rivers using offshore sediments.

1.3 Aims and Objectives

The aims of the study are to correlate the clast and heavy mineral assemblage of the Proto and Meso Orange River gravel terrace deposits and to constrain the timing of deposition of the Atlantic 1 gravel deposits.

To address these aims, the following objectives have been defined:

- i. To reconstruct the drainage history of the lower Orange River using river terrace deposits.

- ii. To investigate extrinsic and intrinsic controls on the clast assemblage and heavy minerals assemblage
- iii. Evaluate the value of a combined approach to understanding continental-scale bedrock river evolution.
- iv. Investigate the sediment distribution patterns in Atlantic 1.
- v. Assess the influence of marine processes (e.g. sea level, ocean currents) on the distribution of heavy mineral assemblages.
- vi. Establish the clast assemblage of the Atlantic 1 gravels from heavy mineral assemblages.
- vii. Establish the depositional sequence of Atlantic 1 gravels with respect to the timing of accumulation of the fluvial lower Orange River deposits.

1.4 Research Questions

Question 1: What factors control heavy mineral and clast assemblages in gravel terrace deposits of continental-scale bedrock rivers, and do terraces of different ages have distinct assemblages?

Terrace deposits of bedrock rivers provide a fragmented record of drainage basin and landscape degradation (e.g., Bridgland and Westaway, 2008; Wegmann and Pazzaglia, 2009), and provide a link to the downstream depositional record. Therefore, understanding the provenance of all components of river terrace deposits help with both understanding long-term landscape evolution, and the composition of offshore deposits. These are key uncertainties during resource exploration, in both oil and gas, and placer mineral industries. Analysis of clast assemblage may reveal changing sediment provenance (Jones, 2000) and drainage re-organisation (Bridgland, 1999). An alternative technique is the use of heavy minerals because they are chemically more resilient during transport and to diagenetic processes post deposition (Hassan, 1976; Morton, 1984, 1991; Goodbred et al., 2014). Despite their respective limitations, the two techniques are rarely combined (e.g., Maher et al., 2007). For the first time, the Proto and Meso Orange River gravel terrace deposits are characterised on basis of their heavy mineral assemblage. Integration of clast and heavy mineral assemblage is

important to help understand the evolution of the Orange River. Therefore the correlation of clast and heavy mineral assemblage signatures in the fluvial Proto and Meso Orange River deposits will help to constrain the stratigraphic record of the marine Atlantic 1 gravels with respect to the Orange River history (Fig. 1.2).

Question 2: How can heavy mineral assemblages be used to characterise seabed marine gravels on passive continental margins?

The application of heavy minerals to offshore settings is synonymous with the oil and gas industry where it is primarily applied to deducing sediment provenance (e.g., Pujos et al., 1990; Morton et al., 2005; Cascalho and Fradique, 2007; Hallsworth and Chisholm, 2008; Tsikouras et al., 2011; Cao et al., 2015) and correlation of sedimentary units for hydrocarbon reservoir evaluation (Morton, 2007; Poulsen et al., 2007). Characterisation of offshore coarse grained gravels using heavy minerals is rarely attempted possibly due to a lack of economic interest. However, Atlantic 1 gravels host important economic diamond deposits. The stratigraphic relationships of the host gravels across the 80 km long Atlantic 1 region is poorly constrained. A good understanding of the stratigraphic record of the gravels, in terms of age of deposition and sediment distribution patterns for these deposits, is important for better resource exploitation and improved sampling and resource exploration techniques. Spatial characterisation of the Atlantic 1 gravels, on the basis of their heavy mineral assemblage, will help in understanding sediment distribution patterns of the Atlantic 1 gravels using the relative chemical and physical stability of heavy minerals. These stratigraphic relationships can be linked to the Proto and Meso Orange River gravels on the basis of their respective heavy minerals.

Question 3: How can onshore and offshore heavy mineral assemblages be correlated?

Linking erosional record of drainage basins with the depositional record of offshore sedimentary basins is challenging because sediments are subjected to modification during transport, in the sediment transfer zone or post sediment deposition (e.g. Romans and Graham, 2013; Clift et al., 2014; Romans et al., 2016). Continental shelves are important in linking sediments from source to sink because they are the first to receive sediments from the rivers before sediments are later transferred to the deep sea by gravity flow and mass movements (Covault and Fildani, 2014). It is important to understand the correlation of heavy minerals between the Orange River gravels and the marine Atlantic 1 gravels because this will help in understanding the timing of the deposition of the marine gravels that may feed into better diamond exploration models. Also, the correlation can help to determine the clast composition of the marine gravels which in turn feeds into better understanding of the evolution of the Orange River drainage basin in terms of the dynamic nature of the landscape evolution.

Question 4: How can a better understanding of long-term relationships between river catchment dynamics and offshore sedimentation patterns be used to improve predictions and reduce uncertainties in exploration for offshore diamondiferous deposits in Atlantic 1?

Heavy minerals have been extensively used in exploration of ore minerals (Gurney et al., 1993; Gurney and Zweistra, 1995; Wyatt et al., 2004; Nowicki et al., 2007; McClenaghan, 2011; Carmody et al., 2014) where they are used as indicator minerals for a range of mineral deposits. This project will investigate the potential for correlating specific heavy minerals with diamond distribution. If such correlations can be established they could underpin efficient sampling methods based on heavy mineral signatures, which may be easier to obtain than diamond grade which demand large sample sizes.

1.5 Thesis Structure

Chapter 2: Geology of the west coast placer

Fluvial, marine and aeolian deposits making up the west coast placer are introduced. Significance and application of heavy mineral analysis to the reconstruction of palaeo-environments is discussed.

Chapter 3: Analytical methods

This chapter provides a detailed description of the sampling techniques. A detailed account of the procedures used in determination of bulk sediment geochemistry, heavy mineral assemblage, mineral composition and mineral surface textures are outlined.

Chapter 4: Long-term controls on continental-scale bedrock river terrace deposition from integrated clast and heavy mineral assemblage analysis: an example from the lower Orange River, Namibia

This chapter is a journal paper that has been modified to a thesis chapter. It presents an integrated approach of clast and heavy mineral assemblage in characterising the Proto and Meso Orange River deposits to understand the drainage evolution of the Orange River basin.

Chapter 5: The relationship between bathymetry, geomorphology and the distribution of heavy minerals

In this chapter factors controlling the heavy mineral assemblage of the Atlantic 1 gravel deposits are assessed. Sediment distribution patterns in the marine environment are discussed.

Chapter 6: Correlation of Orange River and Atlantic 1 gravel deposits using heavy mineral assemblage

The depositional sequence of the Atlantic 1 gravels with respect to the accumulation of the Proto and Meso Orange River deposits is deduced from the heavy mineral assemblage. Factors that have affected the propagation of the heavy mineral assemblage from the river to the marine environment are discussed. In this chapter heavy mineral assemblage data is correlated with diamond grades to assess if heavy mineral assemblages could underpin a predictive methodology.

Chapter 7: Discussion

This chapter provides a synthesis of data presented from Chapters 4, 5 and 6 in the context of the research questions listed in the Introduction chapter (Chapter 1).

Chapter 8: Conclusion and Future Work

This chapter summarises the main findings of this study. Recommended future work is also discussed.

Chapter 2 Geology of the Namibian West Coast

Placer

2.1 Introduction

Alluvial deposits along the lower Orange River (Fig. 2.1), clastic beach and shallow marine gravel deposits, coast-parallel wind deflation deposits, and aeolian deposits along the Namibian coast constitute the Namibian diamond placer. Along the Namibian coast, the marine gravel deposits, wind deflation deposits and aeolian deposits occur over a stretch of 300 km northward from the Orange River mouth (Fig. 2.2). These deposits are genetically related as they consist of Orange River derived exotic clasts from the upstream catchment area (Jacob, 2005). Exotic clasts include agate, chalcedony, Karoo Supergroup shales and sandstone and banded iron formation (BIF). The exotic clasts reflect the geology in the upstream part of the Orange River catchment area (Figs. 2.3, 2.4). Gravel brought to the Atlantic Ocean by the Orange River was transported by a combination of northward longshore drift and wave action forming a series of extensive clastic marine beach gravels along the coast (Spaggiari et al., 2006). The oldest marine preserved gravel is the Eocene gravel which occurs in patches along the coast (Jacob, 2007). Wind assisted erosion of the Eocene gravel under the extreme arid Namib Desert conditions led to the formation of deflation lag deposits (Miller, 2008). Alluvial gravels that form terrace deposits comprise stratigraphically the pre-Proto, Proto and Meso Orange River gravels (Jacob, 2005). The Proto suite has been dated at Early to Middle Miocene, using macrofauna fossils, including *Lopholistriodon moruoroti*, found in Auchas and Arrisdrif gravel terrace deposits of the lower Orange River (Corvinus, 1978; Corvinus and Hendey, 1978; Hendey, 1978; Pickford, 1987; Pickford and Senut, 2002) located 43 km and 30 km from the Orange River mouth, respectively.

From the Orange River mouth, the diamondiferous sediments that reached the Atlantic Ocean, were distributed northwards and westwards by littoral ocean currents including longshore drift, driven by a high-energy southwesterly wind regime, and waves which concentrated diamonds (Bluck et al., 2007). A modern mean height of 2 m for the southwesterly swell (Bosman and Jourbert, 2008) attest to the strength of the wind regime in this region. Pether et al. (2000) advocates that longshore drift begun in Middle Eocene but Bluck et al. (2007) argues for an earlier onset of Early Cretaceous. However, field evidence at Buntfeldschuh attests to Eocene onset as the 42 Ma Eocene basal shoreline marine succession at this locality is directly overlain by a thick (18 m; Bluck et al., 2007) aeolian sandstone (Fig. 2.5A). The direction of the forests within the aeolian sandstone point northwards suggesting that the strong southerly wind regime (which drives the longshore drift) has been in operation since the Eocene (Siesser and Salmon, 1979; Miller, 2008). Additionally, no Early Cretaceous age aeolian sediments have been discovered onshore. However, Wickens and MacLachlan (1990) reported Lower Cretaceous aeolinites with a dominant southwest wind direction from offshore boreholes (Kudu 9A-2 and Kudu-9A-3) in the region.

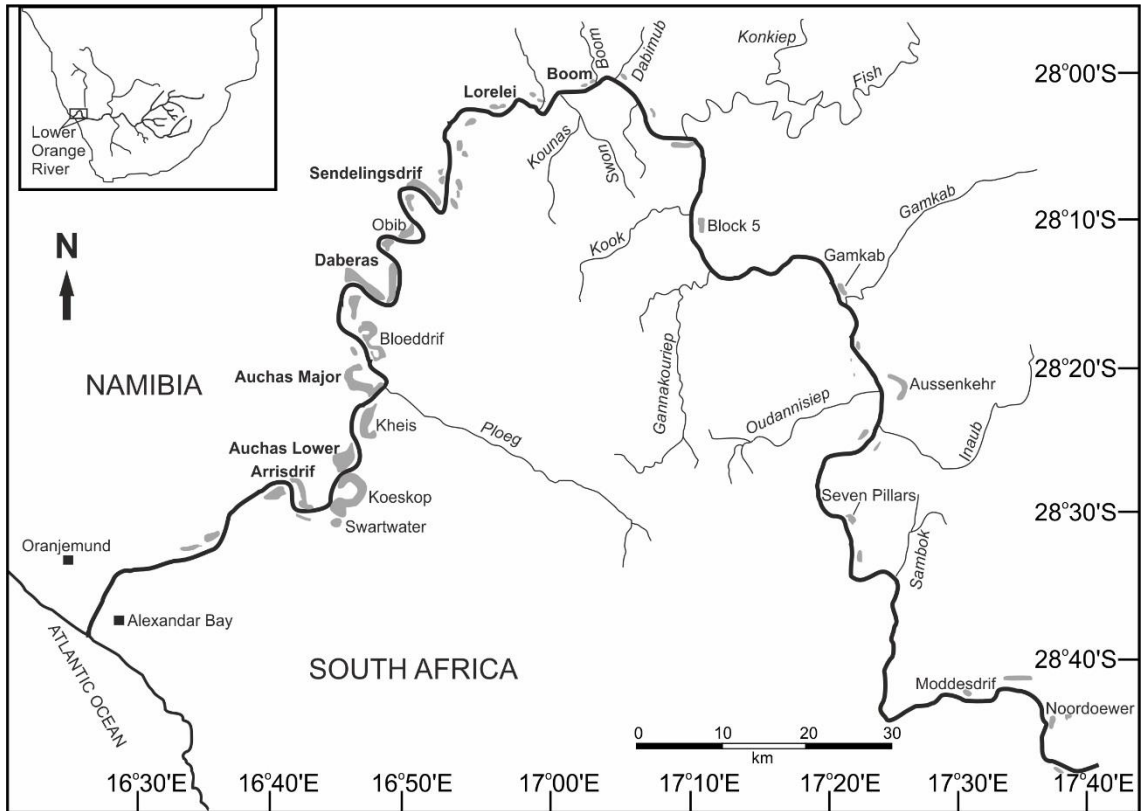


Figure 2.1. Distribution of gravel terrace deposits (grey colour) along the lower Orange River. Deposits analysed in this study are marked in bold. Modified from Jacob et al. (1999).

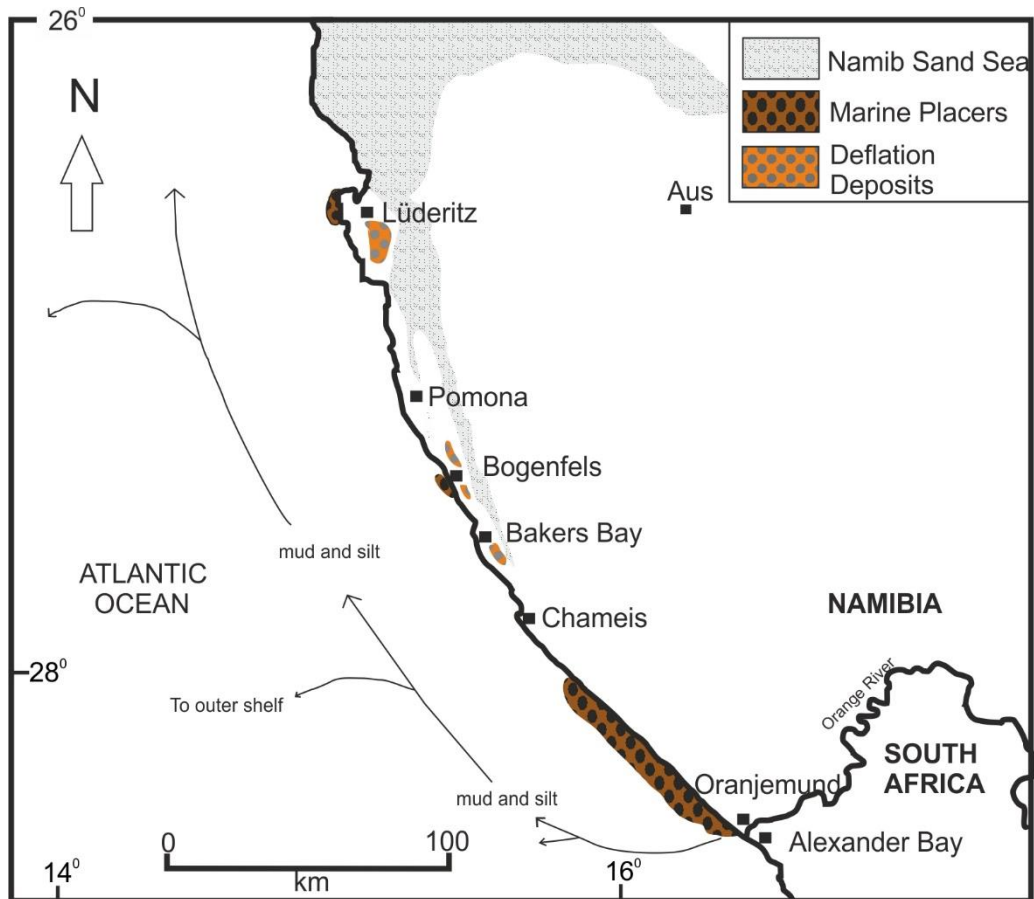


Figure 2.2 Distribution of clastic marine gravel and wind deflation lag deposits along the Namibian coast. Modified from Spaggiari et al. (2006).

There is a systematic decrease in clast size northwards within the clastic marine gravel between the Orange River mouth and Lüderitz. Coarse cobble boulder-bearing gravel is present in the south, close to the river mouth, whereas finer pebble-bearing gravel predominates in pocket beaches in the north close to Bogenfels area (Bluck et al., 2005; Spaggiari et al., 2006; Bluck et al., 2007). Farther north at Lüderitz, the clast size becomes even smaller and occurs as granules. The size of diamonds also follows this trend with the smaller stones occurring at Lüderitz.

The aim of this chapter is to provide an overview of how the deposits, constituting the west coast placer, preserved in different environment settings (alluvial, marine and aeolian), are linked together.

2.2 Regional Geological Setting

The Orange River and its major tributary, the Vaal River, are the main bedrock confined rivers in a $\sim 10^6$ km² catchment in southern Africa (Garzanti et al., 2014). The geology exposed in the catchment is highly variable. In the east, geology comprises the Archaean Kaapvaal Craton (de Wit et al., 1992) (Fig. 2.3) intruded by Cretaceous and older diamondiferous kimberlites (de Wit, 1999; Shirey et al., 2001; Moore and Moore, 2004). The upper Orange River traverses rocks of the extensively eroded Permo-Carboniferous to Jurassic Karoo Supergroup (Visser, 1993; Johnson et al., 1997; Catuneanu et al., 1998, 2005; Key et al., 1998; Bangert et al., 1999). Between Noordoewer (300 km east of the Orange River mouth) and Oranjemund (Fig. 2.3), the lower Orange River cuts through the Mesoproterozoic Namaqua Metamorphic Complex (Thomas et al., 1994; Jacobs et al., 2008) before incising the Neoproterozoic Gariep Belt (Frimmel and Frank, 1998; Frimmel et al., 2004) close to the river mouth on the Atlantic Ocean coast.

The central part of southern Africa is marked by a low relief elevated central plateau (> 1000 m above mean sea level) whereas the coastal margins along the Indian and Atlantic Oceans are characterised by a high relief low elevation coastal plain (Knight and Grab, 2016a) (Fig. 2.4). The two are separated from each other by the Great Escarpment (Gallagher and Brown, 1999).

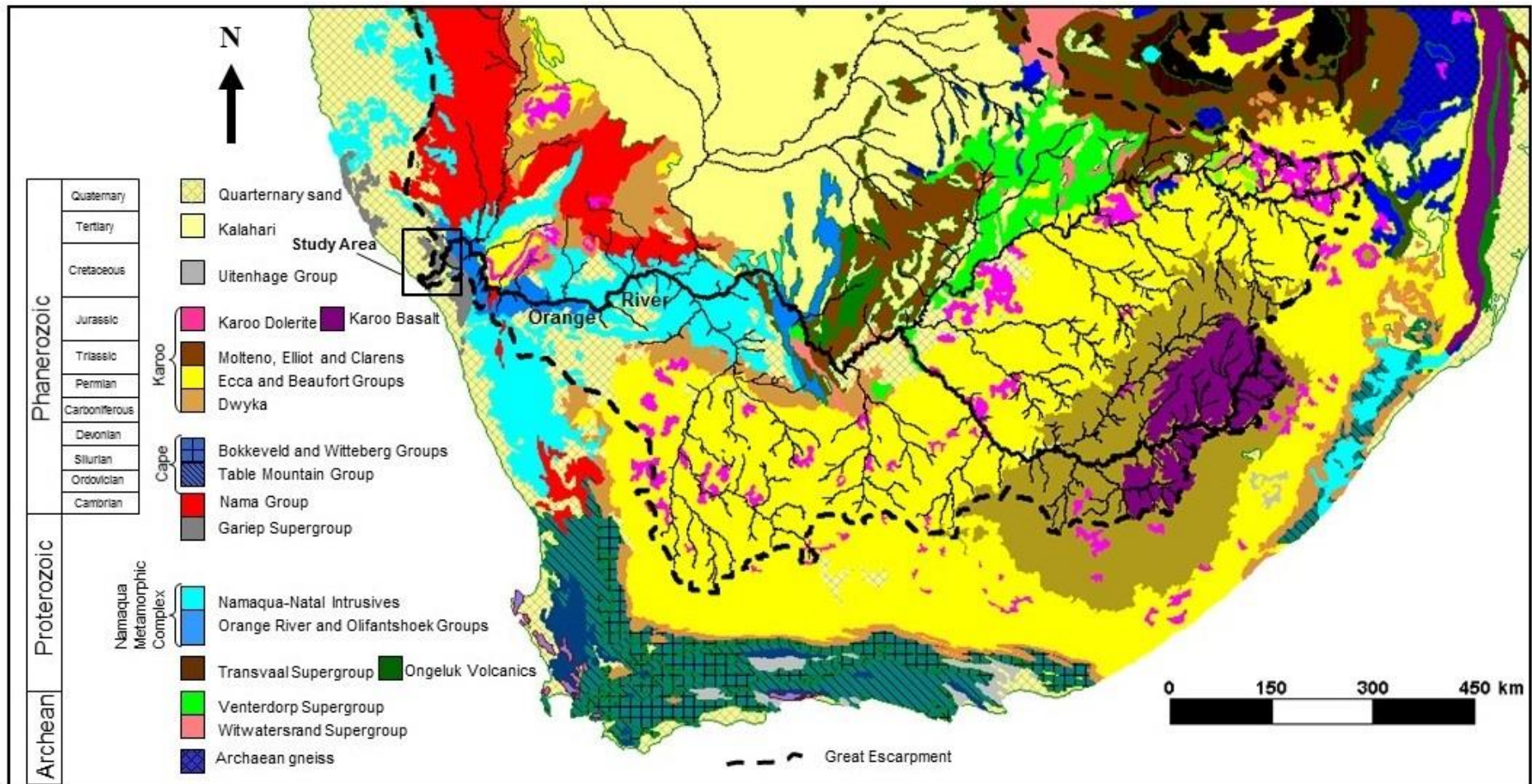


Figure 2.3. Geology of southern Africa. Adapted from Jacob (2005).

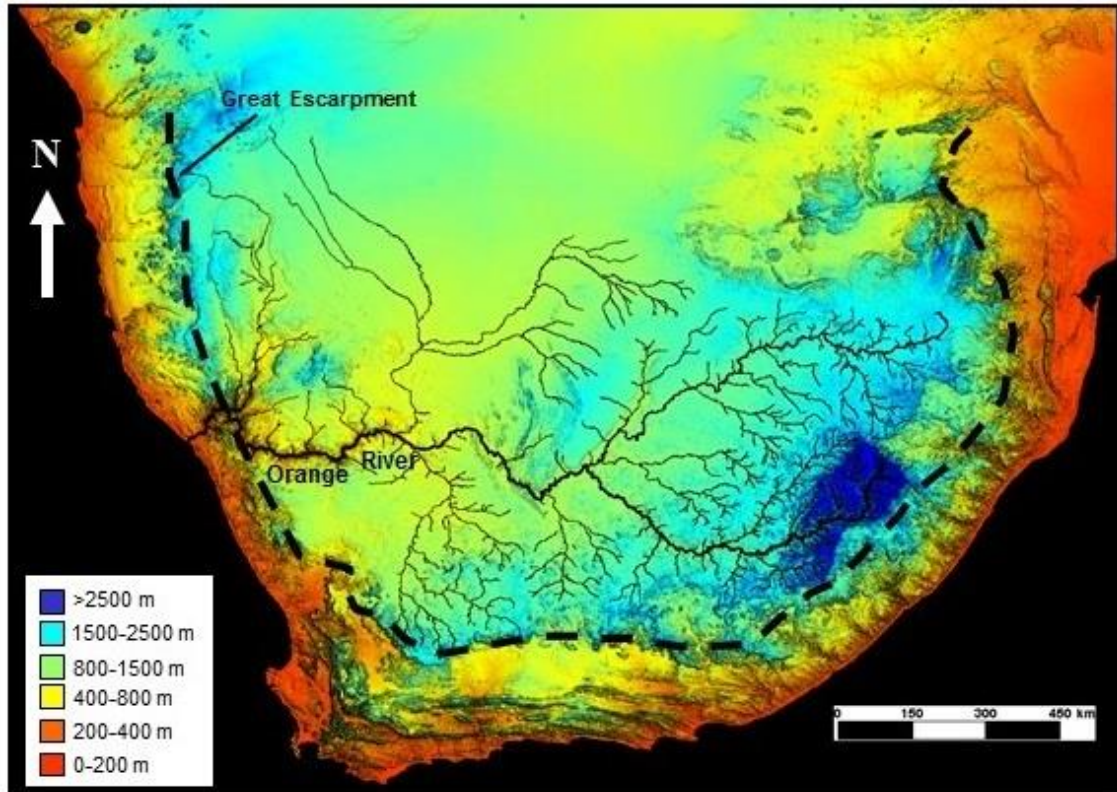


Figure 2.4. Elevation terrain of southern Africa. Note the elevated central plateau. Adapted from Jacob (2005).

2.3 Source of Diamonds

Although a general consensus exists with regard to the palaeo-Orange River being the main transport system that delivered diamonds from the interior of southern Africa to the west coast of Namibia (Jacob et al., 1999; Pether et al., 2000; Bluck et al., 2005; Jacob, 2005; Spaggiari et al., 2006), debate remains as to the provenance of the diamonds on the west coast. de Wit (1999) and Bluck et al. (2005), for example, have argued that the Namibian diamonds originated from erosion of Cretaceous post-Karoo Supergroup kimberlites within the palaeo-Orange River upstream catchment area in central South Africa and Lesotho (Fig. 2.4). However, others have argued for erosion of more proximal Permo-Carboniferous (~300 Ma) Dwyka Group glacial deposits of the inland Karoo Basin as the source (e.g., Sutherland, 1982; Van Wyk and Pienaar, 1986; Moore and

Moore, 2004). Advocates of the Dwyka Group as the diamond source invoke westward ice flow during the Dwyka glaciation coupled with the presence of kimberlitic and diamond indicator minerals such as pyrope garnet within glacial sediments (Bristow et al., 1989; Seggie et al., 1999; Moore and Moore, 2004). However, no single diamond has been recovered from Dwyka glacial sediments to date.

Phillips and Harris (2009) used $^{40}\text{Ar}/^{39}\text{Ar}$ dating technique to establish the age of clinopyroxene inclusions within Namibian diamonds and to reconstruct their provenance. The diamond sample population from which clinopyroxene inclusions were extracted was collected from the lower Orange River terrace deposits, beach placer deposits and the shallow marine offshore deposits with deflation deposits the only one not to be included in the $^{40}\text{Ar}/^{39}\text{Ar}$ dating study. Ages obtained for the majority of the clinopyroxene inclusions are younger (< 300 Ma) than the Dwyka Group glacial deposits constraining the provenance of the majority of the Namibian diamonds to post-Dwyka Group kimberlites as opposed to derivation from erosion of Dwyka Group glacial deposits (Phillips and Harris, 2009). In addition, a significant number of post-Dwyka kimberlites fall within the Orange River upstream catchment area (Shirey et al., 2001). Similarly, any contribution from the Kunene River that drains the Angolan kimberlites to the Namibian diamonds, has been ruled out by Garzanti et al. (2014, 2015) through their provenance study of coastal dune and beach sand between the Orange River mouth and southern Angola using bulk-petrography, heavy mineral data and zircon geochronology. As well the Atlantic Ocean currents, both longshore drift and other littoral currents all flow in a northerly direction (Diester-Haass et al., 1990; Diester-Haass et al., 2002; Monteiro et al., 2005; Bluck et al., 2007; Edelman-Furstenberg, 2014; Nagel et al., 2016) such that any possibility of material delivered to the Atlantic coast by the Kunene River to flow southwards appears unlikely.

Diamond stone size increases from old to young gravels with Eocene gravel showing a small average stone size of 0.2 carats/stone (Millad, 2004) and the Proto Orange River gravel deposits having a larger stone size of 1.1 to 1.3 cts/stn (Jacob et al., 1999). Pliocene to Holocene littoral beach gravel has an average

stone size of 1 to 0.5 cts/stn (Spaggiari et al., 2006). The increase of stone size from Eocene to younger gravels is not known. However, it could also be that the Eocene gravel consist of the top most crater facies diamonds; and continued erosion of the kimberlites through the Proto times exposed deeper parts of the kimberlites, possibly containing larger stones, which were exploited by the Meso Orange River.

2.4 Eocene gravel

Eocene clastic marine gravel is poorly preserved (Jacob, 2007). It occurs along the Namibian coast only in five known locations 6-10 km inland from the present coastline (Jacob, 2007). The most southern outcrop is located ~8 km from the modern Orange River mouth. The other four outcrops occur some 130 to 190 km north of the river mouth at Buntfeldschuh, Eisenkiesenklippenbake, Langetal Valley and Granitiberg. In the south, the Eocene shoreline crops out at lower elevations 3.8 m above mean sea level (amsl) compared to the northern outcrops (160-170 m amsl) (Stocken, 1978; Bluck et al., 2007). Such high elevations suggest that the Eocene shoreline was never drowned, and this might explain why it was poorly preserved given the extreme conditions of the Namib Desert. This agrees with the Miller et al. (2005) global sea level curve, which suggests that sea level fell by 70 to 100 m since the early Miocene.

At Buntfeldschuh, the Eocene basal marine succession sitting on bedrock is overlain by a thick aeolian sandstone (18 m) (Fig 2.5A) (Bluck et al., 2007). A ferricrete layer caps the sequence, which according to Miller (2008) is 6 m thick (Fig. 2.5A). The basal marine unit consist of a lower marine unit (~20 m) and an upper marine unit with an erosional contact between the two units (Miller, 2008). Both units comprise of sandstone, siltstone and pebble gravel lenses. The pebble gravel component is diamondiferous, but with significantly low diamond grade (Miller, 2008). Yellow chalcedony and agate that are the characteristic exotic clasts of Eocene gravel, as documented by Jacob (2005) and Miller (2008), dominate the gravel component (Fig. 2.5B). However, yellow chalcedony is notably scarce in the southern Eocene gravel outcrop. The abundance of shark

teeth in the upper marine unit at Buntfeldschuh proves a marine origin (Böhn, 1926). Dating of the shark teeth yielded a middle Eocene age (42 Ma) for the marine succession. The clay matrix (Fig. 2.5B) in the Eocene gravel further strengthen marine depositional environment.

The fact that the aeolian sandstone overlying the basal marine unit at Buntfeldschuh is thick would mean that the Eocene transgression or high stand, was followed by a prolonged low sea level stand or regression during which beach sand was exposed and thus available to reworking by wind. This hypothesis correlates with the major Oligocene to middle Miocene regression proposed by Siesser and Dingle (1981) for southern Africa, which they inferred lasted for a period of 20 Myr. The magnitude and duration of Oligocene to Miocene regression proposed by Siesser and Dingle (1981) is much greater than the global curve (Miller et al. (2005), which if correct suggests a tectonic component to the relative sea level change.

2.5 Lower Orange River gravel terraces

Along the lower Orange River, gravel terrace deposits occur next to the modern Orange River on both the Namibian side and South African side of the river.

2.6 Marine gravel beaches

In the majority of locations, the raised beach gravel sits on top of the Gariep Belt rocks dominated by schist (Jacob et al., 2006). The only exception is 10 km north of the modern Orange River mouth where the bedrock is fluvial sandstone (Fig. 2.6A) at 1 m above sea level. The sandstone represents the northern bank of the palaeo-Orange River. The deposition of the marine beach gravel on top of fluvial sandstone is a classic example of transgression (Pirazzoli, 1996), which saw the landward migration of the shoreline.

The bedrock overlain by marine gravel is cut by sub-parallel gullies perpendicular to the coast. In some places, the gullies are uniformly spaced (Fig. 2.7A). The average depth of the gullies is 2 m deep (Fig. 2.7B). The process that formed the gullies is not well understood. However, formation by merging of potholes (Wright, 1964) and exploitation of weakness in rocks such as joints have been proposed (Jacob et al., 2006). Other marine related gravel deposits preserved 20 km north of the river mouth include back barrier deposits, front barrier deposits and lagoon deposits.

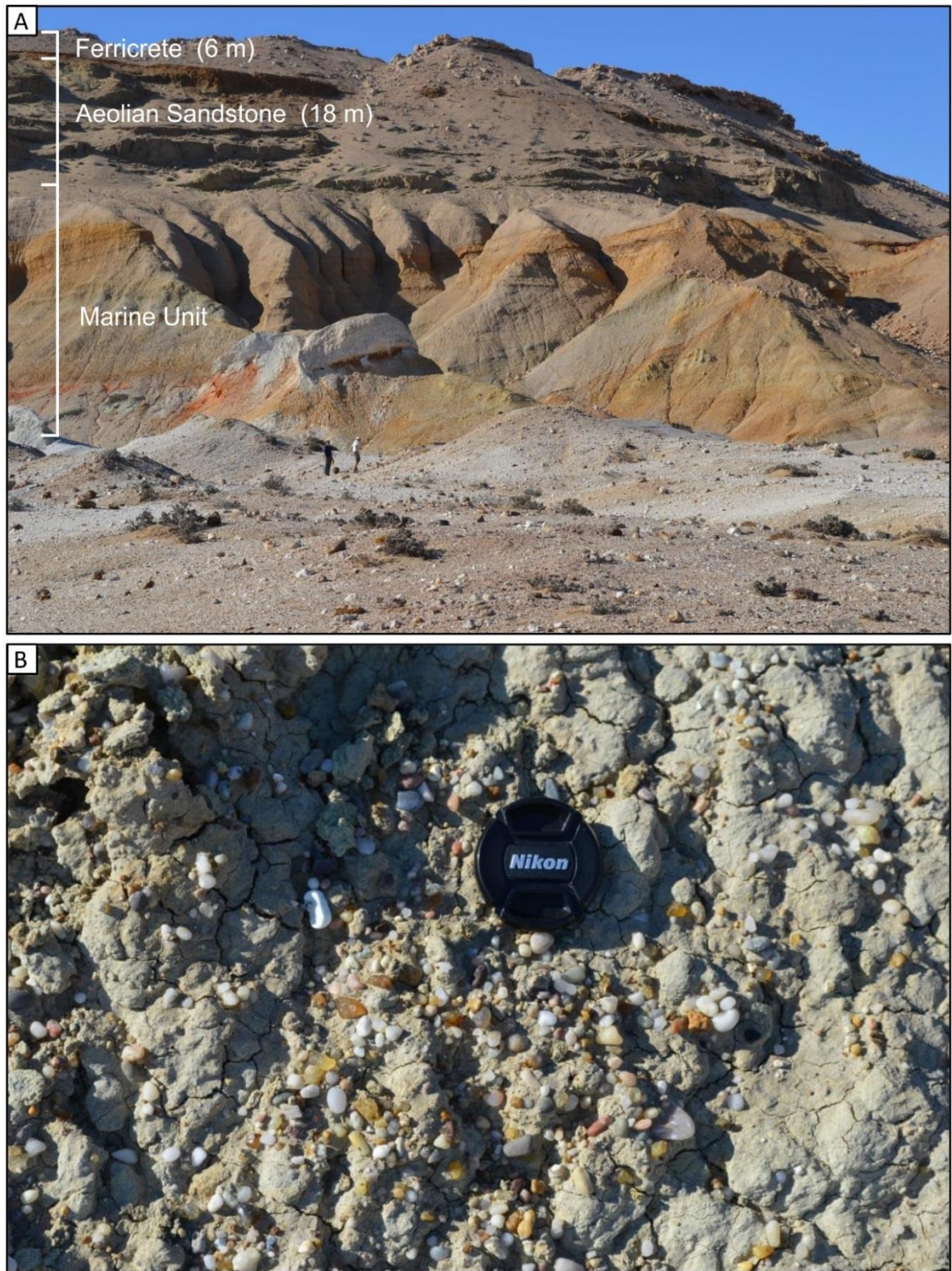


Figure 2.5 (A) Basal Eocene marine succession overlain by a thick aeolian layer, Buntfeldschuh. The sequence is capped by ferricrete. Thickness for aeolian sandstone and ferricrete from Bluck et al. (2007) and Miller (2008), respectively. (B) Clay matrix of the marine gravel. Honey-yellow pebbles are chalcedony. For scale camera lens is 52 mm in diameter.



Figure 2.6 (A) In situ fluvial sandstone bedrock, Mining Area 1 about 10 km north of Orange River mouth. (B) Post mining view of East Cliff where the F-Beach was stacked. The broken white line represents the top surface of F-Beach.

2.6.1 Raised beaches

The raised beaches occur as a series of stacked beaches, which are locally referred to as, from young to old, A, B, C, D, E and F beaches and represent a succession of transgression events (Stocken, 1978). According to Stocken (1978) the beaches are separated from each other by regression events. The average elevation of the oldest beach (F) is 20 - 30 m above mean sea level. At East Cliff (Latitude 0603084, Longitude 6871379), the F-Beach gravel was stacked next to a cliff and reached the same height as the top of the cliff (Fig. 2.6B). No satisfactory age exists for the stacked beaches. However, the youngest beaches (A, B and C) have been dated using C¹⁴ radiometric dating of shells, but only the A-Beach yielded a reasonable age of 5,150 ± 45 years (Stocken, 1978). The ages obtained for the B and C-beaches are inconclusive (Stocken, 1978). The older beaches (D, E and F) are possibly late Pliocene to early Pleistocene based on the presence of *Donax rogersi* fossil (Pether, 1986).

2.6.2 Back barrier, front barrier and lagoon deposits

Front barrier (foreshore) gravel deposits are concentrated within 10 km of the river mouth. The foreshore gravels show a fining upward sequence. In places the gravel is made up of a series of repeating sequences (Fig. 2.8A). Each sequence terminates with a blinding fabric gravel that is solely made up of small pebbles with no sand (Fig. 2.8B). Blinding fabric gravel also occurs in a palaeo fan delta environment located less than 15 km east of the foreshore gravel. Some of the foreshore gravels consists of rip up clay balls (Fig. 2.9A) possibly sourced from lagoonal clay during a transgression period. The clay possibly formed during a regression period but subsequent transgression, that deposited the gravel containing the clay balls, drowned the lagoon.

The back barrier (wash over) sediments are distinguished on the basis of their lack of foresets, which is typical of wash over sediments although foresets have been reported in washover sand deposits (Forbes et al., 1982). These deposits are made up of poorly consolidated gravel layers alternating with sand layers (Fig. 2.9B). The abundance of sand in the wash over sediments is reflected by

the thick sand layers that suggest a protected barrier beach because a beach environment exposed to wave action would lose most of the sand. Bioturbation preserved in the sand layers (Fig. 2.9B) support a protected environment.



Figure 2.7 (A) A series of east-west orientated bedrock gullies, exposed after mining. The average depth and width of the gullies at this location is 1.8 m and 2.1 m, respectively. (B) A 2.3 m wide gully exposed after mining. Pictures taken looking west, Mining Area 1.

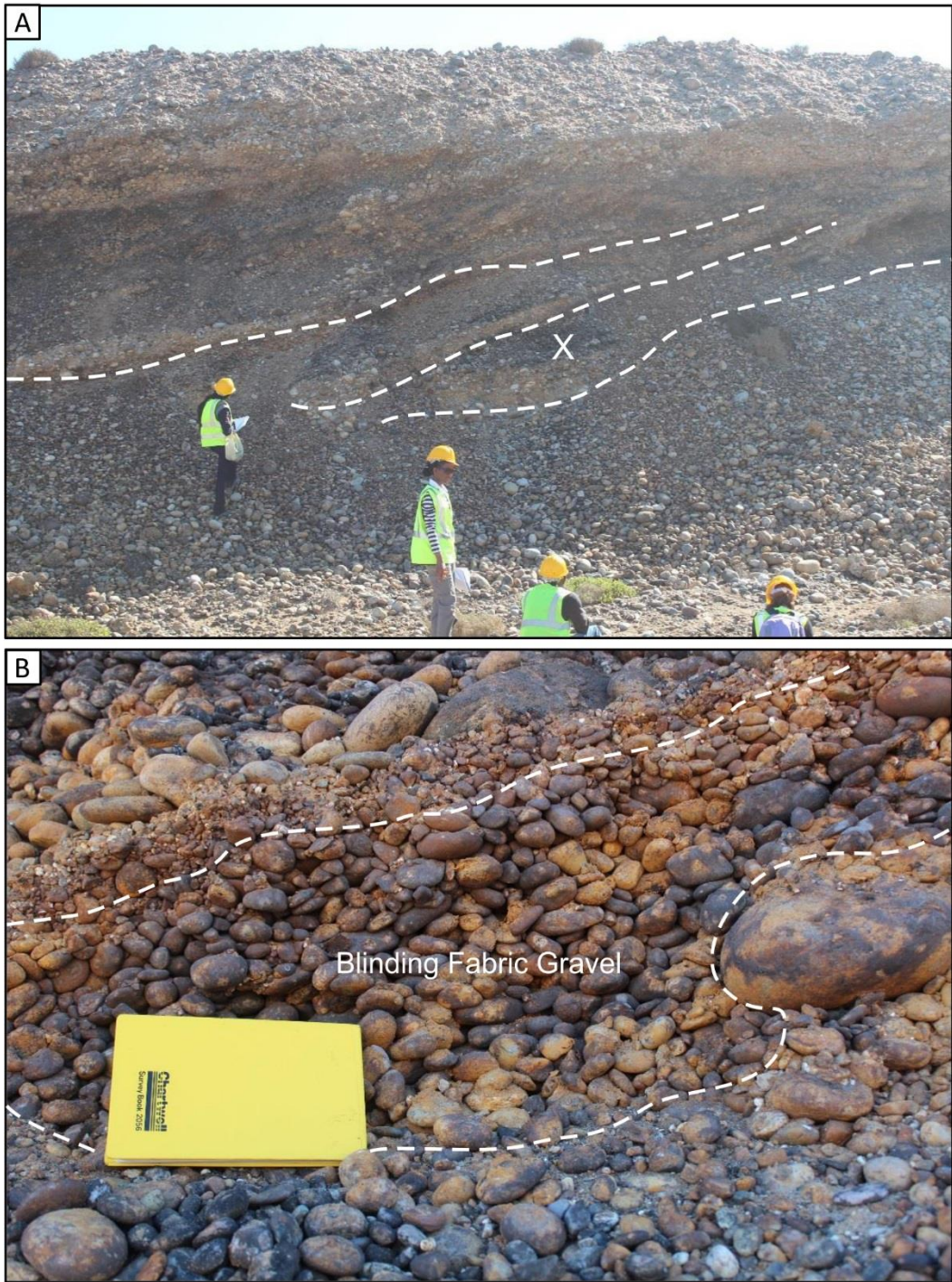


Figure 2.8 (A) Clastic coarse barrier beach gravel with series of repeating sequences (highlighted by broken white line) that terminates in blinding fabric gravel. (B) Close up of blinding fabric gravel, position X in Picture A. Pictures taken looking northeast.

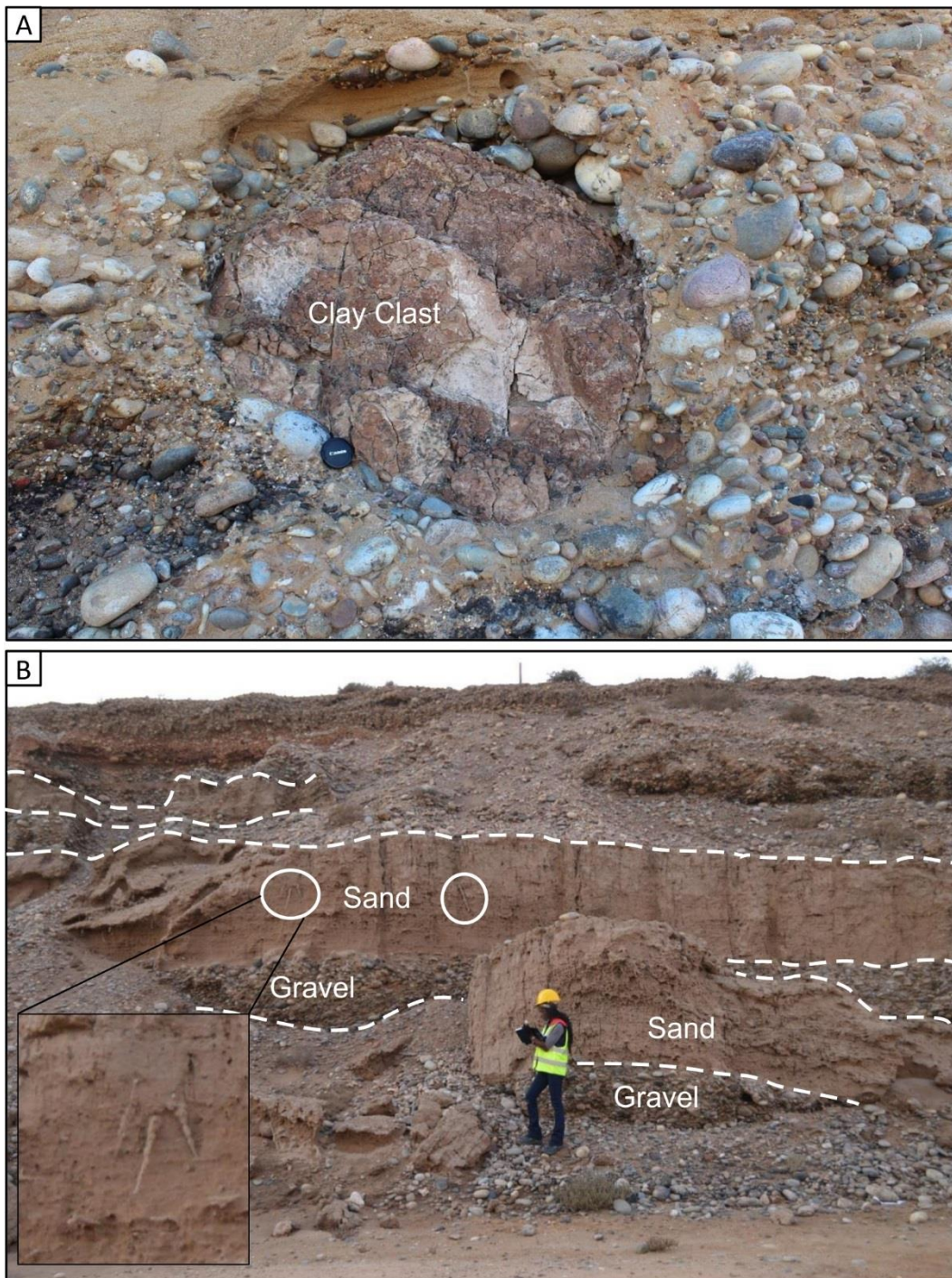


Figure 2.9 (A) Clay rip-up clast in front barrier beach gravels. Camera lens cover for scale. (B) Back barrier beach deposits with alternating sand and poorly consolidated gravel layers. Note bioturbation in sand layers (white circles).

2.6.3 Shallow Marine Atlantic 1 gravels

The Atlantic 1 terrigenous gravels represent the offshore extension of the beach gravels in a shallow marine setting (up to 153 m water depth). These gravels also carry Orange River-derived exotic clasts. Rogers and Li (2002) noted that the Atlantic 1 gravels show a fining upward sequence synonymous with transgression where the basal coarse gravels were originally deposited in a high energy foreshore and surf-zone environments. A lot of uncertainties exist regarding the distribution of Proto-age and Meso-age gravels in Atlantic 1. The current depositional model of the Atlantic gravels (Gray, 2006) assumes that there is no mixing between the Proto-age and Meso-age. However, this is considered highly improbable given the dynamic environment coupled with major sea-level fluctuations that would have exposed wide areas of the shelf. Therefore, some mixing and reworking is likely.

2.7 Deflation deposits

Deflation lag deposits occur farther north in the vicinity of the four northern Eocene shoreline gravel outcrops. The abundance of agate and yellow chalcedony in the Eocene gravel and deflation deposits (Jacob, 2005; Miller, 2008) provides a strong link between the two (Fig. 2.10). Weathering conditions under arid climate in the Namib Desert are extreme (fog and wind), which perhaps facilitated the weathering of the Eocene gravel to form deflation deposits. Conditions are very extreme such that most rocks are completely weathered and only a lag of vein quartz remains as a surface layer (Fig. 2.11A). Wind flute marks on dolomite rock surface (Fig. 2.11B) attest to persistent strong winds.

Although the Eocene gravel originally exhibit low diamond grades, continuous reworking by wind processes has upgraded the gravel to form deflation deposits. The majority of the sand released from original Eocene gravel is transported in mobile sand dunes that form part of the Namib sand sea (Corbett, 1993; Corbett, 1996). The dunes can reach heights of 10 m or more (Garzanti et al., 2014) to a maximum of 50-150 m high (Lancaster, 1981). Using trace element geochemistry Garzanti et al. (2015) proved that the majority of the sand making up the dune

sand is terrigenous, which has been delivered to the coast by the Orange River. Some of this Orange River sand has travelled as far as southern Angola, where it forms part of the Moçâmedes Desert sand dunes, a distance of 1750 km northward of the Orange River mouth (Garzanti et al., 2014).

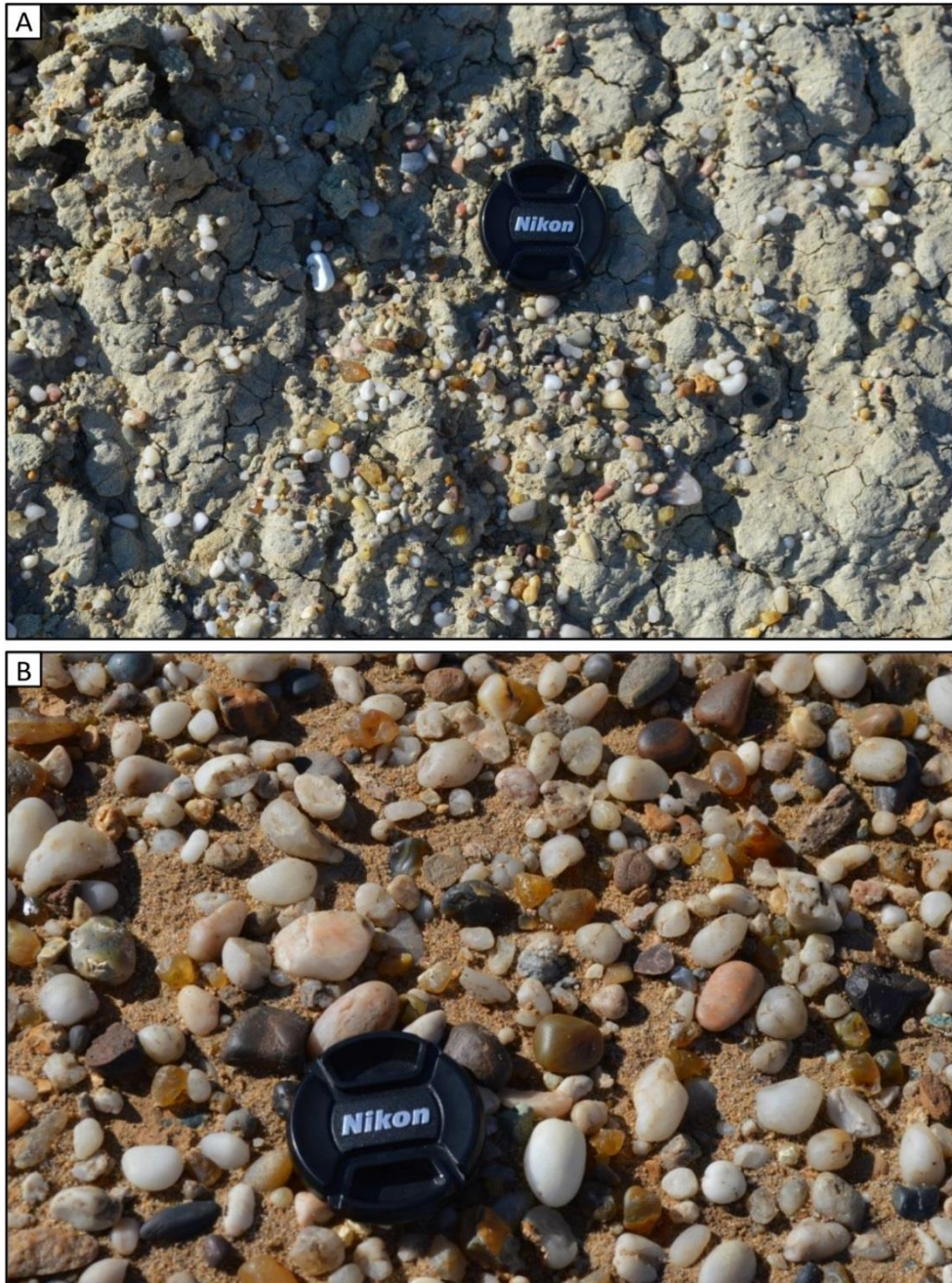


Figure 2.10 Chalcedony (honey-yellow) and agate pebbles in (A) insitu Eocene gravel and (B) deflation deposit at Buntfeldschuh. For scale camera lens is 52 mm in diameter.

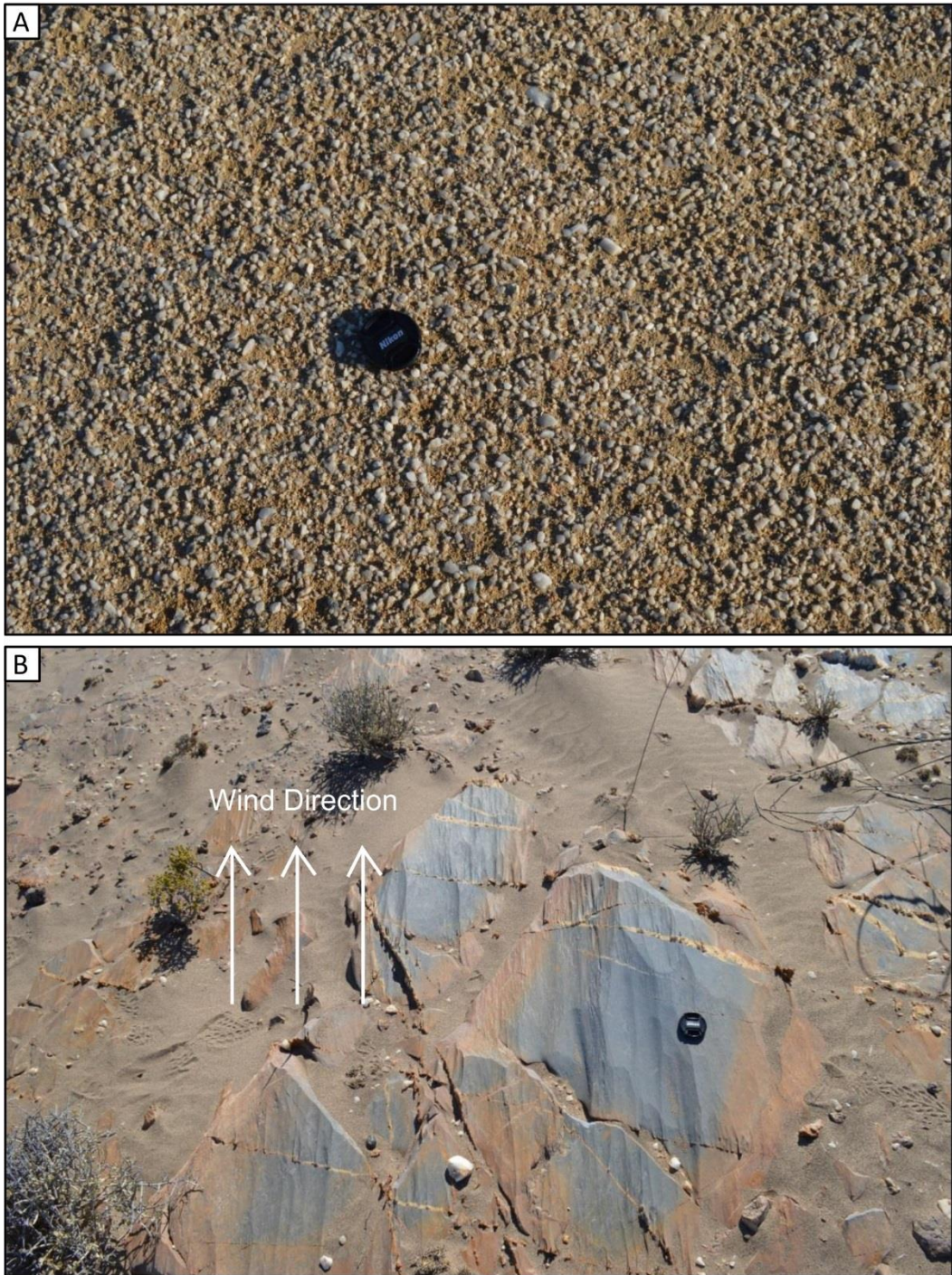


Figure 2.11 (A) Deflation lag of vein quartz after the country rock has been completely weathered, Chameis, Sperrgebiet. (B) Wind formed flutes on dolomite rock surface. Northward wind direction is denoted by arrows. Picture B taken looking north. For scale camera lens is 52 mm in diameter.

2.8 Significance and application of heavy mineral analysis to the reconstruction of palaeo-environments

Heavy mineral assemblage, geochemistry and geochronology (e.g. zircon U-Pb dating) have been used in the reconstruction of palaeo-environments in fluvial, shoreline and shallow-marine settings (Bateman and Catt, 2007; Fleming et al., 2016). Dill (1995) reconstructed the propagation of an alluvial fan on the basis of changes in the assemblage of heavy minerals. Heavy mineral analysis was used by Chen et al. (2009) to establish the timing of the linkage of the Yangtze River to the Yangtze coast, and by Yue et al. (2018) to reconstruct the palaeogeomorphological evolution of the Yangtze Delta. The strengths of heavy mineral applications is that they are chemically more resistant to weathering and may survive multiple phases of post deposition weathering (Hassan, 1976; Morton, 1984; Morton, 1991; Goodbred et al., 2014) in comparison to sediment clasts and light, chemically unstable minerals, such as feldspar. However, the relatively high density of heavy minerals may restrict the degree of transport, and influence accumulation in different sedimentary environments (Komar and Wang, 1984; Komar, 2007).

Isotope geochemistry and detrital geochronology are alternative techniques that can be used in combination with heavy mineral analysis (Jiang et al., 2015; Garzanti, 2016; Morton et al., 2016; Zimmermann and Hall, 2016) in tracing the evolution of fluvial, shoreline and shallow-marine settings. Another complimentary method is optically stimulated luminescence (OSL) of naturally irradiated quartz and potassium feldspar grains (Ballarini et al., 2007; do Nascimento et al., 2015; Rhodes, 2015), which has been used on offshore sands (Mellett et al., 2013), alluvial sediments (Roskosch et al., 2012) and lake sediments (Kadereit et al., 2012; Mischke et al., 2017), although the availability of feldspar in humid wet climate regions may be limited. Also, the OSL component of some quartz or feldspar grains may not be completely reset at the time of burial resulting in overestimation of sediment ages (Ballarini et al., 2007; Chamberlain et al., 2017), and dating is limited to Quaternary sediments that are younger than 1 Ma (Watanuki et al., 2005; Rhodes, 2015). Chamberlain et al. (2017) highlight another limitation of luminescence dating to delta sediments which is the

unsuitable luminescence characteristics of quartz including acceptable sensitivity synonymous with rapid deposition of young clastic sediments such as the Ganges-Brahmaputra-Meghna Delta.

Similarly, radiocarbon dating is only applicable to young sediments of Quaternary age (< 1 Ma). In addition, reworked fluvial organic matter can result in overestimation of sediment ages under the radio carbon dating method (Howarth et al., 2013).

Geochronology dating methods that are suitable for sediments older than 1 Ma years include U-Pb dating of zircon and detrital apatite and zircon fission track. U-Pb method can establish the maximum deposition age of sediments as old as Archean such as the Witwatersrand Supergroup (Robb et al., 1990). The relative abundance of zircon in clastic sedimentary rocks and sediments make U-Pb dating method conducive for reconstruction of palaeo-environments in fluvial, shoreline and shallow-marine settings (Nelson, 2001). However, the limitations of the U-Pb dating of clastic sedimentary rocks is that the accuracy of determining the maximum deposition age is influenced by the variety of the lithologies making up the sediments with sedimentary rocks/sediments that have multiple provenance providing the most accurate age estimate (Nelson, 2001).

The fission track method has been used in deducing erosion rates and palaeogeomorphology (Tinker et al., 2008b) including that of Cretaceous sediments (Barbarand et al., 2013). This provides the age of annealing for zircon and apatite grains, and therefore not the depositional age. Although maximum age can be useful in areas of rapid exhumation, in the case of Namibia the period of rapid exhumation was primarily in the Cretaceous.

In summary, a heavy mineral approach was considered the most appropriate technique to aim correlation between fluvial and marine deposits in this instance because the Orange River gravels and Atlantic 1 gravels are older than Quaternary ruling out the use of OSL dating and radiocarbon dating. Alternative techniques such as fission track thermochronology and detrital zircon could be used

in the future in concert with the heavy mineral assemblages. Finally, the use of heavy mineral assemblage and their chemical composition is a cost effective technique that can be used in mining operations, and is a complimentary technique to traditional clast assemblage analysis of gravels.

Chapter 3 Analytical Procedures

3.1 Previous Work

Jacob (2005) mapped and characterised the lower Orange River gravel terraces (between Noordoewer and the Orange River mouth) into two distinct fining-upward gravel terrace deposits, primarily based on mapped stratigraphic relationships (cross-cutting relationships) and strath and terrace top elevations, and secondarily according to the proportion of exotic clasts. The terrace deposits were named Proto Orange River deposits and Meso Orange River deposits. The palaeo-river courses of the Proto Orange River and the Meso Orange River were mapped during the same study. However no parallel study was undertaken on the offshore sediments.

Most of the Orange River clast assemblage data, has been adapted from Jacob (2005). In that study, heavy mineral samples were co-collected with the clast populations, and this sample suite has underpinned the current study of the relationship between clast analysis and heavy mineral distribution which is a major component of the current project. In addition, replicate sampling for clasts was undertaken at two localities to ensure compatibility of data generated by the two studies.

The present study has developed the original work of Jacob (2005) in two distinct ways. Firstly, the characterisation of heavy mineral concentrates from the same localities as the clast samples has permitted correlation of these data sets to further enhance our understanding of the evolution of the fluvial system. Secondly, the project is the first to gain heavy mineral concentrates from the marine setting through systematic sampling of offshore sediments. These new data sets have been considered in the context of the fluvial heavy mineral suite to interpret the temporal influence of terrestrial sediments on the evolution of the marine facies.

3.2 Clast Analysis

The clast assemblage data of the Orange River deposits from Jacob (2005) study is adapted in this study. In this study, three further samples were collected and the clast assemblage determined (Table 3.1). To standardise the sampling procedure, clast assemblage analysis conducted during this study was based on the same sampling method as the one of Jacob (2005). It was not possible to do a clast assemblage on the Atlantic 1 gravels during this study due to security protocols that preclude handling of diamondiferous material.

After excavation, the gravel was screened on site through stacked sieves splitting the clasts into +40 mm, +25 mm, +16 mm, +8 mm and +4 mm. The clasts were split further with a sample splitter until the desired number of clasts was attained. The less than 3 mm size fraction was bagged for heavy mineral analysis. A minimum of 50 clasts were inspected in the +40 mm and +25 mm size fractions (Table 3.1). A minimum of 100 clasts were analysed for the small size fractions (+16 mm, +8 mm and +4 mm). Some samples contained a large number of clasts in the small size range and the population was split by coning and quartering to provide a suitable population for analysis. The total number of clasts analysed per size fraction per sample is summarised in Table 3.1. Lithology, clast shape and clast roundness were recorded for each individual clast. Clast roundness, which is a reflection of distance travelled and lithology durability, was visually estimated using the roundness chart of Powers (1953).

Table 3.1 Total number of clasts analysed per size fraction for Orange River samples, this study.

Deposit Type	Pre-Proto Orange River Deposit		Meso Orange River Deposit
Deposit Name	Daberas	Sendelingsdrif	Sendelingsdrif
Sample Name	Daberas Zone 13	Sendelingsdrif Zone 7	Sendelingsdrif Zone 7 Meso
+40 mm	51	51	50
+25 mm	69	57	62
+16 mm	104	82	117
+8 mm	145	164	107
+4 mm	105	104	135

3.3 Determination of heavy mineral proportions

3.3.1 Sample Collection

The majority of the Orange River samples (both clast and sand samples) were collected by Jacob (2005) as described in section 3.1.

The majority of the clast assemblage data used in this study is adapted from Jacob (2005) therefore the samples for the heavy mineral analysis needed to be collected from the same samples from which the clast assemblage was done. For the Atlantic 1 samples, heavy mineral samples were collected from the less than 3 mm size fraction which is the same size range as the Orange River sample analysed for heavy minerals.

3.3.1.1 Orange River samples

Heavy minerals were recovered from -3 mm sand samples. These sand samples were collected at the same time as the clast analysis samples described in Section 3.1. Of the 26 samples analysed for heavy mineral assemblage in this study, 25 samples have been collected by Jacob (2005) during his PhD study

while the remaining sample (Sendelingsdrif Zone 7 Meso) was collected during this study. For comparison purposes, two modern Orange River samples from Sendelingsdrif and Auchas Major deposits were analysed for heavy mineral assemblage.

3.3.1.2 Atlantic 1

Sampling on the sea bed poses challenges. Grab samples is a common method used to sampling unconsolidated seabed sediments (e.g., Cascalho and Fradique, 2007). Sampling in Atlantic 1 was undertaken by the MV Mafuta mining vessel. A total of 28 samples were collected. During mining, the gravel is extracted from the sea floor by a remote controlled crawler and conveyed onto the vessel via an umbilical pipe. On the vessel, the gravel is split into four equivalent process streams (Fig. 3.1). Each stream is screened into different size fractions. The undersize -3 mm size fraction or slimes are directed to a pipe which feeds the Additional Minerals Plant holding cyclone (Fig. 3.1). The Additional Minerals Plant is designed specifically for recovering gold and platinum grains. The samples used in this study were collected from the end of the pipe feeding into the Additional Minerals Plant holding cyclone (Fig. 3.1). Samples were collected by holding a bucket over the cyclone-feeding pipe and placed into porous cotton bags. The samples were then partially dried on the vessel before shipment to the Oranjemund facility where they were fully dried and weighed. The sample location coordinates were provided by the Debeers Marine Survey team.

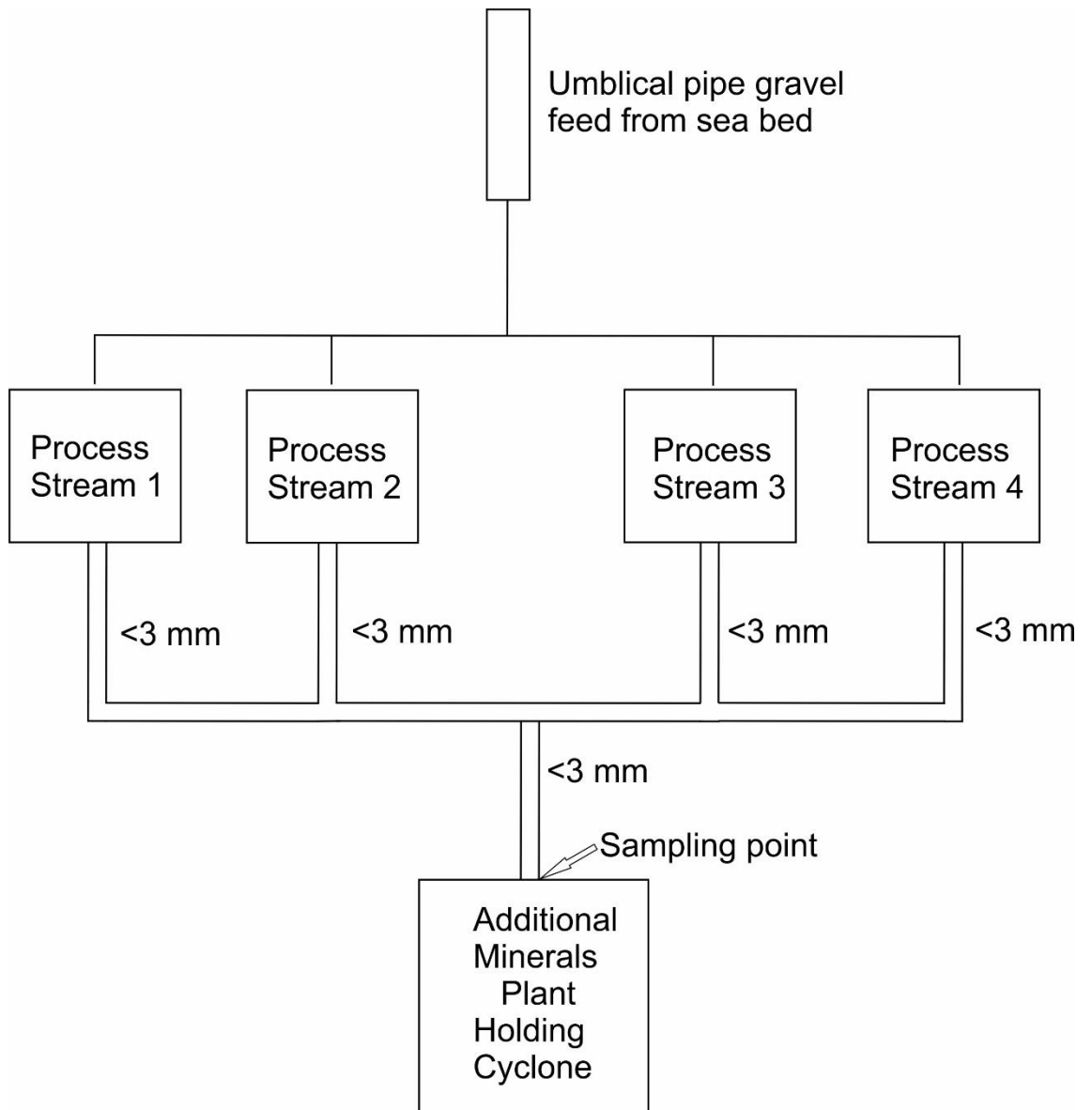


Figure 3.1 Flow sheet of gravel processing on the MV Mafuta mining vessel. Sample collection point indicated by arrow.

3.3.2 Sieving

Gravity separation machines are most efficient when the feed is pre-classified. Consequently each sample was sieved into 2-3 mm, 1-2 mm, 0.5-1 mm, 0.25-0.5 mm, 0.125-0.25 mm, 0.063-0.125 mm and <0.063 mm size fractions prior to processing on the gravity separation Mineral Processing Table. In addition, consideration of size fractions permits identification of size ranges of specific heavy minerals. Each sample was sieved for a period of 10 minutes using an automatic electrical sieve shaker.

3.3.3 Bulk Sediment Geochemistry

To get an indication of possible heavy minerals present in the samples bulk sediment geochemistry was conducted on selected size fractions prior to doing heavy mineral assemblage analysis. Selected size fractions (0.25-0.5 mm, 0.125-0.25 mm, 0.063-0.125 mm and <0.063 mm) were analysed for bulk sediment chemistry using an Innovex X-5000 X-ray Fluorescence (XRF) machine. A machine calibration check followed by analysis of two stream sediments standards were conducted prior to analysis of the samples at the start of each analytical day.

3.3.3.1 XRF Machine Analytical Accuracy

Selected Orange River and Atlantic 1 samples were analysed for repeat analysis. For the Orange River samples, there is a strong positive correlation between the first analysis and repeat analysis for both major (Fe, $R^2 = 0.9795 - 0.9992$) and minor elements (Mn, $R^2 = 0.9522 - 0.9987$) (Figs. 3.2, 3.3).

For the marine samples, the XRF machine is more accurate for the elements that are in high concentration. However, the accuracy is low for elements in trace amounts particularly for the 0.125-0.250 mm size fraction. Ca, for example, being high in concentration shows a good positive correlation between the first and repeat analysis (Ca, $R^2 = 0.9846 - 0.999$) (Fig. 3.4). However, Mn shows no correlation between the first and repeat analysis in the 0.25-0.50 mm size fraction

(Mn, $R^2 = 0.0307$) (Fig 3.5A) but shows a positive correlation for the finer size fraction (Ca, $R^2 = 0.8648 - 0.9925$) (Fig. 3.5B, C, D).

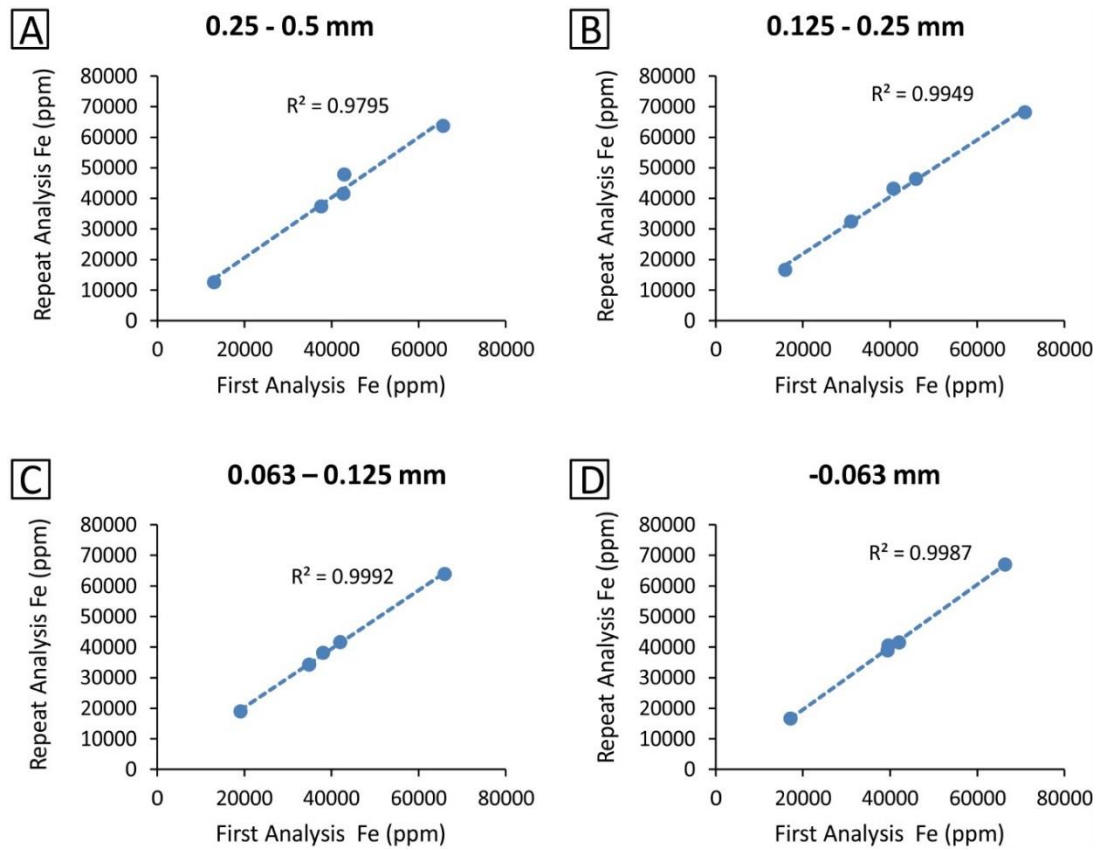


Figure 3.2. Comparison of Fe content between first and repeat XRF analyses, Orange River samples.

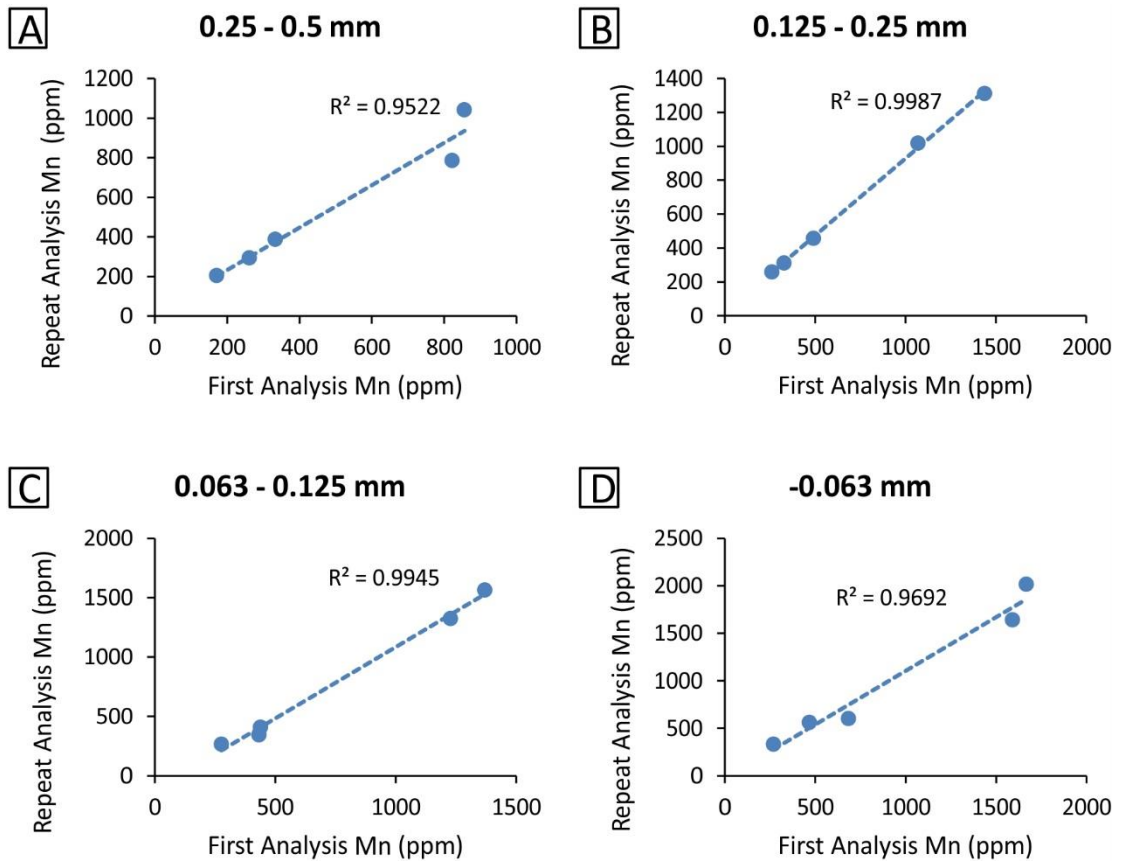


Figure 3.3 Comparison of Mn content between first and repeat XRF analyses, Orange River samples.

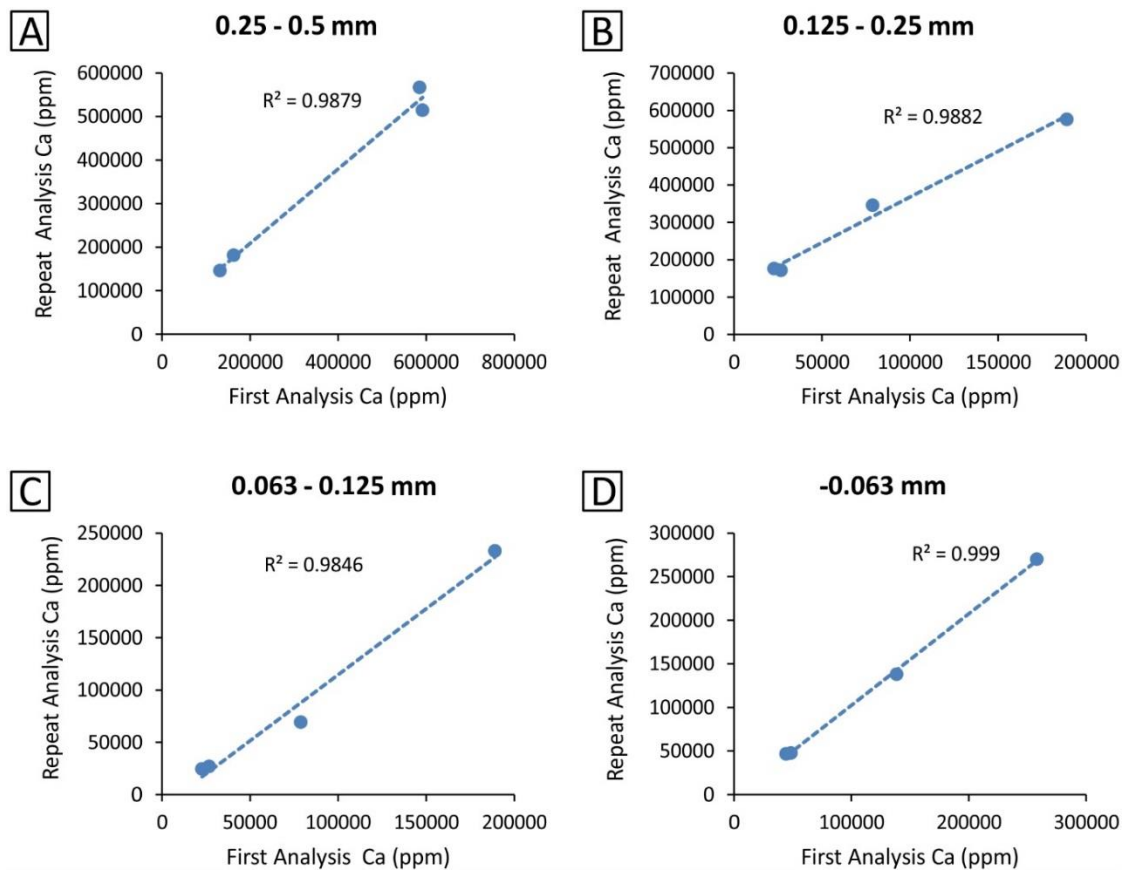


Figure 3.4 Comparison of Ca content between first and repeat XRF analyses, Atlantic 1 samples.

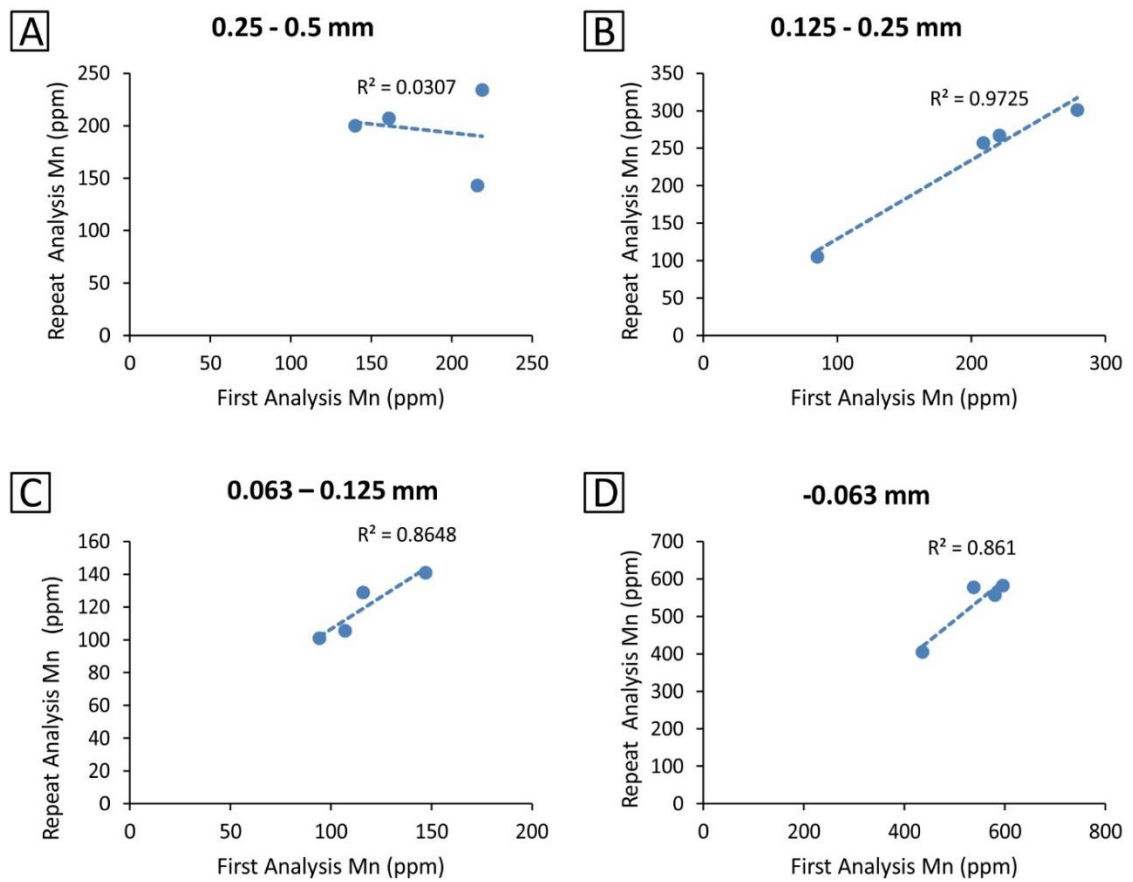


Figure 3.5 Comparison of Mn content between first and repeat XRF analyses, Atlantic 1 samples.

3.3.4 Gravity Settling Table

Several methods that utilise density separation have been used for separation of heavy minerals from light minerals in sediments or crushed hard rocks. These include shaking tables (Olivarius et al., 2011) and heavy liquids (e.g., Komar and Wang, 1984; Dunlevey and August, 2010; Garzanti et al., 2014). The use of heavy liquids has become less widespread in recent years due to the toxic nature of the heavy liquids. In this study heavy minerals were separated from sediment samples by using the Laboratory Minerals Separator manufactured by Metsolve, Vancouver.

After the sieved size fraction were analysed on the XRF machine for bulk sample geochemistry, the samples were processed on a gravity settling shaking table. Heavy minerals were separated from the rest of the sieved sample material using

a Met-Solve Analytical Table, a gravity settling shaking table, producing a heavy mineral concentrate (Fig. 3.6). Only the 1-2 mm, 0.5-1 mm and 0.25-0.50 mm size fractions were processed on the gravity settling table for heavy mineral recovery. Initial results has indicated that the 2-3 mm size range does not contain any heavy minerals because no single heavy mineral was recovered from processing of this size fraction of a Sendelingsdrif Pre-Proto sample. The selected size fractions (1-2 mm, 0.5-1 mm and 0.25-0.50 mm) were processed at 1° slope angle, 1.5 litres/minute water flow rate and 60 strokes/minute rocking speed. The 1-2 mm size fraction was also processed at a slope angle of 1°, as opposed to the manufacturer recommended steeper angle of 2° (Table 3.2) because even a slope angle of 1.5° is too steep to effect the separation of garnets, the dominant heavy mineral in this size fraction, from the light grains. At 1.5° garnet grains rolled off the table together with the light minerals.

Samples were processed by feeding small wet portions at a time onto the table deck. When a heavy mineral concentrate was visible on the table deck (Figs. 3.7, 3.8) after the first feed the table was turned off. The light minerals were guided off the table into the tailings drainage pipe using a small spray pipe that is attached on the side of the table (denoted by B in Fig 3.6). The heavy mineral concentrate was guided to the top end of the table with a spray pipe. In order to avoid loss of lower specific density heavy minerals, such as amphiboles, to tailings a small band of light minerals was also guided to the top of the table together with the heavy mineral concentrate. The second feed was introduced just downslope of the heavy mineral concentrate-sand mixture from the first feed. This process was repeated until the last feed of the sample. After the last feed of the sample had gone through, the heavy mineral concentrate was sucked up with a plastic bottle and then transferred into glass vials. After the concentrate has been recovered, the table deck was cleaned with a spray water pipe. To get rid of any remaining grains the table was run for 20 seconds at a high water flow rate of 2.5 litres per minute. After the table was purged for 20 seconds, the tailings pipe was cleaned by pouring water three times down the tailings pipe with a one litre jug. This ensured that no material were carried over to the next sample. The sample tailings were then recovered from the sedimentation tank by lifting a

tailings capturing small tub out of the main sedimentation tank (denoted by F in Fig 3.6). Tailings were placed in the same Ziploc plastic bag pre-table processing. Heavy mineral concentrates were dried and weighed.

Table 3.2 Manufacturers recommended operating parameters for the Mineral Processing Table.

Size Fraction (mm)	Slope (°)	Speed (Strokes/min)	Water Flow (Litres/min)	Deck Shape
0.106 - 0.15	1.5	80	3.5	Flat
0.150 - 0.212	1.5	80	3.5	Flat
0.212 - 0.300	2	60	1.5	V-Shape
0.300 - 0.425	2	60	1.5	V-Shape
0.425 - 0.600	2	60	1.5	V-Shape
0.600 - 0.850	2	60	1.5	V-Shape
0.850 - 1.170	2	50	1.5	V-Shape
1.170 - 1.700	2	50	1.5	V-Shape



Figure 3.6 Laboratory Mineral separator. A = water inlet (light blue), B = spray pipe (dark blue), C = sample feed point, D = tailings outlet, E = tailings pipe (green), F = sedimentation tank (white).

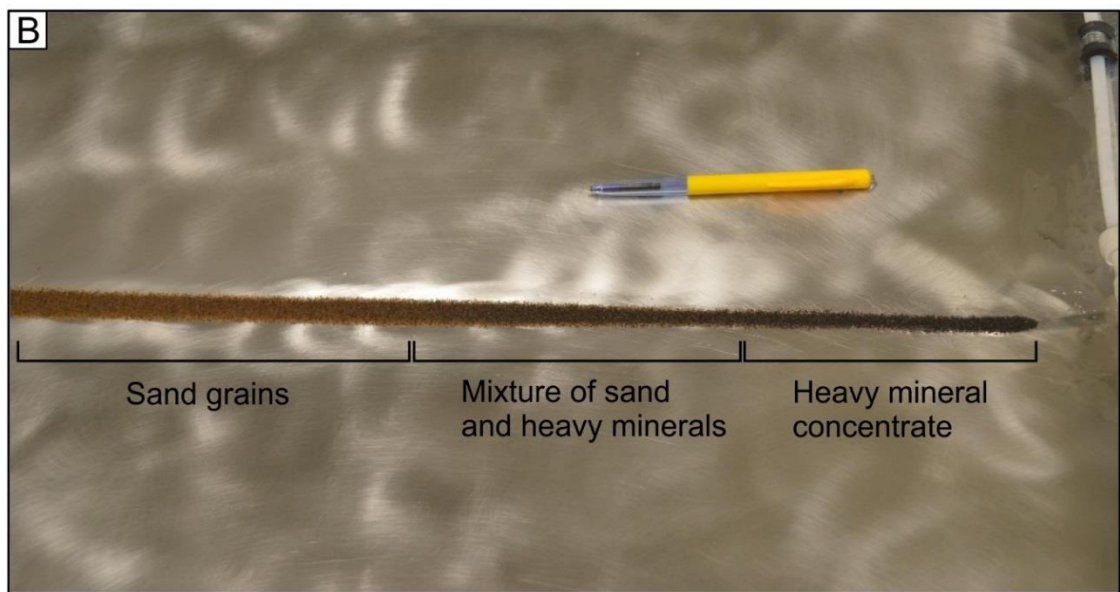
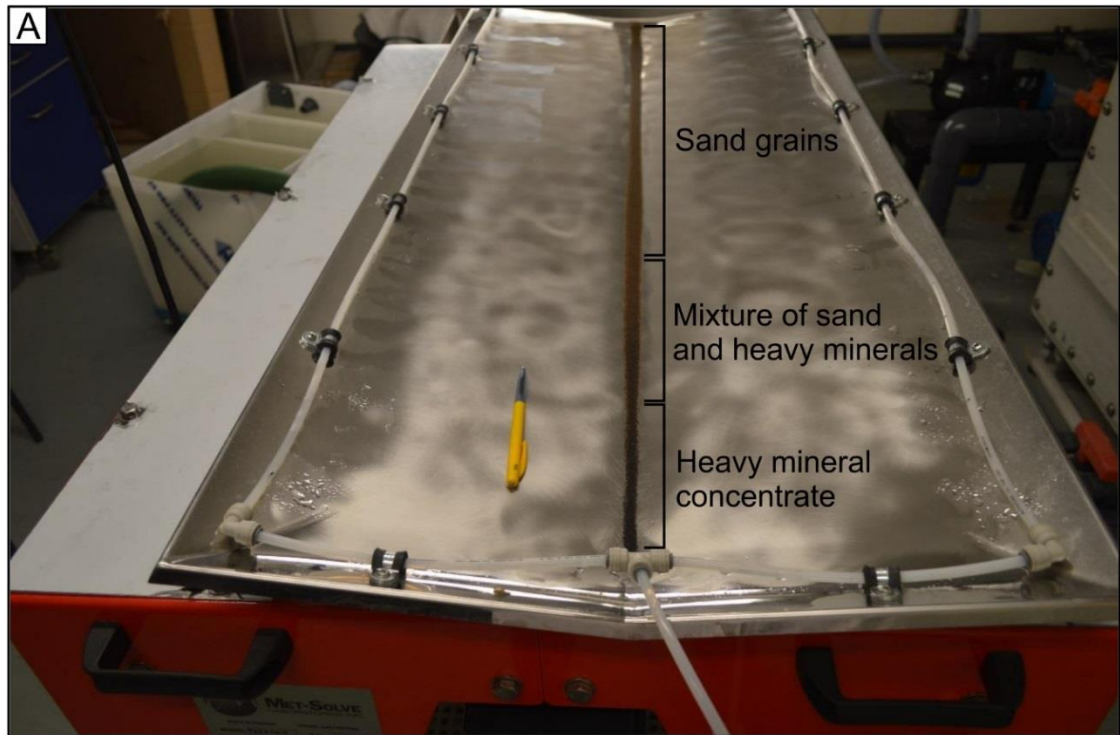


Figure 3.7 (A) Heavy minerals concentrate (dark) and light minerals during processing after separation on the gravity table of 0.5-1 mm size fraction of Auchas Lower Meso sample. (B). Close up view of Picture A bottom.

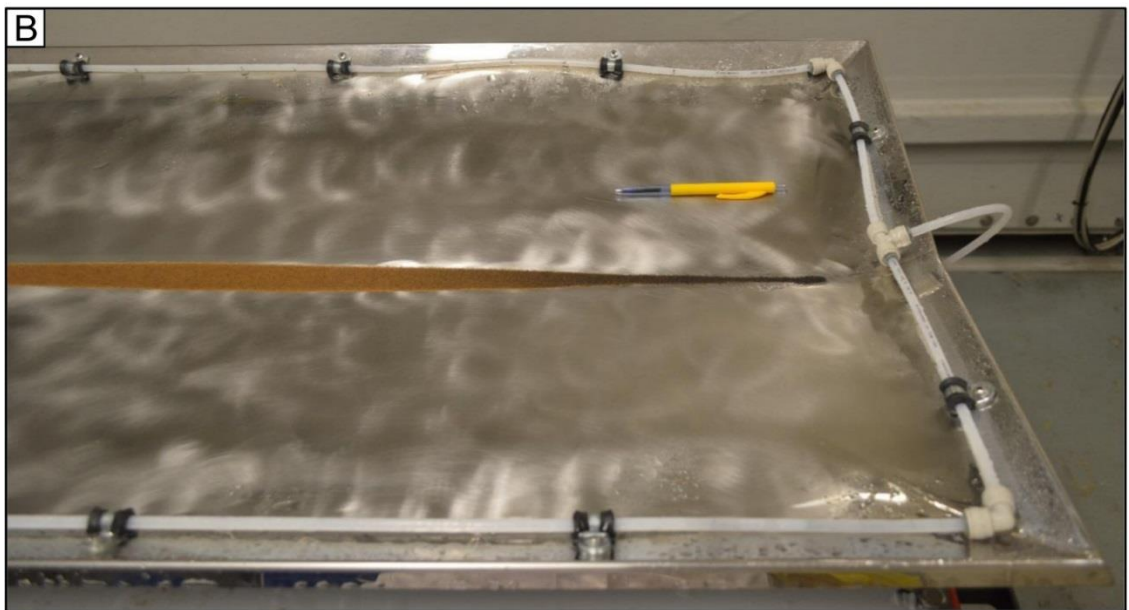
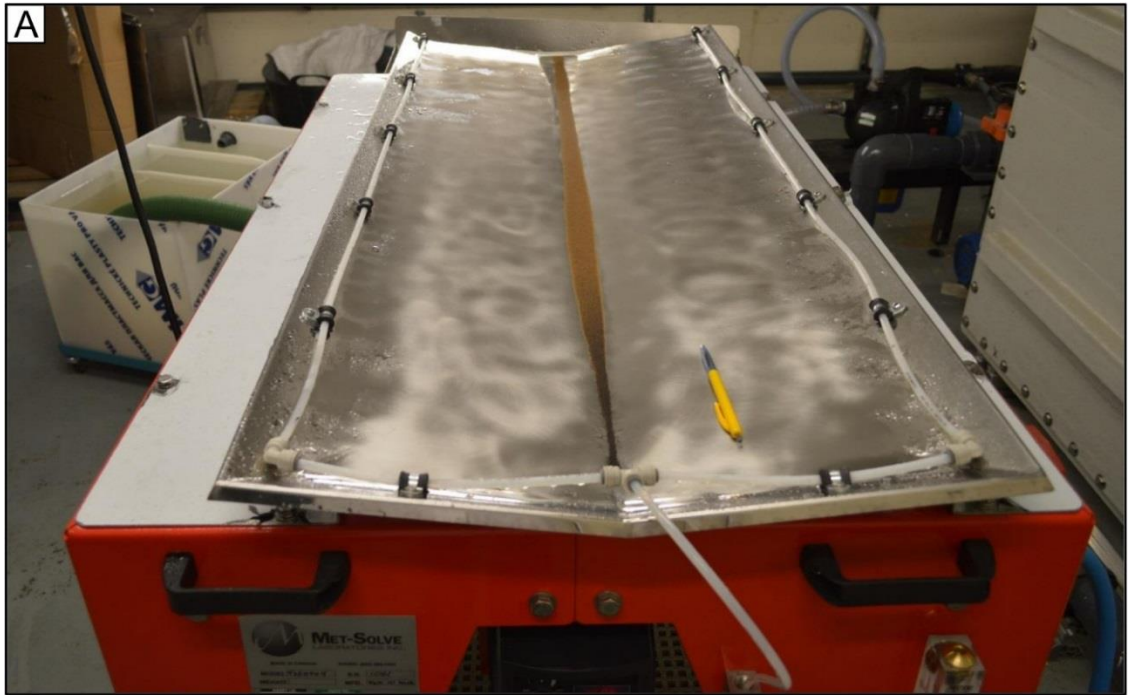


Figure 3.8 Heavy minerals concentrate (dark) and light minerals after separation on the gravity table of 0.5-1 mm size fraction of Auchas Outlet Meso Trench sample. Close up view of Picture A bottom.

3.3.5 Grain counting using polarizing microscope Stereo Zoom microscope

Techniques for determining heavy mineral proportions include Mineral Liberation Analyser (MLA), Quantitative Evaluation of Minerals by Scanning Electron Microscopy (QEMSCAN), X-Ray Diffraction (XRD) and grain counting. Both MLA and QEMSCAN are accurate methods but were not available to this study. The limitation of XRD is that most heavy minerals such as ilmenite and garnet have overlapping X-ray peaks and thus makes it difficult for separating the peaks and getting accurate values (Webster et al., 2003; Passchier, 2007). Most heavy mineral studies have used petrographic optical microscopy in quantifying heavy mineral assemblages by counting 200-300 grains per sample (Dill, 1998; Bynum, 2007; Durn et al., 2007; Faupl et al., 2007; Scheneiderman and Chen, 2007; Uddin et al., 2007; Garzanti et al., 2014; Garzanti et al., 2015; Krippner et al., 2016). Heavy mineral proportions were determined by counting a minimum of 300 grains per size fraction per sample under a binocular microscope following the methodology of Dill (1998), Faupl et al. (2007), Scheneiderman and Chen (2007), Garzanti et al. (2015) and Krippner et al. (2016). The sample was reduced in size by coning and quartering to generate a sub sample of 300 grains per sample. Magnetite was removed using a hand magnet, and grain counts according to mineral type were undertaken on the remaining sub sample. The counted grains were placed in separated glass vials according to mineral type. Minerals that could not be identified on the microscope were mounted on polished epoxy blocks and identified with a FEI Quanta FEG 650 Scanning Electron Microscope (SEM), using a 20 KV accelerating voltage and 5 nm spot size.

To test the reproducibility of the grain counting method four Orange River samples (Table 3.3; Figs. 3.9, 3.10) were selected for repeat counting. The repeat samples were selected on the basis of samples with heavy mineral assemblage that deviates from the rest of the samples. The heavy mineral sample split from which the repeat heavy mineral counting was done was obtained in the same way as the initial heavy mineral split. Repeat analysis was done for size fractions 0.5-1 mm and 0.25-0.50 mm. No repeat analysis was done for the 1-2 mm size fraction because after the initial grain counting there was not enough heavy mineral concentrate left to make a minimum total of 300 grains.

Table 3.3 Orange River samples analysed for repeat grain counting.

Deposit Type	Sample Name	Size Fraction	Mineral	First Analysis (number of grains)	Repeat Analysis (number of grains)	Average (number of grains)	Standard Deviation
Proto Orange River	Arrisdrif Proto Lower	0.5-1 mm	Magnetite	49	86	67.5	26.16
		0.5-1 mm	Garnet	198	172	185	18.38
		0.5-1 mm	Amphibole-Epidote	3	2	2.5	0.71
		0.5-1 mm	Ilmenite	70	46	58	16.97
		0.5-1 mm	Zircon	1	0	0.5	0.71
	Boom Proto Upper	0.25-0.50 mm	Magnetite	193	186	189.5	4.95
		0.25-0.50 mm	Garnet	26	26	26	0.00
		0.25-0.50 mm	Amphibole-Epidote	2	3	2.5	0.71
		0.25-0.50 mm	Ilmenite	91	120	105.5	20.51
	Meso Orange River	Arrisdrif Young Terrace	0.5-1 mm	Magnetite	88	70	79
0.5-1 mm			Garnet	159	181	170	15.56
0.5-1 mm			Amphibole-Epidote	72	30	51	29.70
0.5-1 mm			Ilmenite	44	35	39.5	6.36
Auchas Outlet Meso Trench		0.25-0.50 mm	Magnetite	161	150	155.5	7.78
		0.25-0.50 mm	Garnet	126	82	104	31.11
		0.25-0.50 mm	Amphibole-Epidote	6	1	3.5	3.54
		0.25-0.50 mm	Ilmenite	85	76	80.5	6.36

3.3.6 Mineral Identification on SEM and Mineral Surface Texture Analysis

Minerals that could not be identified via microscopy were identified with a FEI Quanta FEG 650 SEM using current of 20 kV and spot size of 3. This was done by mounting a representative number of grains per unknown mineral onto polished epoxy blocks (Tables 3.4, 3.5).

The objective of analysing mineral surface textures is to assess if there is any further reworking of the heavy minerals in the marine environment that may have altered the mineralogy of heavy mineral assemblage from source to sink. Garnet, magnetite and epidote were selected for mineral surface analysis textures from the Proto and Meso Orange River terrace deposits, and Atlantic 1 samples. Garnet in particular was chosen because it is abundant in both Orange River and Atlantic 1 gravels. Also, the type of grain surface textures formed on garnet are sensitive to the chemistry of environment of alteration compared to other silicate minerals (Salvino and Velbel, 1989). Magnetite is sensitive to oxidising and reducing conditions of the geochemical environment for example between river and marine environment (e.g., Weibel and Friis, 2007). The analysed minerals were selected from the 0.5-1 mm size fraction. Analysis of mineral surface textures was carried out using the SEM at 20 kV, spot size of 3 and aperture of 7.

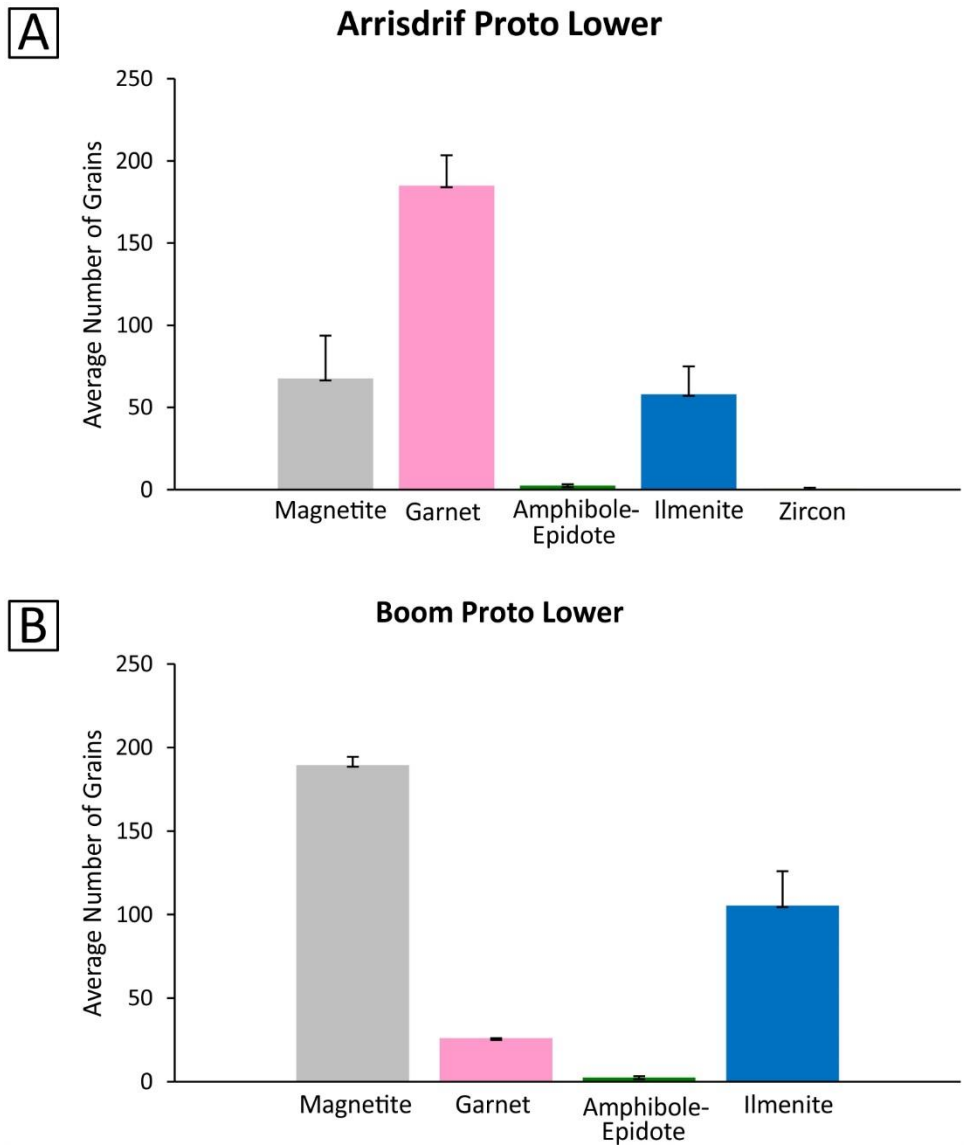


Figure 3.9 Comparison between first and repeat heavy mineral assemblage for Proto Orange River samples. Size fractions are (A) 0.5-1 mm and (B) 0.25-0.50 mm. The error bars indicate deviation from the average value.

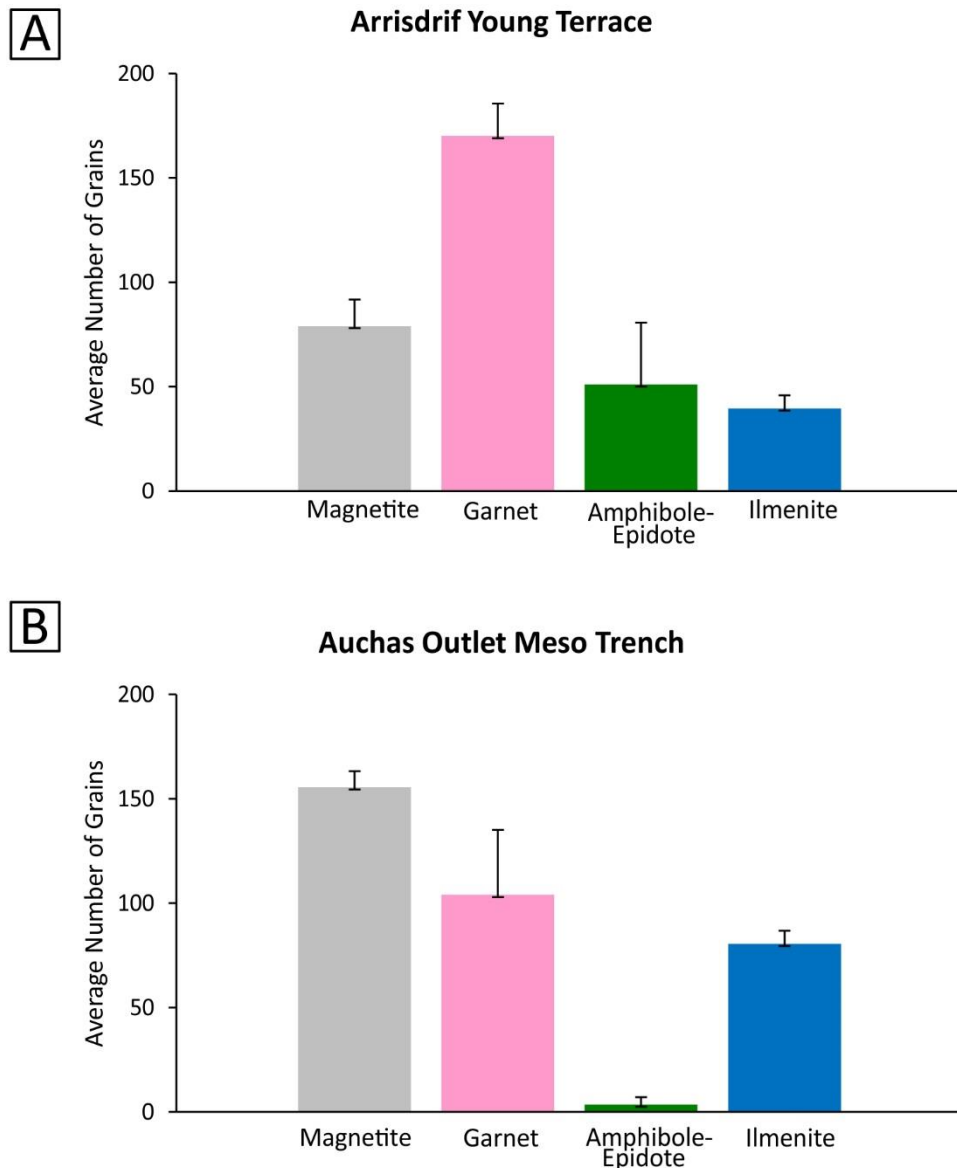


Figure 3.10 Comparison between first and repeat heavy mineral assemblage for Meso Orange River samples. Size fractions are (A) 0.5-1 mm and (B) 0.25-0.50 mm. The error bars indicate deviation from the average value.

3.3.7 Mineral Composition

Garnet, magnetite and epidote compositions were determined with a JEOL JXA8230 electron microprobe at 20 kV accelerating voltage, 30 nA beam current, 30 seconds on peak count time and 15 seconds off-peak count time. This was done by mounting a representative number of grains per mineral onto polished epoxy blocks (Tables 3.6, 3.7).

Table 3.4 Total number of mineral grains identified on the SEM for Orange River samples.

Mineral	1-2 mm	0.5-1 mm	0.25-0.50 mm
Garnet	6	4	0
Titanite	0	2	2
Epidote	0	0	2
Amphibole	7	5	4
Zircon	0	1	0

Table 3.5 Total number of mineral grains identified on the SEM for Atlantic 1 samples.

Mineral	0.25-0.50 mm
Clinopyroxene	7
Ilmenite	6
Apatite	18
Apatite (with silicate growth)	4
Epidote	1

Table 3.6 Number of garnet, magnetite and epidote grains from selected Orange River samples analysed for composition with the JEOL JXA8230 electron microprobe.

Deposit Type	Deposit Area	Sample Name	Garnet	Epidote	Magnetite
Proto Orange River Deposit	Boom	Boom Proto Lower	3	3	3
		Boom Proto Upper	3	3	3
	Sendelingsdrif	Sendelingsdrif Sample 7 Lower	4	4	4
	Auchas Major	AM59 Lower	4	4	4
	Arrisdrijf	Arrisdrijf Proto Lower	3	3	3
		Arrisdrijf Proto Upper	3	3	3
Meso Orange River Deposit	Boom	Boom Meso Lower	3	3	3
		Boom Meso Upper	3	3	3
	Sendelingsdrif	Sendelingsdrif Zone 7 Meso	4	4	4
	Auchas Major	Auchas Outlet Meso Trench	4	4	4
	Arrisdrijf	Arrisdrijf Meso	3	3	3
		Arrisdrijf Young Terrace	3	3	3

Table 3.7 Number of garnet, magnetite and epidote grains from selected Atlantic samples analysed for composition with the JEOL JXA8230 electron microprobe.

Mining Region	Sample Name	Garnet	Epidote	Magnetite
Region K	Region K-S1	4	4	4
	Region K-S5	4	4	4
Region N	Region N-S4	4	4	4
	Region N-S6	4	4	4
Region V	Region V-S7	4	4	4
	Region V-S9	4	4	4
Region W	Region W-S1	4	4	4
	Region W-S6	4	4	4

Chapter 4 Long-term controls on continental-scale bedrock river terrace deposition from integrated clast and heavy mineral assemblage analysis: an example from the lower Orange River

4.1 Introduction

Constraining the long-term landscape evolution of drainage basins requires data from the detrital record in genetically-related sedimentary basins (e.g., Morton, 1991; Dickinson and Gehrels, 2003; Mange and Otvos, 2005; Bhattacharya et al., 2016; Romans et al., 2016). A fragmented archive of drainage basin evolution is provided by terrace deposits within bedrock rivers (e.g. Bridgland and Westaway, 2008; Wegmann and Pazzaglia, 2009). This depositional record in sites of landscape degradation help to improve our understanding on the timing and character of river systems during sediment transfer from the continents (source) to oceans (sink) (Pazzaglia and Gardner, 1993; Aalto et al., 2008; Marsaglia et al., 2010; Kuehl et al., 2016). Generally, when sediments are transferred from continents to oceans environmental signals (e.g., climate, tectonic uplift) are modified either during transport in the sediment transfer zone or after deposition (Romans et al., 2016). Lithological information is also subject to modification. Analysis of clast assemblages is the most common approach to investigate the changing provenance of fluvial gravels and to establish the denudation and drainage evolution of catchments (Gibbard, 1979; Green et al., 1982; Bridgland, 1999). An alternative technique is the use of heavy minerals, because they are more physically and chemically resilient than many clasts, and may survive multiple phases of weathering and transport (Hassan, 1976; Morton, 1984, 1991; Goodbred et al., 2014).

Most drainage reconstruction studies have either used clast assemblage analysis (Gibbard, 1979; Dowdeswell et al., 1985; Bridgland, 1999; Jones, 2000; Mikesell et al., 2010) or heavy mineral assemblage (Uddin et al., 2007; Morton et al., 2011). Maher et al. (2007) present a rare example of combining the two techniques to reconstruct a river capture event of the Rio Alias, southeast Spain. Both techniques are problematic. Clasts derived from mechanically or chemically unstable bedrock might be preferentially degraded owing to abrasion during transport or chemically weathered post deposition (Green et al., 1980), which hinders accurate finger-printing of source areas. Heavy mineral studies also contain inherent weaknesses (Smale and Morton, 1987; Dill, 1994; Morton and Hallsworth, 1999; Faupl et al., 2007; Morton and Hallsworth, 2007; Uddin et al., 2007; Tsikouras et al., 2011; Wong et al., 2013; do Nascimento et al., 2015; Caracciolo et al., 2016; Krippner et al., 2016). For example, the relatively high density of heavy minerals may restrict the degree of transport, and influence accumulation in different sedimentary environments (Komar and Wang, 1984; Komar, 2007).

In this study, clast assemblage and heavy mineral signatures are integrated within a critical part of source-to-sink systems, the transfer zone where a depositional record is found within net erosional settings to provide information on the controls of sediment provenance, transport/bypass, and deposition. The lower Orange River was chosen because it is a continental scale bedrock river with a well-constrained geology of the drainage basin, and comprises accessible gravel terrace deposits with very good exposures owing to the arid climate and active mining operations (Fig. 4.1A). Furthermore, the gravel terrace deposits represent multiple cycles of degradation and aggradation, allowing investigation of changing controls through time. Specific objectives are i) to reconstruct the drainage history of the lower Orange River using two river terrace deposits, ii) to investigate extrinsic and intrinsic controls on the clast assemblage and heavy minerals assemblage, and iii) to evaluate the value of a combined approach to understanding continental-scale bedrock river evolution.

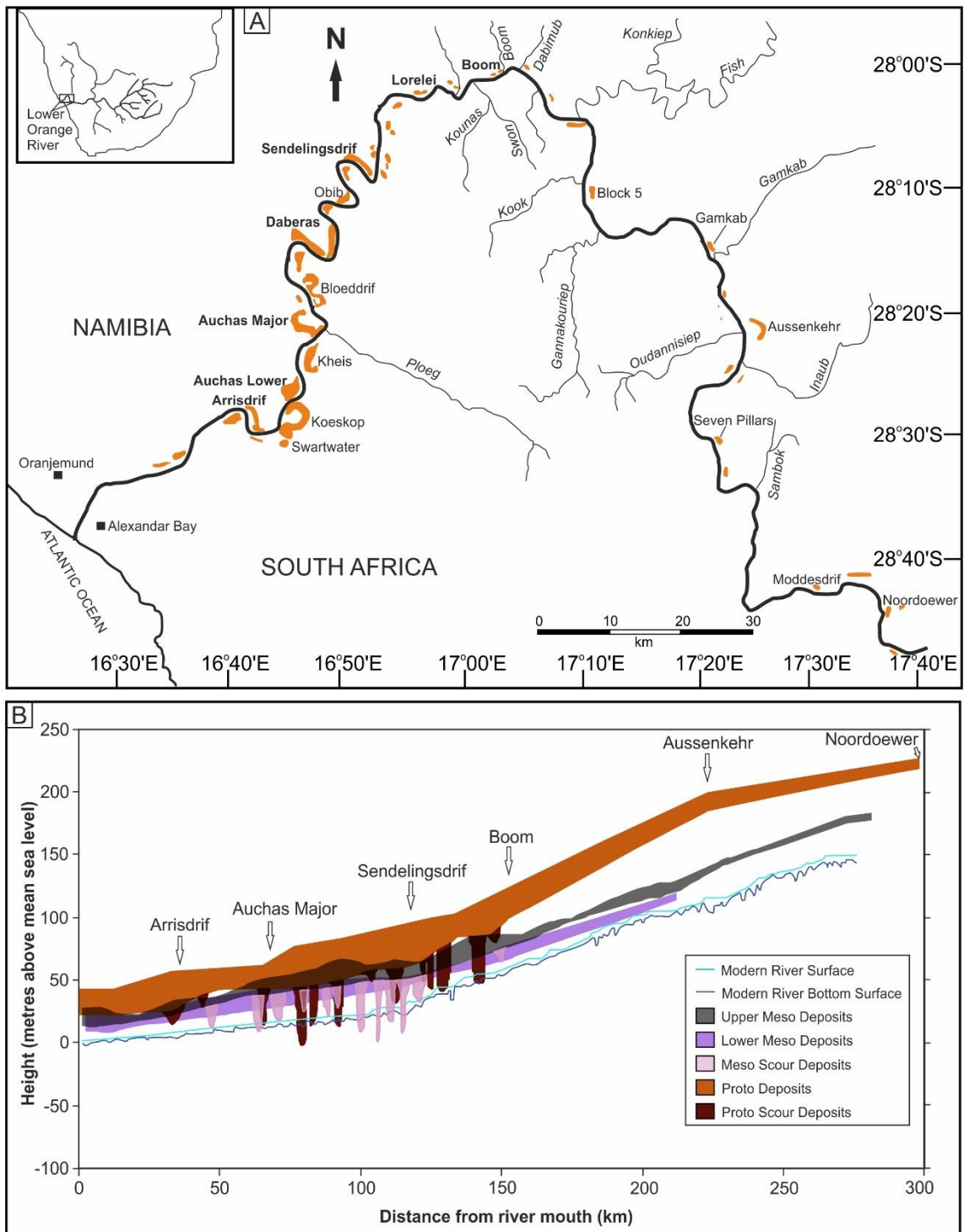


Figure 4.1 (A) Study area with distribution of gravel terrace deposits (orange colour) along the lower Orange River. Deposits analysed in this study are marked in bold. (B) Proto Orange River and Meso Orange River profiles relative to the modern Orange River profile. Figures A and B modified from Jacob et al. (1999) and Jacob (2005), respectively.

4.2 Geological Setting and Geomorphology

4.2.1 Geological Setting

The Orange River and its major tributary, the Vaal River, are the main bedrock confined rivers in a $\sim 10^6$ km² catchment (Garzanti et al., 2014). The term catchment area refers to the upstream part of the Orange River and this has been adapted throughout the thesis. The geology of the upstream catchment is highly variable. In the east, the geology comprises the Archaean Kaapvaal Craton (de Wit et al., 1992) intruded by Cretaceous and older diamondiferous kimberlites (de Wit, 1999; Shirey et al., 2001; Moore and Moore, 2004). The upper Orange River traverses rocks of the extensively eroded Permo-Carboniferous to Jurassic Karoo Supergroup (Visser, 1993; Johnson et al., 1997; Catuneanu et al., 1998; Key et al., 1998; Bangert et al., 1999; Catuneanu et al., 2005). Between Noordoewer (300 km east of the Orange River mouth) and Oranjemund (Fig. 4.2), the lower Orange River cuts through Mesoproterozoic Namaqua Metamorphic Complex (Thomas et al., 1994; Jacobs et al., 2008), before incising the Neoproterozoic Gariiep Belt (Frimmel and Frank, 1998; Frimmel et al., 2004) close to the river mouth on the Atlantic Ocean coast (Fig. 4.2). The Namaqua Metamorphic Complex form the basement of the area. The Gariiep Belt, which also extends into northwestern South Africa (Fig. 4.2), comprises mainly of metamorphosed sediments, including chert, quartzite, meta-greywacke, metapelite and metadiamictite (Frimmel et al., 1996; Frimmel and Frank, 1998; Basei et al., 2005). Around the Noordoewer area, the Ediacaran to early Cambrian Nama Group, a foreland basin succession (DiBenedetto and Grotzinger, 2005; Grotzinger et al., 2005; Grotzinger and Miller, 2008) cap the Namaqua Metamorphic Complex basement (Fig. 4.2). These rocks are possible sources of sediment in the Orange River terrace deposits. Along the lower Orange River, three distinct terrace deposits are recognised based on terrace elevation, bedrock strath level and exotic clast suite, which Jacob (2005) informally termed, in stratigraphic order, Pre-Proto Orange River deposits, Proto Orange River deposits, and Meso Orange River deposits. This nomenclature has been adopted in the present study. This study concentrates on Proto Orange River and Meso Orange River gravels in terms of the clast assemblage and heavy minerals.

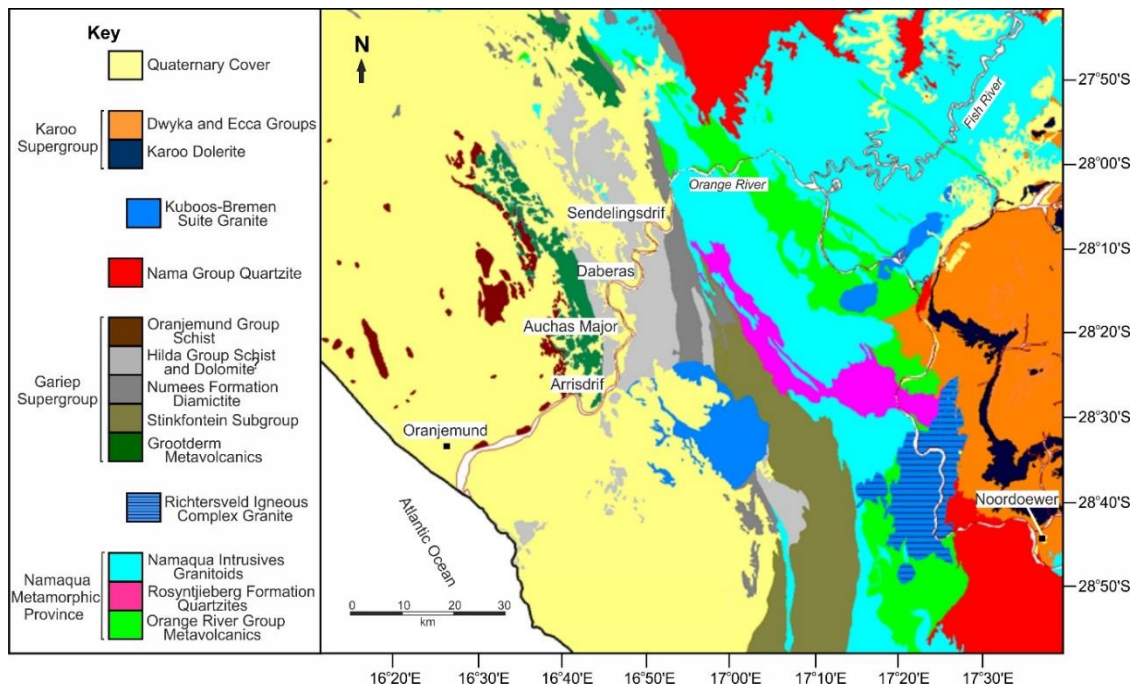


Figure 4.2 Simplified geology of the lower Orange River. Locations of Sendelingsdrif, Daberas, Auchas and Arrisdrif deposits are indicated for reference. Namibia GIS-based data obtained from the Geological Survey of Namibia. South African data after de Villiers and Sohng (1959).

4.2.2 Geomorphology

4.2.2.1 Regional Geomorphology

Over the last 66 Ma, the southern African landscape has been shaped by tectonics, climate and geomorphic processes (Knight and Grab, 2016a) although feedback produced by tectonics and climate are often difficult to isolate (Knight and Grab, 2016b). Periods of uplift and associated increased erosion in southern Africa include the Cretaceous (de Wit, 1999; Stevenson and McMillan, 2004; Richardson et al., 2017), the Miocene and the Pliocene (Partridge and Maud, 2000; Green et al., 2017). van der Beek et al. (2002) are in disagreement with a major uplift event as a precursor to the increased erosion, and propose that the topography of the southeast African margin is a result of thin elastic lithosphere (~10 km). Evidence of major Cretaceous uplift is recorded offshore where sediment supply rates in the Orange Basin offshore Namibia and South Africa (Rust and Summerfield, 1990; Aizawa et al., 2000; Rouby et al., 2009) and the

Outeniqua Basin, offshore South Africa (Tinker et al., 2008a; Sonibare et al., 2015) show a significant increase. There is a general consensus that erosion rates have decreased from the Cretaceous to the present, as shown by apatite fission track (Brown et al., 1999; Tinker et al., 2008b; Wildman et al., 2015) and cosmogenic work (Fleming et al., 1999; Cockburn et al., 2000; Bierman et al., 2014). Although the amount of erosion remains contentious (Hawthorne, 1975; Brown et al., 1999; Gallagher and Brown, 1999; Cockburn et al., 2000; Tinker et al., 2008b; Hanson et al., 2009; Decker et al., 2011, 2013; Wildman et al., 2015; Richardson et al., 2017), uplift is believed to have been much greater in the eastern parts of southern Africa, which forced rivers to flow westwards to lower lying areas towards the Atlantic Ocean (de Wit et al., 2000; Partridge and Maud, 2000). However, there is also a possibility that the eastern subcontinent might have already been relatively more elevated than the western subcontinent prior to uplift (Roberts and White, 2010; Richardson et al., 2016).

During the Miocene, southeastern Africa underwent a maximum uplift of 250 m, almost twice that of the western subcontinent (150 m) (Partridge and Maud, 2000). This is in agreement with Hanson et al. (2009), who estimated high erosion rates for the Monastery kimberlite pipe (~1350 m) in eastern South Africa, relative to the Kimberley and Koffiefontein pipes (~850 m) in central South Africa. Apatite fission track studies have estimated 2.5 to 3.5 km of erosion for the late Cretaceous (Brown et al., 1999; Gallagher and Brown, 1999; Tinker et al., 2008b; Decker et al., 2013; Wildman et al., 2015; Green et al., 2017). Green et al. (2017) argues that the uplift events have increased the erosive power of rivers in southern Africa.

The central part of southern Africa is marked by a low relief elevated central plateau (> 1000 m above mean sea level) whereas the coastal margins along the Indian and Atlantic Oceans are characterised by a high relief low elevation coastal plain. The two are separated from each other by the Great Escarpment (Gallagher and Brown, 1999), which occurs between 50-200 km inland from the coast (Partridge and Maud, 1987, 2000; Partridge et al., 2010). In addition to uplift, rivers have also played an important role in shaping the southern African landscape. The Orange River is one of the major drainage systems in southern Africa, and with its many tributaries, has played a major role in shaping the

landscape since the late Mesozoic. According to Jacob (2005) the Orange River denuded the landscape between 600-1000 m following the Cretaceous uplift. However, contrasting views regarding the evolution and development of the Orange River fluvial system remain (Jubb, 1964; Dingle and Hendey, 1984; Skelton, 1986; de Wit, 1999; de Wit et al., 2000).

4.2.2.2 Geomorphology of the lower Orange River

Outcrops of both Namaqua Metamorphic Complex and Gariep Belt rocks together with the Orange River make up the main geomorphic features in the area. The area between Noordoewer and the Orange River mouth is characterised by a low relief coastal plain and high relief inland area. High relief in the area is a product of the resistant lithologies that comprise the Namaqua Metamorphic Complex rocks (Fig. 4.2). Ephemeral tributaries to the lower Orange River include the Gamkab River, Fish River and Boom River. From Noordoewer towards the river mouth, the palaeo-Orange River valley (early to middle Miocene) widens from 550 m to 2300 m, and its gradient decreases downstream (from 0.87 m/km to 0.38 m/km) with an overall gradient of 0.69 m/km (Jacob, 2005) (Fig. 4.1B).

4.3 Results

4.3.1 Gravel Characterisation

Thick gravel terrace successions deposited on bedrock flanking the lower Orange River on both the Namibian and South African sides (Fig. 4.1A) provide a partial record of the long-term fluvial evolution of the Orange River. During degradational phases, the palaeo-Orange River incised into the local bedrock forming deep scours (10-30 m) below the bedrock strath level that were filled with gravel during aggradational phases (Figs. 4.1B, 4.3B, 4.3C). The scours are associated with meander bends, tributary inputs points and structural features e.g. faults and joints (Jacob, 2005). Multiple cycles of bedrock incision and aggradation resulted in a series of highly dissected terrace deposits (Fig. 4.3A). Some terrace deposits,

particularly at Daberas and Sendelingsdrif, are greater than 10 m thick (Fig. 4.3A). The depth of incision (Figs. 4.1B, 4.3B, 4.3C), size of imbricated clasts (Fig. 4.4A) and coarse grained cross bedding (Fig. 4.4B) suggest a high energy river system (e.g., Dott and Bourgeois, 1982). The overall makeup of the gravel is a combination of both exotic clasts and locally derived clasts, with the large cobble size fractions (> 25 mm) dominated by quartzite clasts. Exotic clasts include agate (Fig. 4.5A), Karoo Supergroup shales and sandstones (Fig. 4.5B), Karoo Supergroup basalt and banded iron formation (BIF) (Fig. 4.5C). These clasts are derived from the Orange River upstream catchment area. The relative abundance of each clast in a given gravel deposit is related to the timing and geomorphic evolution of the Orange River drainage basin. The provenance of the key clast types that comprise the gravels is summarised in Figure 4.6. The mineralogy of the Namaqua Metamorphic Complex rocks and Gariep Belt rocks is summarised in Table 4.1.

According to Jacob (2005) the Proto Orange River deposits represent a significant period of aggradation. The Meso Orange River deposits comprise of older high lying Upper Meso units and younger Meso units that represent short phases of incision and aggradation (Jacob, 2005). Compared to the Meso Orange River course, the Proto Orange River is a high sinuosity river whereas the younger gravels were deposited by a low sinuosity Meso Orange River with a course similar to that of the modern Orange River. Deposition of the older and younger gravels occurred due to a combined effect of base level rise and increase in supply of material from tributaries (Jacob, 2005).

Table 4.1 Mineralogy of the Namaqua Metamorphic Complex and Gariep Belt rocks.

Source Lithology	Heavy Minerals Density > 2.8 g/cm ³	Other Minerals	References
Namaqua Metamorphic Complex	Garnet Amphibole Epidote Spinel Pyroxene Ilmenite Magnetite Sillimanite Zoisite	Plagioclase Feldspar Biotite Cordierite Chlorite	Botha and Grobler (1979) Waters (1989) Robb et al. (1999) Diener et al. (2013) Bial et al. (2015)
Gariep Belt	Amphibole Epidote Ilmenite Titanite	Biotite Plagioclase	Frimmel et al. (1996) Frimmel and Frank (1998)



Figure 4.3 (A) Representative photograph of the thick Proto Orange River terrace deposit at Sendelingsdrif deposit. Photograph taken looking east. (B) and (C) Photograph of deep scours cut into bedrock below the bedrock strath level at Auchas deposit. Note the smooth walls of the scours formed by abrasion.



Figure 4.4 Imbricated clasts (marked by white lines) (A) and coarse cross bedding (B) as seen in Proto Orange River unit and above Meso Orange River unit, respectively. (C) Meso Orange River gravel.



Figure 4.5 Agate (A), Karoo sedimentary rocks (B) and BIF (C) clasts that comprise the exotic clast suite of the Orange River derived gravels. (D) Fresh non-weathered feldspar clasts from Proto Orange River gravel, Daberas deposit.

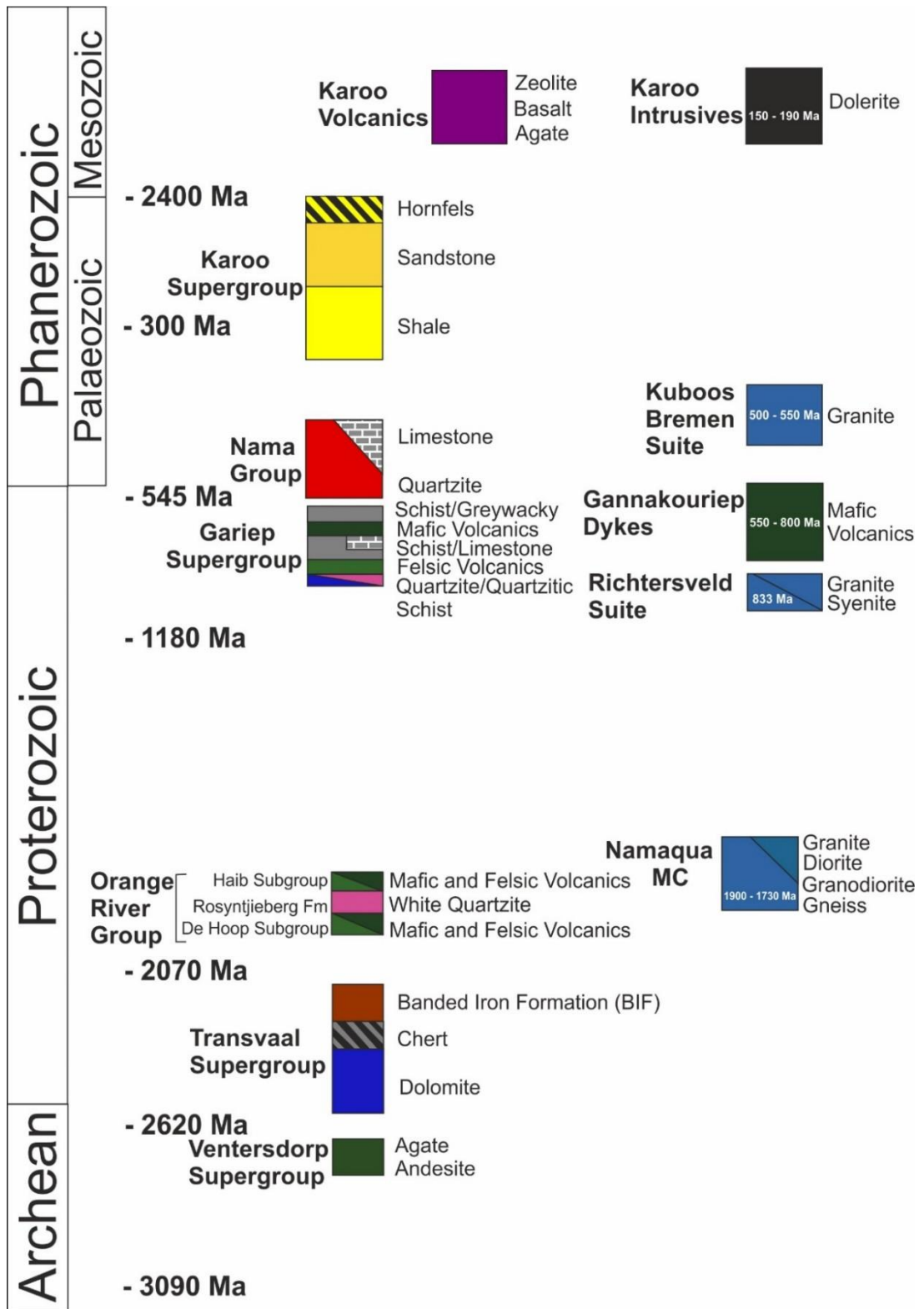


Figure 4.6 Key clasts of the Orange River gravel terrace deposits and their respective provenances. Namaqua MC denotes Namaqua Metamorphic Complex. Modified from Jacob (2005).

4.3.1.1 Clast Assemblage

Of the size fractions analysed for clast assemblage, the data reported in Figure 4.7 is for size fractions 16-25 mm, 8-16 mm and 3-8 mm because these are the size fractions where the exotic clast suite is most readily identified. The Proto Orange River gravel terrace signature is characterised by a dominance of Karoo Supergroup shales and sandstones among the exotic clasts (Figs. 4.5B, 4.7). The exotic clast suite of Meso Orange River gravels is dominated by banded iron formation (BIF) relative to the other exotic clasts (Figs. 4.5C, 4.7). For example, in the 16-25 mm size fraction, Karoo Supergroup sediments constitute 22% and 7% of the Proto Orange River and Meso Orange River gravels, respectively, and BIF is 6% in the Proto Orange River gravel and 10% in the Meso Orange River gravel (Fig. 4.7). At Auchas Major, the Meso Orange River gravel has an uncharacteristic abundant Karoo shales and sandstones (Fig. 4.7) (Jacob, 2005). Another feature of Meso Orange River gravel is the presence of significant amounts of Karoo Supergroup basalt clasts (Fig. 4.7), sourced from the early Jurassic (190-183 Ma) Drakensberg Flood Basalts (Duncan et al., 1997; Marsh et al., 1997; Jacob, 2005; Jourdan et al., 2007), but these are rare in the older gravels (Fig. 4.7A). Feldspar clasts were recorded in the small size fractions (8-16 mm and 3-8 mm) in both Proto and Meso Orange River gravels (Figs. 4.5D, 4.7).

Eocene marine gravel is the oldest Orange River-derived sediments on the west coast and is preserved at 160 m palaeo sea level (Stocken, 1978). The Eocene gravel is characterised by abundant agates and chalcedony as the dominant exotic clasts (Jacob, 2005; Miller, 2008). However, no equivalent Eocene age gravel is preserved in the lower Orange River. The age of Pre-Proto Orange River deposits remains unknown. The Proto Orange River suite has been dated as early to middle Miocene, using macrofauna fossils, (including *Lopholistriodon moruoroti*), found in gravel terrace deposits at Auchas and Arrisdrif of the lower Orange River (Corvinus and Hendey, 1978; Hendey, 1978; Pickford, 1987; Pickford and Senut, 2002) (Fig. 4.1A). The Meso Orange River gravel suite has not been dated, but is inferred to be Plio-Pleistocene (2-5 Ma) based on correlations with littoral beach gravel deposits (Pether, 1986). Proto Orange River gravel terrace deposits are 50-70 m above present river level, whereas the Meso

Orange River terrace deposits are 30-40 m above the modern river level (Jacob et al., 1999) (Fig. 4.1B). The younger bedrock strath terraces formed at lower elevations after incision of the bedrock during net degradational phases of the Orange River.

4.3.1.2 Clast Roundness

The lithology of a clast and the distance it travels before deposition is reflected by the degree of rounding (Lindsey et al., 2007; Miao et al., 2010). Proto Orange River gravels show a higher degree of rounding than the Meso Orange River gravels (Fig. 4.8). For size fractions smaller than 40 mm, clast roundness decreases exponentially with decreasing clast size in both the Proto and Meso Orange River gravels as reported by Jacob (2005) (Fig. 4.8).

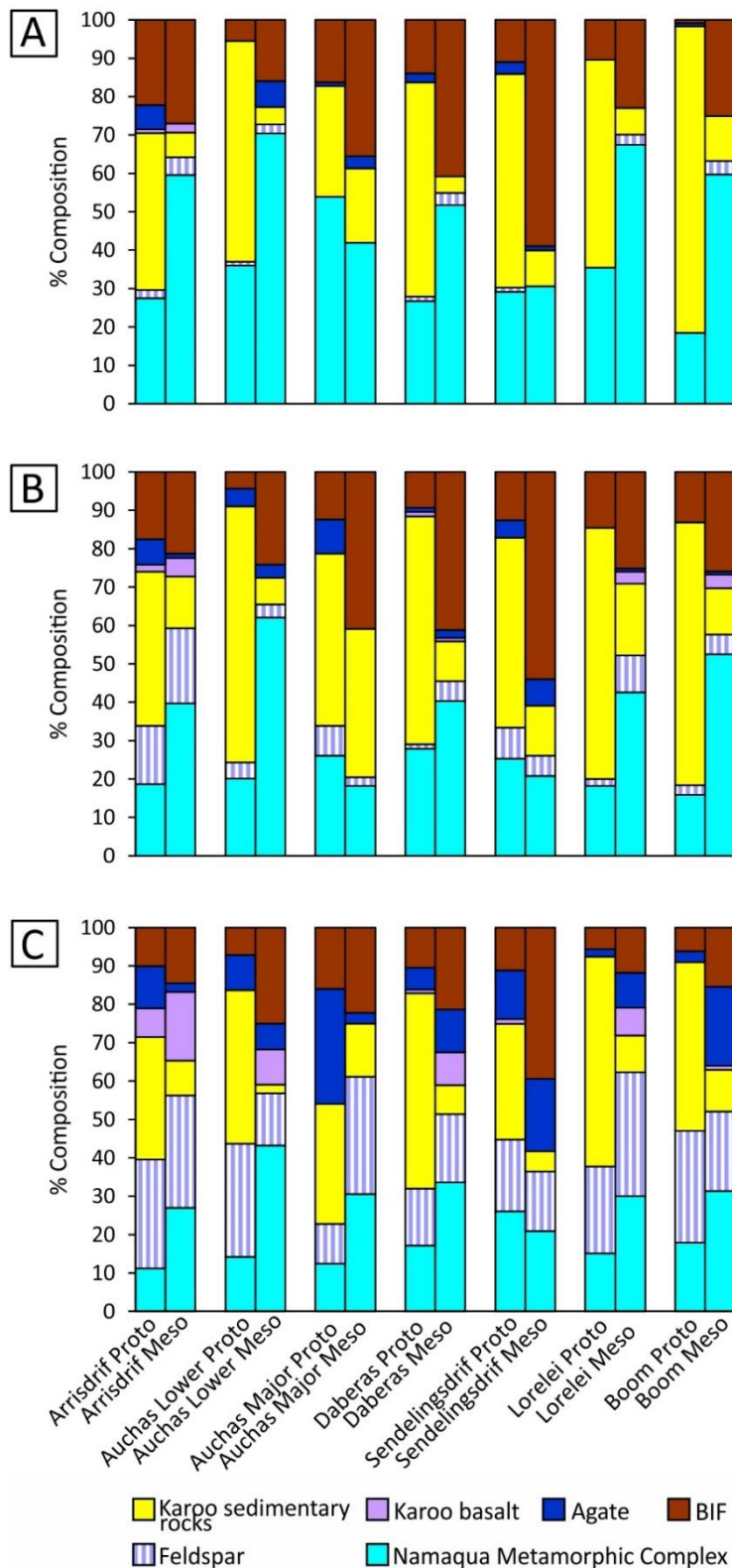


Figure 4.7 Clast assemblage of Proto and Meso Orange River gravels for size fractions (A) 16-25 mm, (B) 8-16 mm and (C) 3-8 mm. Data from Jacob (2005). Sample locations are indicated in Figure 4.1A.

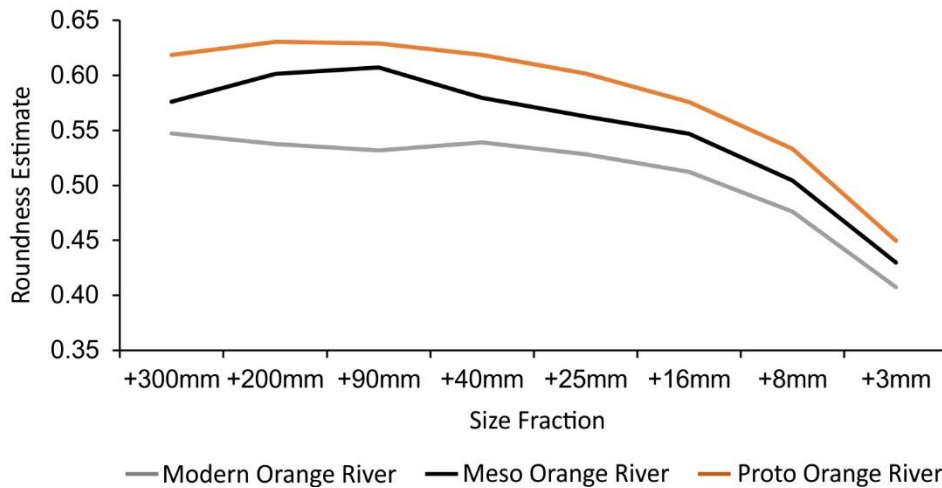


Figure 4.8 Clast roundness of the Proto and Meso Orange River gravels. Modern Orange River data is included for comparison. Data from Jacob (2005).

4.3.2 Heavy Mineral Assemblages of the Proto and Meso Orange River gravels

The heavy minerals present in the Proto and Meso Orange River gravels are magnetite, garnet, epidote, amphibole and ilmenite. Titanite and zircon are present in trace amounts. Figures 4.9-4.13 illustrate the relative abundance of individual heavy minerals within the overall heavy fraction according to locality and gravel stratigraphy. In plotting the heavy mineral assemblages, the lower density minerals amphibole (2.97-3.13 g/cm³) and epidote (3.3-3.6 g/cm³) have been grouped together, because they have similar chemical stabilities (Table 4.2; Morton and Hallsworth, 2007; Andò et al., 2012). These are referred to as amphibole-epidote and this terminology has been adapted throughout the thesis.

The Proto Orange River gravel shows relatively higher magnetite and ilmenite contents than the Meso Orange River gravel for the 0.5-1 mm and the 0.25-0.50 mm size fractions (Figs. 4.9, 4.11). Most of the garnets in the Proto Orange River gravel are in the coarsest size fraction such that garnet abundance decrease by more than half from the coarse size fraction (1-2 mm) to the fine size fraction (0.25 mm-0.50 mm) (Fig. 4.9). In contrast, in the Meso Orange River deposits, garnet reduces gradually from the coarse size fraction to the fine size fraction

(Fig. 4.9). For example, at Arrisdrif garnet content reduces from an average of 89% of the total heavy mineral in the 1-2 mm size fraction to 30% in the 0.25-0.50 mm, whereas in the Meso Orange River it changes from 34% to 26% (Fig. 4.9).

The Meso Orange River samples are characterised by a relative higher abundance of amphibole-epidote minerals than the Proto Orange River samples (Figs. 4.9-4.13). Within the amphibole-epidote group, amphibole is less abundant in the Proto Orange River deposits than in the Meso age gravel (Fig. 4.10). The distinction between the Proto and Meso Orange River deposits in terms of amphibole-epidote content is clear at Arrisdrif, Auchas Lower, Daberas, Lorelei and Boom (Figs. 4.9, 4.11). In contrast, at Auchas Major and Sendelingsdrif deposits, the Meso Orange River samples have low amphibole-epidote content that is similar to the Proto Orange River samples (Figs. 4.9, 4.11).

In the Meso Orange River gravel, amphibole-epidote content increases downstream from Boom to Arrisdrif, whereas magnetite decreases downstream most especially for the 0.5-1 mm size fraction (Fig. 4.11B). However, neither trend is observed in the Proto Orange River gravel (Fig. 4.11). At Boom, for example, the average amphibole-epidote/magnetite ratio of the Lower Meso Orange River sample is 0.3 in the 0.5-1 mm size fraction, whereas further downstream at Arrisdrif it is 0.96 in the same size fraction (Fig. 4.11B). Where there are Lower and Upper Meso units, at Daberas, Lorelei and Boom, the Upper Meso units show higher amphibole-epidote content than the Lower Meso units irrespective of size fraction. At Boom, for example, the average amphibole-epidote/magnetite ratio is 0.07 for the Boom Meso Lower sample whereas it is significantly higher (0.58) for the Boom Meso Upper sample (Fig. 4.11).

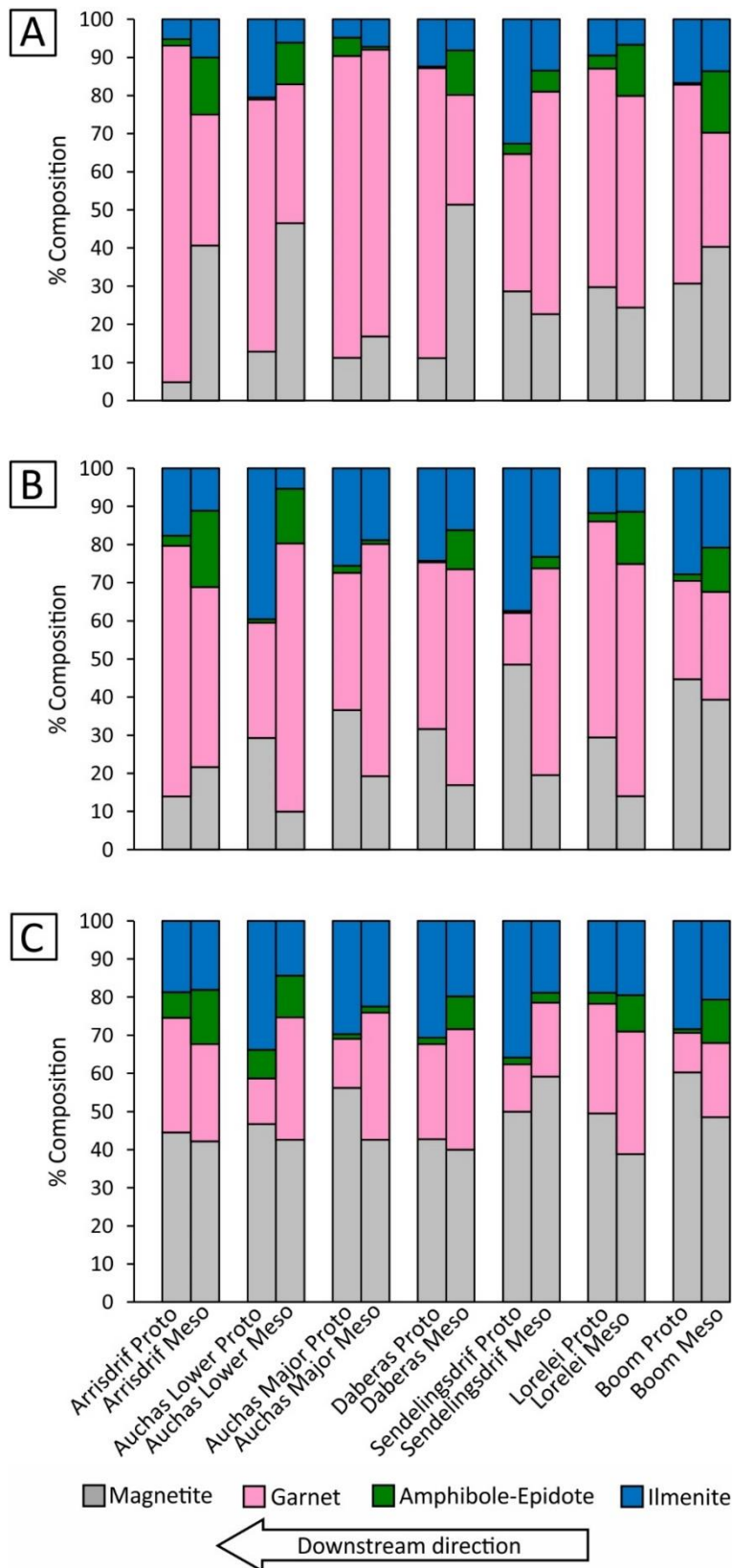


Figure 4.9 Heavy mineral assemblage of Proto and Meso Orange River deposits for size fractions (A) 1-2 mm, (B) 0.5-1 mm (C) and 0.25-0.50 mm. Sample locations are indicated in Figure 4.1A.

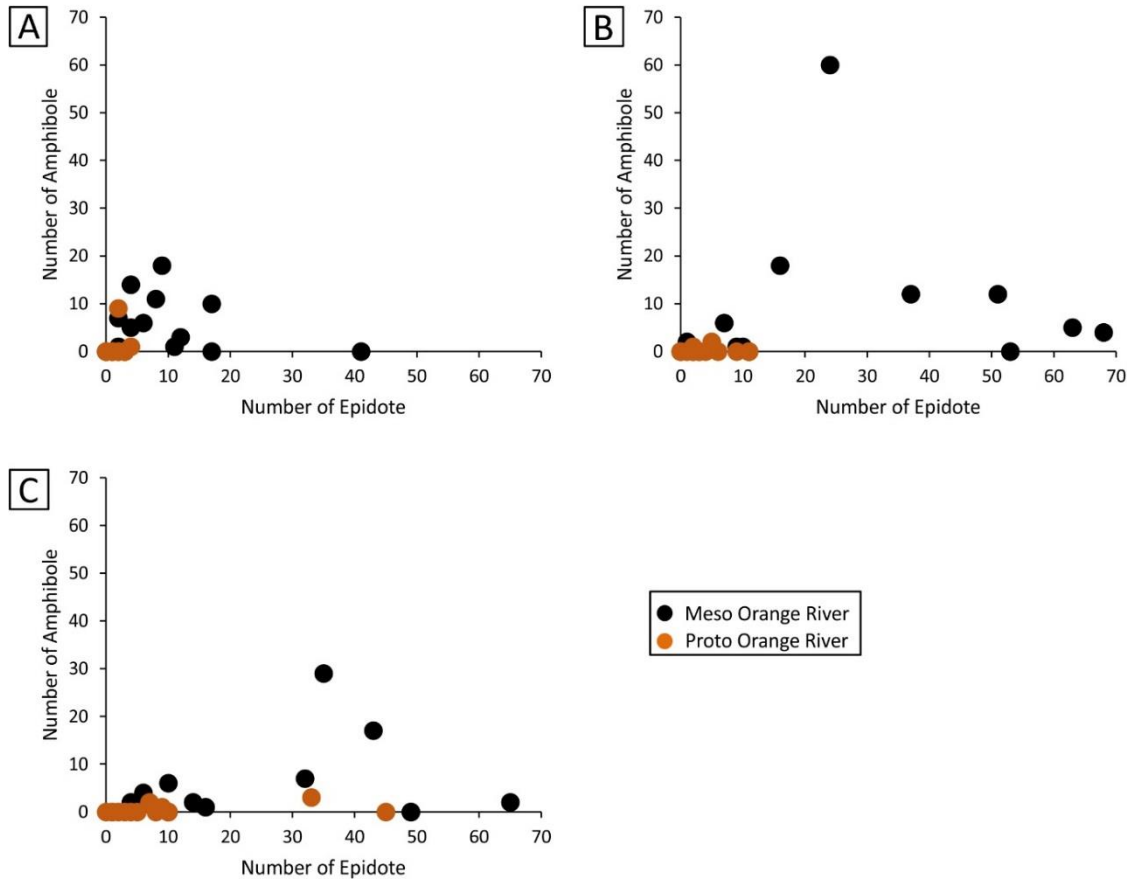


Figure 4.10 Variation in the proportions of amphibole and epidote proportions between the Proto and Meso Orange River deposits for size fractions (A) 1-2 mm, (B) 0.5-1 mm and (C) 0.25-0.50 mm.

4.3.3 Distinction of the Proto and Meso Orange River deposits on basis of clast and heavy mineral assemblage

There is a clear distinction between the Proto and Meso Orange River gravels, at both clast and heavy mineral scales (Fig. 4.12). The Proto Orange River gravel is characterised by a high percentage of Karoo shales and sandstones and low amphibole-epidote content, and the Meso Orange River gravel is characterised by high BIF and amphibole-epidote contents (Fig. 4.12). Amphibole-epidote shows a positive correlation with Namaqua Metamorphic Complex basement clasts (Fig. 4.13). The bulk of Proto and Meso Orange River garnets show similar, FeO-rich compositions at ~32 wt.% FeO (Fig. 4.14B, D). However, a small number of garnets from Proto Orange River deposits (n = 4) and Meso Orange

River deposits (n = 2) show slightly lower FeO than the rest of the group, coupled with strongly elevated MnO (up to 25 wt.%, Fig. 4.14). When compared to the composition of the Namaqua Metamorphic Complex garnets reported by Humphreys and Van Bever Donker (1990), Diener et al. (2013) and Bial et al. (2015) the Orange River garnets are mostly similar to the Namaqua Metamorphic Complex garnets in both their FeO, MgO and MnO contents (Fig. 4.14). The exceptional low FeO, high MnO garnets are most similar to the Gariep Belt garnets presented by Diener et al. (2017), (Fig. 4.14B, D).

Table 4.2 Relative chemical stability of heavy minerals, from Morton and Hallsworth (2007).

Olivine	Least Stable
Pyroxene	
Amphibole	
Epidote	
Titanite	
Kyanite	
Staurolite	
Garnet	
Tourmaline, Spinel	
Rutile, Zircon, Apatite	

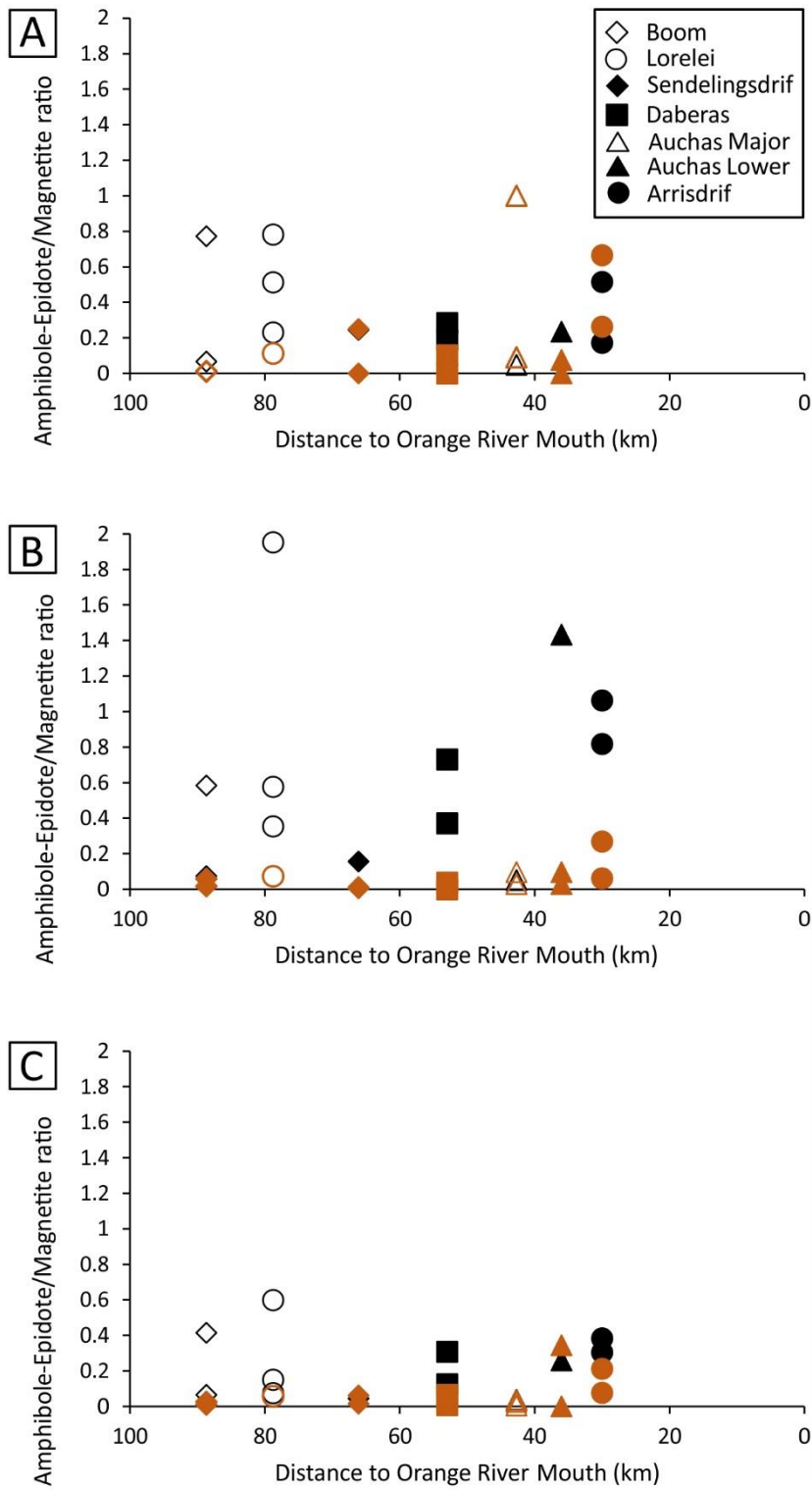


Figure 4.11 Downstream change in amphibole-epidote/magnetite ratio from Boom to Arrisdrif for the Proto Orange River gravel (orange symbols) and Meso Orange River gravel (black symbols). (A) 1-2 mm, (B) 0.5-1 mm and (C) 0.25-0.50 mm. Meso Orange River samples with anomalous amphibole-epidote/magnetite ratios are for the Upper Meso units.

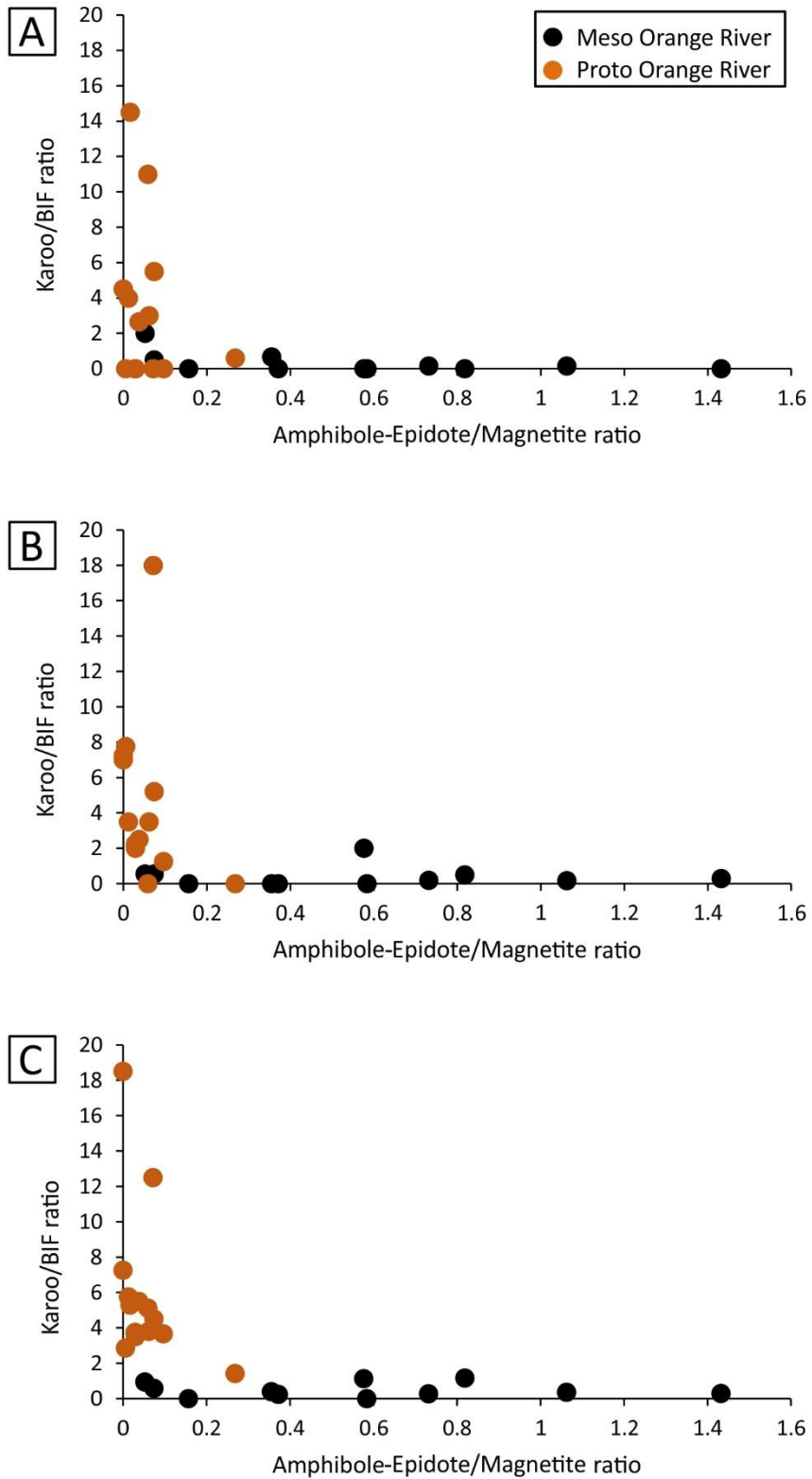


Figure 4.12 Clast assemblage and heavy mineral assemblage variations between Proto Orange River and Meso Orange River gravel. Heavy mineral assemblage data is from 0.5-1 mm size fraction whereas clast assemblage data is for (A) 16-25 mm, (B) 8-16 mm and (C) 3-8 mm.

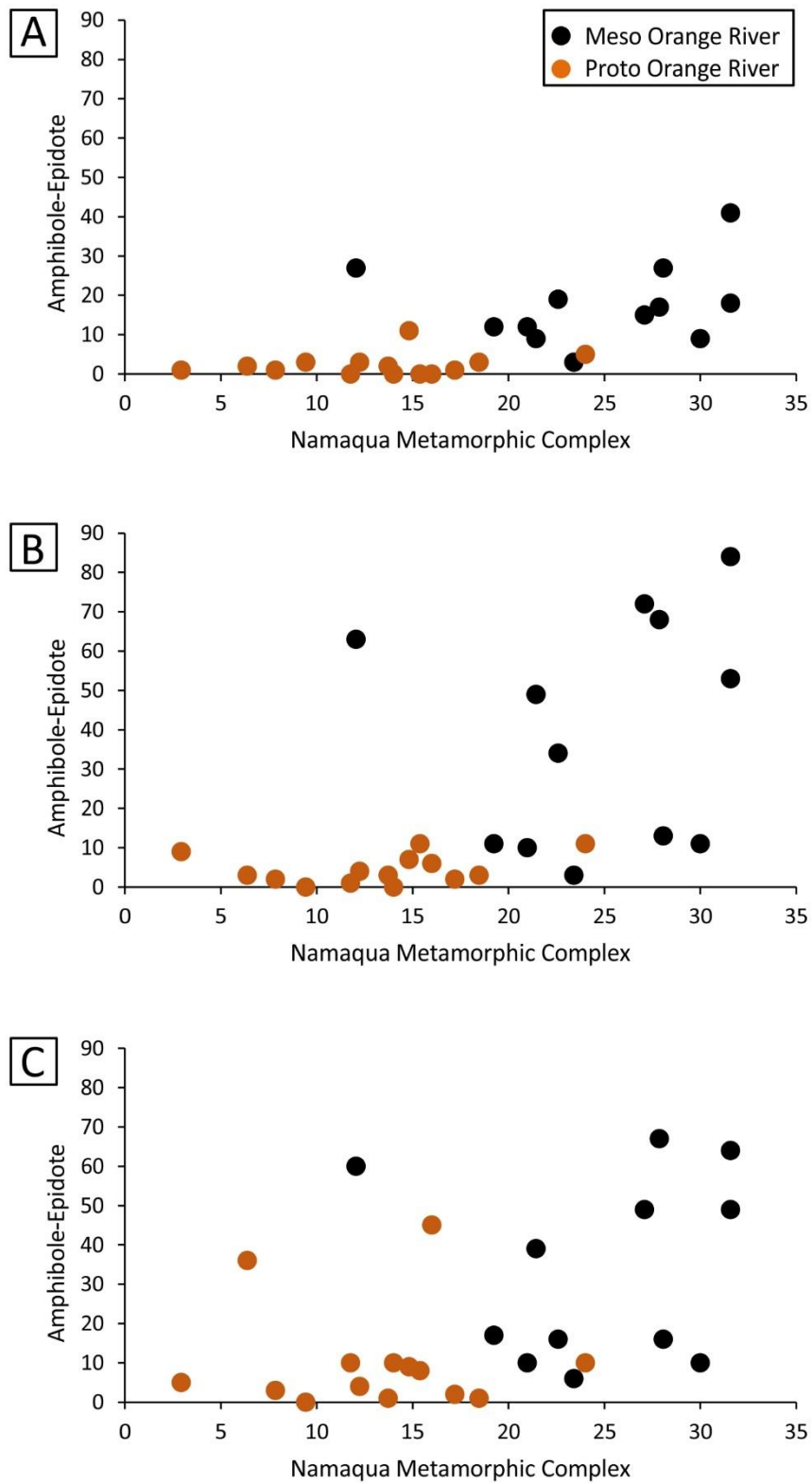


Figure 4.13 Comparison of Namaqua Metamorphic Complex clasts and amphibole-epidote content. (A) 1-2 mm, (B) 0.5-1 mm (C) and 0.25-0.50 mm.

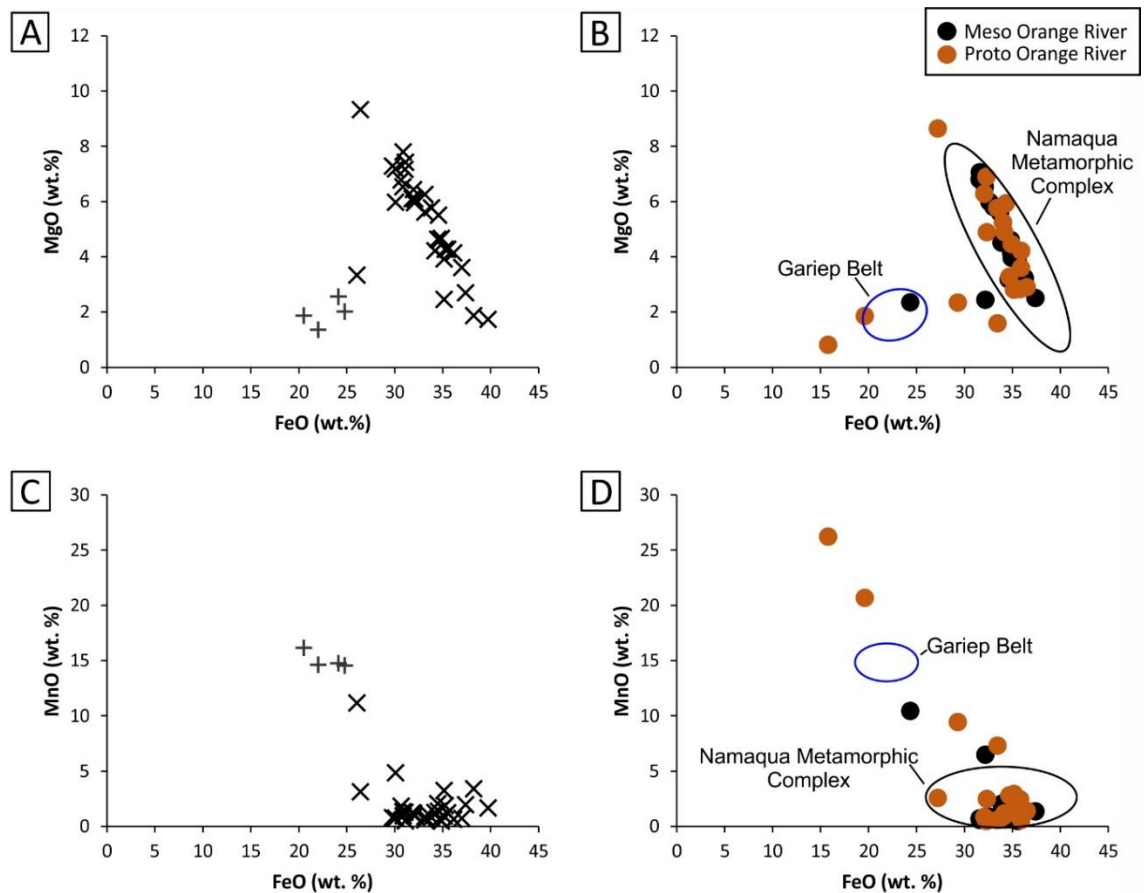


Figure 4.14 (A) Garnet compositions in MgO versus FeO from the Namaqua Metamorphic Complex (Humphreys and Van Bever Donker, 1990; Cornell et al., 1992; Diener et al., 2013; Bial et al., 2015) and Gariep Belt garnets (Diener et al., 2017). (B) Data for Proto and Meso Orange River garnets. (C) MgO versus FeO from the Namaqua Metamorphic Complex and Gariep Belt (D) Data for Proto and Meso Orange River garnets.

4.4 Discussion

4.4.1 Controls on clast assemblage differences

An interplay of key controls, including changes in provenance, palaeohydraulics, and reworking, influence clast assemblages in the different terrace units. Source is widely invoked as a dominant control on compositional differences between sediments on a regional or local scale (e.g., Gibbard, 1979; Green et al., 1982; Bridgland, 1999; Roberts et al., 2008; Claude et al., 2017). Clast provenance can vary through time due to changes in surface exposure and availability of different rock types, or through drainage re-organisation (e.g., Mather, 2000). Re-

organisation of drainage basin networks can be caused by tectonism and volcanism (e.g., Maddy et al., 2012; Richardson et al., 2016), or through drainage capture events (e.g., Mather, 2000; Maher et al., 2007) during the evolution of degradational landscapes. Periods of uplift, and increased erosion and sediment flux in southern Africa include the Cretaceous (de Wit, 1999; Stevenson and McMillan, 2004; Tinker et al., 2008b; Guillocheau et al., 2012; Richardson et al., 2016, 2017), and the Miocene and Pliocene (Partridge and Maud, 2000; Green et al., 2017). A Pliocene period of uplift, which occurred after deposition of the Proto Orange River gravel, could be invoked to have driven drainage re-organisation and influenced clast assemblage differences between the Proto and Meso Orange River gravels. However, there is neither a diagnostic clast lithology in either Proto Orange River or Meso Orange River gravels, nor geomorphological evidence for drainage re-organisation reported for the Orange River catchment during this period.

Only the relative dominance of exotic clasts distinguishes the clast assemblages between the stratigraphically distinct Proto and Meso Orange River successions in the Orange River gravel deposits (Figs. 4.7, 4.12). This suggests that there has not been a major change in sediment provenance available to the Orange River through time, although different lithologies have been entrained during different periods. For example, the proportions of Karoo shales and sandstones suggest that the majority of the Karoo Supergroup sediments were eroded by the end of Proto-Orange River times and were less available to the Orange River in Meso-Orange River times. The opposite is true for the BIF (Figs. 4.7, 4.12). In summary, changes in the availability of rocks exposed in the drainage basin were a more significant control on differences between the Proto and Meso Orange River deposits clast assemblages than drainage re-organisation.

Rivers vary in their discharge capacity and power through time due to changes in channel dimensions, drainage basin area, gradient, and climate (Schumm and Lichty, 1965; Bull, 1979; Charlton, 2008; Hamers et al., 2015). This impacts their ability to erode and transport sediment of different calibre (size and density), and the clast character (Charlton, 2008). The higher degree of clast roundness in the Proto Orange River gravel relative to the Meso Orange River (Fig. 4.8) either suggests a higher sediment load and/or a higher supply of relatively abrasive

quartzite (Lindsey et al., 2007; Miao et al., 2010). The thicker, and volumetrically larger, Proto Orange River gravel terrace deposits (up to 50 m thick) (Figs. 4.1B, 4.3A) provide evidence for a more powerful river, with higher sediment load, during the incisional phase compared to the Meso Orange River incisional phase with thinner gravel terrace deposits (6-23 m thick) (Fig. 4.1B).

The magnitude of the Cretaceous and Miocene uplift events were greater in the eastern part of the subcontinent (de Wit et al., 2000; Partridge and Maud, 2000) where the Orange River headwaters are located. Within the study area, there is a steeper river gradient of the Proto age Orange River (0.69 m/km) compared to the Meso age Orange River (0.60 m/km) (Fig. 4.1B). A steeper surface gradient would increase the power and carrying capacity of the Proto age Orange River, despite the more sinuous planform.

There is a paucity of Karoo Supergroup basalt clasts in the Proto Orange River gravel (1%) relative to the Meso Orange River gravel (3%) (Fig. 4.7) even though they are derived from the Drakensburg Karoo Supergroup, the youngest member of the Karoo Supergroup (Duncan et al., 1997; Marsh et al., 1997; Jourdan et al., 2007; Hanson et al., 2009), which could be expected to have eroded relatively early in the erosional history of the drainage basin. There are two possible explanations for this difference. Firstly, a wetter and more humid climate both before and during the Proto Orange River period may have eliminated basalt preferentially through chemical weathering (Amiotte Suchet and Probst, 1993; Louvat and Allègre, 1997; Dessert et al., 2001; Malvoisin et al., 2012; Cox et al., 2016). Secondly, the majority of the basalt clasts might have been mechanically broken down during transport in the Proto Orange River period, which would explain their presence only in the smaller size fractions of 3-8 mm (Fig. 4.7C). The presence of unweathered feldspar clasts, in the Proto Orange River gravel (Fig. 4.5D), does not support the hypothesis of climate induced chemical weathering of basalt (Pellant, 2000; Maddy et al., 2012; Tan et al., 2017). In addition, Bluck et al. (2007) and Miller (2008) reported that arid conditions in the region were prevalent in the Eocene, based on the occurrence of thick (18 m) aeolian sandstone overlying basal marine gravel at Buntfeldschuh, an Eocene outcrop of shoreline deposits about 130 km north of the Orange River mouth. Therefore, both Proto and Meso deposits were exposed to similar arid conditions.

Evidence from incision rates and clast roundness suggests that the Proto-Orange River was a higher energy environment than the Meso-Orange River sedimentary system, and one in which basalt clasts would be preferentially mechanically degraded (Fig. 4.8). However, the garnet composition data suggest that the heavy minerals are sourced locally from the Namaqua Metamorphic Complex and Gariiep Belt rocks located in the lower Orange River area (Fig. 4.14). Therefore the heavy mineral anomalies that have been liberated from the mechanical disintegration of catchment area derived Karoo Supergroup basalts could not be established in this study.

The Proto Orange River and older deposits were incised by the Meso Orange River system, and were available to be reworked and incorporated into the Meso Orange River deposits. Locally, downstream reworking of older deposits can be an important process as suggested by the uncharacteristic abundance of Karoo Supergroup shales and sandstones in the Auchas Major Meso deposit (Fig. 4.7). However, in general, the absence of significant reworking of the Proto Orange River deposits is striking (Fig. 4.7). The lack of evidence for extensive reworking is possibly because the Orange River evolved to a straighter planform during the Meso period (Jacob, 2005), such that the Proto Orange River gravel terraces are well preserved because they are largely situated outside the influence of the Meso Orange River. Similarly, the decrease in clast roundness from the Proto to the Meso Orange River deposits suggest minimal reworking and redeposition of older deposits within the study area (Fig. 4.8).

4.4.2 Controls on mineralogy of heavy mineral assemblages

Physical sorting, mechanical breakdown, and dissolution by chemical weathering influence the preservation of heavy mineral assemblages (Morton and Hallsworth, 2007; Weibel and Friis, 2007). The distance a heavy mineral grain travels before deposition depends both on its density and size (Komar and Wang, 1984).

Amphibole-epidote minerals as a group show significant changes in proportion as a fraction of total heavy minerals between the Proto and Meso Orange River deposits (Figs. 4.9, 4.11, 4.13). Amphibole-epidote minerals are sourced from the

local Namaqua Metamorphic Complex rocks (Table 4.1) on the basis that they show a positive correlation with the Namaqua Metamorphic Complex basement clasts (Fig. 4.13). In addition, the similarity in composition of the Orange River garnets and the Namaqua Metamorphic Complex garnets, and to a lesser extent the Gariep Belt garnets, constrain the provenance of the detrital heavy minerals in the Orange River gravels to these rocks (Fig. 4.14). Among the trace minerals in the Orange River gravels (titanite and zircon), titanite has only been reported in the Gariep Belt rocks (Frimmel et al., 1996; Frimmel and Frank, 1998) (Table 4.1) and not in Namaqua Metamorphic Complex rocks. Therefore, titanite provides further evidence for a contribution of the Gariep Belt rocks to the lower Orange River gravels, in addition to the Namaqua Metamorphic Complex rocks among the local rocks.

When considering the burial and diagenetic stability of amphibole and epidote, both minerals have relatively low stabilities (Table 4.2; Morton and Hallsworth, 2007). Commonly, amphibole is absent in buried sediment owing to its chemical instability at depths greater than 600 m (Morton, 1984; von Eynatten and Gaupp, 1999; Mange and Morton, 2007). Similarly, epidote is unstable at depths greater than 1100 m (Morton and Hallsworth, 2007). However, loss of amphibole and epidote due to chemical dissolution alone cannot explain their relatively low abundance in the Proto Orange River deposits, that have a maximum thickness of 50 m (Jacob, 2005) (Fig. 4.1B) and a thin sand cover (< 2 m). Furthermore, chemical weathering is considered unlikely given the presence of unweathered feldspar (Fig. 4.5D) which is very susceptible to hydrous alteration (Deer et al., 2001). The increase of amphibole-epidote content from the Proto to the Meso Orange River deposits (Figs. 4.9, 4.13) could be influenced by the interpreted decrease in river energy that improved the preservation potential of mechanically weaker and softer minerals like amphibole (hardness 5-6) and epidote (hardness 6-6.5; Deer et al., 1992). However, the dominant control on the increase in the proportion of amphibole and epidote (Figs. 4.9, 4.13) is interpreted as a consequence of the larger influx of Namaqua Metamorphic Complex-derived material, as amphibole-epidote display a positive correlation with Namaqua Metamorphic Complex basement clasts (Fig. 4.13).

The downstream decrease of magnetite and increase of amphibole-epidote between Boom and Arrisdrif in the Meso Orange River gravel (Fig. 4.11) coincides with the downstream decrease in gravel grain size and increase in sand content for both Proto and Meso Orange River deposits. Given that both magnetite and amphibole-epidote were liberated from Namaqua Metamorphic Complex rocks and Gariep Belt rocks (Figs. 4.13, 4.14), their different downstream changes in concentrations may be controlled by density, of 5.2 g/cm³ (magnetite) and 2.97-3.13 g/cm³ (amphibole) and 3.3-3.6 g/cm³ (epidote) (Pellant, 2000) where most of the magnetite is retained in the upstream deposits. This trend also suggests that there is no further addition of Namaqua Metamorphic Complex material to the Orange River downstream of Boom. The low abundance of amphibole-epidote in the Auchas Major Meso Orange River sample (Fig. 4.9) coincides with its uncharacteristic high abundance of Karoo Supergroup shale and sandstone (Fig. 4.7), which are characteristic features of the Proto Orange River deposits. This suggests that reworking of the Proto Orange River gravel affected the clast and heavy mineral assemblages by diluting the amphibole-epidote content of the sand sized fractions at this location.

A large percentage of the garnets in the Proto Orange River gravel are relatively coarse (1-2 mm) (Fig. 4.9A) whereas the fine grained garnets (0.5-1 mm and 0.25-0.50 mm) appear to be much less common (Figs. 4.9B, C), presumably removed by higher energy in the Proto period and transported offshore. Imbricated clasts in the Proto Orange River gravel attest to a high energy bedload-dominated river system (e.g., Ashley et al., 1988; Wittenberg, 2002) (Fig. 4.4A).

4.4.3 Implications for river terrace deposits analysis

The clast assemblage of the Proto and Meso Orange River gravel terrace deposits is controlled by catchment-scale processes (Fig. 4.15). In contrast, differences in the heavy mineral assemblages between the two gravels (Figs. 4.9, 4.12) is influenced by local controls, i.e., availability of Namaqua Metamorphic Complex rocks to the Orange River and the preservation potential of amphibole and epidote. This implies that extrinsic controls on clast assemblage and intrinsic

controls on heavy mineral assemblage of the Orange River gravels need to be considered in evaluation of terrace deposits of other bedrock river systems globally. The sand size fraction and the clasts can be derived from different sources such that they carry different provenance signatures and reflect different transport histories. This is likely to be a similar scenario in other continental-scale bedrock rivers. Therefore, prediction of the nature of the fine size fraction on the basis of clast provenance alone is problematic. Mechanically weaker rocks such as basalt may be lost. For example, in this study basalt was mechanically degraded in Proto Orange River deposits. Therefore, using clast assemblage to reconstruct the drainage history of high energy river systems should take into account the possibility of loss of mechanically weaker clasts. Bridgland (1999) used clast analysis to reconstruct the drainage evolution of the Thames River, England, and has argued, on the basis of changes in the composition of clasts, that tributaries have been re-organised over its history and that the river has diverted its course in response to middle Pleistocene glaciation. However, chalk is an important rock type exhumed in the Thames drainage basin. Therefore reconstructing palaeo tributaries that have drained solely through chalk on the basis of clast assemblage alone is problematic in this case because chalk is mechanically weak. Through clast analysis of late Quaternary sediments, Jones (2000) noted a downstream decrease of granite clasts in the Pineta Basin, Spain, and attributed it to mechanical breakdown. If these Pineta Basin sediments were deposited by a higher energy river system, the granite clasts might have been broken down and their signature lost. In such cases, an integrated analysis of clast assemblages and heavy mineral assemblages would be a better approach because heavy minerals would have survived mechanical breakdown and retained the granite signature. Therefore, the heavy mineral assemblage technique is a useful tool for studying drainage basin evolution in areas where rivers and their associated tributaries drain areas whose geology is dominated by mechanically weaker rock types. Studies that have used clast analysis to deduce provenance of sediments have made an implicit assumption that sand sized sediments are also from the same source as the clast size sediments (e.g., Bridgland, 1999; Mikesell et al., 2010). Such studies of clast assemblages are not able to investigate whether the provenance signature carried by the pebble size clasts is only for the clast population and not for the sand size fractions.

This study has shown that assessment of the controls on clast and heavy mineral assemblages needs to be treated separately due to the differences in density and surface area that affect the preservation and behaviour of pebble size clast and sand sized heavy minerals. However, despite different factors controlling the clast assemblage and heavy mineral contents of the lower Orange River gravels, the Proto and Meso Orange River deposits differ in terms of both clasts and heavy minerals. The heavy mineral data in this study, as exemplified by a downstream decrease in magnetite content suggests that the signal propagates downstream. This has implications for the predictions and assessment of offshore records of sediment provenance.

In summary, most studies have reconstructed the drainage evolution of rivers by either using clast assemblage or heavy mineral assemblage insolation. Here, a rare integrated dataset that clasts and sand-sized matrix material of gravel deposits can have different provenance and controls, and this is reflected in the different transport distances. Therefore, clast assemblage analysis should not be used uncritically as a proxy for the character of the matrix and vice versa. An integrated approach in analysis of these important but fragmented archives is recommended to improve prediction of offshore resources using source-to-sink approaches.

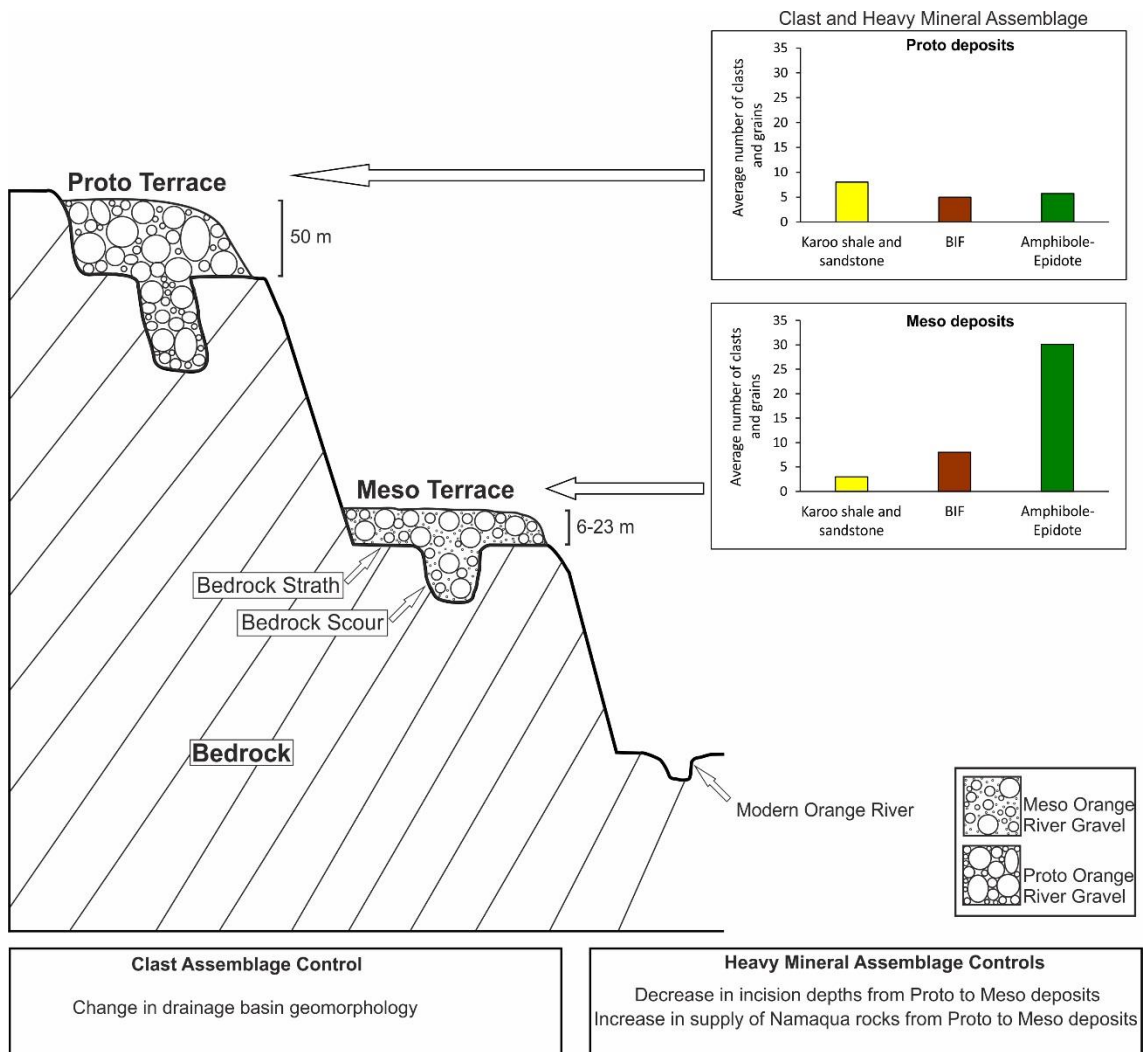


Figure 4.15 Clast and heavy mineral assemblage of the Proto Orange River and Meso Orange River deposits and the respective controls affecting the differences.

4.5 Conclusions

This study has integrated clast assemblage and heavy mineral assemblages to investigate the character and controls in a series of bedrock confined river terrace deposits formed during degradation and aggradation cycles by the palaeo-Orange River, a continental-scale river system. The Proto Orange River gravel at Auchas Major Deposit has been reworked by the Meso Orange River introducing a significant amount of Karoo Supergroup sedimentary clasts into, and diluting the amphibole-epidote content of, the Meso Orange River gravel. There is only local evidence of reworking of Proto Orange River gravel into other deposits at Auchas Major. The differences in clast character and type between the Proto and Meso Orange River deposits can be linked to a more powerful river system during Proto times driven by a changing drainage basin geomorphology, rather than reworking of older deposits or changes in provenance. The decrease in incision depths, and sediment transport from Proto to Meso Orange River deposits was accompanied by an increase in the proportion of sediments supplied to the river from local lithologies including Namaqua Metamorphic Complex rocks. This change is reflected by the increase of amphibole-epidote in the heavy mineral assemblages, which was derived from the erosion of Namaqua Metamorphic Complex rocks, from Proto to Meso Orange River times. This study indicates that clast assemblage analysis should not be uncritically used as a proxy for the character of the matrix and vice versa, and that an integrated approach is needed to improve the prediction of heavy minerals, including placer minerals, in ancient river terrace deposits and their offshore time equivalent deposits. An integrated approach is recommended when assessing these important archives of the links and controls between drainage basin evolution, and the stratigraphic record of sedimentary basins.

Chapter 5 The relationship between bathymetry, geomorphology and the distribution of heavy minerals

5.1 Introduction

The application of heavy minerals to continental shelf and deep sea sediments studies has concentrated mostly on constraining sediment provenance (e.g., Pujos et al., 1990; Morton et al., 2005; Cascalho and Fradique, 2007; Hallsworth and Chisholm, 2008; Tsikouras et al., 2011; Cao et al., 2015) and sediment transport pathways (e.g., Frihy and Dewidar, 2003). Heavy minerals in offshore settings have also been widely used in the oil and gas industry where they are used in hydrocarbon reservoir evaluation particularly in correlating sedimentary units which lack biostratigraphic markers and primary sedimentary structures (Morton, 2007; Poulsen et al., 2007). Studies that have used heavy minerals to characterise sediments and assess sedimentation patterns in offshore settings are rare (e.g., Frihy, 2007). Despite extensive and detailed clast characterisation of Proto and Meso Orange River deposits conducted by Jacob (2005), no detailed clast assemblage work has been done on the coeval Atlantic 1 gravel deposits. In this study the Proto and Meso Orange River deposits have been further classified using heavy mineral assemblage; and the clast assemblage and heavy mineral assemblage have been correlated (Chapter 4). In the absence of clast assemblage, heavy minerals are used for the first time to characterise the Atlantic 1 gravels and assess their evolution and sedimentation patterns in response to incision and aggradation cycles on the lower Orange River (Fig 5.1).

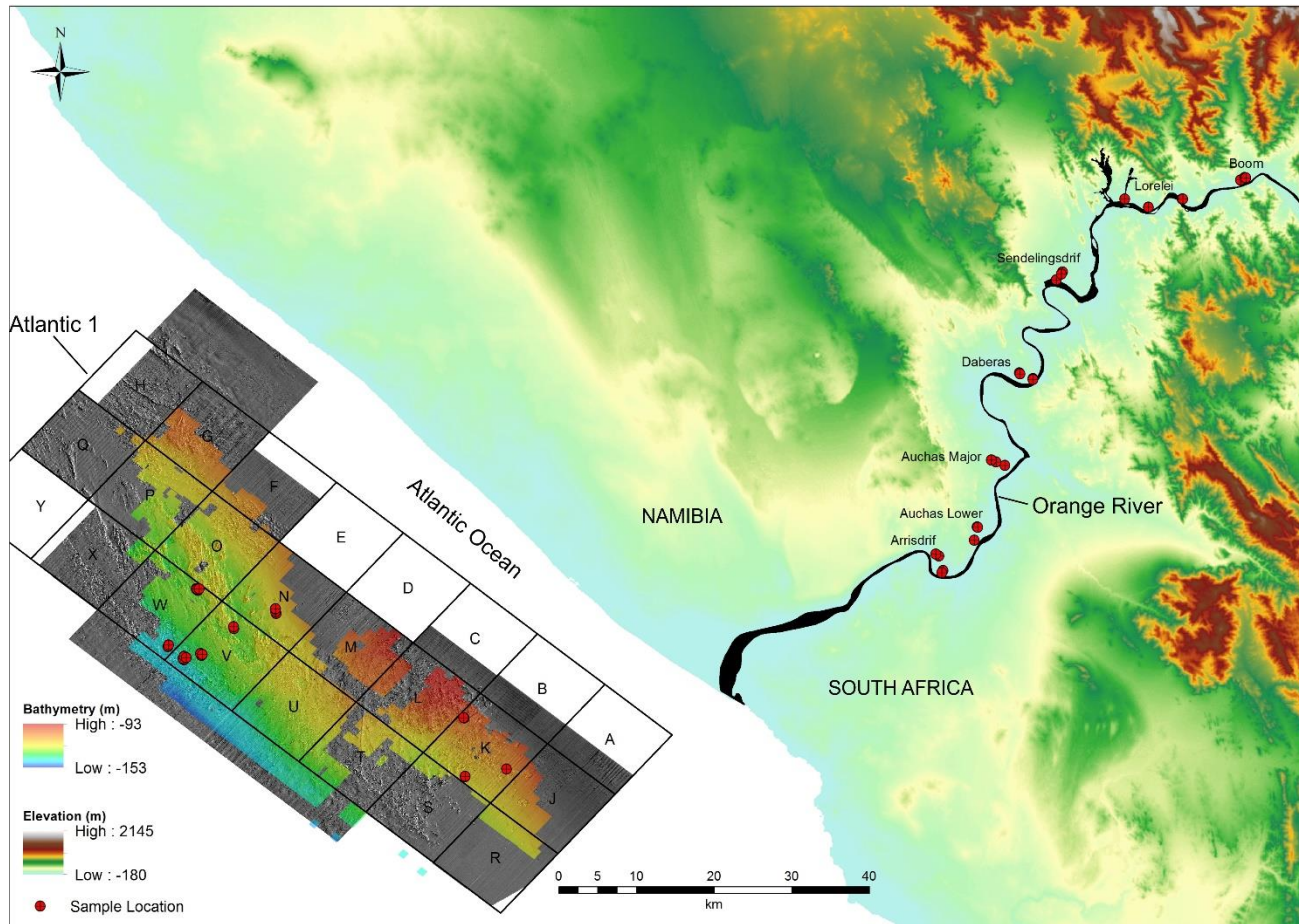


Figure 5.1. Location map of Atlantic 1 with respect to the lower Orange River. Onshore elevation after Jarvis et al. (2008).

5.2 Geological Setting

The geology of Atlantic 1 is made up of Cretaceous, Eocene, Miocene and Pleistocene sedimentary units (Fig. 5.2A). These sedimentary units form a basement to the diamondiferous gravel that is in turn overlain by unconsolidated overburden sand. The thickness of the gravel is variable but gravel in excess of 7 m has been reported (Mubita et al., 2015). The Cretaceous unit comprising of clay and sandstone occur along the eastern margin of Atlantic 1 (Fig. 5.2A). Eocene clay, cemented sandstone and conglomerate occur primarily offshore of the Cretaceous unit. The Miocene unit consisting of clay, unconsolidated sand and conglomerate occur further offshore in the west and they are bordered on the western side by Miocene carbonates (Fig. 5.2B) (Mubita et al., 2015). Sporadic Pleistocene unit consisting of sandstone and conglomerate occurs in the southern part of Atlantic 1 (Fig. 5.2A). Although the Cretaceous, Miocene and Eocene sedimentary units predominates in certain areas of Atlantic 1, they are faintly expressed in other areas of Atlantic 1. An exception are the Miocene carbonates that are restricted to the most offshore area of Atlantic 1 (Fig. 5.2B).

5.2.1 Cretaceous unit

The entire eastern margin of Atlantic 1 from north to south, is made up of Cretaceous clay and sandstone. The thick and soft to hard clay footwall is punctuated by a series of offshore dipping (5°) grey to light brown sandstone layers (Fig. 5.2B) that are believed to have been tilted during rifting (Mubita et al., 2015) possibly during the same rifting event that led to the formation of the Cambrian foreland Nama Basin (Frimmel and Frank, 1998; Grotzinger and Miller, 2008). Cretaceous clay is very thick and no drilling has been done through the clay to determine if there is any hard rock below the clay. Also no geophysical data is available on the lithology below the thick clay (Fig. 5.2B). In addition to being sandwiched between clay, sandstone also outcrops in places. Sandstone in the most southern part (Region K and Region J) is cemented.

5.2.2 Eocene unit

Clay, gritty sandstone and conglomerate make up the Eocene unit. The Eocene clay is overlain by outcropping coarse grained cemented gritty sandstone and sporadically by conglomerate outcrops (Mubita et al., 2015). In places, the cemented sandstone has been eroded forming north-south orientated linear depressions that are perpendicular to the coastline. Within the depressions, the underlying clay is exposed and the depressions are filled with gravel together with slabs of the weathered cemented sandstone (Mubita et al., 2015).

5.2.3 Miocene unit

The offshore area of Atlantic 1 is covered by Miocene sediments (stratified sandstone, conglomerate, clay and unconsolidated sand) of clastic origin. Miocene clastics are deposited on top of either the Cretaceous clay or the Eocene unit (Fig. 5.2B). The marine Miocene carbonates, spatially restricted to the offshore most part of Atlantic 1, are exclusively underlain by Miocene clastics (Fig. 5.2B).

5.2.4 Pleistocene unit

Minor sporadic occurrences of the Pleistocene unit, consisting of sandstone and conglomerate, occur in the southern part of Atlantic 1 (Fig. 5.2A). The Pleistocene unit is deposited on a flat Cretaceous clay and it is overlain by Holocene mud (Fig. 5.2).

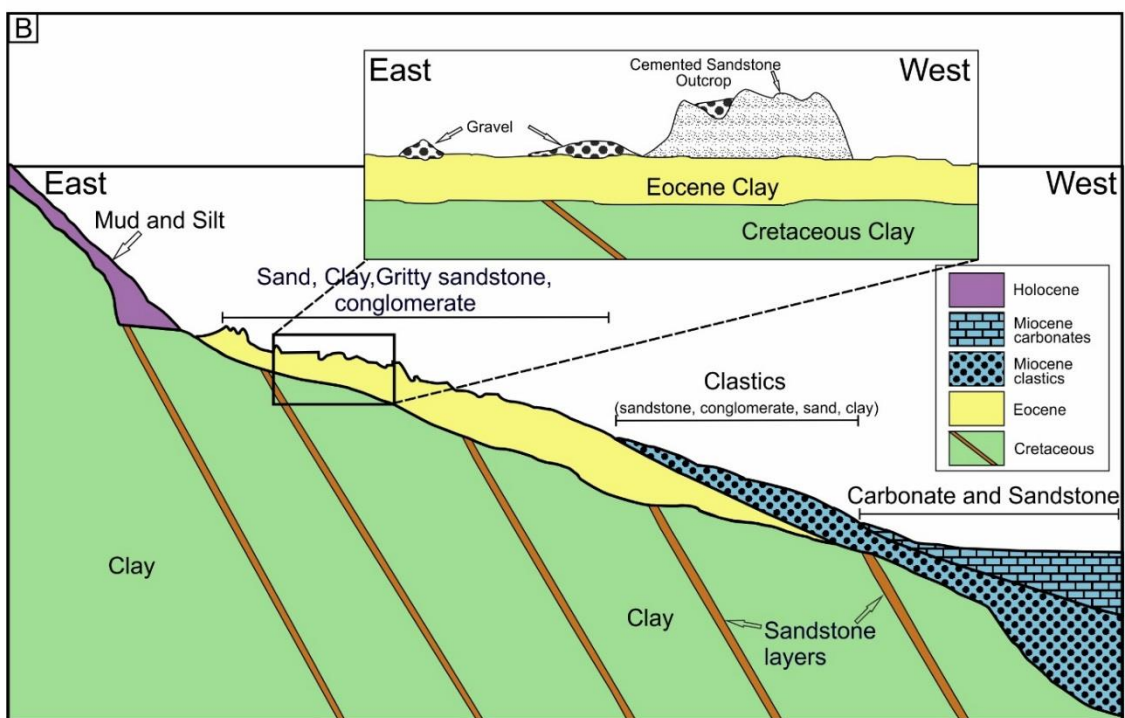
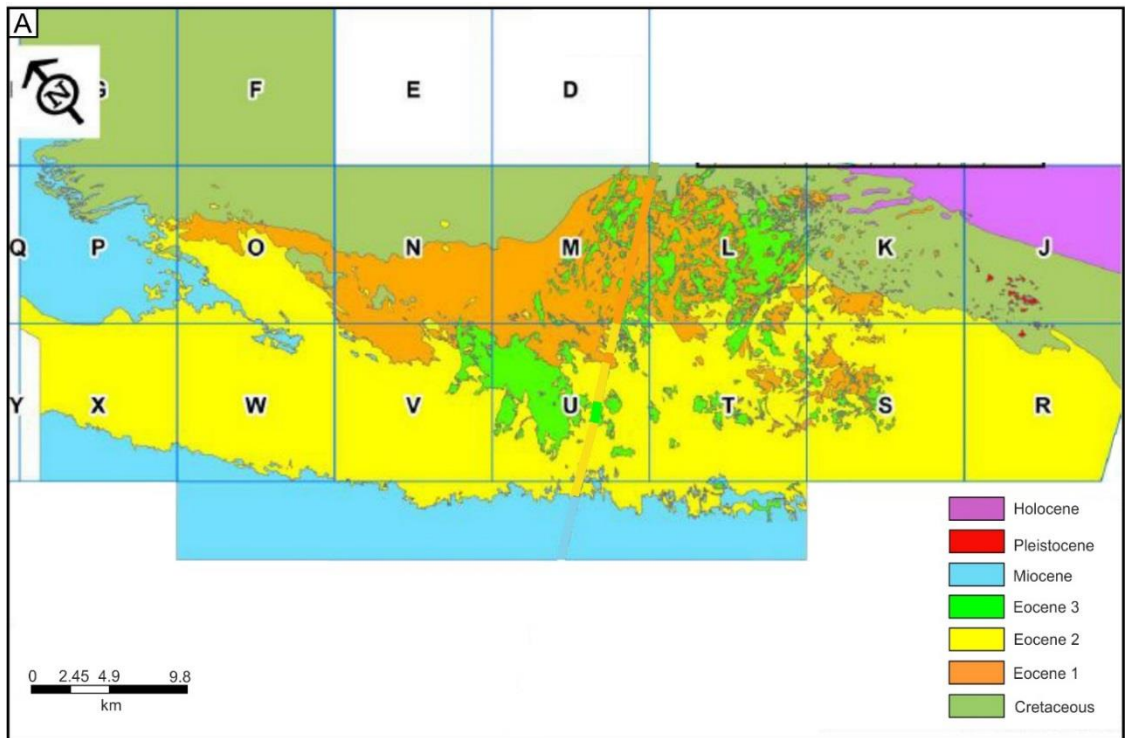


Figure 5.2 (A) Stratigraphy of Atlantic 1 geology. (B) Representative cross section of sedimentary geology of Atlantic 1. Both figures modified from Mubita et al. (2015).

5.3 Sea Level Changes in Southern Africa

Changes in relative sea level affects the distribution of sediments in shallow marine settings (Leeder, 1999). A fall in relative sea level exposes shelf sediments to entrainment and redistribution by fluvial and aeolian erosion (Leeder, 1999). To understand the evolution of the terrigenous gravel deposits in the Atlantic 1 region, it is important to understand relative sea level changes that have affected the southwestern African continental margin.

Global sea level changes is well-documented albeit subject to disagreements on the rate and magnitude of eustatic sea level change (e.g., Vail et al., 1977; Haq et al., 1987; Miller et al., 1991a; Miller et al., 1991b; Miller et al., 1998; Miller et al., 2004; Miller et al., 2005; Lambeck et al., 2014; Dutton et al., 2015). A general consensus exists regarding the main drivers of global sea level changes: waxing and waning continental ice sheets (Vail et al., 1977; Miller et al., 1998; Leeder, 1999; Miller et al., 2005; Lambeck et al., 2014) and plate tectonics (Pirazzoli, 1996; Leeder, 1999; Miller et al., 2005). Important variations from the global sea level curve, such as isostatic variations from ice loading, and tectonic activity (Kuhlmann et al., 2010) are minimal to absent offshore Namibia. Similarly, the effects of thermal subsidence on sea level in southern Africa should be minor to absent because the rate of thermal subsidence on passive continental margins over the last 135 Ma has been low (0.03 mm/yr) (Pirazzoli, 1996). Therefore, the global sea level curve of Miller et al. (2005) can be used as proxy for the southern African region.

Most of the sea level work done in the region has concentrated on the Quaternary period (e.g., Ramsay, 1995; Ramsay and Cooper, 2002; Compton, 2006; Stollhofen et al., 2014), with limited research undertaken on the relative sea level record of southern Africa during the Paleogene and Neogene. Siesser and Dingle (1981) investigated shoreline movements around southern Africa from the Paleogene to present, and identified three major events: i) Late Paleocene-Early Eocene transgression, ii) Oligocene regression, and iii) Middle to Late Miocene transgression (Fig. 5.3). The Orange River-derived Eocene marine gravel

outcropping along the Namibian coast (160-170 m above sea level) (Stocken, 1978; Bluck et al., 2007) supports the Late Paleocene-Early Eocene transgression (Fig. 2.5A, Chapter 2). The Oligocene regression is marked by a widespread unconformity on the continental shelf (Dingle, 1971; de Vera et al., 2010) that is supported by Oligocene fluvial river channel incision in the Cape Canyon (Pether et al., 2000). The Middle to Late Miocene transgression around southern Africa is evidenced by the occurrence of estuarine *Serpulid Polychaete* worm tubes found in the Miocene gravels at Arrisdrif located 30 km northeast of the modern Orange River mouth (Corvinus, 1978; Hendey, 1978) indicating higher sea levels. The magnitude of the regressions and transgressions of Siesser and Dingle (1981) appears to be overestimated in comparison to the global record (Miller et al. 2005).

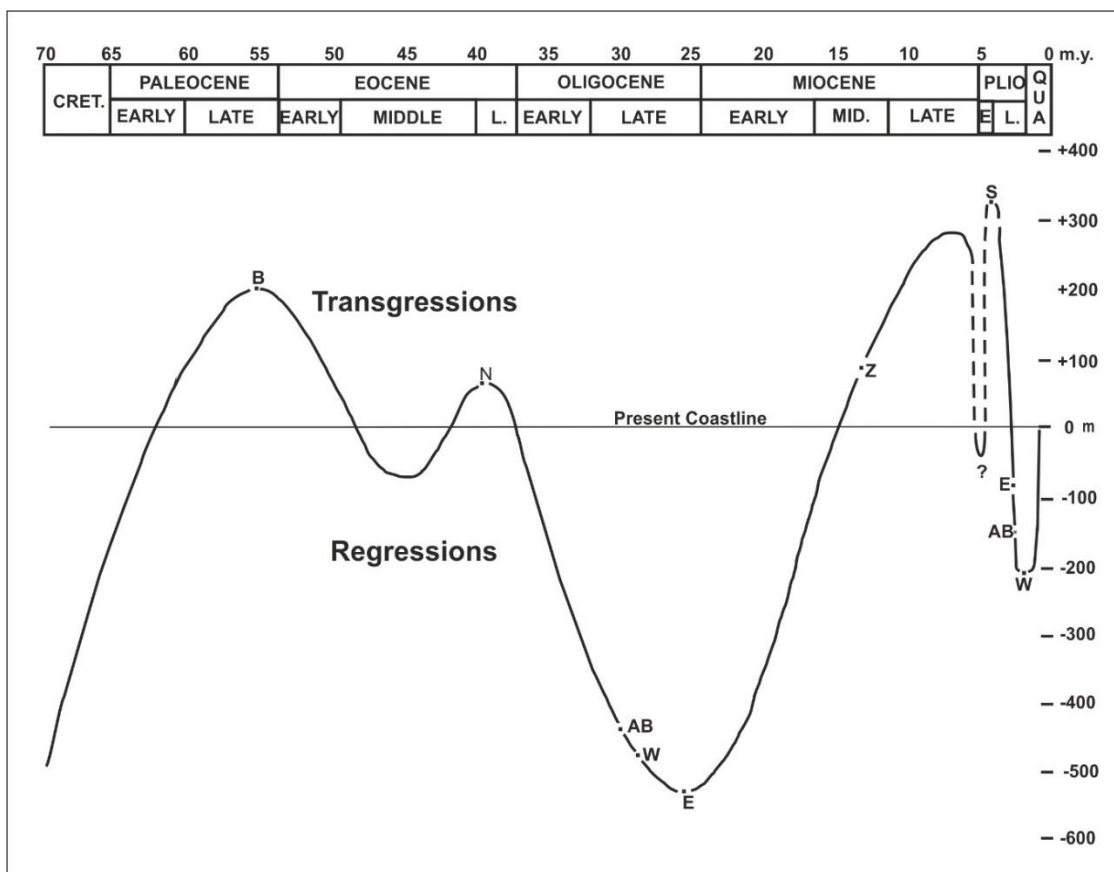


Figure 5.3 Sea levels associated with shoreline movements in southern Africa between the Cretaceous period and Quaternary. Outcrop localities on which the interpretation are based are denoted by letters; AB – Agulhas Bank, B- Birbury, E- east coast, N – Namibia, S – south coast, W – west coast, Z – Zululand. Modified from Siesser and Dingle (1981).

During the Late Paleocene-Early Eocene, global sea level is suggested to have risen to 70-100 m, and then fell 70 to 100 m since the Early Eocene (Miller et al., 2005). The magnitude of Early Miocene sea level drop (Miller et al., 2005) agrees with the non-drowning of the Eocene shoreline, that sits at 160-170 m above mean sea level along the Namibian coast (Stocken, 1978; Bluck et al., 2007). During the last glacial maximum of Late Pleistocene, sea level reached 120 m below mean global sea level (Miller et al., 2005; Lambeck et al., 2014; Dutton et al., 2015).

Warm water bivalve shells at Bogenfels Pan, 165 km north of the Orange River mouth, have prompted Compton (2006) to suggest a middle Holocene high sea level stand of 3 m above mean sea level. This middle Holocene high sea level stand has also been recorded globally (Miller et al., 2005; Lambeck et al., 2014).

5.4 Oceanographic Setting

The Atlantic 1 gravel deposits are located offshore southern Namibia, on the continental shelf (Fig. 5.1). The Namibian continental shelf is unusual in that it is wide (35-100 km) (Dingle, 1973; Bremner, 1981; Bremner and Willis, 1993; Goudie and Viles, 2015) and deep (inner shelf up to 130 m, middle shelf 200 m and outer shelf 200-400 m) (Bremner and Willis, 1993; Compton and Bergh, 2016). Globally, the deepest continental shelves are those on glacial margins of the Arctic Oceans (average depth of 405 m) (Paris et al., 2016). The Atlantic 1 region is on the inner shelf (Rogers and Li, 2002) with the seabed at 90-153 m below mean sea level (mbmsl). Another distinctive characteristic is the thin sediment veneer on the shelf due to limited subsidence (Dingle, 1973) since the Cretaceous. The thin sediment veneer on the inner shelf can either be explained by transfer of terrigenous sediments to the offshore Orange Basin on the continental slope or northward aeolian transfer of the sand and finer size sediments in mobile sand dunes of the extensive Namib Sand Sea (34 000 km²) (Lancaster, 1985). The extensive size of the Orange Basin (160 000 km²)

(Kuhlmann et al., 2010) and its thick depocentre (1500-2200 m) (Brown et al., 1995; Hirsch et al., 2010; Guillocheau et al., 2012) all suggest that the Orange Basin has been a sink for most of the sediments that may have accumulated on the inner shelf. Offshore Namibia, submarine canyons (18 km long and 400-500 m deep) occur on the outer shelf and the upper slope (Bagguley and Prosser, 1999) and these present another important mechanism for transporting sediments from the continents to the deep sea. However, Bagguley and Prosser (1999) noted that the majority of the canyon systems (four out of six canyons) that formed during the Cretaceous-Cenozoic boundary in the Orange Basin are detached canyons dominated by mass transport systems as opposed to transporting fluvial sediments. If Orange River-derived sand that comprise the Namib Sand Sea as far as 1750 m from the mouth of the Orange River (Garzanti et al., 2014; Garzanti et al., 2015) had remained in the marine environment the sediments on the shelf would have been thicker to an extent in light of limited accommodation space.

Waves along the Namibian coast originate from the southwest (Decker, 1988; Compton and Bergh, 2016) with an average height of 2 m (Bosman and Jourbert, 2008), driven by a strong south-westerly wind that has been in operation since the Eocene (42 Ma) (Bluck et al., 2007). However, winter storm waves can reach excess of 5 m high (Rossouw, 1984). The south-westerly wind plays an important role in transporting sand and finer sediments northward. The tidal range in the region is microtidal (Goudie and Viles, 2015) with spring tide amplitudes at 1.4 m (Laudien et al., 2003). At Oranjemund, in the vicinity of the Orange River mouth, the tidal range is 1.8 m (Bluck et al., 2007).

The Benguela current is an important upwelling system on the inner shelf, which is driven by longshore trade winds (Diester-Haass et al., 2002; Monteiro et al., 2005; Edelman-Furstenberg, 2014; Nagel et al., 2016). The Benguela current brings cold nutrient-rich water to the surface (Kristmannsson, 1999) and operates within a 50 km wide band (Mohrholz et al., 2014).

The exhumed Neoproterozoic basement of metamorphic rocks and granites is restricted to the shelf area near the coastline, in a 4-12 km wide stretch from the coastline westward (Dingle, 1973). Locally, Orange River-derived gravel deposits overlie Cretaceous mudstone (Mubita et al., 2015). Diester-Haass et al. (1988)

and Holtar and Forsberg (2000) relate the mudstone to an Orange River origin. No coring results in the public domain confirm the thickness of the Cretaceous mudstone succession. The stratigraphic transition from Orange River derived Cretaceous clay to Cenozoic gravel on the Namibian shelf prompted Bluck et al. (2007) to argue that the Orange River evolved from a fine grained river system to a coarse grained cobble and pebble river system. Aizawa et al. (2000) reached a similar conclusion that during the Cretaceous more than 90% of sediments delivered by the Orange River to the Atlantic was mud. This transition coincides with a major Late Cretaceous uplift and exhumation event in southern and western Africa (de Wit, 1999; Stevenson and McMillan, 2004; Tinker et al., 2008b; Guillocheau et al., 2012; Richardson et al., 2016; Richardson et al., 2017).

5.5 Seabed Morphology and Bathymetry

5.5.1 Bathymetry and landforms

For comparison purposes in this study Atlantic 1 is divided into four domains based on bathymetry data and seabed geomorphology. These are Southeast, Northeast, Northwest and Southwest (Fig. 5.4). The Atlantic 1 regions sampled in this study are Region K, Region N, Region V and Region W (Fig. 5.4). Of these sampled regions, Region K falls in the Southeast Domain, Region N is located in the Northeast Domain whereas Regions V and W are part of the Northwest Domain (Fig. 5.4). The western most part of Regions V and W make up the Southwest Domain.

5.5.2 Southeast Domain

This domain is the closest to the Orange River mouth (Fig. 5.4). The water depth is much shallower (100-122 mbmsl) meaning long periods of exposure during sea level lowstands. The Southeast Domain is characterised by thick sediments. Sediment thickness decreases from the eastern part towards the western part of the domain (Fig. 5.5). The seabed character of the Southeast Domain is a smooth seabed marked by absence of topographic features. Linear erosional features

are notably absent (Fig. 5.5), and minor isolated gritty sandstone outcrops occur (Fig. 5.6). There are two styles of bathymetry in the Southeast Domain, a subdued smooth area and also rough patchy areas (Fig. 5.6).

5.5.3 Northeast Domain

The seabed has little relief from bedforms with no significant undulations. Mubita et al. (2015) attributed the smooth sea bed to thick overburden sand. A broad shallow depression (water depth range: 119-123.5 mbmsl) that is sheltered on the western side by a low Eocene sandstone ridge occurs in Region N and part of Region M (Fig. 5.7). The shallow depression with a smooth seabed expression and the absence of major geomorphic features indicate that this domain may have represented a low energy environment, such as a lacustrine system or inlet, during sea-level lowstands.

5.5.4 Northwest Domain

The most distinctive features in Atlantic 1 are north-to-south erosional features and east-to-west orientated ridges that are parallel and perpendicular to the coastline, respectively (Figs. 5.8, 5.9, 5.10). The north-to-south orientated erosional features are within cemented Eocene sandstone (Mubita et al., 2015) and are 147-2136 m wide, 7-16 km long, and are 6-7 m deep. In this domain, the seabed occurs at much deeper water depths (120-130 mbmsl). There is a second set of shallow depressions that are perpendicular (east-west oriented) to the coastline and these occur in the northern part of the Northwest Domain (Fig. 5.8). According to Mubita et al. (2015), the east-west oriented features are sandstone ridges. Where the ridges are prominent, the area is characterised by thin overburden sand cover (Mubita et al., 2015). Spatially, the difference between the north-to-south and east-to-west features is that the latter were completely exposed during the Pleistocene low sea level (Fig. 5.4). The gullies in the Neoproterozoic metamorphic basement of the raised beach gravels have the same east-west orientation (Jacob et al., 2006) (Fig. 5.11).

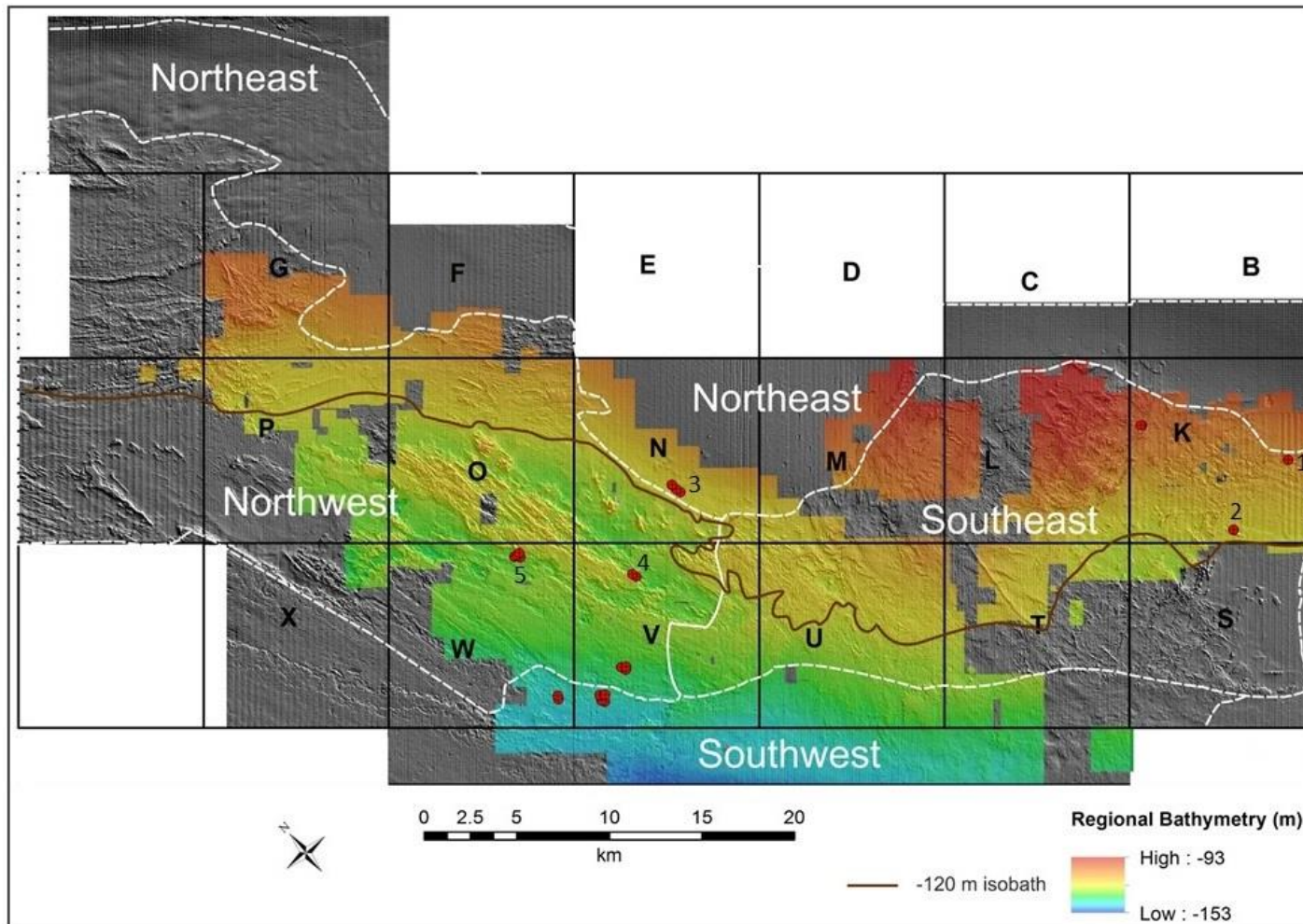


Figure 5.4 Bathymetry domains of the Atlantic 1 region. Red symbols denotes sample locations. The brown solid line represent the approximate last sea level low stand (-120 m isobath). Numbers 1, 2, 3, 4 and 5 indicate the location of the bathymetry sections shown in Figures 5.4, 5.5, 5.6, 5.8 and 5.9, respectively.

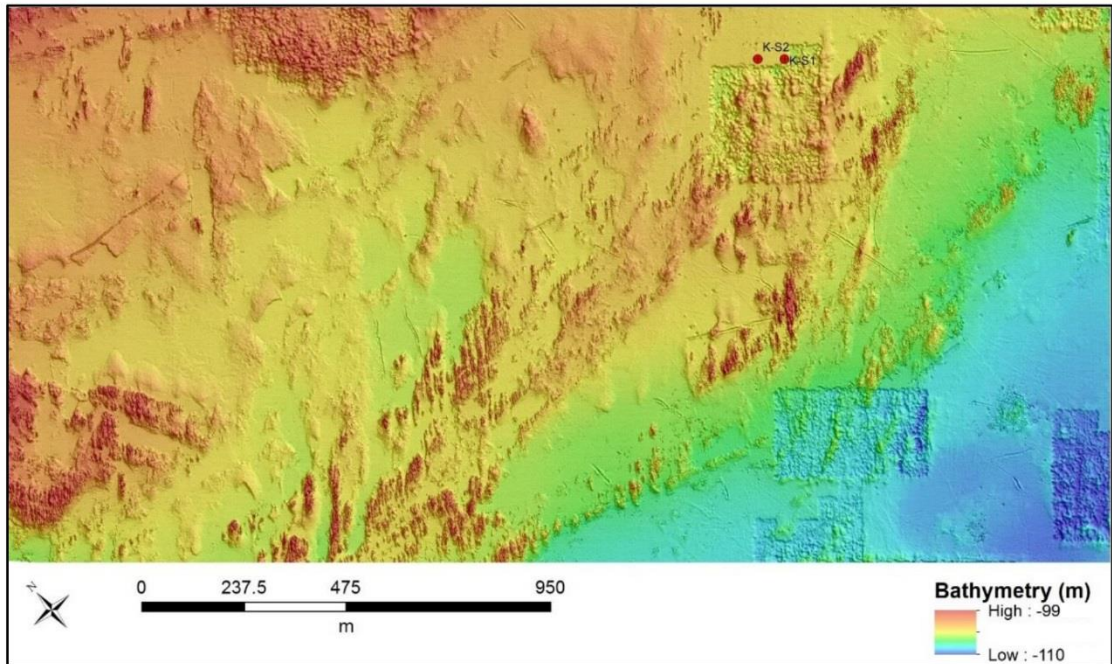


Figure 5.5 Representative bathymetry of the Southeast Domain. Location of the area shown is denoted by 1 in Figure 5.3. Red dots indicate sample positions.

5.5.5 Southwest Domain

This domain is the deepest and farthest offshore of the four domains and is marked by the seaward end of erosional features in the Northwest Domain, possibly due to sediment infill. Day et al. (1992) reported erosional features covered by sediments on the middle shelf. However, analysis of the seismic sections taken from this domain has not revealed any covered erosional features.

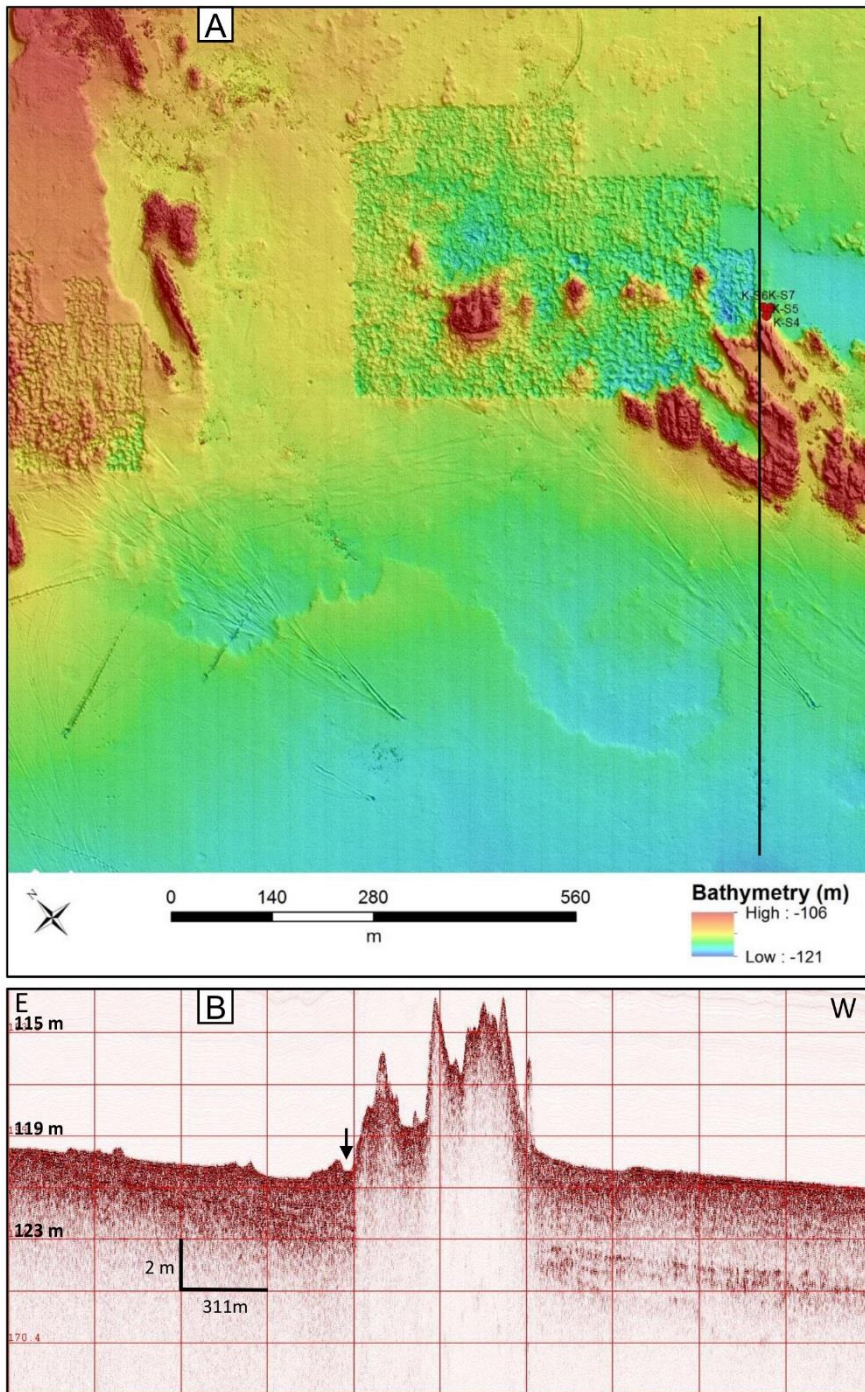


Figure 5.6 Representative sea bed morphology of the Southeast Domain as seen from the bathymetry and associated seismic data. The location of the area shown is denoted as 2 in Figure 5.3. Sample positions (red dots) indicated on the bathymetry map in (A) are denoted on the seismic section in (B) by the black arrow. Black line in Figure A marks the position of the seismic section.

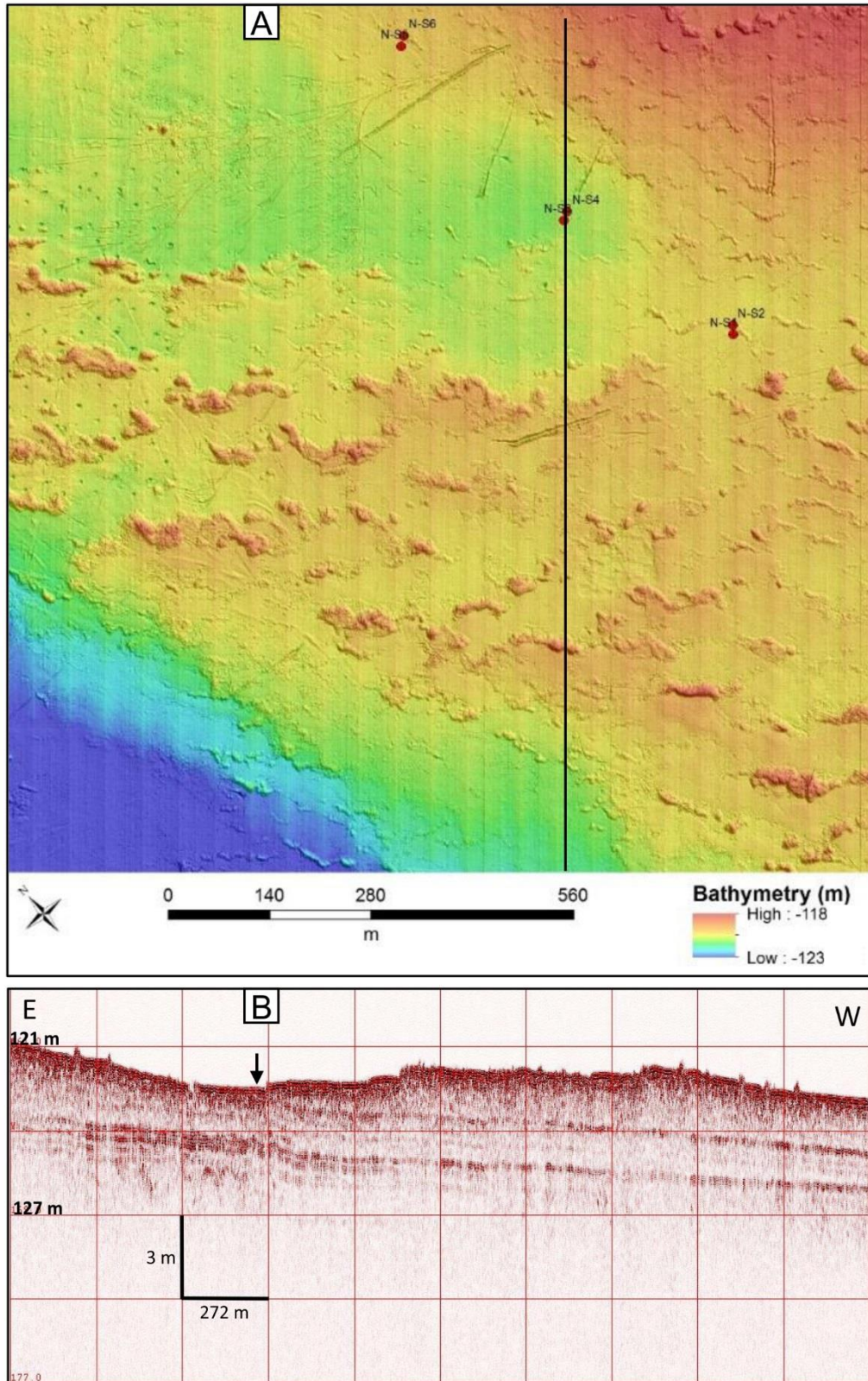


Figure 5.7 Shallow broad depression bordered in the west by a ridge, Region N, Northeast Domain. Location of the area shown is denoted by 3 in Figure 5.3. Black line in Figure A marks the position of the seismic section.

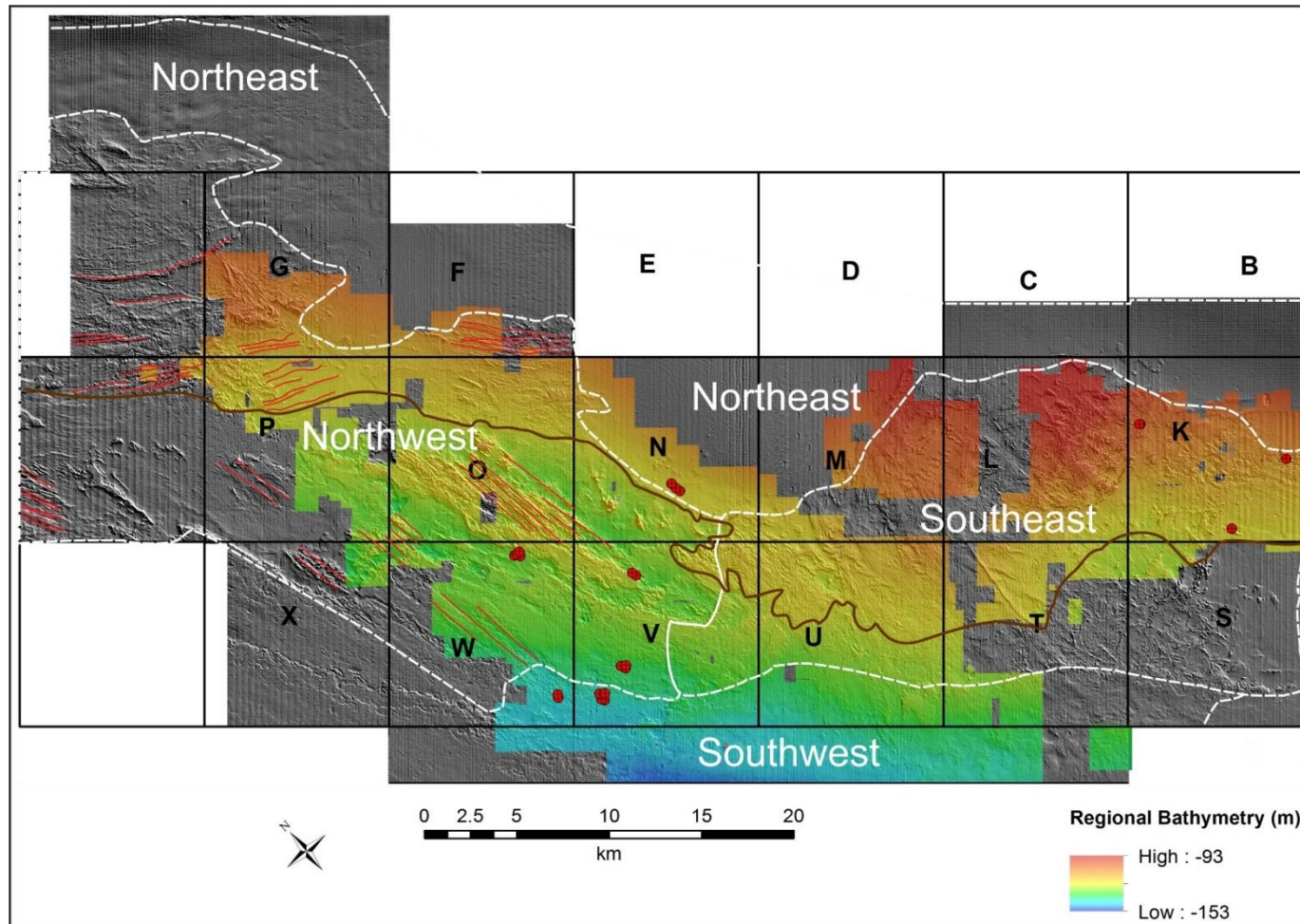


Figure 5.8 Coast parallel and coast perpendicular linear features (red lines) in the Northwest Domain. Red symbols denotes sample locations. The brown solid line represent the approximate last sea level low stand (-120 m isobath). Refer to Figure 5.1 for regional reference.

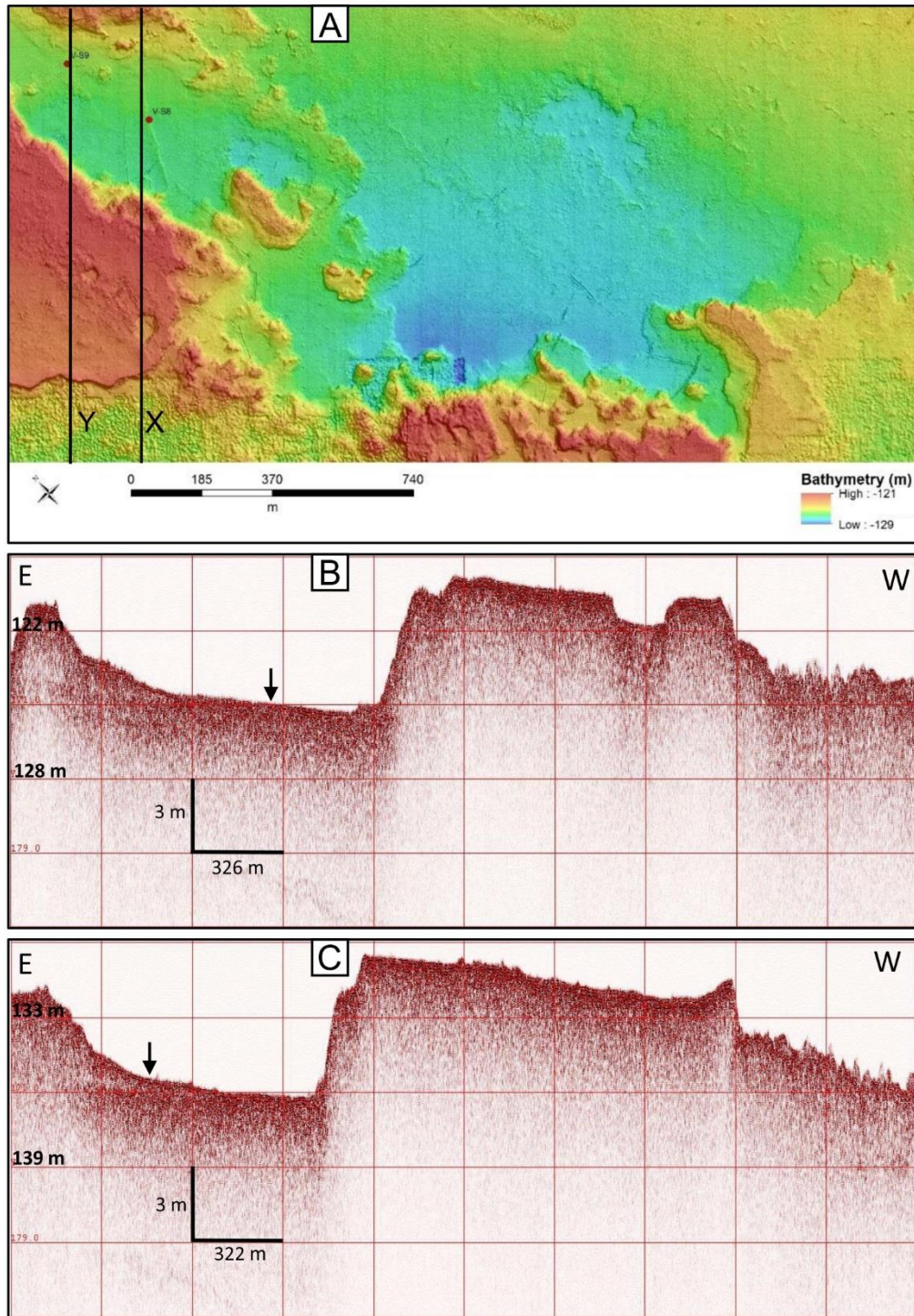


Figure 5.9 Coast parallel erosional features in Region V, Northwest Domain. Location of the area shown is denoted by 4 in Figure 5.3. Black lines in Figure A labelled X and Y indicate positions of seismic sections for Figure B and Figure C, respectively. Arrows in Figures B and C indicate sample locations denoted by red circles in Figure A.

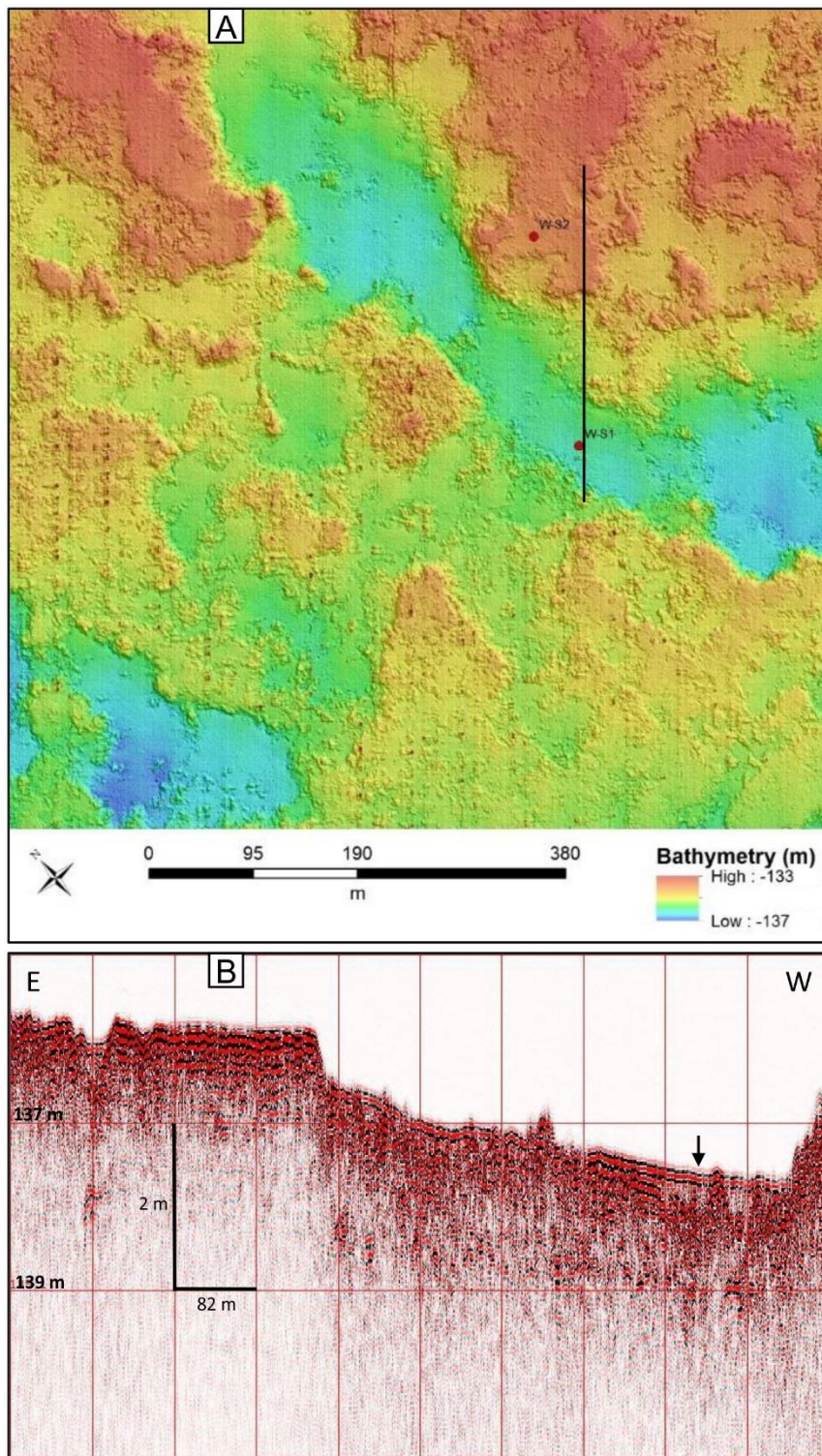


Figure 5.10 Coast parallel features in the Region W, Northwest Domain. Location of the area shown is denoted by 5 in Figure 5.3. Black line in Figure A marks the position of the seismic section in Figure B.

5.6 Heavy Mineral Assemblages

Heavy minerals present in Atlantic 1 gravel are garnet, magnetite, ilmenite, epidote and amphibole, clinopyroxene and apatite (Figs. 5.12 - 5.16). There is no substantial difference between all the sampled regions in terms of the proportion of garnet (Fig. 5.16). In both the eastern and western domains, magnetite displays a northward decreasing trend (Figs. 5.16, 5.17B). Amphibole-epidote content is higher in Region K, and decreases offshore to Regions V and W, particularly in the 0.5-1 mm and 0.25-0.50 mm size fractions (Fig. 5.16). Region N samples have amphibole-epidote content similar to, but lower than, that of Region K samples in the 0.25-0.5 mm size fraction, but trace amphibole-epidote content in the coarse size fractions (1-2 mm and 0.5-1 mm) (Fig. 5.16). For example, in the 0.25-0.50 mm size fraction, amphibole-epidote content is 12.1% and 9.3% in Region K and Region N, respectively whereas it is lower in Region V (1.7%) and Region W (1.1%). Clinopyroxene occurs only in Region K gravel (Figs. 5.12, 5.16B, 5.16C) with the exception of four clinopyroxene grains recorded from a single Region V sample (V-S8) (Fig. 5.14C). The clinopyroxene grains contain intergrowths of plagioclase and titanomagnetite (Fig. 5.18).

Apatite grains are black, brown and green in colour. There are two sets of apatite, namely biogenic and authigenic (Fig. 5.19). The biogenic apatites, dominantly made up of animal shells, are black and brown whereas authigenic apatite grains are green. Therefore, the authigenic apatite have been plotted separately. Also, the authigenic apatites show a distinct offshore increase (Region V and W) (Figs. 5.16B, C). For example, the average authigenic apatite concentration is 3%, 3.3%, 8.4% and 12.6% for Regions K, N, V and W, respectively, in the 0.25-0.50 mm size fraction (Fig. 5.16C).

When compared, there is no notable difference in heavy mineral concentrations between samples located within north-south orientated erosional linear depressions and those that are located outside the linear features from the same region, Region V (Fig. 5.20). A similar pattern could not be established for Region W, which also has linear features, because all the samples from this region are located within the linear features. The composition of the Atlantic 1 garnets is

similar to that of the Namaqua Metamorphic Complex and the Gariiep Belt garnets (Fig. 5.21).

5.7 Mineral Grain Size Distribution

None of the regions display a strong preferential enrichment in minerals of specific sizes (Fig. 5.22). For example, amphibole-epidote content is higher as a fraction of all heavy mineral grains in Region K in both the coarse size fractions (1-2 mm) and the finer size fractions (0.5-1 mm and 0.25-0.5 mm) (Fig. 5.22C). Garnet is the only mineral that shows a slight enrichment of coarse garnets (1-2 mm) in the offshore direction where the average number of garnet grains are 74, 60, 151 and 82 for Region K, Region N, Region V and Region W, respectively whereas the trend is reversed in the fine size fraction (0.25-0.50 mm; Region K = 218, Region N = 239, Region V = 200, Region, W = 226). It is notable that in the fine size fraction (0.25-0.50 mm) the elevated ilmenite content in Region V (Fig. 5.22D) coincides with its higher magnetite content in the same size fraction (Fig. 5.22A). The sand size fraction of Region K and Region N gravel is much coarser than that of Regions V and W (Fig. 5.23).



Figure 5.11 Coast perpendicular gullies in the bedrock of raised beach gravels exposed after mining. Photographs taken looking west.

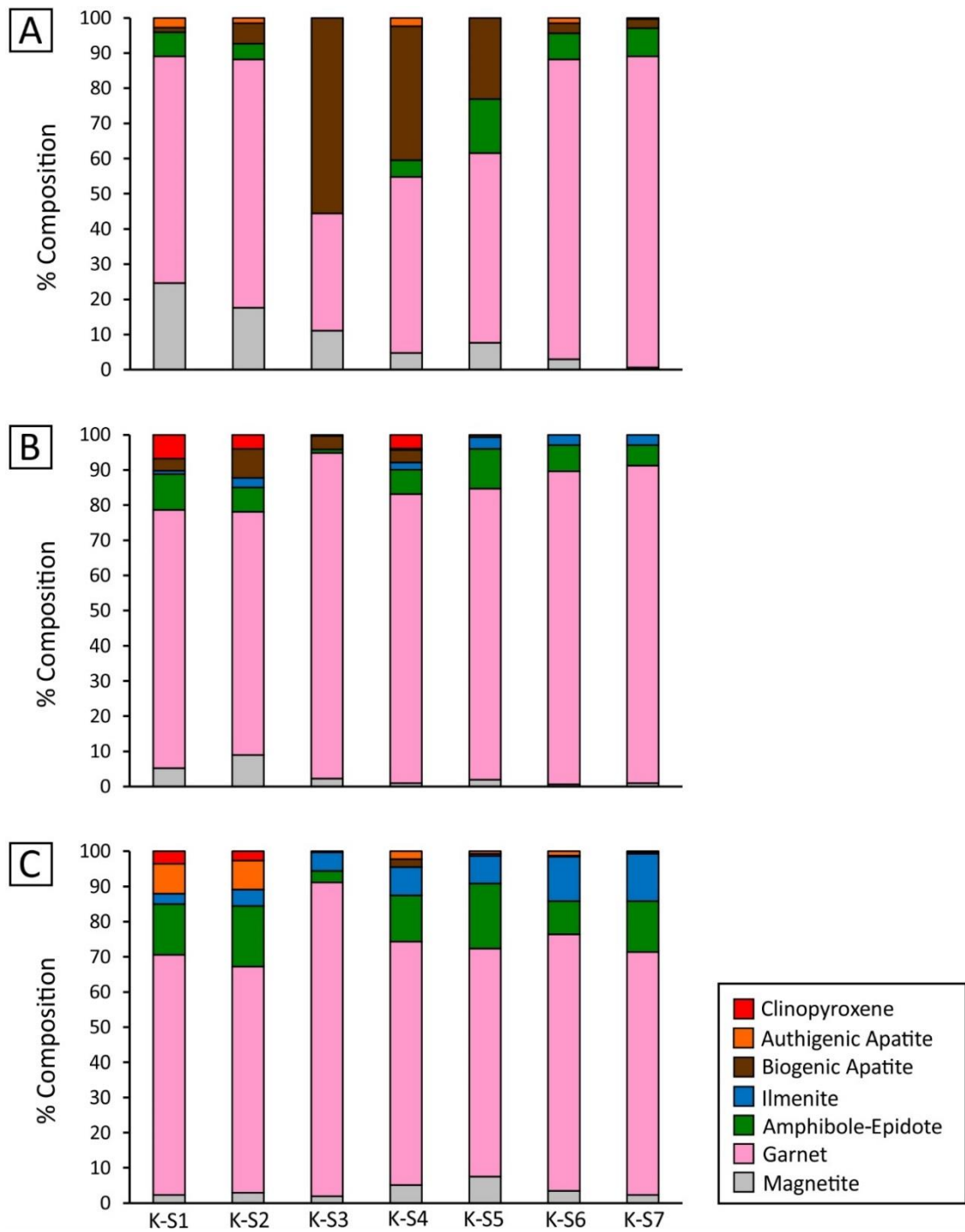


Figure 5.12 Heavy mineral assemblage of Region K. Figures A, B, C represent size fractions 1-2 mm, 0.5-1 mm and 0.25-0.50 mm, respectively.

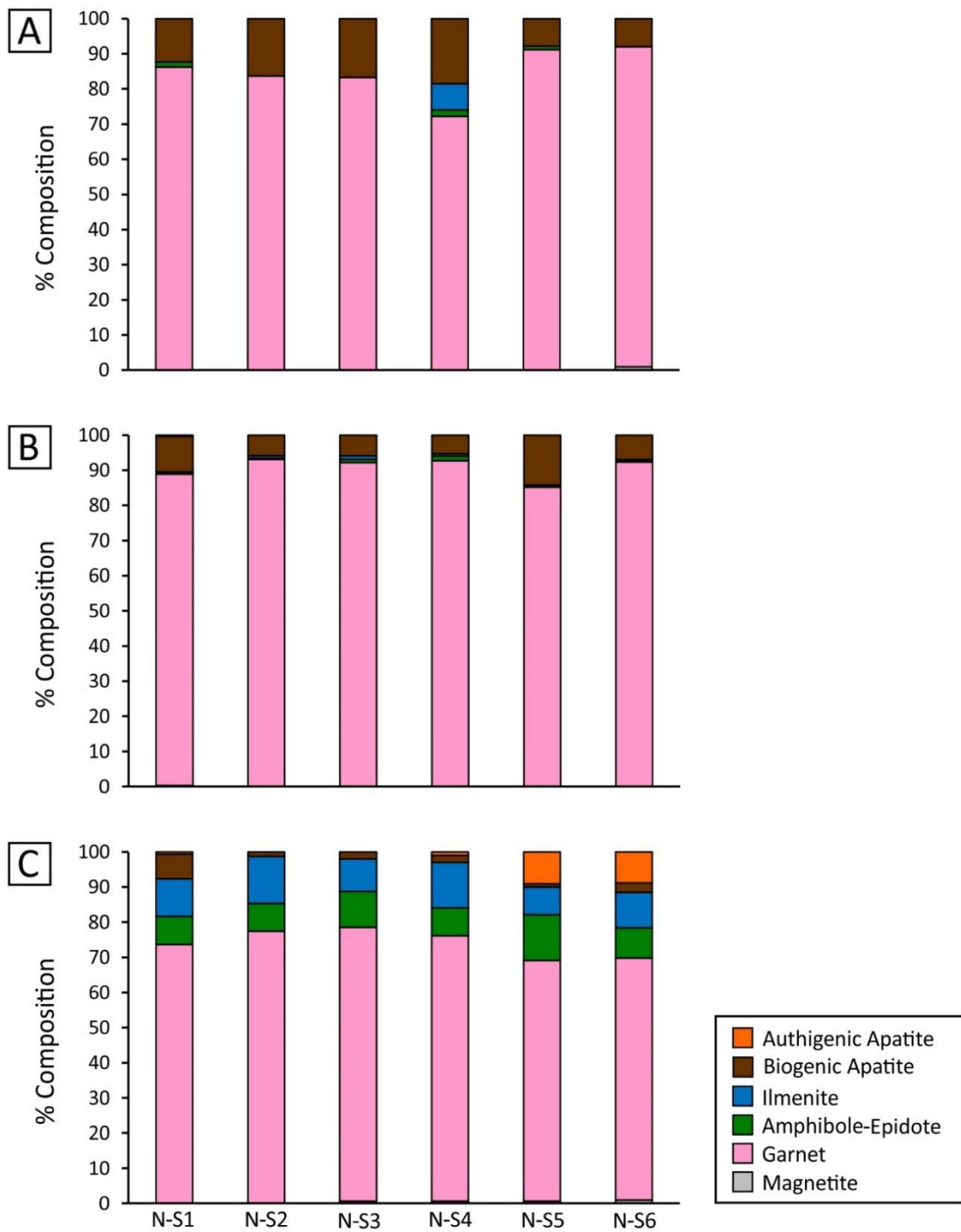


Figure 5.13 Heavy mineral assemblage of Region N. Figures A, B and C represent size fractions 1-2 mm, 0.5-1 mm and 0.25-0.50 mm, respectively.

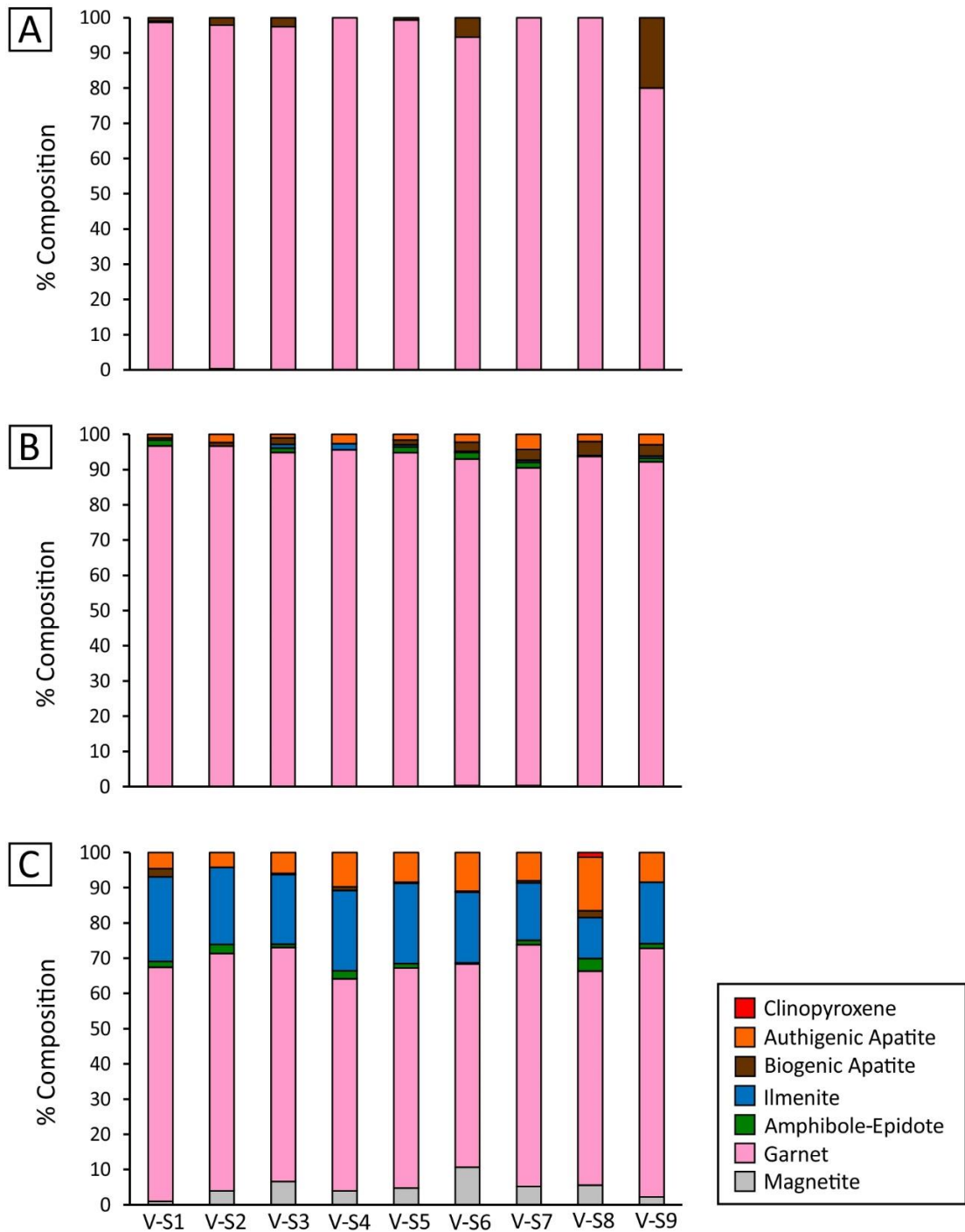


Figure 5.14. Heavy mineral assemblage of Region V. Figures A, B, C represent size fractions 1-2 mm, 0.5-1 mm and 0.25-0.50 mm, respectively.

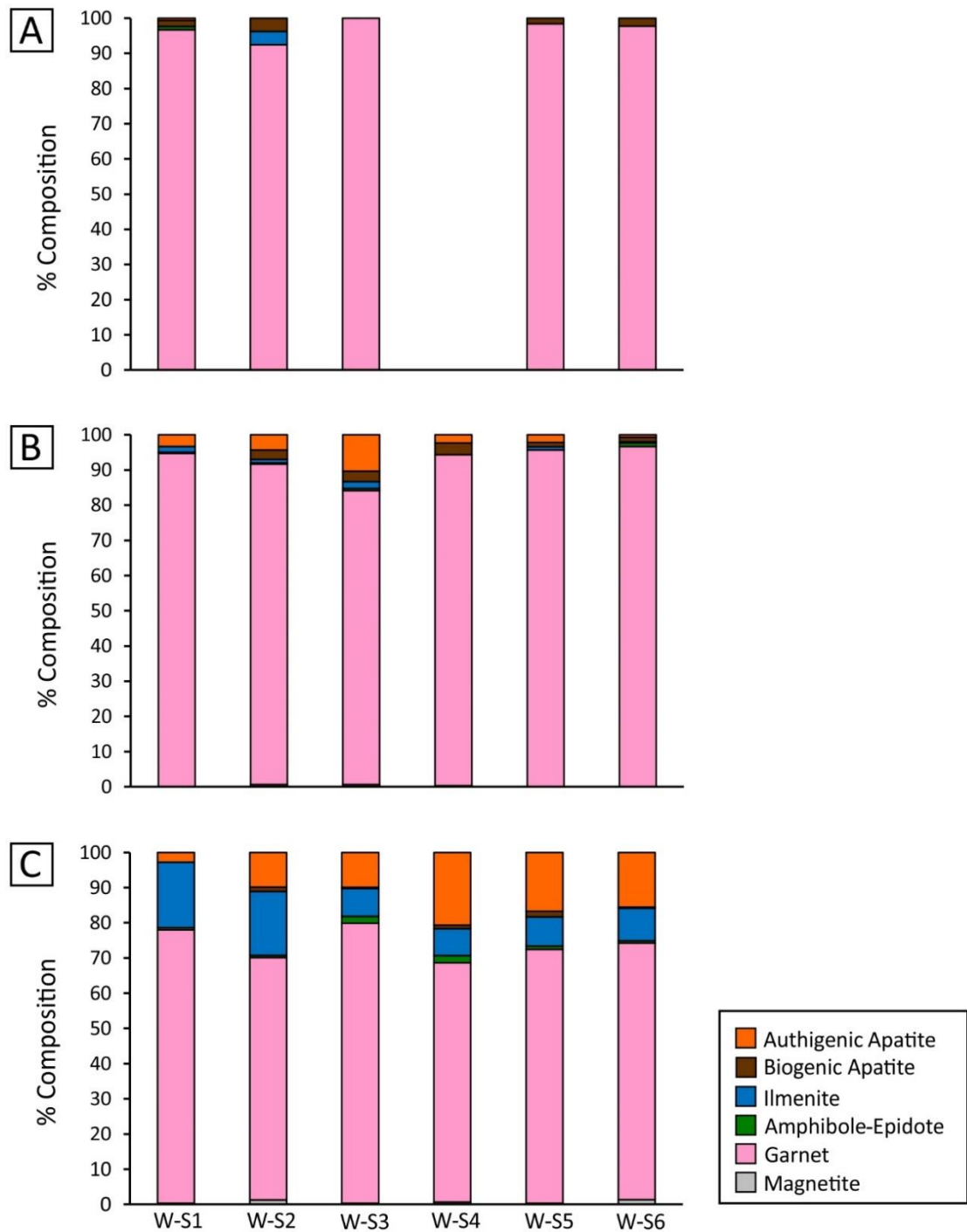


Figure 5.15. Heavy mineral assemblage of Region W. Figures A, B, C represent size fractions 1-2 mm, 0.5-1 mm and 0.25-0.50 mm, respectively. No heavy mineral was recovered in sample W-S4 in the 1-2 mm size fraction.

5.8 Discussion

With the exception of apatite, the heavy minerals present in Atlantic 1 (magnetite, garnet, ilmenite, epidote and amphibole) are the same minerals that are present in the Proto and Meso Orange River gravels (Figs. 5.12, 5.13, 5.14, 5.15, 5.16). Clinopyroxene recorded in Region K is present in the modern Orange River gravels. Therefore, the majority of the Atlantic 1 heavy minerals can be considered to have been transported to the coast, together with diamonds, by the Orange River, with redistribution by the interplay of marine (including tidal), fluvial and aeolian processes. The heavy minerals are sourced from Namaqua Metamorphic Complex and Gariep Belt rocks that form the basement of the lower Orange River, as evidenced by a positive correlation between amphibole-epidote and Namaqua Metamorphic Complex rocks clasts (Fig. 4.13, Chapter 4). Importantly, garnet composition of the Atlantic 1 deposits are similar to that of the Namaqua Metamorphic Complex and, to a lesser extent, Gariep Belt garnets (Fig. 5.21). Also, these minerals are reported to be present in the Namaqua Metamorphic Complex rocks (Eglington, 2006; Bial et al., 2015). Offshore in Atlantic 1, the footwall on which the basal gravel rest is sedimentary either thick clay (>8 m) or sandstone (Fig. 5.2). Neither the thickness of the clay footwall nor the rock type below the clay is known because these have not been intersected with core.

Apatite is authigenic or marine detrital in origin, and was formed *in situ* in Atlantic 1. This is supported by apatite absence in the alluvial lower Orange River gravels. Regionally, authigenic apatite has been reported both south and north of the Orange River mouth. *In situ* authigenic phosphorite nodules occur in basal gravels along the Namaqualand coast, within 20 km south of the Orange River mouth (Pether, 1986). North of the Orange River mouth offshore Walvis Bay extensive (24, 700 km²) high grade (19 wt.% P₂O₅) phosphorite deposits have been reported by Compton and Bergh (2016).

Factors that may have influenced the heavy mineral distribution in Atlantic 1 include sea bed geomorphology, sea water chemistry, sediment transport and sea level and these are discussed in detail below.

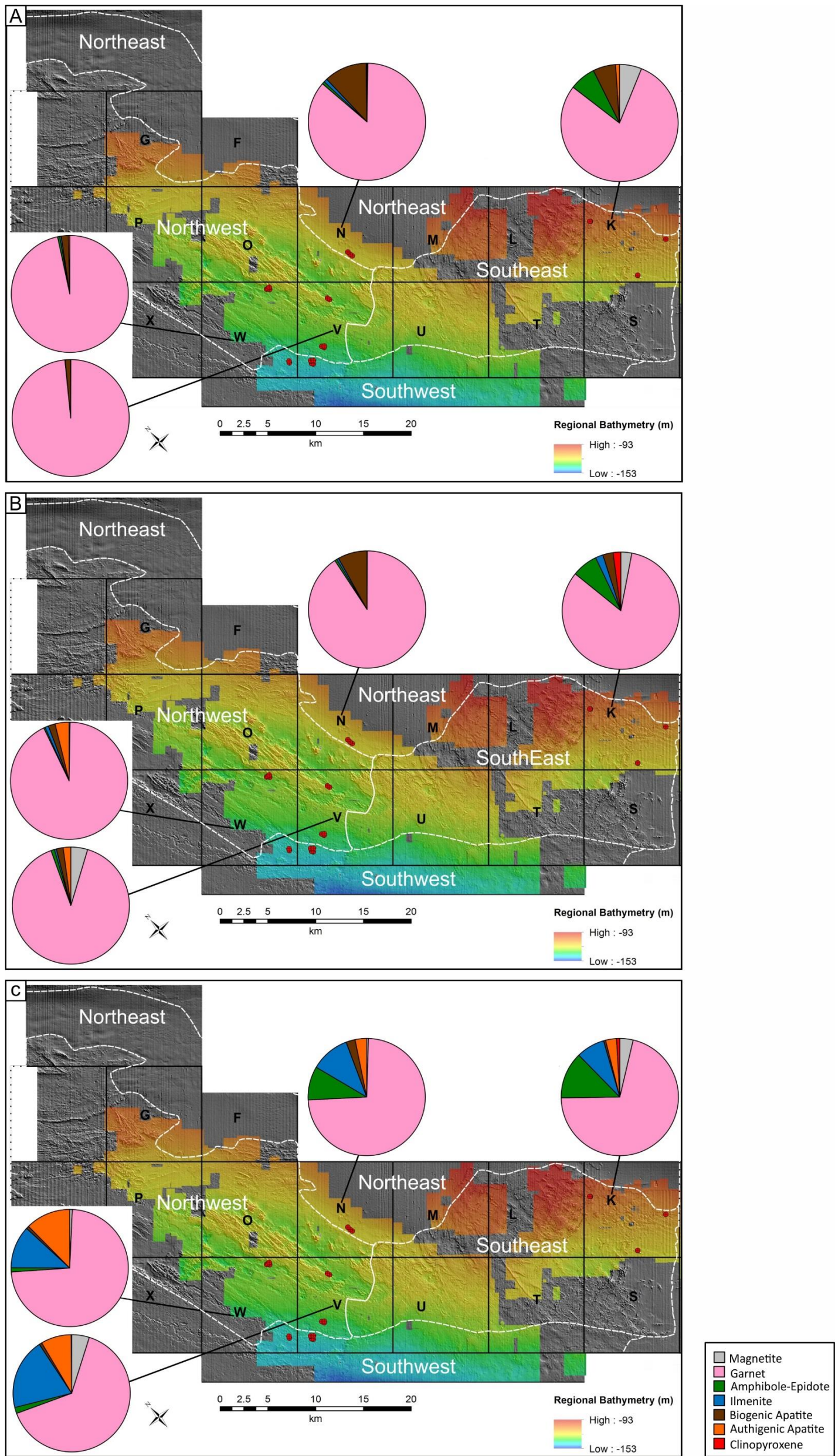


Figure 5.16 Spatial distribution of heavy mineral assemblage in Atlantic 1. Figures A, B and C represent 1-2 mm, 0.5-1 mm and 0.25-0.50 mm, respectively.

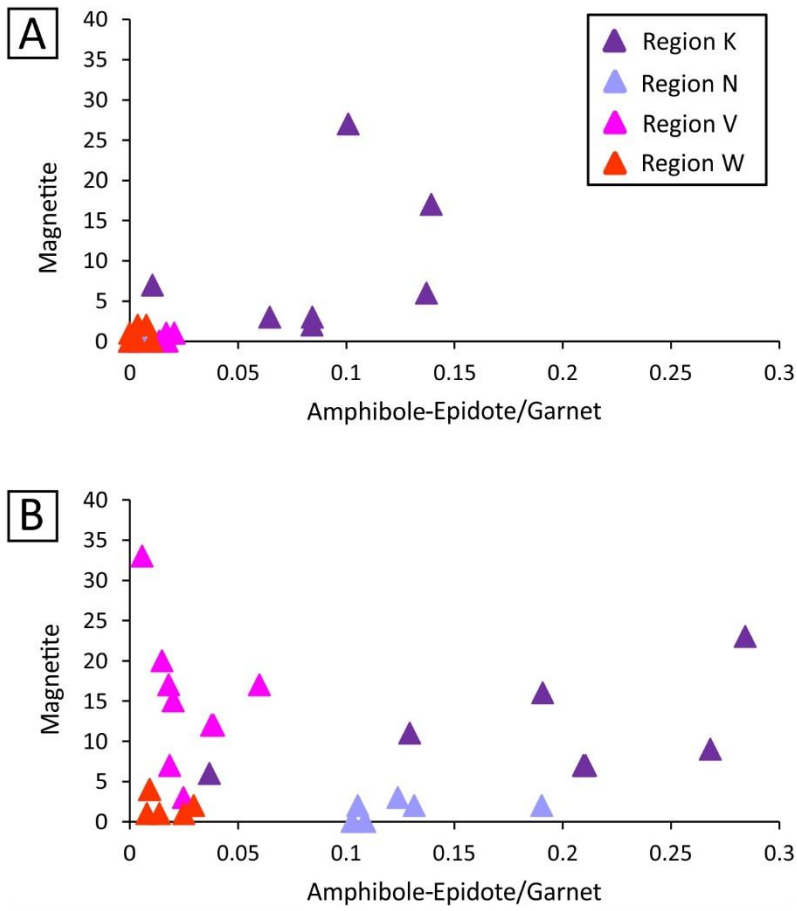


Figure 5.17 Difference in magnetite content between Regions K, N, V and M. Figures A and B represent size fractions 0.5-1 mm and 0.25-0.50 mm, respectively.

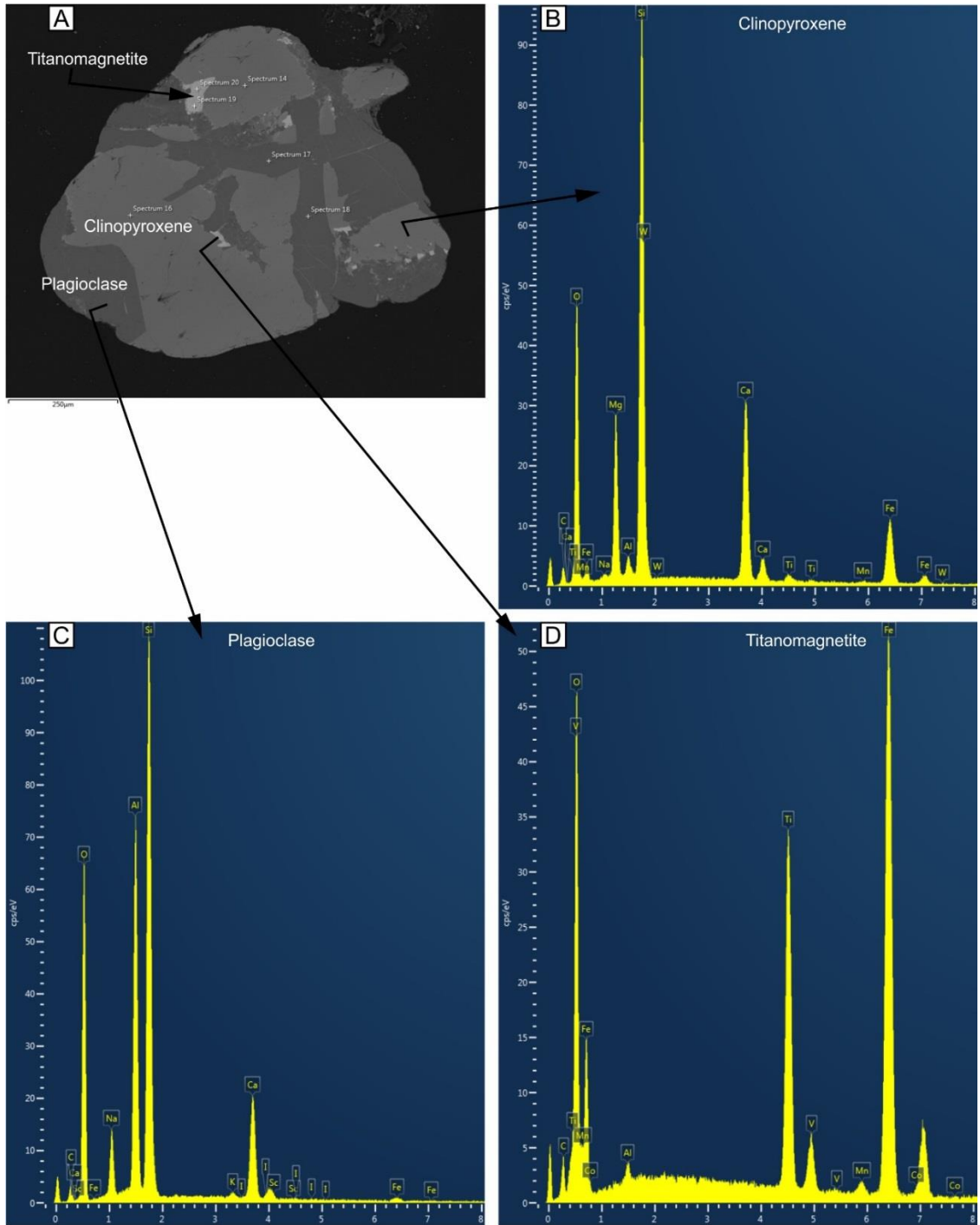


Figure 5.18 (A) SEM image of clinopyroxene (light grey) with plagioclase (dark grey) and titanomagnetite (white) intergrowth. Figures B, C and D show EDS spectrums of clinopyroxene, plagioclase and titanomagnetite, respectively. The y-axis in Figures B, C and D represent peak count intensity.

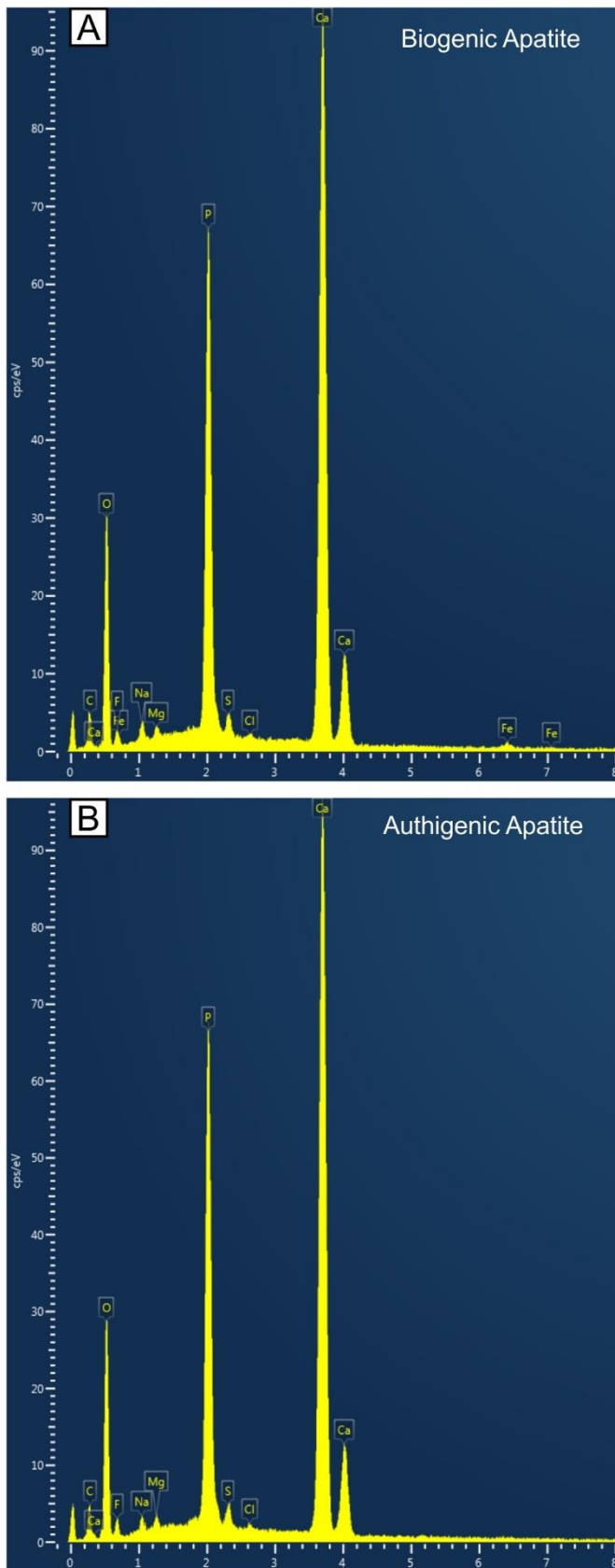


Figure 5.19 Compositional difference between biogenic apatite (A) and authigenic apatite (B). The y-axis in Figures A and B represent peak count intensity.

5.8.1 Sea Bed Geomorphology

The coast parallel features carved in cemented Eocene sandstone in the southern part of the Northwest Domain are enigmatic (Fig. 5.8), and their process of origin is poorly constrained. Day et al. (1992) reported similar 15-20 m deep coast parallel features on the middle shelf, 80 km north of the Orange River mouth, that they have interpreted to be fluvial channels. There is no evidence of a palaeo river north of the Orange River mouth that can be linked to these coast parallel features, and their straight morphology and orientation suggests they are not fluvial in origin. The coast parallel features on the inner shelf in Atlantic 1 could have been formed by aeolian erosion. Their north-south orientation is the same as the prevailing southerly wind direction along the Namibian coast (Bluck et al., 2007), and there are many landforms attributed to net erosional aeolian processes farther to the north (Miller, 2008). However, this area remained submerged even at the lowest Pleistocene sea-levels (Fig. 5.4).

Another set of erosional features that have a different orientation are east-west orientated features that are perpendicular to the coast (Fig. 5.8). Their orientation is different from the wind direction but they have the same orientation as the gullies of the raised beaches located in the surf-zone suggesting that they were formed at similar water depth (Fig. 5.11). Of note is that these east-west orientated features were exposed during the lowest Pleistocene sea-levels (Fig. 5.4). Although still not well understood processes proposed to have formed the gullies of the raised beaches are formation by merging of potholes (Wright, 1964) and exploitation of weakness in rocks such as joints (Jacob et al., 2006). Therefore the coast perpendicular features in Atlantic 1 are possibly formed by the same processes to that of the gullies of the raised beaches because they have the same east-west orientation despite different lithology in which the gullies are carved. The east-west orientated features in Atlantic 1 are within Cretaceous sandstone (Mubita et al., 2015) whereas the gullies of the raised beaches are within Neoproterozoic Gariiep Belt metamorphic rocks (Jacob et al., 2006).

In the Northwest Domain, there is no difference in either garnet, magnetite, amphibole-epidote or ilmenite content between samples that are located within the coast parallel linear depressions and those that are outside the linear features (Fig. 5.20). Therefore, the geomorphology of the sea bed did not influence the

distribution of the heavy minerals in Atlantic 1. This lack of relationship is striking because heavy minerals would be expected to be preferentially trapped and concentrated inside the linear features. This further supports the argument that Atlantic 1 gravels did not undergo extensive erosion and recycling of sediments. Erosion would have preferentially concentrated heavy minerals inside the linear depressions as they are deep enough (6-7 m). Also if erosion was extensive the mobile minerals amphibole and epidote would have been much lower in the samples that are located outside the linear features. However, the fact that the south-north linear depressions are open on both ends (Figs. 5.8, 5.10) may have made it difficult for the heavy minerals to be trapped and retained inside since the longshore drift current also runs in a northward direction.

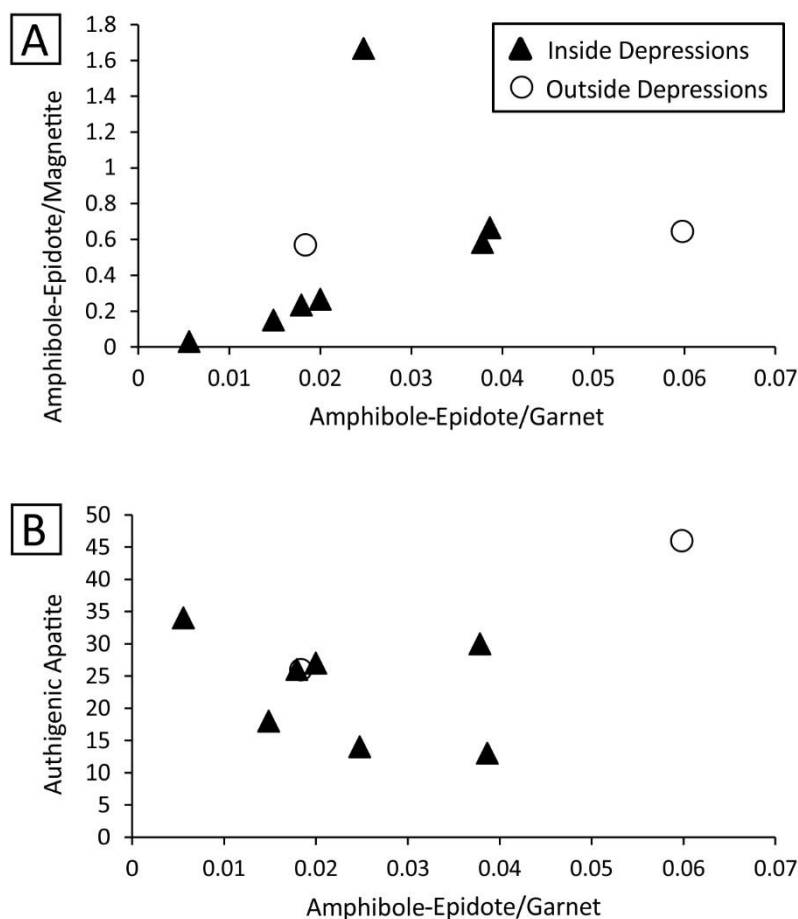


Figure 5.20 Comparison between samples that are located inside and samples that are located outside linear depressions from the same region, Region V. Data for 0.25-0.50 mm size fraction.

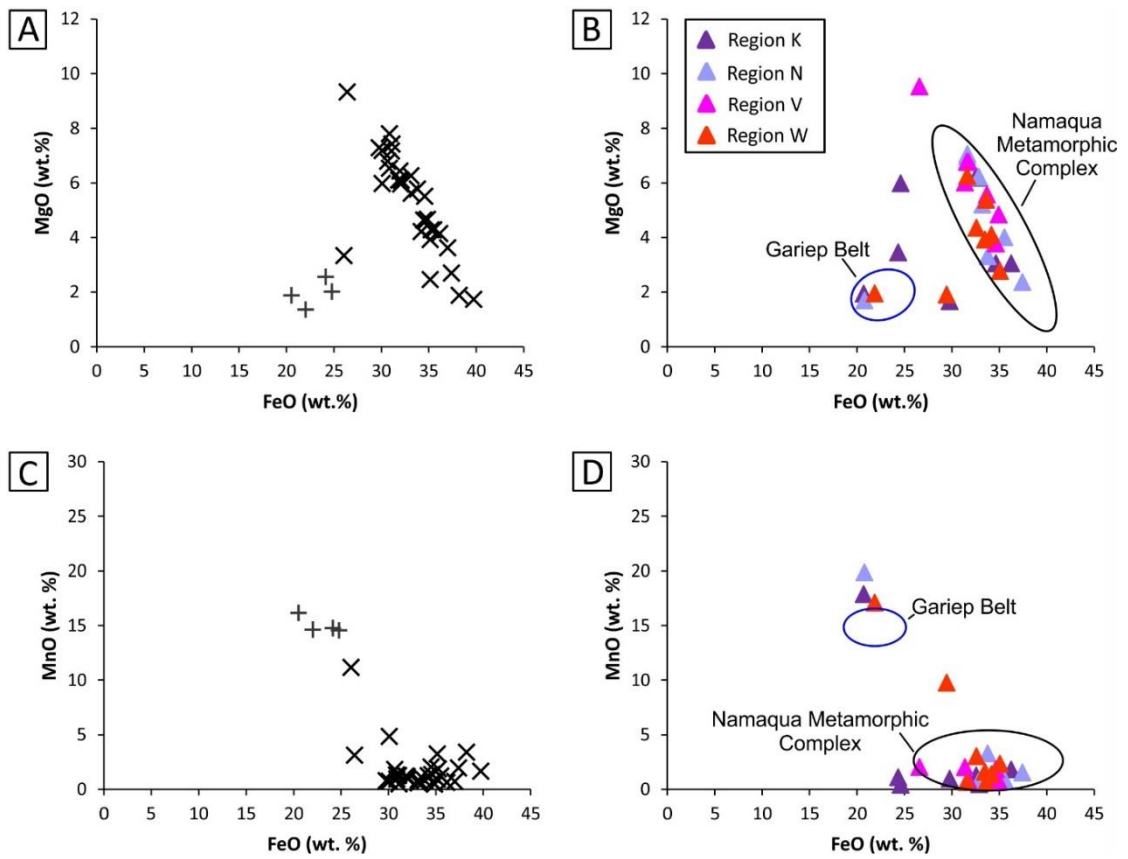


Figure 5.21 Comparison of Atlantic 1 garnets with Namaqua Metamorphic Complex and Gariep Belt garnets. Data for Namaqua Metamorphic Complex garnets from Humphreys and Van Bever Donker (1990), Cornell et al. (1992), Diener et al. (2013) and Bial et al. (2015) whereas Gariep Belt garnet data after Diener et al. (2017).

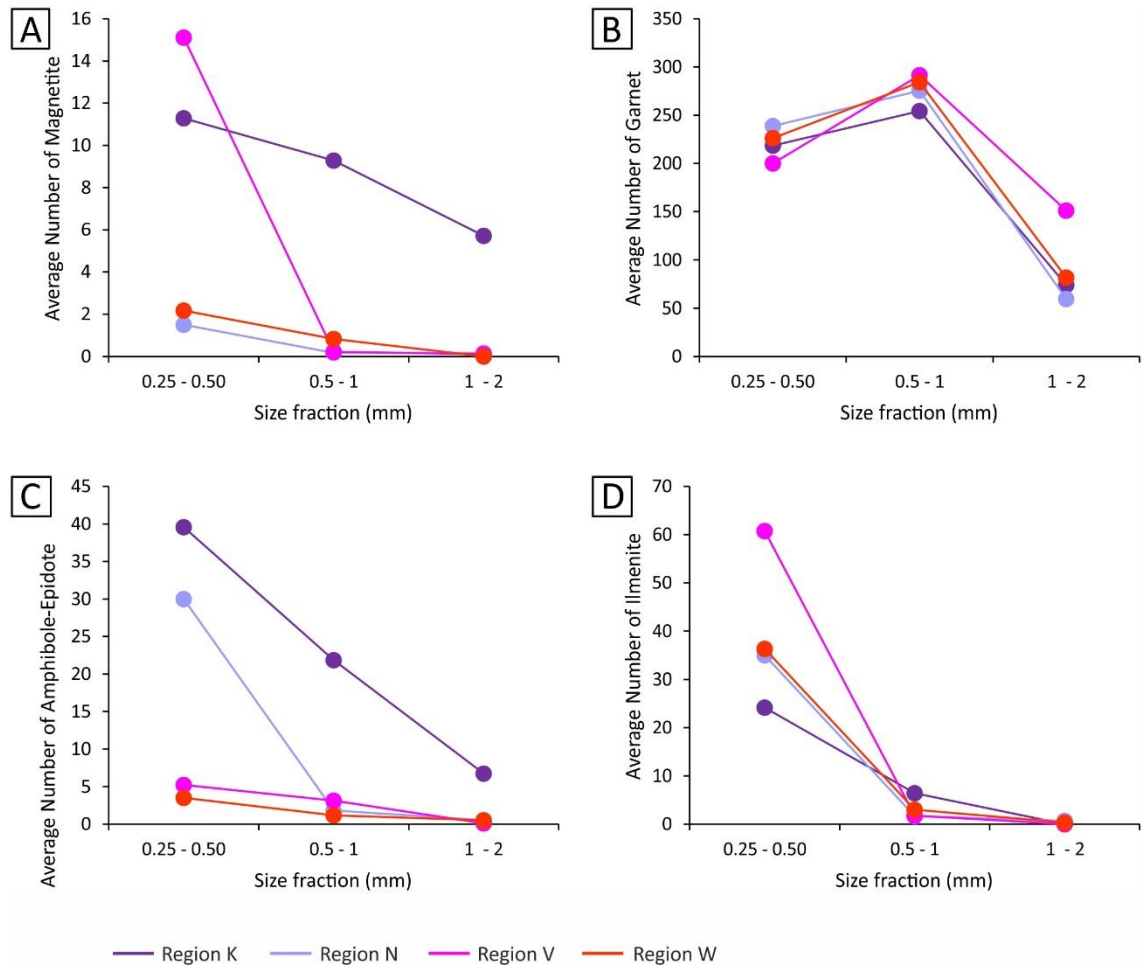


Figure 5.22 Comparison of (A) magnetite, (B) garnet, (C) amphibole-epidote and (D) ilmenite grain size between the Atlantic 1 regions.

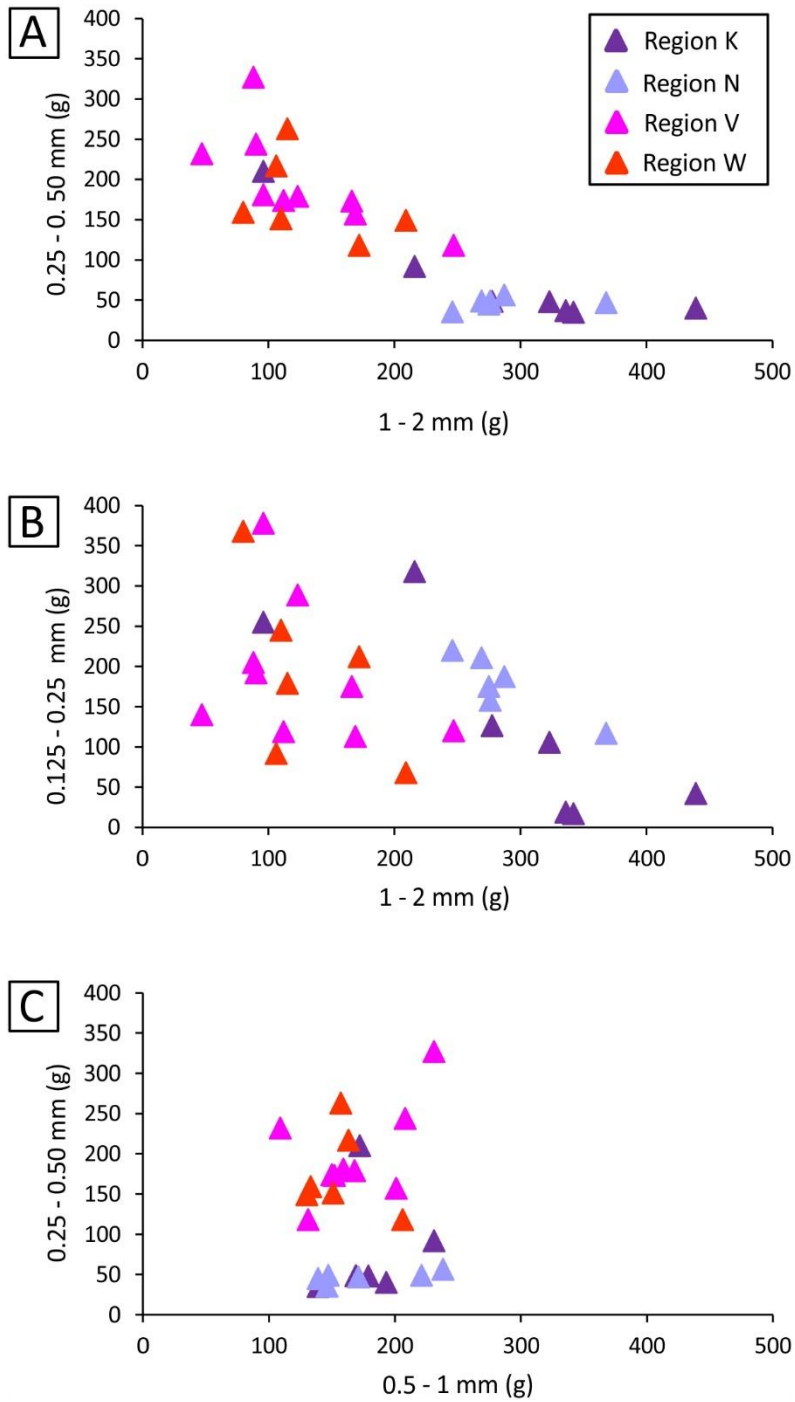


Figure 5.23 Variation of sand coarseness among the Atlantic 1 regions.

5.8.2 Effect of Sea Water Chemistry

The preservation potential of detrital Fe-oxide minerals including magnetite and ilmenite is influenced by the reducing and oxidising conditions of the depositional environment (Dill, 2007; Weibel and Friis, 2007). The marine gravels all show similar ilmenite content (Fig. 5.16) whereas magnetite decreases northward in both the eastern domains and western domains (Figs. 5.16B, 5.16C). Therefore, magnetite is the mineral discussed here. Amphibole-epidote, another minerals that show differences in concentration between the four domains, are not influenced by the reducing and oxidising conditions of the depositional environment. Under reducing conditions magnetite is dissolved by reacting with hydrogen sulphide (H_2S) to form authigenic pyrite (FeS_2) (Canfield and Berner, 1987; Weibel and Friis, 2007). Depending on the equilibrium between organic carbon and reactive Fe, dissolution of magnetite can also form authigenic greigite in addition to pyrite (Rowan et al., 2009). According to Kasten and Jørgensen (2000), hydrogen sulphide, which is responsible for dissolution of magnetite in a marine environment, is produced by reduction of sulphate by bacteria. Sulphate reduction rates are high in marine environments that are highly enriched in organic matter (Brüchert et al., 2003) such as the Namibian continental shelf where the upwelling Benguela current operates (Diester-Haass et al., 2002; Monteiro et al., 2005; Edelman-Furstenberg, 2014; Nagel et al., 2016).

Magnetite may be dissolved either partially or completely. The degree of magnetite dissolution depends on the surface area of magnetite (Canfield and Berner, 1987; Rowan et al., 2009), concentration of dissolved sulphide and the time period during which magnetite is in contact with sulfidic pore fluids (Canfield and Berner, 1987). In general, rapid sedimentation enhances the preservation of magnetite. Dissolution is therefore likely to occur when the rate of sediment deposition is low, and when mineral grains are fine grained (Rowan et al., 2009). However, complete dissolution of detrital magnetite can still occur in rapidly deposited sediments such as the Holocene sediments (~ 7 cm/kyr) found offshore California and Oman as reported by Rowan et al. (2009). In Atlantic 1, magnetite shows a northward decreasing trend in both the eastern domains

(from Region K to Region N) and western domains (from Region V to Region W) in the fine size fraction (Fig. 5.16C). If scarcity of magnetite in Region N and W is a result of dissolution of magnetite then these two regions will also have high pyrite content. However, no pyrite grains have been recovered from either of the regions in this study either because they are absent or they are smaller than 0.25 mm which is the cut-off size for the heavy mineral assemblage analysis. Another possible explanation could be that the magnetite grains that reached Region W were finer than the magnetite grains that remained in Region K, which is much coarser and thus less prone to dissolution. The interpreted larger surface area (with respect to volume) of the magnetite in Region W could have enhanced the complete dissolution of magnetite. Alternatively the sedimentation rate of Region W might have been slower than in Region K such that magnetite was exposed to sulfidic pore fluids for a longer period. However, it is difficult to constrain the mean sedimentation rates at different time periods given that the shelf has a highly fragmented sedimentary record with varying mean sedimentation rates in different windows. Furthermore, slow sedimentation in Region W relative to Region K is unlikely because since the major Cretaceous uplift in southern Africa sedimentation rates offshore increased significantly as recorded in the offshore Orange Basin (Rust and Summerfield, 1990; Aizawa et al., 2000; Rouby et al., 2009; Guillocheau et al., 2012). Following the peak sedimentation induced by the uplift event, sedimentation is believed to have decreased thereafter through time (de Wit, 1999; Guillocheau et al., 2012). Gravels in Region V and Region W are older than Region K gravels therefore the former should have been deposited under relatively faster rate than the Region K sediments. Therefore the decrease of magnetite from south to north is more likely to be a function of the high density of magnetite, where most of the magnetite remained closer to the Orange River mouth.

5.8.3 Effect of Sea Currents

Shallow marine currents that operate along the Namibian coast include northward longshore drift (Pether et al., 2000; Bluck et al., 2007) and Benguela current (Diester-Haass et al., 2002; Mohrholz et al., 2014; Nagel et al., 2016). Amphibole-epidote in Atlantic 1 decreases offshore away from the river mouth. Region K, the most southern region sampled, has a higher amphibole-epidote content relative to the other regions despite the mobile nature of amphibole and epidote that are easily entrained by waves and currents (Cascalho and Fradique, 2007; Frihy, 2007; Garzanti et al., 2015). If the northward longshore drift current preferentially transported amphibole-epidote northward then Region N, north of Region K, would be predicted to have a higher amount of amphibole-epidote, which is not the case (Figs. 5.16B, 5.16C). Interestingly, Garzanti et al. (2015) also found a similar pattern in beach sands along the Namibian coast over a distance of 300 km where amphibole content decreases northward of the Orange River mouth. In parallel, magnetite decreases northward in both the western and eastern domains, which is expected as magnetite is much more dense and less mobile. The northward decrease of amphibole-epidote could be explained if amphibole-epidote was broken down by mechanical processes as a result of wave action, producing a northward decreasing trend. However, amphibole-epidote does not show preferential enrichment in finer sizes in the amphibole-epidote poor regions (Fig. 5.22). Therefore longshore sea currents are interpreted to have limited influence on the distribution of heavy minerals in Atlantic 1 gravels except for magnetite. The offshore decrease of amphibole-epidote could be related to age of the gravels, because the amount of Namaqua Metamorphic Complex rocks, the source of amphibole and epidote, has increased through time as discussed in Chapter 4. The period during which the offshore gravels (Region V and Region W) were deposited was clearly at the time when the amount of sediments supplied from Namaqua Metamorphic Complex source was lower.

5.8.4 Effect of Sea Level

There are two ways that sea level could have affected the distribution of Atlantic 1 sediments and their associated heavy mineral assemblage. Firstly, sea level controls where the sediments are initially deposited. Secondly, sea level controls the redistribution of sediments post primary deposition. According to Filippelli (2011) the amount of phosphorite (apatite) increases with age of deep water. Therefore the relatively higher authigenic apatite content in the Northwest Domain and Southwest Domain (Fig. 5.16C) suggest that the gravels in the Northwest Domain and Southwest Domain have been stable for a longer time period (following subsequent sea level rise). In contrast the eastern domains (Southeast and Northeast) have been exposed during the last glacial maximum in the Late Pleistocene (Fig. 5.4). The sand size fraction of the Southeast and Northeast domains is much coarser than that of Northwest Domain and Southwest Domain (Fig. 5.23) implying that the eastern domains were exposed to subaerial conditions for a longer period that allowed aeolian processes to remove much of the silt and sand grain-size populations (Fig. 5.23). Therefore, sea level fluctuations have affected the distribution of apatite in the Atlantic 1 gravels.

In the 0.5-1 mm size fraction, Region V and Region W that make up the Northwest Domain and Southwest Domain show similar sand size distribution (Fig. 5.23) and amphibole-epidote content (Fig. 5.16C, 5.17). If northward aeolian processes that have been in operation since the Eocene (Miller, 2008) transported heavy minerals then a northward increasing amphibole-epidote trend from Region K to Region N would have been produced because amphibole and epidote are mobile owing to their lower densities (Casalho and Fradique, 2007; Frihy, 2007; Garzanti et al., 2015). During the late middle Miocene sea level increased to 25 m above current mean sea level for a short period of 1 Ma and thereafter sea level dropped again (Miller et al., 2005). The late middle Miocene sea level rise (Miller et al., 2005) coincides with the interpreted deposition of Southeast and Northeast domain gravels.

The western domains (Southwest and Northwest) have always been under water whereas the eastern domains (Southeast and Northeast) were exposed to subaerial conditions during the low sea level stand in the Pleistocene (Fig. 5.4).

During the Pleistocene lowstand, the eastern domains gravels were exposed to northward aeolian processes that could have carried amphibole-epidote northward, owing to their mobile nature relative to garnet and magnetite (Cascalho and Fradique, 2007; Frihy, 2007; Garzanti et al., 2015). As a result, such processes should produce a northward increasing trend in amphibole-epidote. However, amphibole-epidote proportion displays a northward decreasing trend from the Southeast Domain to the Northeast Domain, suggesting that the difference in amphibole-epidote content between the eastern and western domains was not influenced by sea level. Therefore, in the eastern domains, amphibole-epidote was likely broken down by mechanical processes as sediments are carried northward by the longshore drift current.

In summary, sea level fluctuations affected the distribution of authigenic apatite but not amphibole-epidote content.

This study has demonstrated that the distribution patterns of heavy mineral in Atlantic 1 were not controlled by either seabed geomorphology or oceanographic currents (longshore drift). By contrast, the distribution patterns of coarse grained sediments (> 3 mm) indicate northward transport by longshore drift where the clast grain size (including that of diamonds) decreases northward as a function of particle size and density along the Namibian coast from the Orange River mouth towards Lüderitz in beach and intertidal environments. However, amphibole-epidote content, the lower density heavy mineral, does not show a northward increasing trend which suggests that sand sized heavy minerals in Atlantic 1 show different transport and distribution patterns to the clast size (> 3 mm) sediments. This pattern has also been observed in the alluvial gravels along the lower Orange River where the clast size and sand sized heavy minerals show different transport histories, as discussed in Chapter 4. In contrast, several provenance studies have made an assumption that sand size grains and clast size particles are derived from the same source and that they reflect the same transport history.

5.9 Conclusions

Atlantic 1 gravels are characterised by heavy mineral assemblage comprised of garnet, magnetite, amphibole, epidote, ilmenite and apatite (biogenic and authigenic). Rare clinopyroxene occurs closer to the Orange River mouth. Amphibole-epidote and apatite distinguish the gravels of the eastern domains (Southeast and Northeast) and western domains (Northwest and Southwest), with the eastern domains showing a relatively higher amphibole-epidote content and lower proportion of authigenic apatite relative to the western domains. The higher apatite in the western domains relative to the eastern domains can be attributed to the fact that the western domains have been under water for a longer period whereas the eastern domains have been exposed to subaerial conditions during the last low sea level in the Pleistocene because the conditions of apatite formation requires deep water that has been stable for long periods. The northward decreasing trend of magnetite in both the eastern and western domains is a function of magnetite density in relation to the northward longshore drift.

The northward decreasing trend of amphibole-epidote in the eastern domains is neither a function of northward longshore drift nor geomorphology of the seabed. Sea level fluctuations also did not influence the distribution of amphibole-epidote in Atlantic 1 gravels but instead the distribution of these two minerals is interpreted to be a function of the relative amount of Namaqua Metamorphic Complex derived sediments, and mechanical breakdown during transport.

Chapter 6 Correlation of Orange River and Atlantic 1 gravel deposits using heavy mineral assemblage

6.1 Introduction

Linking the erosional record of onshore drainage basins with the depositional record of offshore sedimentary basins is a major challenge in geosciences (e.g., Allen, 2008; Romans and Graham, 2013; Clift et al., 2014; Romans et al., 2016). Gravel terrace deposits of continental-scale rivers provide both a fragmented record of drainage basin evolution, and a means to predict and unravel the depositional record of quasi-contemporaneous marine sediments. Continental shelves are important in linking sediments from source to sink because they are the first marine environment to receive sediments from the rivers before sediments are later transferred to the deep sea by gravity flow and mass movements (Covault and Fildani, 2014). On continental shelves sediments are subject to the effects of relative sea level change, ocean currents, and waves, fluvial and aeolian processes as well as post depositional modification that may alter the volume and composition of the sediments delivered by rivers to the coast. Studies that have correlated heavy minerals assemblages of river and continental shelf sediments are primarily focused on deducing sediment provenance (Casalho and Fradique, 2007). In this study, the Orange River gravel terrace deposits and the Atlantic 1 continental shelf gravels (Fig. 6.1) are compared in terms of their heavy mineral assemblages in order to assess the transfer and evolution of sediments between the Orange River and the continental shelf. In addition mineral surface textures are studied in order to assess the effect of post deposition modification on the mineralogy of heavy mineral assemblage as sediments are transferred from the river environment to the marine environment. The study area is unique with respect to other large continental scale river systems such as the Mississippi, Nile and Amazon (Hartley *et al.*, 2017), because the sediments of the Orange River delivered to the coast

are not preserved in the delta location but most of the sand has been displaced to form the Namib Desert sand dunes. Coarse sediments preferentially remained on the continental shelf.

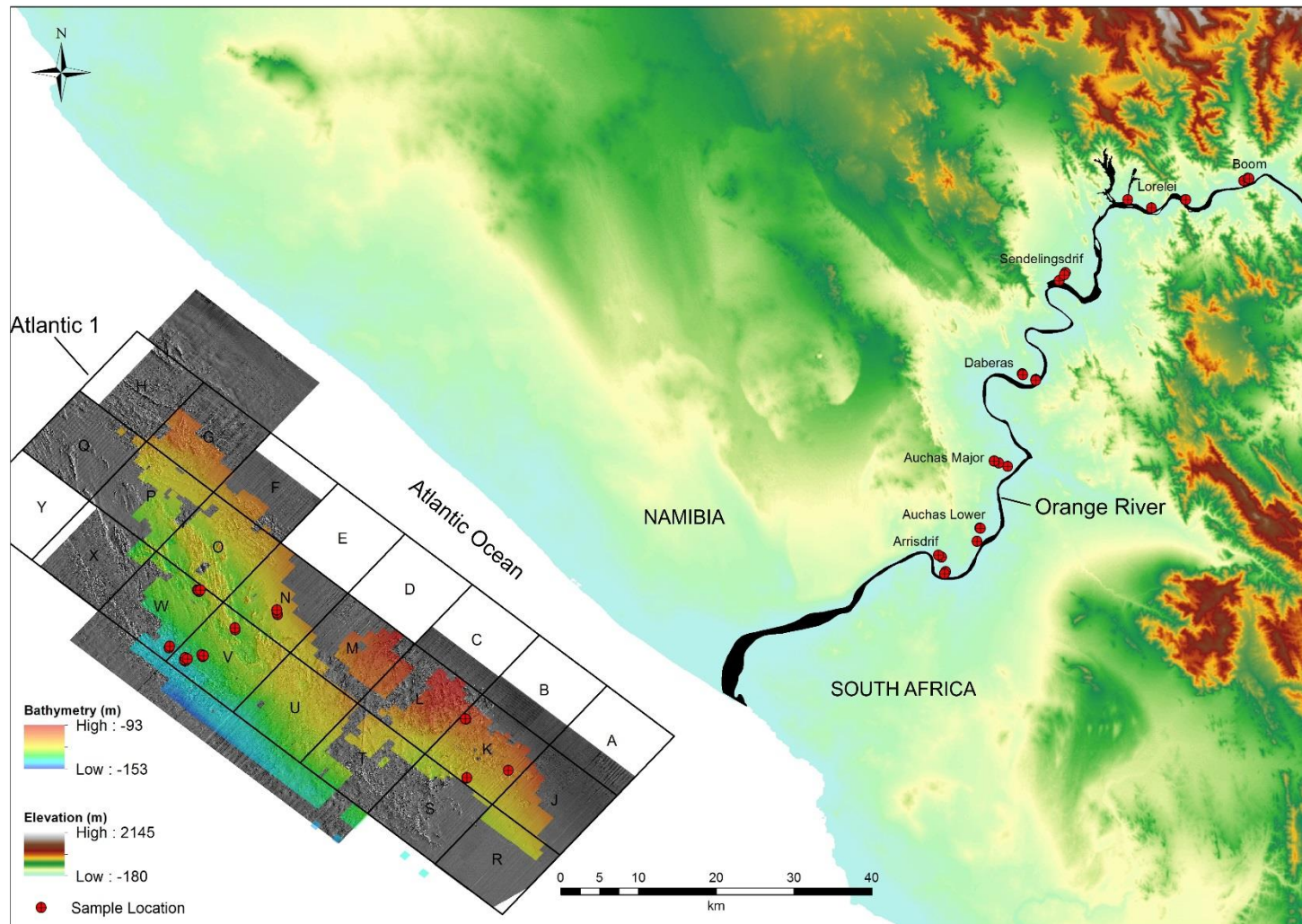


Figure 6.1 Orange River and Atlantic 1 study area. Red symbols represent sample locations. Onshore elevation data from Jarvis et al. (2008).

6.2 Heavy mineral assemblage

The heavy mineral assemblages of Orange River and Atlantic 1 gravels are presented and discussed in detail in Chapters 4 and 5, respectively. In this chapter the heavy mineral assemblages of the two are compared. The histograms presented in Figures 6.2 and 6.3 have been arranged so that the change in heavy mineral assemblage downstream with increasing distance offshore may be followed by scanning left to right.

The magnetite content decreases from all the Orange River deposits to the Atlantic 1 deposits (Figs. 6.2, 6.3). Figure 6.4 directly compares the abundance of magnetite and garnet in fluvial and marine sediments, and highlights the influence of particle size on the ratio of these minerals in the different settings. Coarse (>0.5 mm) ilmenite is rare in the marine samples. Garnet shows an opposite trend to magnetite and ilmenite where it is higher in the Atlantic 1 gravels relative to the Orange River gravels for the 0.5-1 mm and 0.25-0.50 mm size fractions (Fig. 6.5). The Orange River gravels contain coarser garnets with elevated garnet proportion in the 1-2 mm size fraction than the Atlantic 1 gravels (Fig. 6.4A).

Figures 6.6-6.9 illustrate the spatial variation in heavy mineral assemblages according to age of fluvial gravels. In each case the compositions of heavy minerals in the fluvial gravels (1-2 mm and 0.5-1 mm) are compared with the results of the parallel studies on marine gravels. This approach permits inspection of evolution of particle size for the same heavy mineral suite from onshore to offshore. General trends in the abundance of garnet, magnetite and ilmenite have been discussed above, but Figures 6.6-6.9 clearly illustrate the differing proportions of amphibole-epidote in sediments of Proto and Meso Orange River gravels and Atlantic 1 gravels. Gravel from Regions K and N (relatively nearshore) exhibit the amphibole-epidote signature of fluvial Meso Orange River gravels (Figs. 6.8, 6.9), whereas the offshore localities (Regions V and W) show amphibole-epidote content characteristic of the Proto Orange River gravel (Figs. 6.6, 6.7). Clinopyroxene is present in Region K but was not observed in either the Proto Orange River or Meso Orange River gravels (Figs. 6.9C, D). However,

clinopyroxene was observed in the modern Orange River gravels (Fig. 6.10), where they contribute up to 40% of the heavy mineral grain inventory.

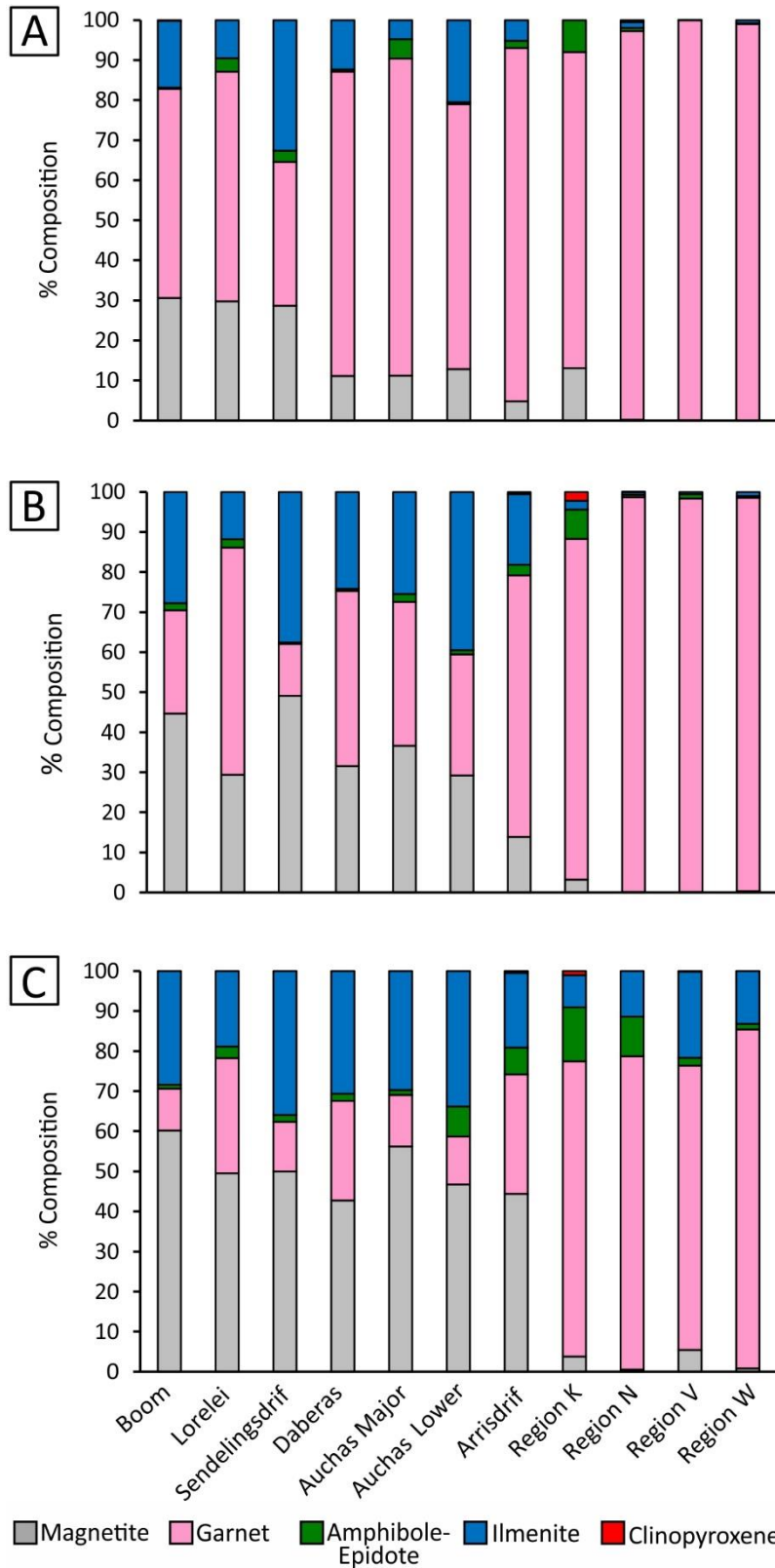


Figure 6.2 Heavy mineral assemblage of Proto Orange River and Atlantic 1 deposits. Figures A, B, C represent size fractions 1-2 mm, 0.5-1 mm and 0.25-0.50 mm, respectively. Due to absence of apatite in the river samples, apatite data is excluded from this plot for ease of comparison.

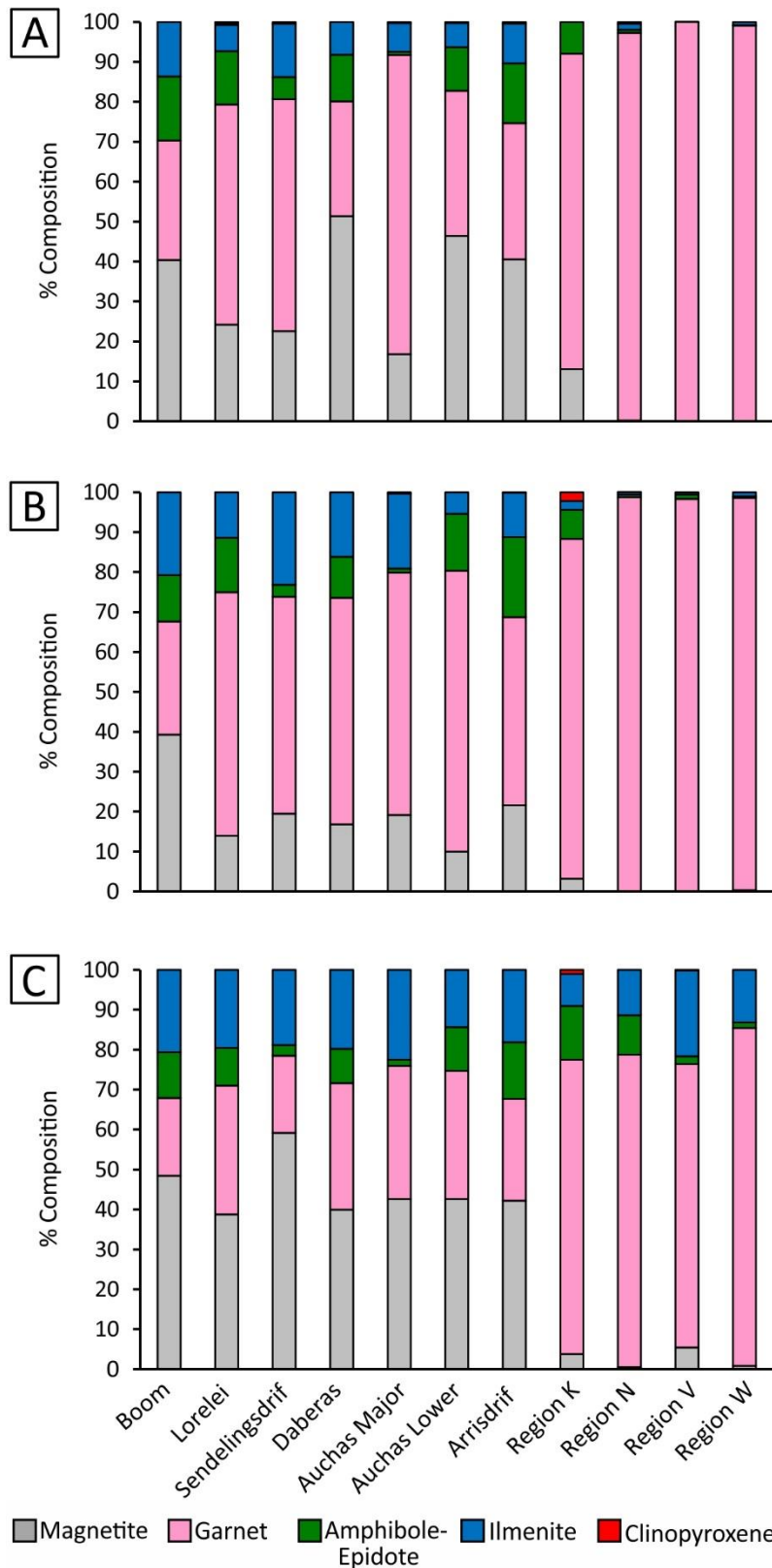


Figure 6.3 Heavy mineral assemblage of Meso Orange River and Atlantic 1 deposits. Figures A, B, C represent size fractions 1-2 mm, 0.5-1 mm and 0.25-0.50 mm, respectively. Due to absence of apatite in the river samples, apatite data is excluded from this plot for ease of comparison.

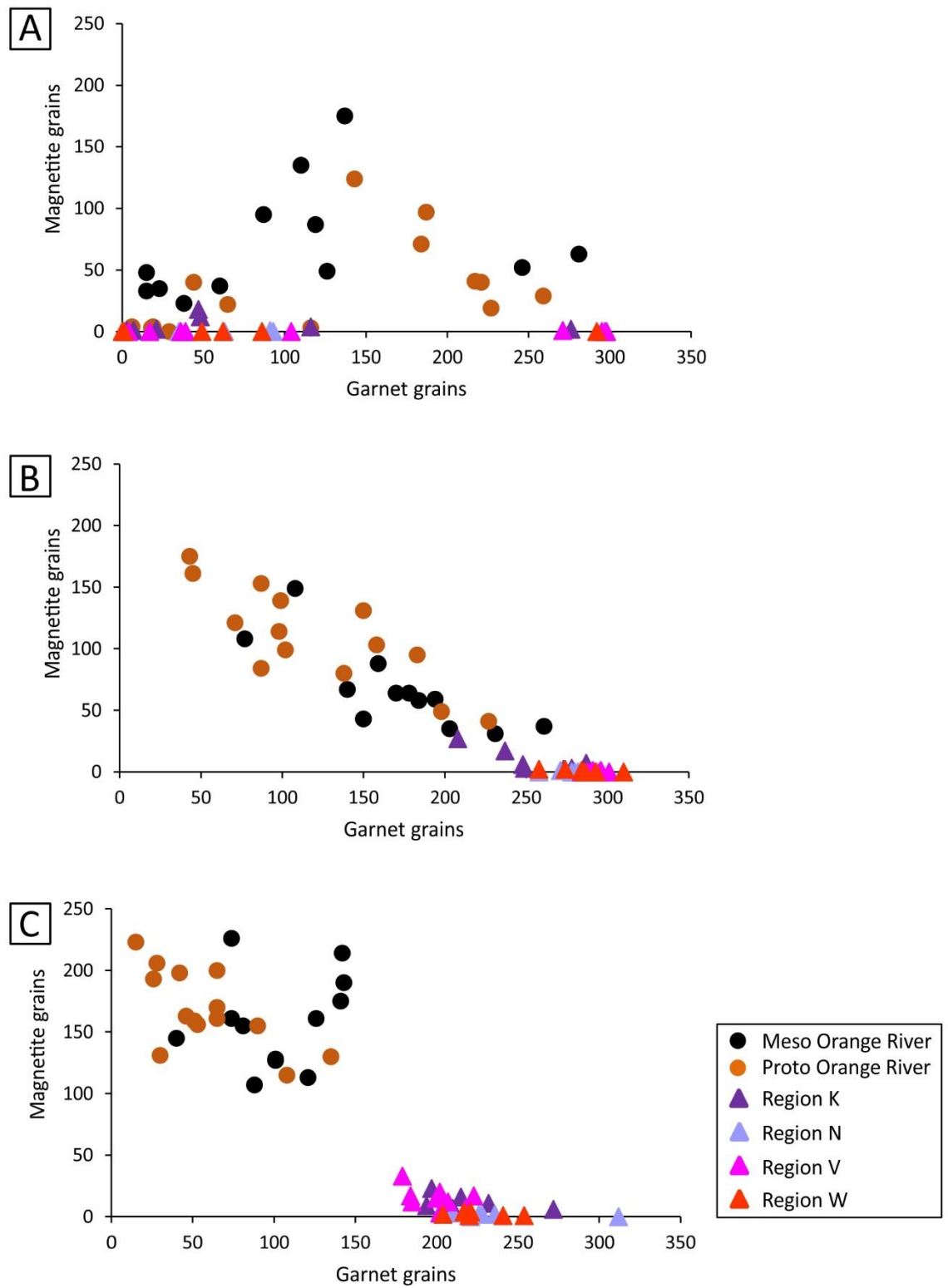


Figure 6.4 Comparison of garnet and magnetite content between the river and marine deposits. Figures A, B, C represent size fractions 1-2 mm, 0.5-1 mm and 0.25-0.50 mm, respectively.

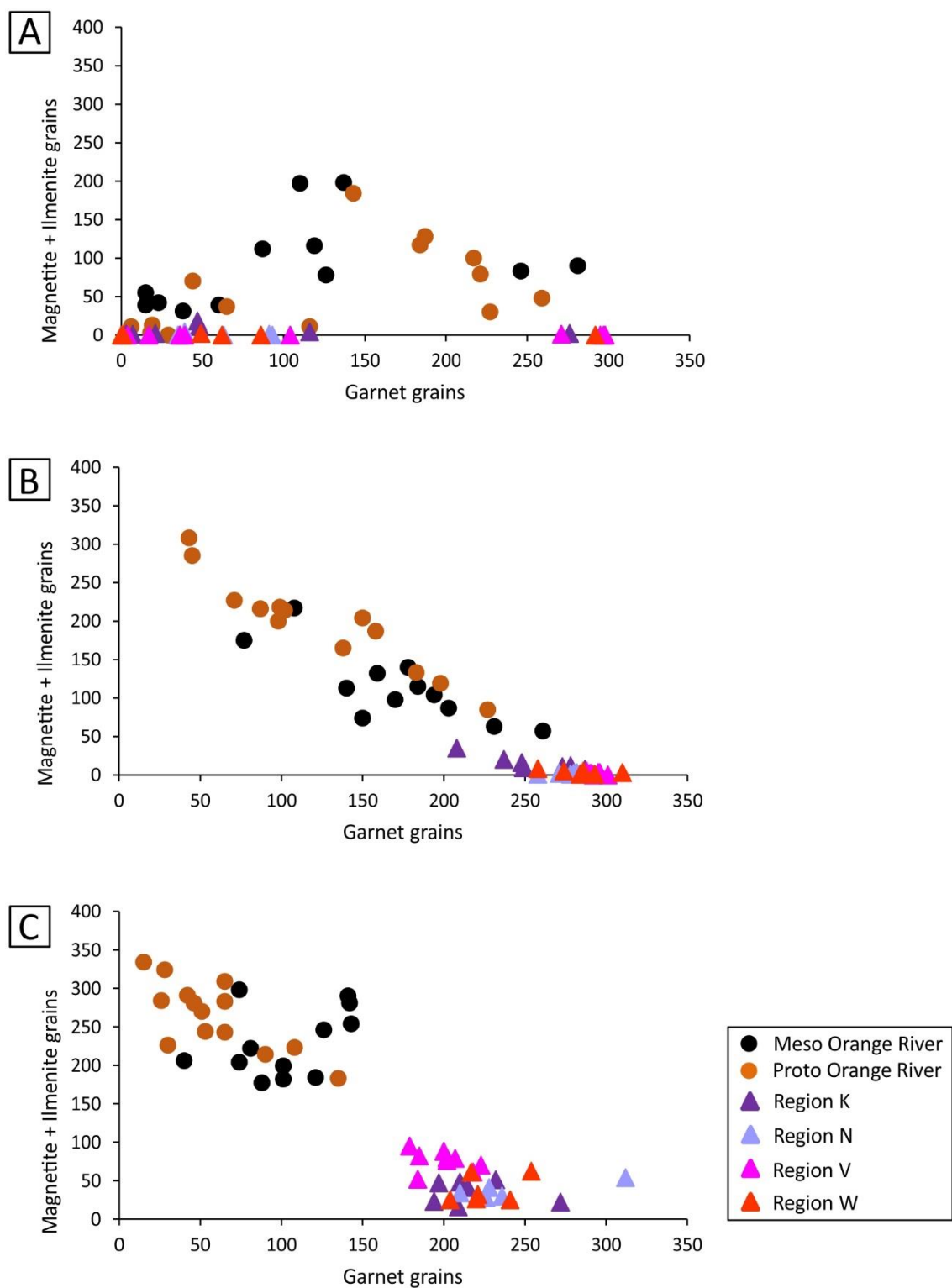


Figure 6.5 Comparison of garnet, magnetite and ilmenite content between the river and marine deposits. Figures A, B, C represent size fractions 1-2 mm, 0.5-1 mm and 0.25-0.50 mm, respectively.

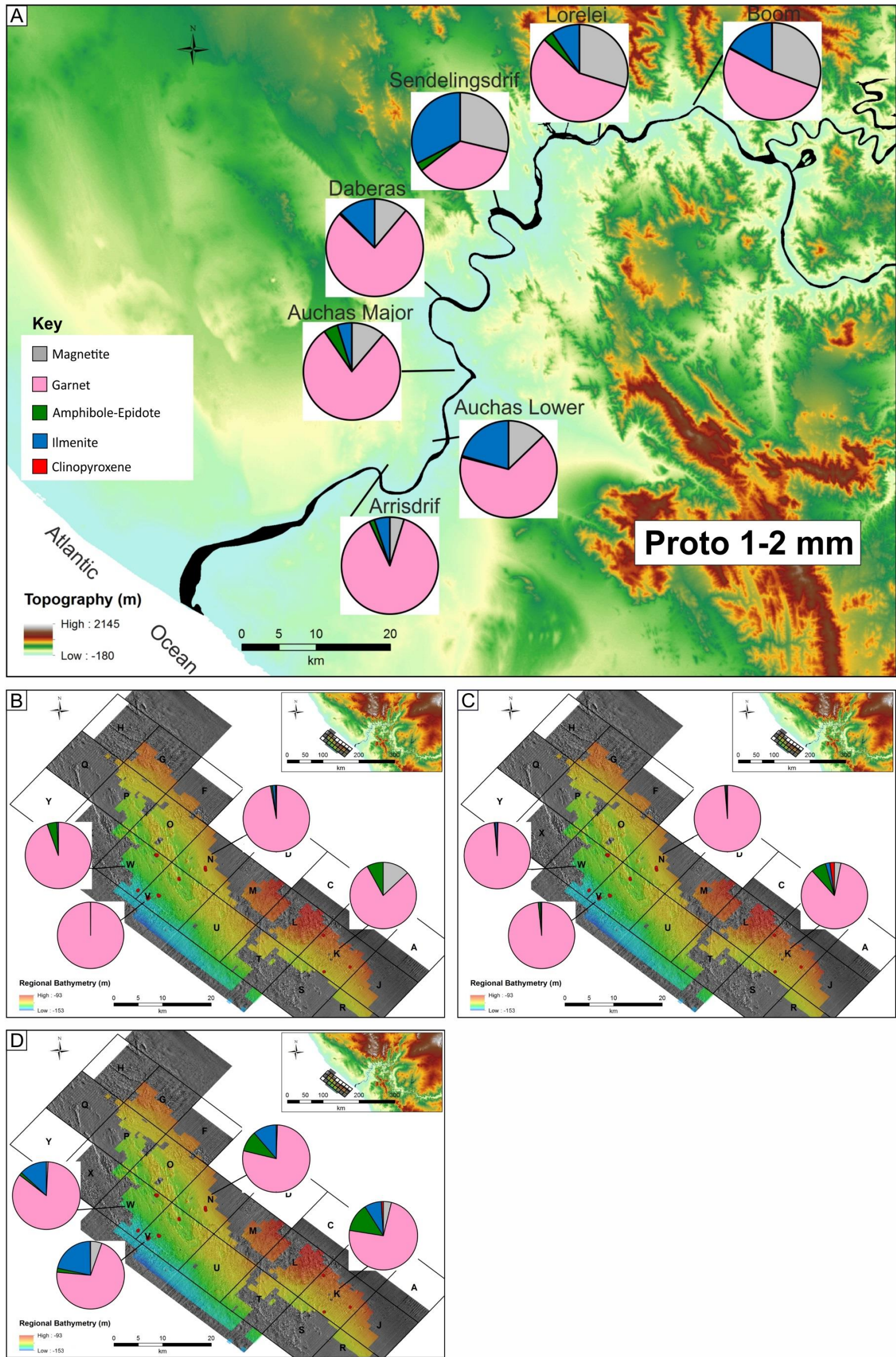


Figure 6.6 Spatial variation of heavy mineral assemblage in the Proto Orange River deposits (A) and Atlantic 1 samples (B, C and D). Heavy mineral data for the Proto Orange River deposits is for 1-2 mm whereas data for Atlantic 1 deposits in B, C and D is for 1-2 mm, 0.5-1 mm and 0.25-0.50 mm size fractions, respectively. Due to absence of apatite in the river samples, apatite data is excluded from this plot for ease of comparison. Elevation data for Orange River area from Jarvis et al. (2008).

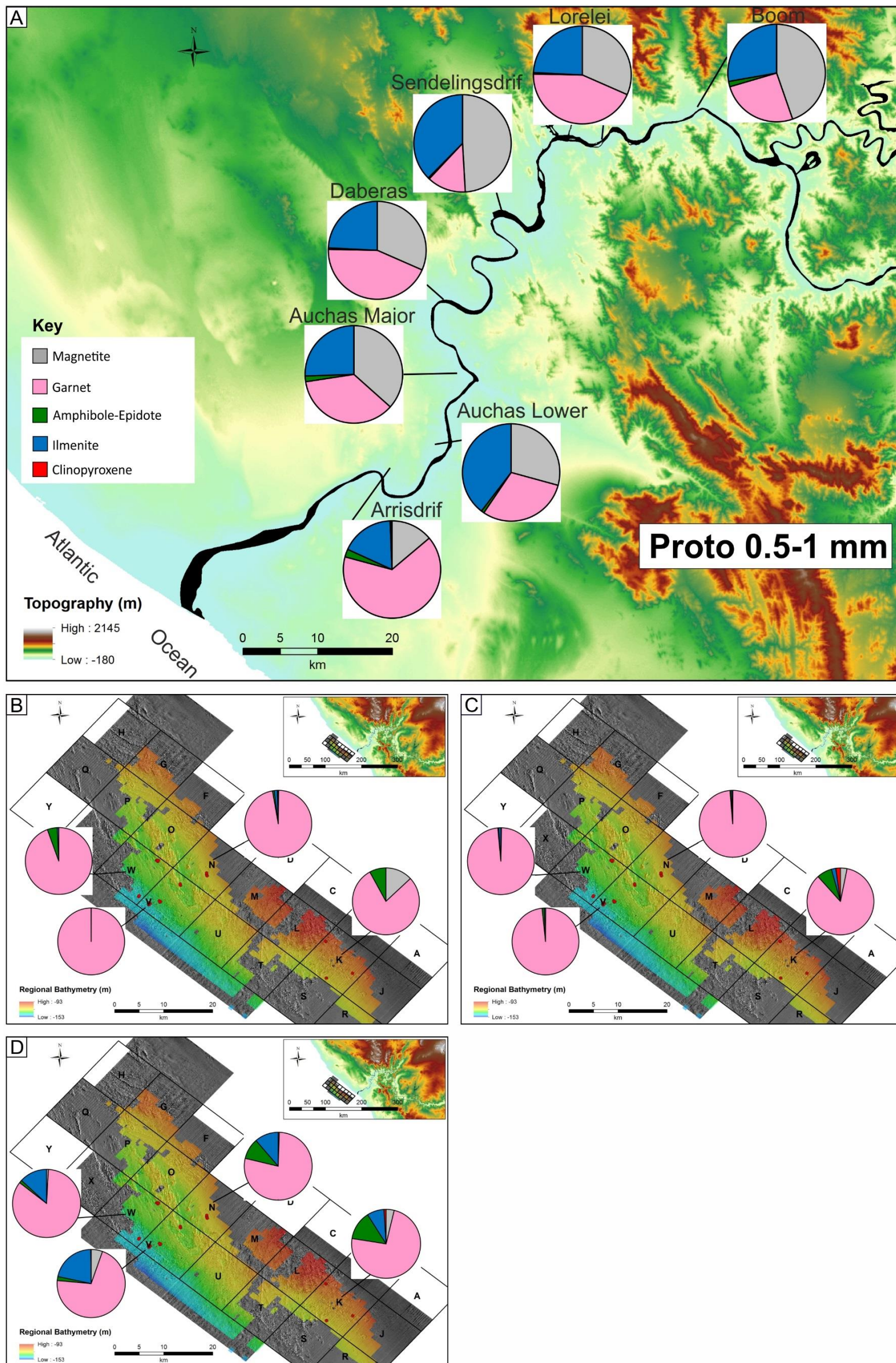


Figure 6.7 Spatial variation of heavy mineral assemblage in the Proto Orange River deposits (A) and Atlantic 1 samples (B, C and D). Heavy mineral data for the Proto Orange River deposits is for 0.5-1 mm whereas data for Atlantic 1 deposits in B, C and D is for 1-2 mm, 0.5-1 mm and 0.25-0.50 mm size fractions, respectively. Due to absence of apatite in the river samples, apatite data is excluded from this plot for ease of comparison. Topography data for Orange River area from (Jarvis et al., 2008).

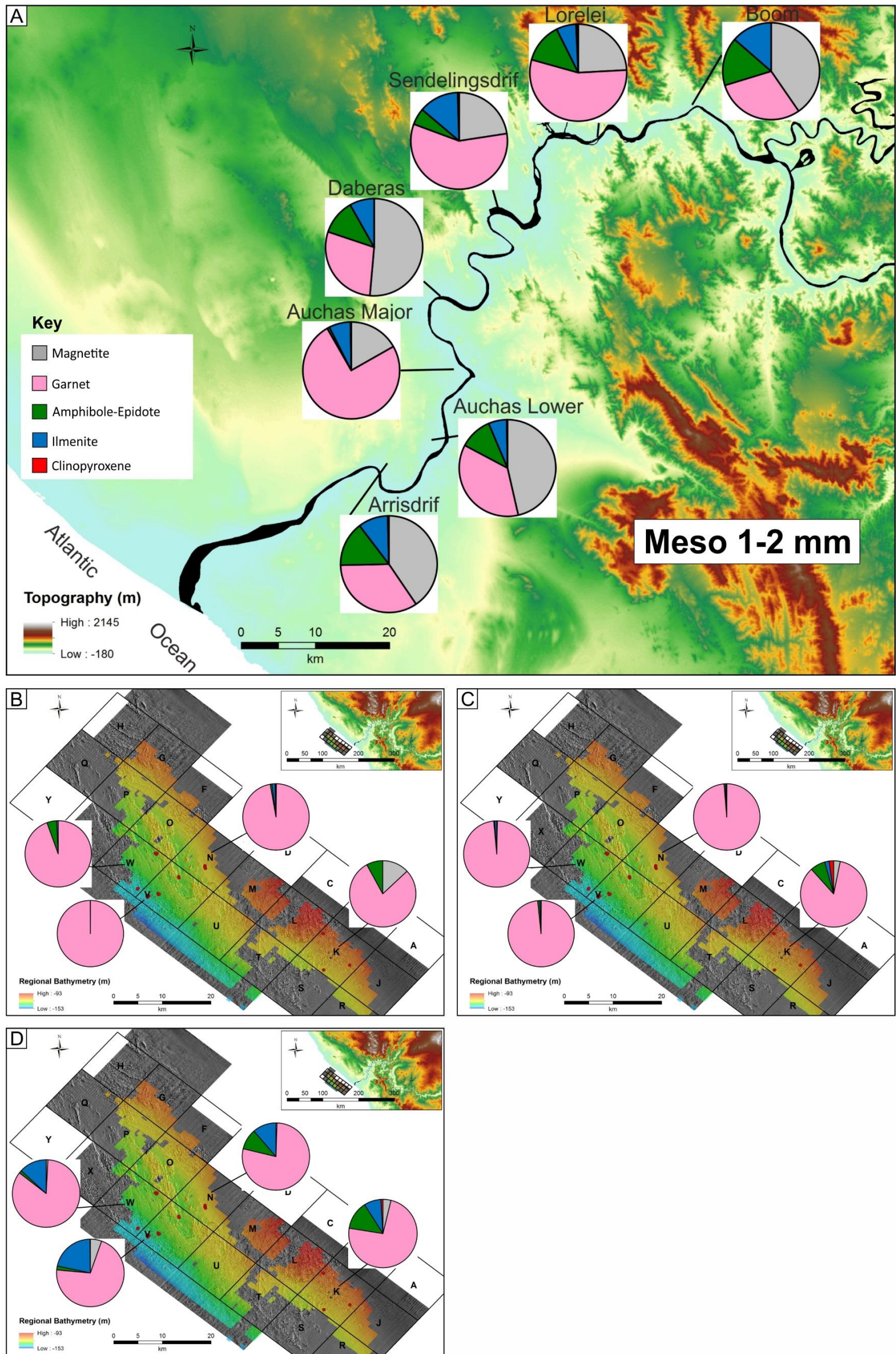


Figure 6.8 Spatial variation of heavy mineral assemblage in the Meso Orange River deposits (A) and Atlantic 1 samples (B, C and D). Heavy mineral data for the Meso Orange River deposits is for 1-2 mm whereas data for Atlantic 1 deposits in B, C and D is for 1-2 mm, 0.5-1 mm and 0.25-0.50 mm size fractions, respectively. Due to absence of apatite in the river samples, apatite data is excluded from this plot for ease of comparison. Topography data for Orange River area from Jarvis et al. (2008).

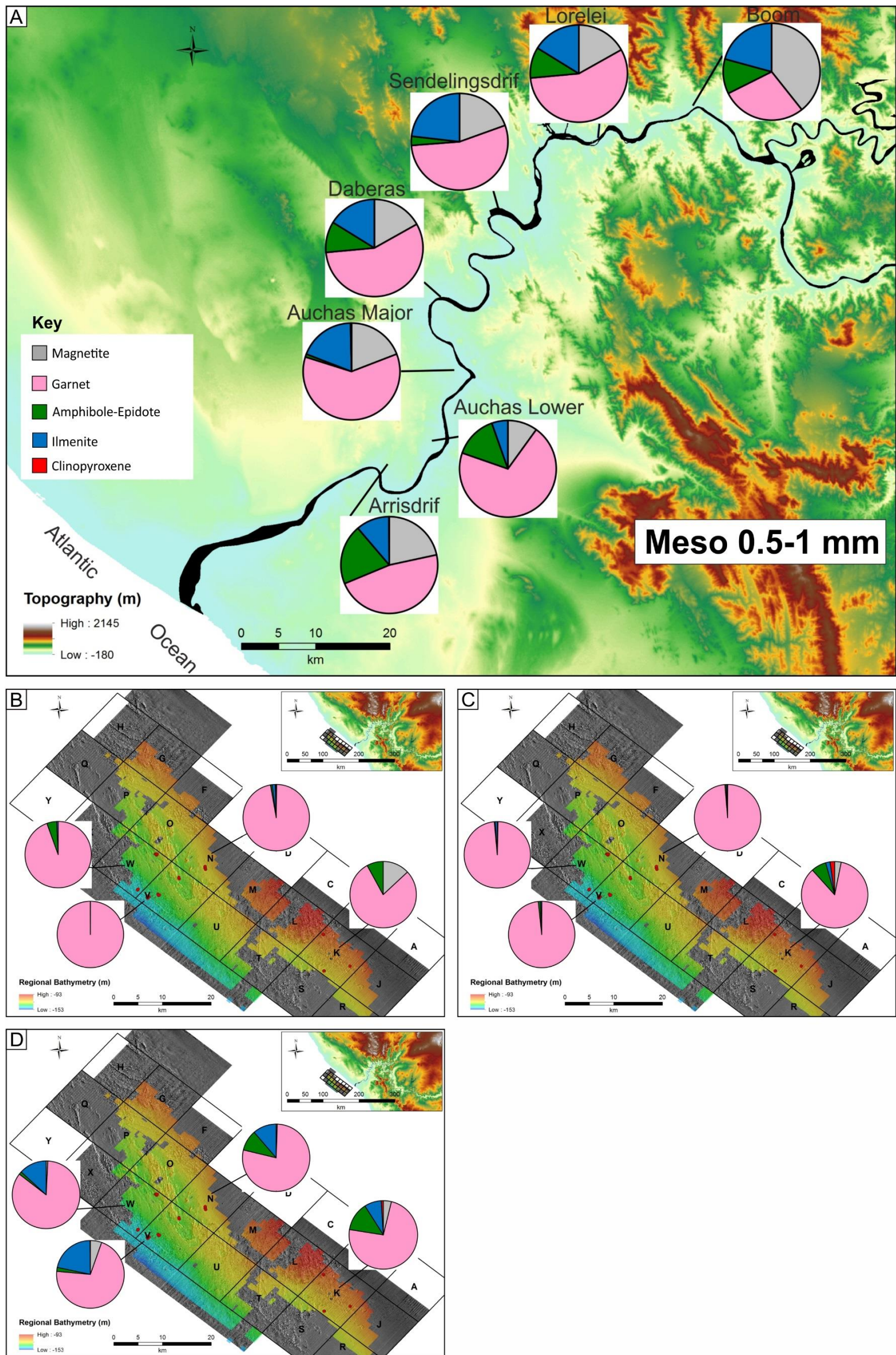


Figure 6.9 Spatial variation of heavy mineral assemblage for the Meso Orange River deposits (A) and Atlantic 1 samples (B, C and D). Heavy mineral data for the Meso Orange River deposits is for 0.5-1 mm whereas data for Atlantic 1 deposits in B, C and D is 1-2 mm, 0.5-1 mm and 0.25-0.50 mm size fractions, respectively. Due to absence of apatite of apatite in the rive samples, apatite data is excluded from this plot for ease of comparison. Topography data for Orange River area from (Jarvis et al., 2008).

6.3 Geochemical composition of bulk samples

Bulk samples of fluvial and marine gravels were analysed by XRF to provide chemical data for comparison with the heavy mineralogy assemblage. In addition, bulk analyses can provide information on the smallest size fractions where the mineralogical approach is challenging. Bulk chemical analyses were determined for four size fractions (0.25-0.50 mm, 0.125-0.250 mm, 0.063-0.125 mm and -0.063 mm). Details of the sample preparation and analytical methods are reported in Chapter 3, Section 3.3.3. Of the four size fractions analysed, the data described below relates to the 0.25-0.50 mm size range because this correlates with one of the size fractions for which mineralogical data is available.

The elements present in the heavy minerals reported in this study are specified in Table 6.1 according to whether they are major or minor components. It is clear that some elements are present in different mineral species. Figure 6.11 presents bivariate plots illustrating element ratios for the major elements identified in Table 6.1. Orange River samples and Atlantic 1 samples can be distinguished on the basis of their Ti/Fe, Ti/V, V/Fe, and Cr/Fe ratios with the fluvial samples showing higher Ti, Fe, V and Cr contents. The fluvial and marine samples show overlapping ranges of Mn content although the marine samples generally yield lower values.

Bulk sample geochemical compositions have been compared with specific mineral abundance in Figure 6.12. This approach permits evaluation of the proportions of specific elements associated with the different mineral species. The high magnetite proportion in the Orange River samples coincides with their higher V, Ti, Cr and Fe contents, (Fig. 6.12). In contrast, lower magnetite proportions in the Atlantic 1 samples coincides with their lower V, Ti, Cr and Fe contents. The abundance of garnet does not correlate with Fe and Cr contents. Vanadium may be present in both magnetite and ilmenite (Table 6.1) both of which are present in higher proportions in fluvial sediments (Figs. 6.2C, 6.3C). This is reflected in the positive correlation between magnetite abundance and V values illustrated in Figure 6.12F. In contrast, ilmenite does not show any correlation with V content (Fig. 6.12G). Chromium values correlate with magnetite rather than garnet abundance (Figs. 6.12A, B). Although the marine

gravels have higher garnet proportions in the 0.25-0.50 mm size fraction, they are characterised by lower Fe content in the same size fraction (Fig. 6.12D).

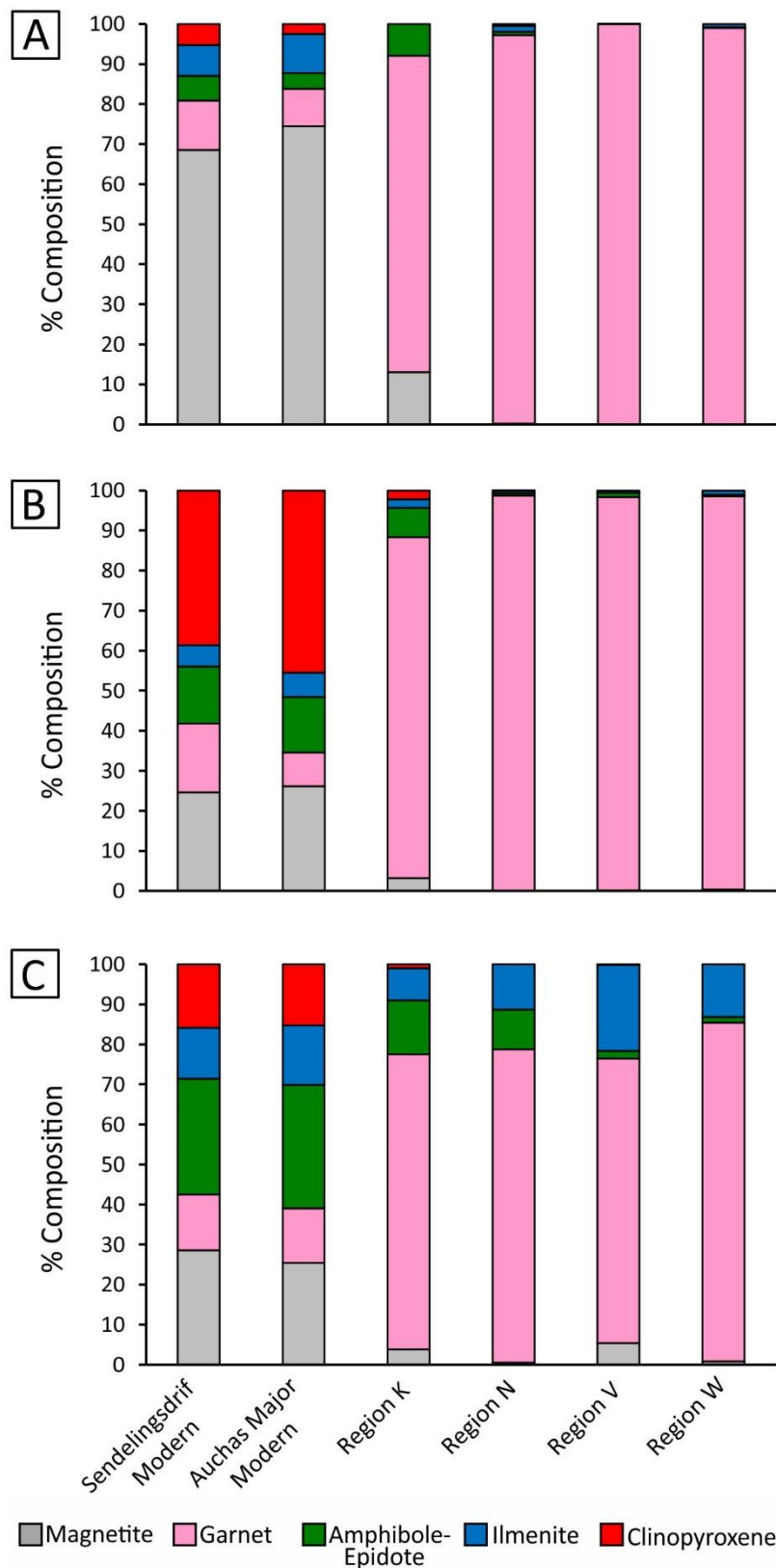


Figure 6.10 Comparison of two modern Orange River samples with Atlantic 1 gravels. Figures A, B, C represent size fractions 1-2 mm, 0.5-1 mm and 0.25-0.50 mm, respectively.

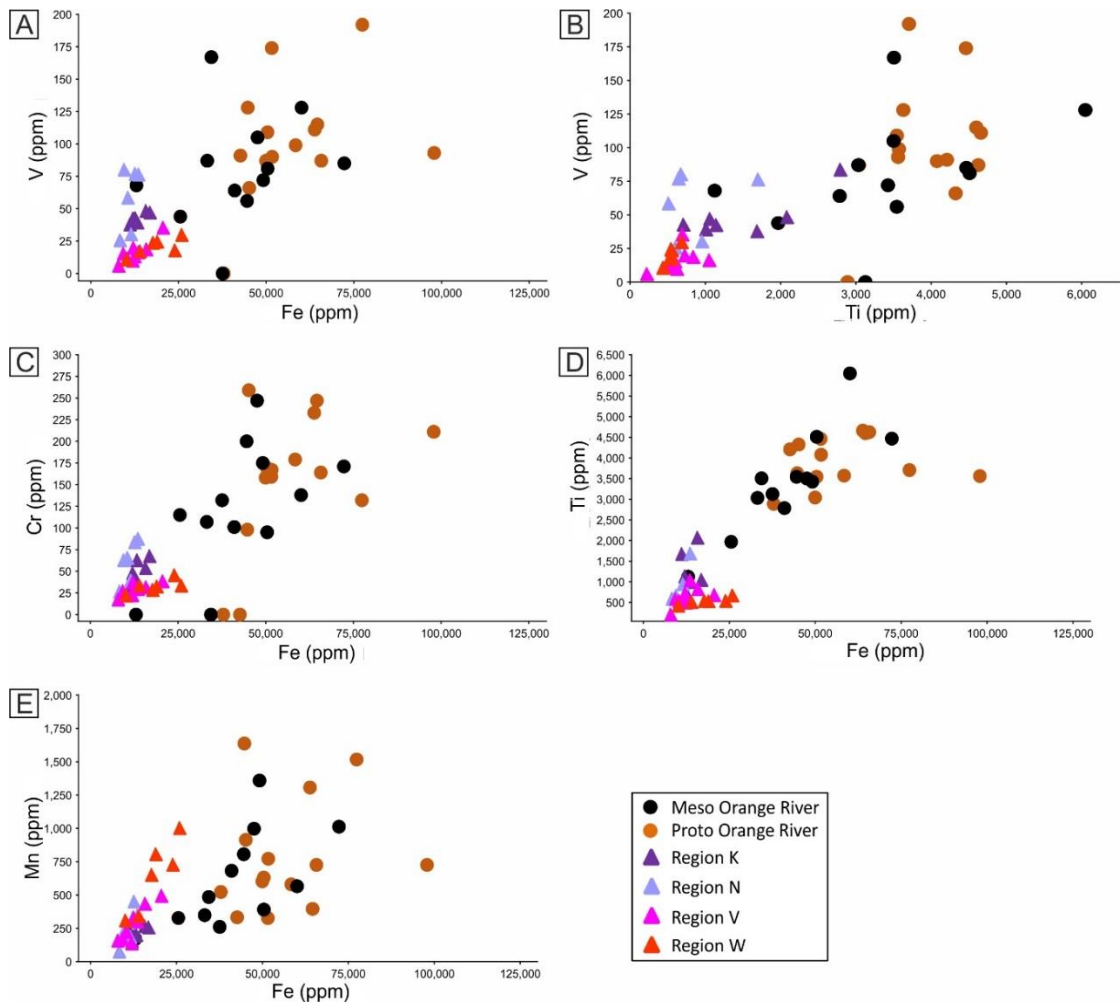


Figure 6.11. Comparison of bulk sample composition between Proto Orange River samples, Meso Orange River samples and Atlantic 1 samples for 0.25-0.50 mm size fraction. Anomalous sample K-S3 from Region K (Fe = 385, 860 ppm) is excluded from Figures A, C, D and E.

Table 6.1 Common major and minor elements that make up the heavy minerals of the river and marine samples.

Mineral	Major Elements	Minor Elements
Magnetite	Fe, Ti, V	Cr
Garnet	Fe, Mg, Mn, Ca	Al, Cr
Epidote	Ca, Fe	Al
Amphibole	Ca, Mg, Fe, Na, K	Al
Ilmenite	Ti, Fe V	
Clinopyroxene	Ca, Mg, Fe, Na	Mn, Sc, Cr, Li, Al
Apatite	Ca, P Mn, Sr	

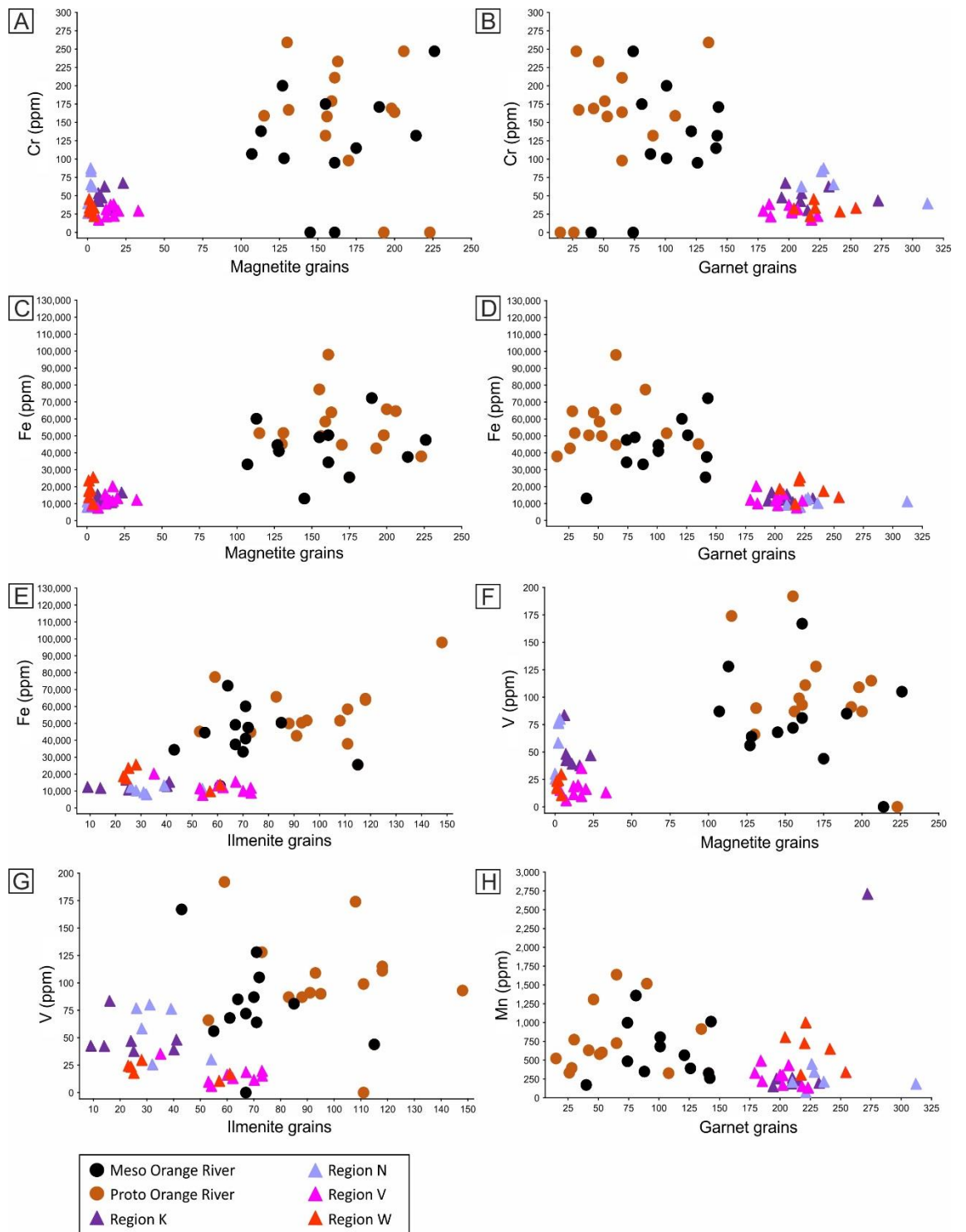


Figure 6.12 Covariation of bulk sample composition and heavy mineral assemblage in Proto Orange River samples, Meso Orange River samples and Atlantic 1 samples for 0.25-0.5 mm size fraction.

6.4 Mineral surface textures

The objective of analysing mineral surface textures is to evaluate the degree of physical reworking in the marine environment which could influence the observed mineralogy of the heavy mineral assemblages between the river and marine environments. Garnet, epidote and magnetite in the 0.5-1 mm size fraction were selected for further study in this regard. The 0.5-1 mm size fraction was chosen because it is the size fraction in which the three minerals are widely present. Among the lower density minerals, epidote was chosen for mineral surface texture analysis because it is more common in both the fluvial and marine gravels than amphibole. The grain surface textures formed on garnet are most sensitive to the chemistry of the environment of alteration compared to other silicate mineral species (Salvino and Velbel, 1989). Magnetite stability is a function of redox state, and could be expected to vary between river and marine environments (e.g., Weibel and Friis, 2007).

6.4.1 Orange River samples

Surface textures on garnets comprise conchoidal fractures (Figs. 6.13A, B) and etch pits (Figs. 6.13, 6.14). Etch pit textures include euhedral triangular pits (Figs. 6.13C, D) and pits superimposed on conchoidally fractured surface (Figs. 6.13B, 6.14B). A 'cobble' texture was also recorded (Fig. 6.14B, C). There is no difference in the range of grain surface textures on garnets between the Proto and Meso Orange River gravels. For example, the 'cobble' texture is present on garnets from both the Proto Orange River gravel (Fig. 6.14B) and the Meso Orange River gravel at Sendelingsdrif.

Epidote shows much more extensive chemical etching relative to garnet (Figs. 6.15, 6.16). Compared to garnet, the etch pits on epidote are anhedral (Fig. 6.15). Saw tooth terminations are present on Meso Orange River epidotes (Fig. 6.16) but none was recorded in the Proto Orange River gravels.

Magnetite shows a much lower degree of dissolution textures (Fig. 6.17) compared to garnet and epidote. Etch pits are present but rare (Fig. 6.17A). Honeycomb texture was recorded on magnetite (Fig. 6.17D).

6.4.2 Atlantic 1 samples

Conchoidal fractures are the dominant surface textures on garnets from Atlantic 1 (Figs. 6.18A, B, C). Small, anhedral, dissolution etch pits occur (Fig. 6.18D) but euhedral triangular dissolution pits are notably absent on garnets. Rare imbricate wedge marks (Figs. 6.18E, F) were recorded.

Epidote grains display more pronounced dissolution. Irregular shaped dissolution etch pits were recorded including on a rounded epidote (Fig. 6.19). Saw tooth terminations are common (Fig. 6.20).

Magnetite grains exhibit dissolution textures (Fig. 6.21). Large irregular shaped etch pits were recorded on some of the magnetite grains (Figs. 6.21A, B).

6.4.3 Comparison of Orange River and Atlantic 1 samples using mineral surface textures

A summary of grain surface textures of garnet, epidote and magnetite grains derived from Proto Orange River, Meso Orange River and Atlantic 1 gravels is presented in Table 6.2. Conchoidal fractures are present on both Orange River garnets (Figs. 6.13A, 6.13B, 6.14B) and Atlantic 1 garnets (Figs. 6.18A, B, C), but are more common on garnets from the marine environment (Table 6.2). In general, the etch pits on the Atlantic 1 garnets are smaller in both size (Fig. 6.18D) and number relative to the Orange River garnets (e.g., Fig. 6.13D). The triangular etch pits common on the Proto and Meso Orange River garnets (Figs. 6.13C, 6.13D, 6.14A, 6.14D) are absent on the Atlantic 1 garnets. In contrast the etch pits on Atlantic 1 garnets have irregular shapes (Fig. 6.18D). The 'cobbled' texture (Fig. 6.14B, C) is also absent on the Atlantic 1 garnets. Imbricate wedge marks are rare but were observed on a single Atlantic 1 garnet (Figs. 6.18E, F) but this feature was not recorded on the Proto and Meso Orange River garnets (Table 6.2). Saw tooth terminations common on epidote grains from Atlantic 1 (Fig. 6.20) are rare on Meso Orange River epidotes (Fig. 6.16) but absent on the Proto Orange River epidote. In general, magnetite from the river samples shows a much lower degree of dissolution than magnetite from the marine samples (e.g., Figs. 6.17, 6.21).

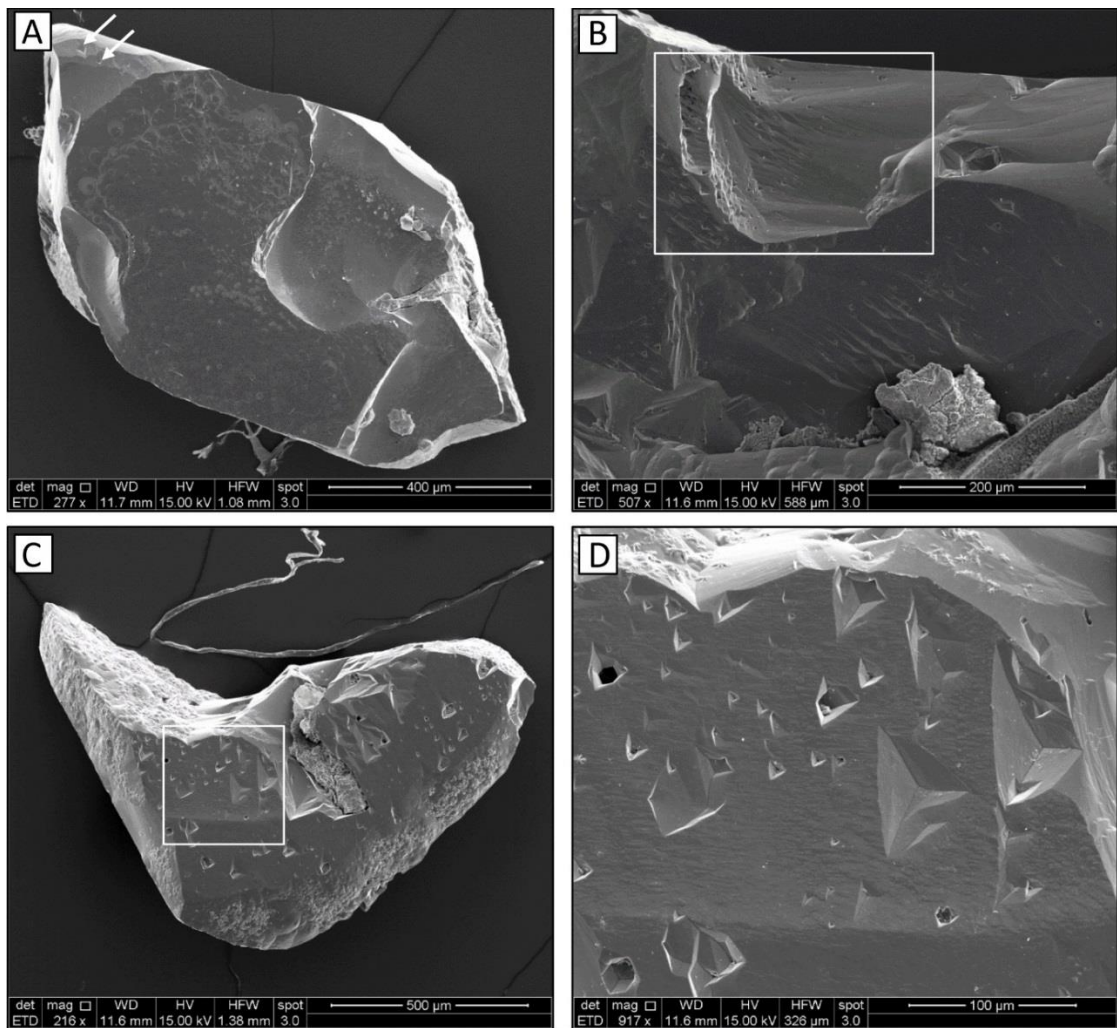


Figure 6.13 Garnet: (A) Conchoidal fractures, Proto Orange River gravel, Auchas Major Deposit. Note the few etch pits (arrows) on the fractured surface. (B) Etch pits superimposed on conchoidally fractured surface (white rectangle), Proto gravel, Arrisdrif Deposit. (C) Large euhedral pits, Proto Orange River gravel, Boom Deposit. (D) Close up view of area inside white square in Picture C.

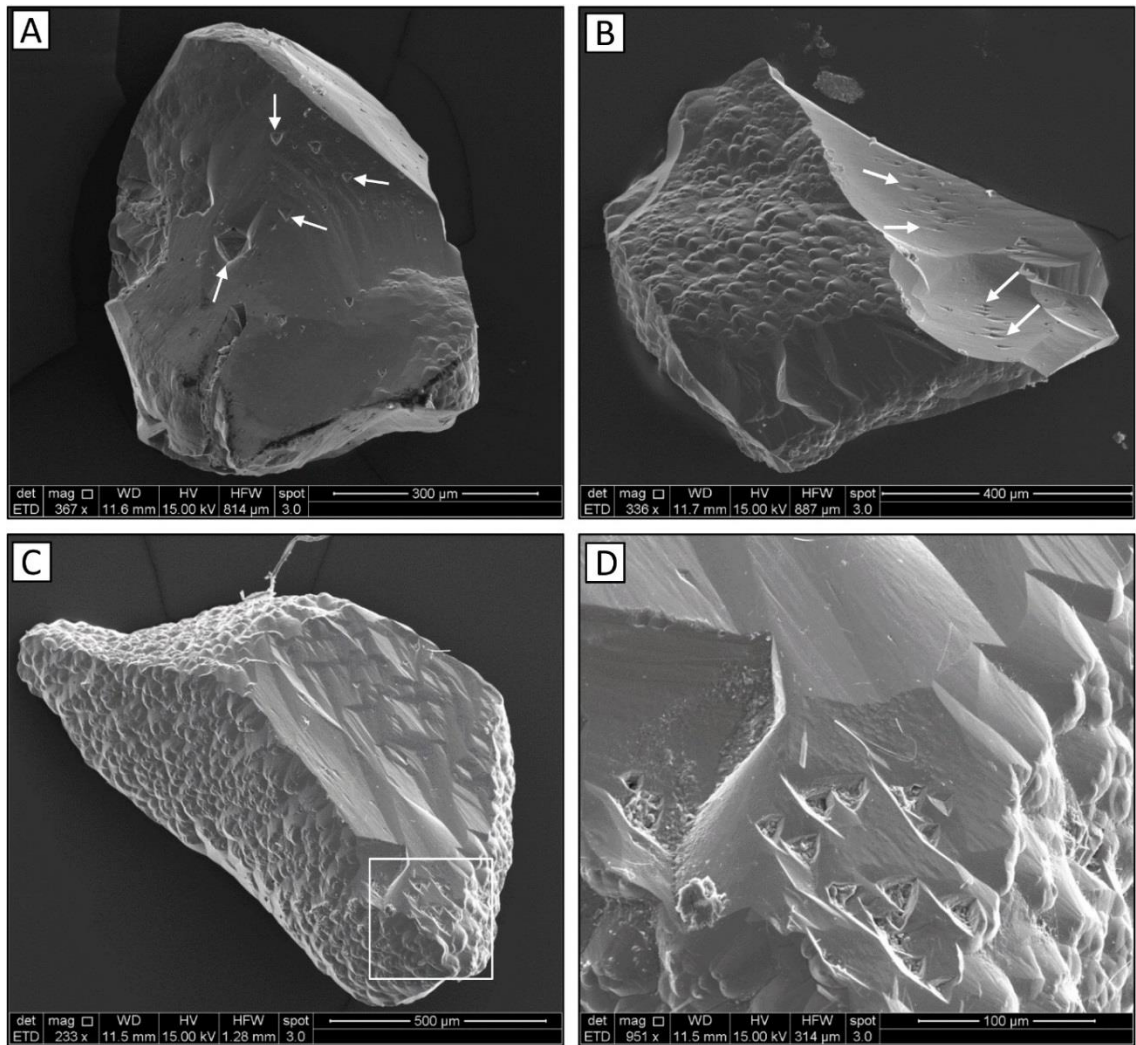


Figure 6.14 Garnet: (A) Euhedral etch pits (arrows), Meso Orange River Boom Deposit. (B) Cobbled structure and etch pits (arrows) on conchoidally fractured surface, Proto Orange River Sendelingsdrif Deposit. (C) Cobbled structure and euhedral etch pits (white square) Proto Orange River gravel, Auchas Major Deposit. (D) Close up of euhedral etch pits inside white square in Picture C.

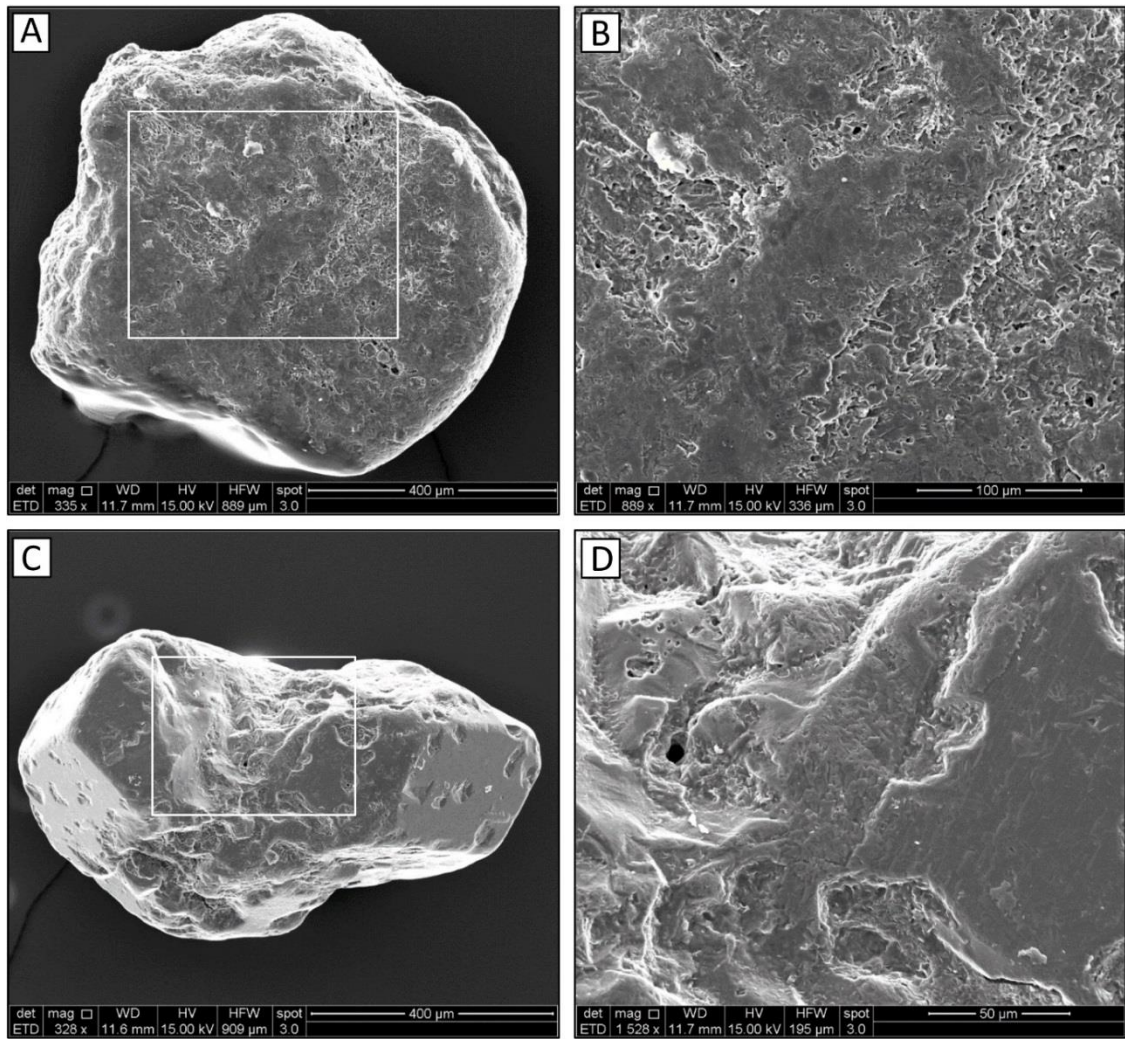


Figure 6.15 Epidote: (A) Extensive chemical etching. (B) Close up view of white boxed area in Picture A. (C) Etch pits on epidote from Meso Orange River gravel. (D) Close up view of Picture C. Both grains from Meso Orange River gravel, Sendelingsdrif Deposit.

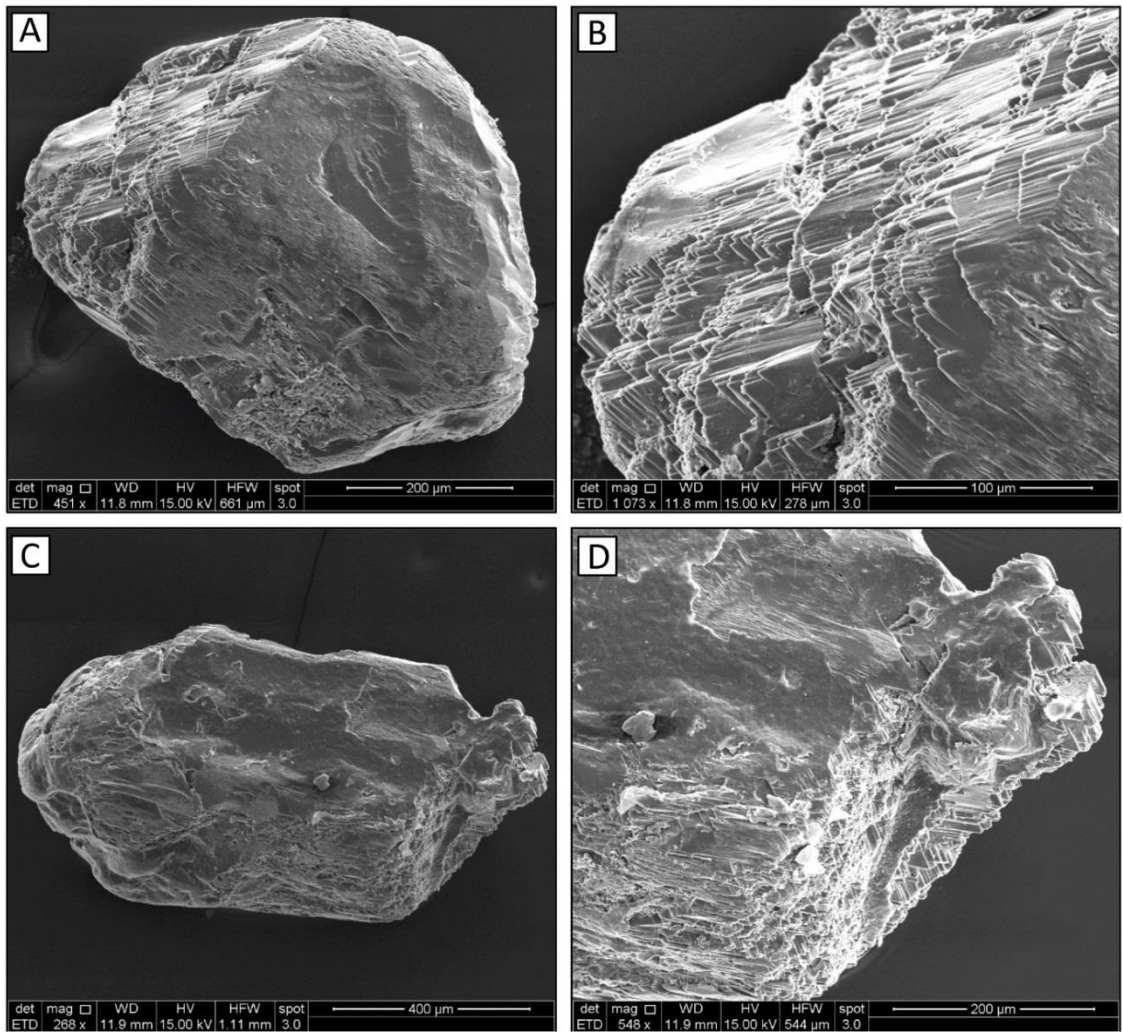


Figure 6.16 Epidote: Saw tooth terminations on epidote from Meso Orange River gravel, Arrisdrijf Deposit.

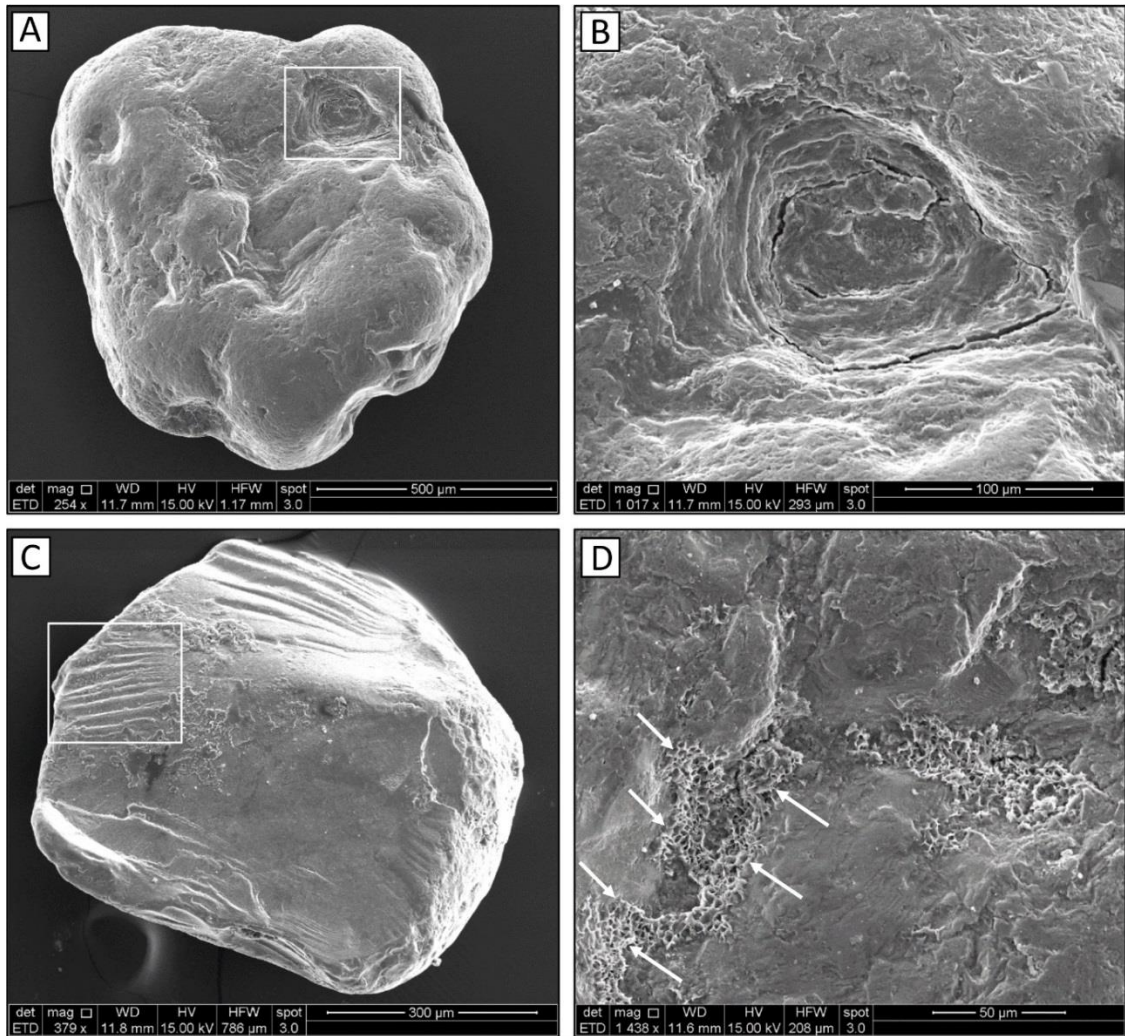


Figure 6.17 Magnetite: (A) Large fractured dissolution pit (white square), Meso Orange River gravel, Sendelingsdrif Deposit. (B). Close up of dissolution pit in Picture A. (C) Conchoidal fracture (white square) on magnetite, Proto Orange River gravel, Sendelingsdrif Deposit. (D) Honeycomb dissolution texture (white arrows), Proto Orange River gravel, Arrisdrif Deposit.

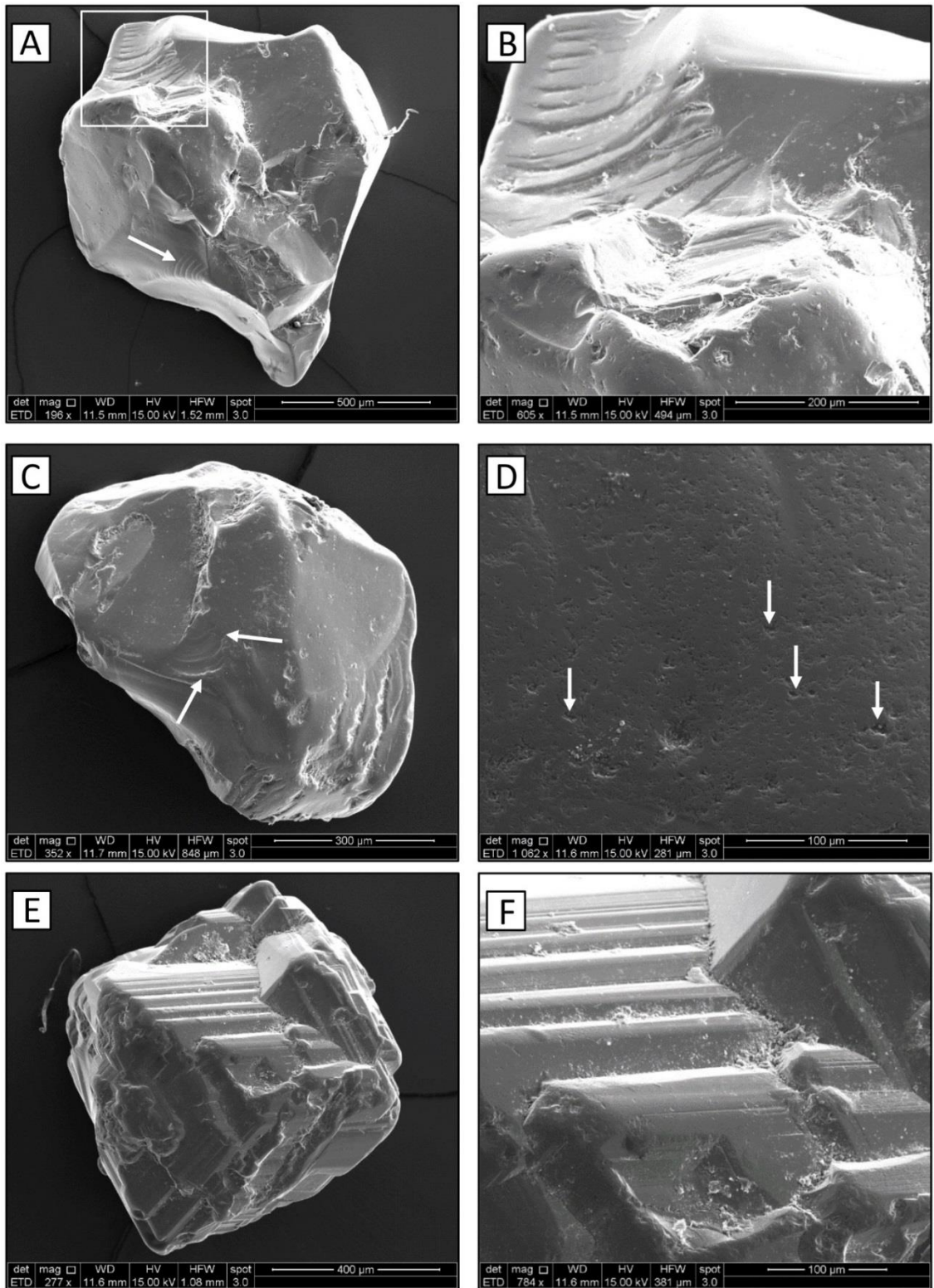


Figure 6.18 Garnet: Conchoidal fractures on garnets from Region K (A and B) and Region V (C). Picture D shows small dissolution pits (arrows), Region N. Imbricate wedge marks on garnet, Region W (E and F).

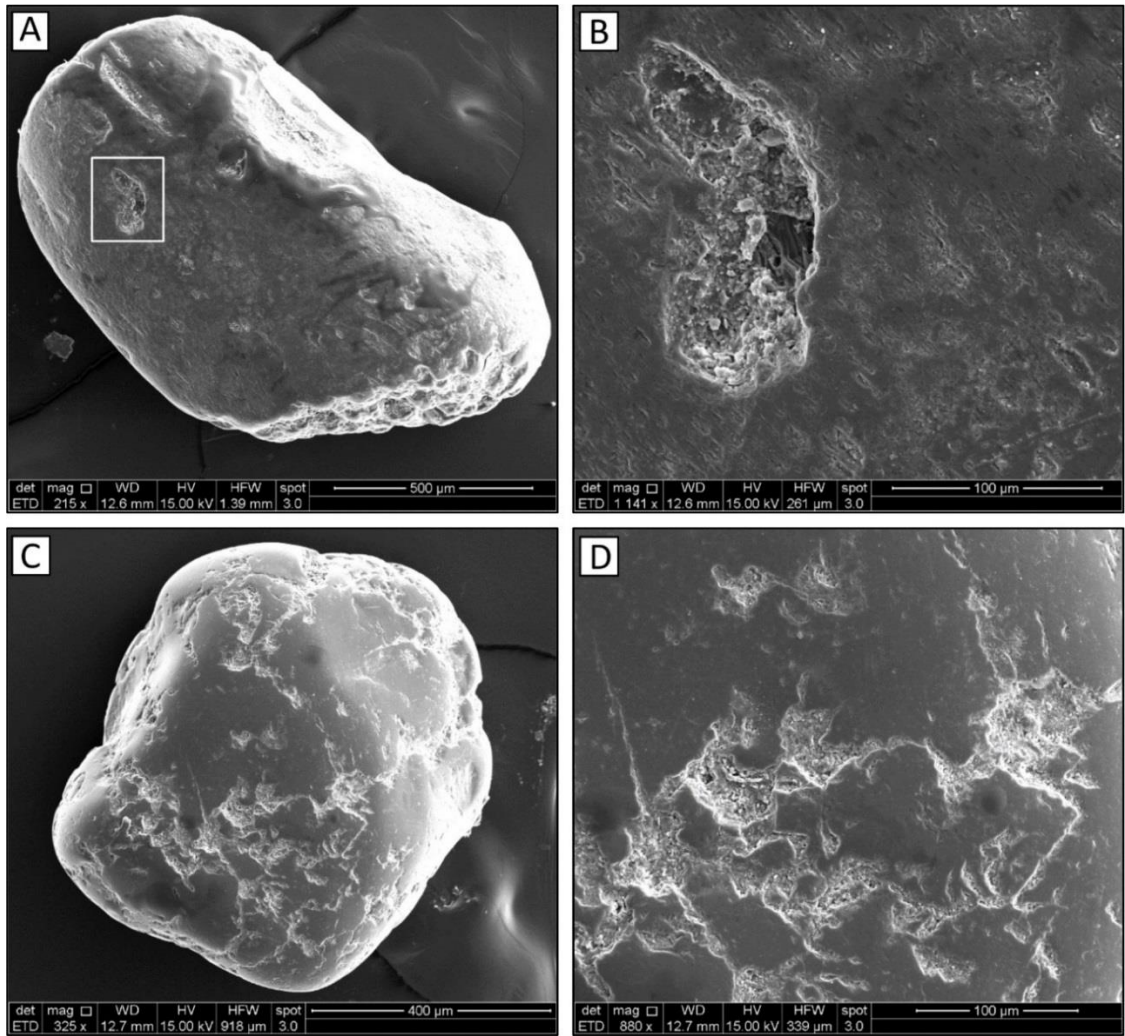


Figure 6.19 Epidote: Large dissolution pit (A and B). Irregular dissolution pits on a rounded epidote (C and D). All grains from Region V.

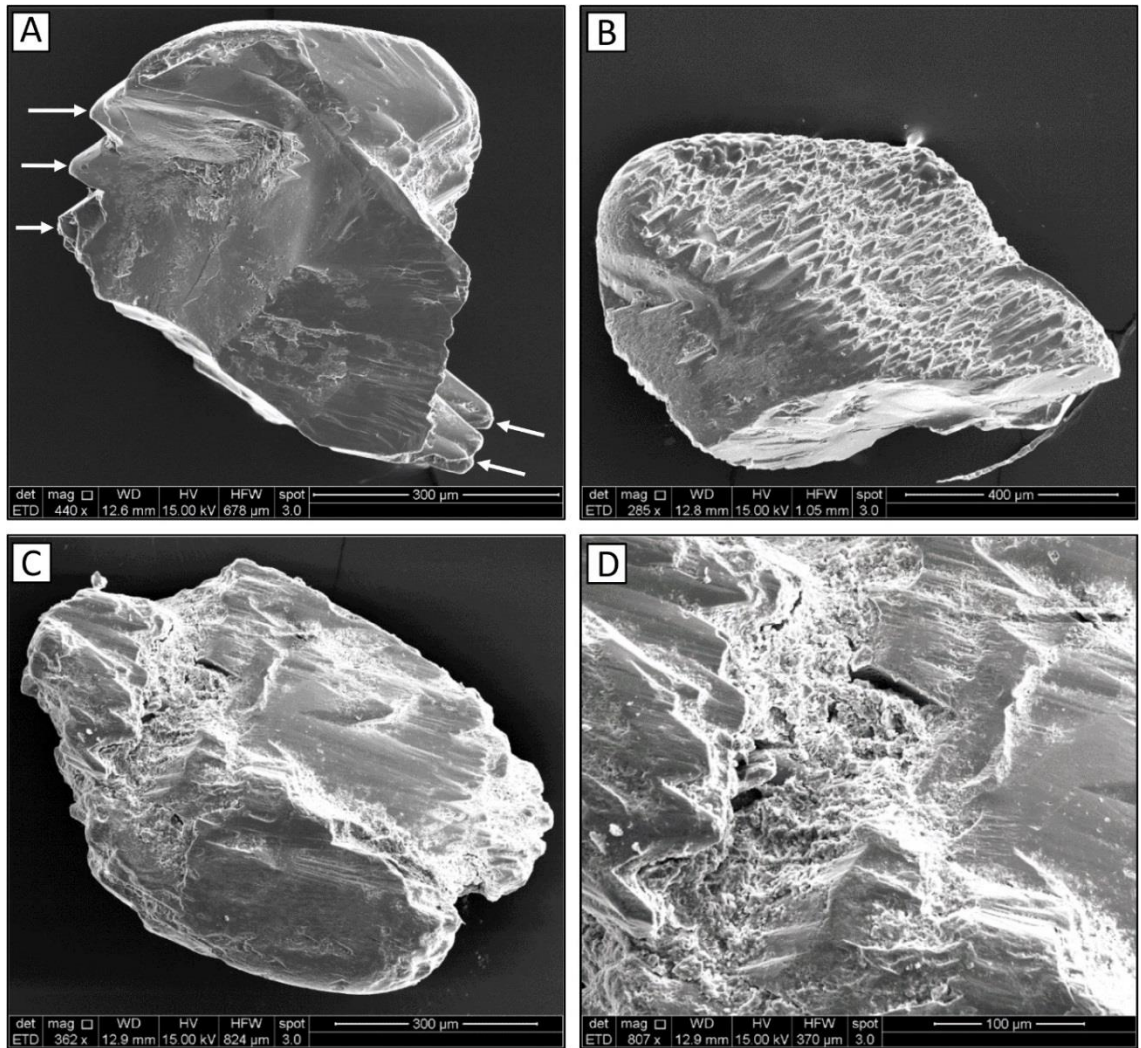


Figure 6.20 Epidote: Saw tooth terminations (arrows in A) from Region K (A and B) and Region V (C and D).

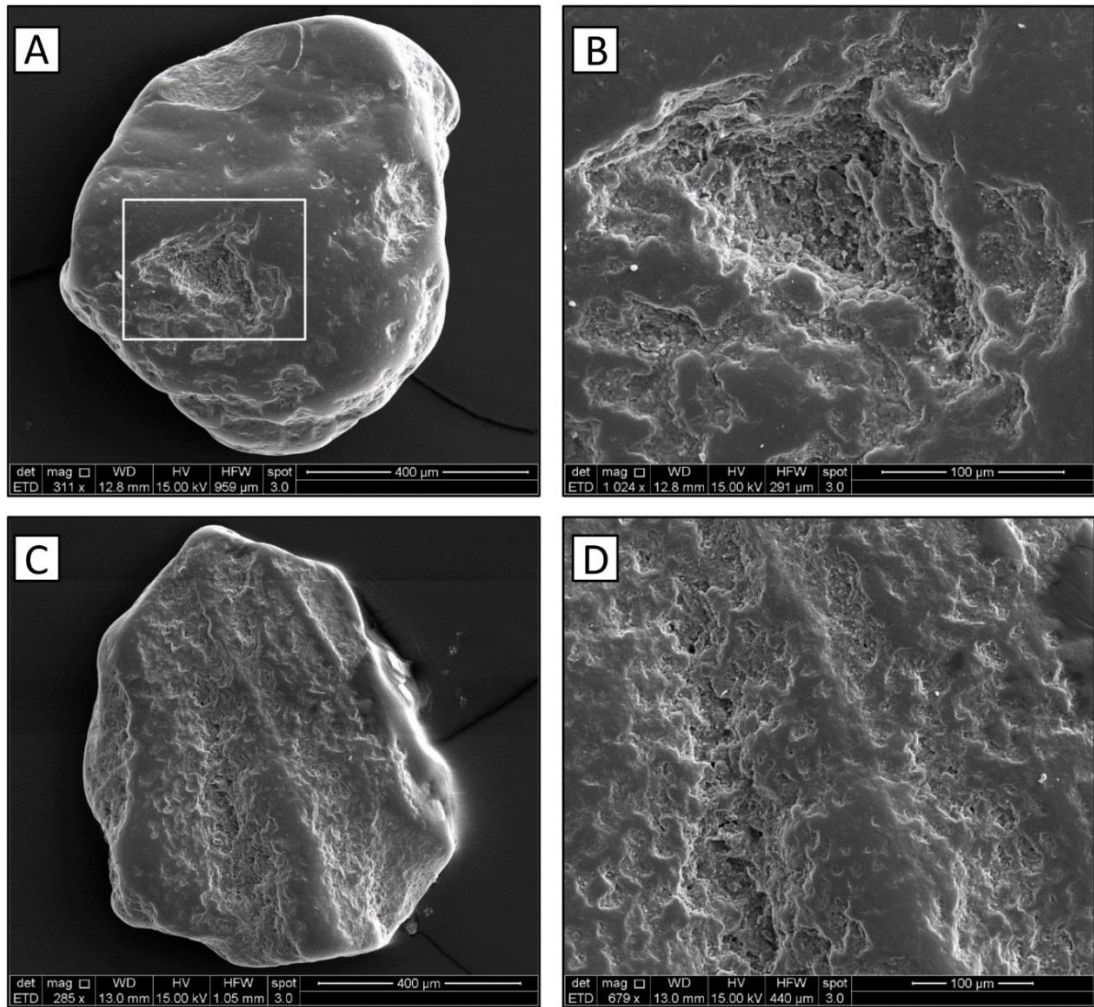


Figure 6.21 Magnetite: Irregular dissolution pits, Region N.

Table 6.2 Comparison of surface textures between Proto Orange River gravels, Meso Orange River gravels and Atlantic 1 gravels.

Mineral	Grain Surface Texture	Process Type of Formation	Proto Orange River gravel	Meso Orange River gravel	Atlantic 1 gravel
Garnet	Conchoidal fracture	Mechanical	Present	Present	Abundant
	Etch pits superimposed on conchoidal fractures	Chemical	Present	Present	Absent
	Triangular etch pits	Chemical	Present	Present	Absent
	Irregular shaped etch pits	Chemical	Present	Present	Present
	Cobbled texture	Chemical	Present	Present	Absent
	Imbricate wedge marks	Chemical	Absent	Absent	Present
Epidote	Etch pits	Chemical	Present	Present	Present
	Saw tooth terminations	Chemical	Absent	Present	Abundant
Magnetite	Etch pits	Chemical	Present	Present	Present

6.5 Mineral composition

Each of the heavy minerals discussed above could be derived from different lithologies and if so, these different provenances could be reflected in their element chemistry. The mineral species selected for chemical composition comparison are garnet, epidote and magnetite because of their relative

importance in the heavy mineral suites as described above. The target size fraction was 0.5-1 mm size fraction because it is the size fraction from which grain surface textures were analysed. In addition each of the three minerals exhibits different physical and chemical durability which could influence longevity in the fluvial and marine systems. Garnet is resistant to alteration (Morton, 1984). Epidote was chosen because it is the key discriminator (in addition to amphibole) between the Proto and Meso Orange River gravels as well as between the western and eastern gravels from Atlantic 1 as discussed in section 6.2. Magnetite is sensitive to oxidising and reducing conditions of the geochemical environment for example between river and marine environments (e.g., Weibel and Friis, 2007).

6.5.1 Garnet

Garnet populations from fluvial and marine sediments have been compared in terms of their FeO/MgO and FeO/MnO ratios (Fig. 6.22). Figures 6.22A and 6.22C show compositional data for garnets derived from the Gariep Belt and Namaqua Metamorphic Complex, and these data have been used to identify the compositional fields outlined in Figures 6.22B and 6.22D, which also include the results of the present study. Both Orange River garnets and Atlantic 1 garnets show a similar, but very narrow range of FeO composition (Fig. 6.22). The majority of garnets in the fluvial and marine gravels show compositions similar to that of the garnets from the Namaqua Metamorphic Complex. A few garnets with a composition consistent with those from the Gariep Belt have been recorded in Proto Orange River deposits (n = 4), Meso Orange River deposits (n = 2) and in Atlantic 1 (n = 4) from different locations (Fig. 6.22).

6.5.2 Epidote

The epidote display a narrow range of Ca compositions (Fig. 6.23). Epidote grains from the Proto and Meso Orange River deposits and Atlantic 1 deposits show similar ranges of Ca, and Fe contents (Figs. 6.23). A few epidote grains show

lower Ca content (18.5-20.21 wt.%) from the rest of the group and these are from Meso Orange River deposits (n = 7) and to a less extent from Proto Orange River deposits (n = 2) and Atlantic 1 deposits (n = 3).

6.5.3 Magnetite

There are two sets of magnetite in the Orange River deposits and the Atlantic 1 deposits (Fig. 6.24). The first group has high FeO (79.27-91.44 wt.%) and low TiO₂ (< 11 wt.%) contents. The second group is characterised by lower FeO (38.05-49.81 wt.%) and high TiO₂ (46.26-55.13 wt.%) (Fig. 6.24A). Most of magnetite in Atlantic 1 belong to the high TiO₂ group. Within the low TiO₂, high FeO magnetite group, the Proto and Meso Orange River magnetite show slightly higher FeO and lower TiO₂ than the Atlantic 1 magnetite. For example, FeO content is 80.42-91.20 wt.% and 80.47-91.44 wt.% for the Proto Orange River and Meso Orange River magnetite, respectively whereas it is slightly lower for Atlantic 1 magnetite (79.27-82.91 wt.%) (Fig. 6.24A). In addition, the low TiO₂ magnetites are also characterised by very low MnO content (< 0.4 wt.%) whereas the high TiO₂ magnetite have elevated MnO content (0.47-10.22 wt.%) (Fig. 6.24B).

6.6 Relationship between heavy mineral distribution and diamond grade in Atlantic 1

The heavy mineral fraction of sand size sediment may be of use in predicting the presence or abundance of detrital diamonds in two ways. Firstly, specific minerals may share a common provenance with the diamonds, i.e. they may represent minerals derived from diamondiferous kimberlite. Secondly, the minerals may have a separate origin from the diamonds but act as a diamondiferous facies marker.

6.6.1 Diamond grade

The term 'diamond indicator minerals' is commonly used to describe heavy minerals that have characteristic compositions relative to the same mineral types from non-diamondiferous rocks (McCandless and Gurney, 1989; Wyatt et al., 2004). Such minerals have been applied to exploration of alluvial diamond deposits (Marshall and Baxter-Brown, 1995). Among the suite of diamond indicator minerals, garnet and ilmenite occur in both the Atlantic 1 gravels and the Proto and Meso Orange River gravel terrace deposits. One aim of this section is to establish the relative importance of diamond indicators derived from kimberlites with other mineralogically similar heavy minerals sourced from more local lithologies

The diamond data presented in Table 6.3 was provided by Debeers Marine Namibia, and it is based on production data from Atlantic 1. The grade (carats/m²) and stone size (carats/stone) are calculated for 25 m x 25 m blocks, referred to as panels. The data reported here relates to panels for which heavy mineral data is also available from the present study. The diamond grade is obtained by dividing the number of diamond stones recovered by the total area of the panel. Similarly, stone size is calculated by dividing the amount of carats recovered from a panel by the number of diamonds. In this study, several samples were collected from the same panel, and therefore they have the same diamond grade and stone size (Table 6.3).

Regionally across Atlantic 1 there is no significant trend in either diamond grade or stone size based on the data set (Fig. 6.25). Also the stone size does not correlate with diamond grade (Fig. 6.26). For example in Region K, the samples that have the highest grade show the lowest stone size. Within Region V and Region W the diamond grade increases in the offshore direction (Fig. 6.25).

6.6.2 Correlation of heavy mineral concentration with diamond grade

The relationship between abundance of different heavy minerals in specific size ranges to diamond grade is illustrated in Figures 6.27 and 6.28. Overall the concentrations of heavy minerals are independent of diamond grade and stone size. It might be expected that the coarse grained heavy minerals (1-2 mm) would

be most likely to show a positive correlation, but this is not the case for garnet, ilmenite or amphibole-epidote (Fig. 6.28). There is a weak positive correlation between diamond grade and the coarsest size fraction of magnetite in Region K, (Fig. 6.27A, B,) and the same relationship is observed with the 0.5-1 mm fraction and grade (Fig 6.27C), but not stone size (Fig 6.27D). This association is not evident in the fine grained magnetite (0.25-0.50 mm) (Fig. 6.27E, F).

6.7 Discussion

The variation in geochemical signature of bulk samples, heavy mineral assemblage, mineral grain surface textures and mineral composition between the Orange River gravels and Atlantic 1 marine gravels (Fig. 6.1) can be influenced by a wide range of factors and these are discussed below.

6.7.1 Integration of bulk geochemistry and heavy mineral assemblage

Linking bulk sample geochemistry to individual heavy minerals is challenging because elements may be hosted in two related, but different minerals. Elements may also vary in their relative proportion within individual mineral species. Consequently the mineral-element correlations are prone to scatter. Elements can also be hosted in completely different minerals such that their overall contribution to the chemical analyses reflects the abundance of the different mineral species (Table 6.1).

In the Orange River and Atlantic 1 samples, magnetite and garnet are the two possible sources of Cr (Table 6.1). The Orange River bulk samples exhibit higher Cr and Fe content relative to the Atlantic 1 samples (Fig. 6.11C). In the same size fraction (0.25-0.50 mm), the marine samples have higher garnet proportion but lower magnetite relative to the river samples. Therefore the majority of the Cr content in the Orange River and marine samples is associated with magnetite (Fig. 6.12A).

Magnetite and ilmenite may contain V (Table 6.1). The higher Fe and V contents of the Orange River gravels (Fig. 6.11A) correspond to higher abundance of

magnetite (Fig. 6.12F). In contrast, the river and marine samples are not easily discernible on the basis of V/ilmenite ratio (Fig. 6.12G). On this basis, most of the V is associated with magnetite instead of ilmenite.

Garnet compositions can vary according to the proportion of the dominant major element (Fe, Mg, Mn and Ca). Although the marine samples have relatively high garnet proportions, their Mn proportions overlaps with that of the river samples (Fig. 6.12H). This can in part be explained by the observation that Orange garnets from the two study environments are Fe-rich (almandine) (Fig. 6.22B) although they contain some Mn (Fig. 6.22D).

In summary the principal mineral–chemical associations are magnetite-Cr, magnetite-Fe and magnetite-V. The other Fe-containing phases, garnet and ilmenite do not show correlation with Fe. The implication of this result for studies of this kind is that the integration of bulk sediment geochemistry and mineral assemblage requires caution because elements can occur in more than one mineral type making it difficult to link bulk sediment composition data to mineral proportion data. The use of mineral composition is recommended because it allows for identification of specific elements that are hosted by more than one mineral.

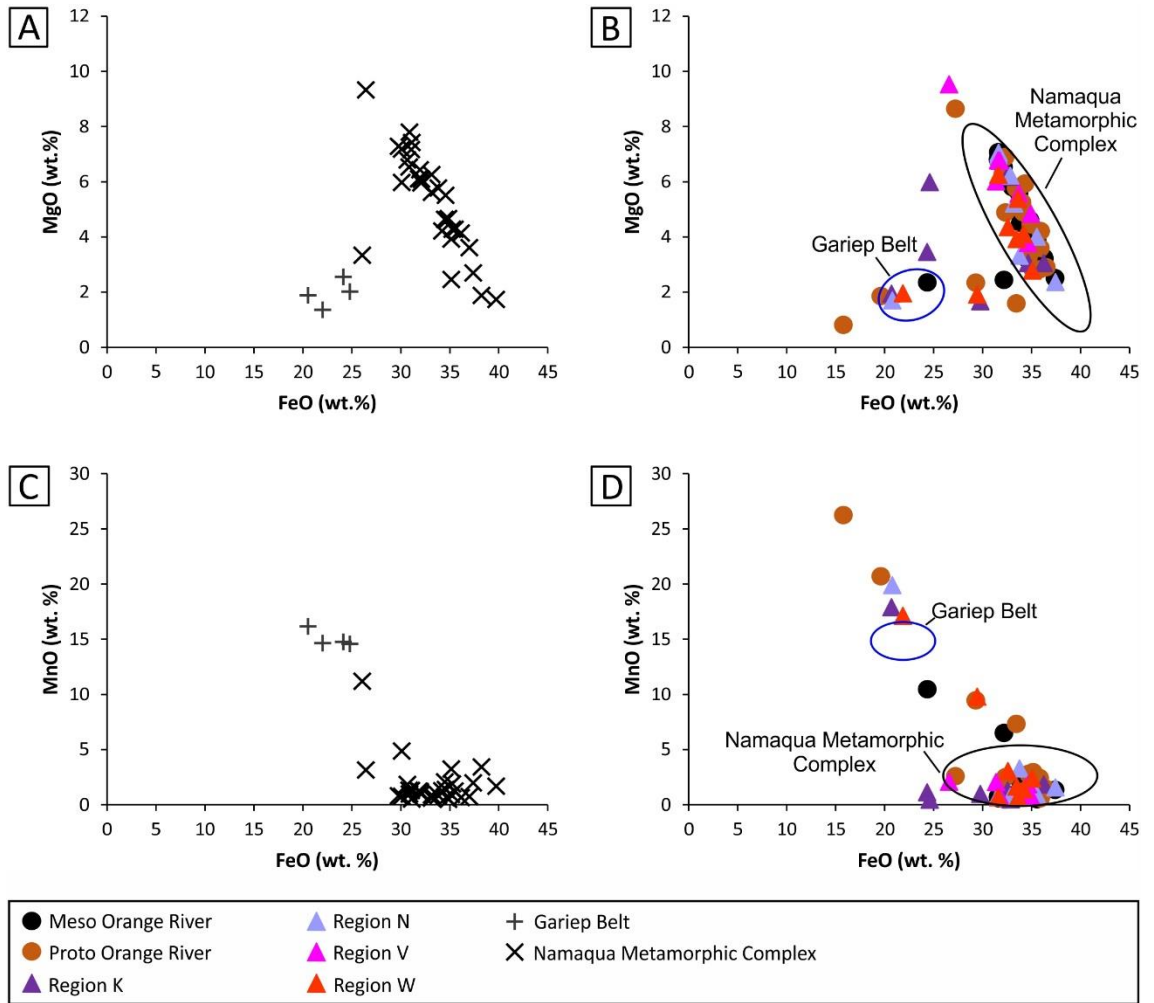


Figure 6.22 (A) Garnet compositions in MgO versus FeO from the Namaqua Metamorphic Complex (Humphreys and Van Bever Donker, 1990; Cornell et al., 1992; Diener et al., 2013; Bial et al., 2015) and Gariep Belt garnets (Diener et al., 2017). (B) Data for Proto and Meso Orange River and Atlantic 1 garnets. (C) MgO versus FeO from the Namaqua Metamorphic Complex and Gariep Belt. (D) Data for Proto and Meso Orange River and Atlantic 1 garnets.

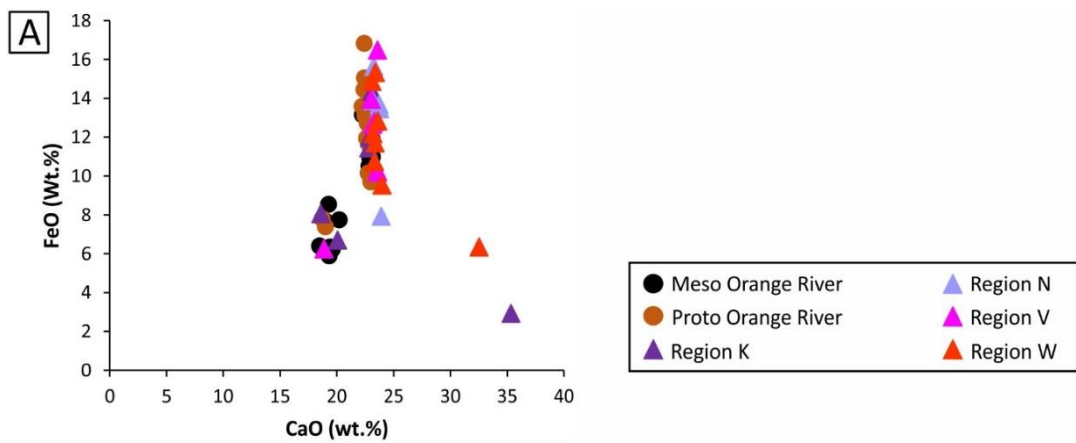


Figure 6.23 Epidote composition from Proto Orange River deposits (n = 20), Meso Orange River deposits (n = 20) and Atlantic 1 deposits (n = 32).

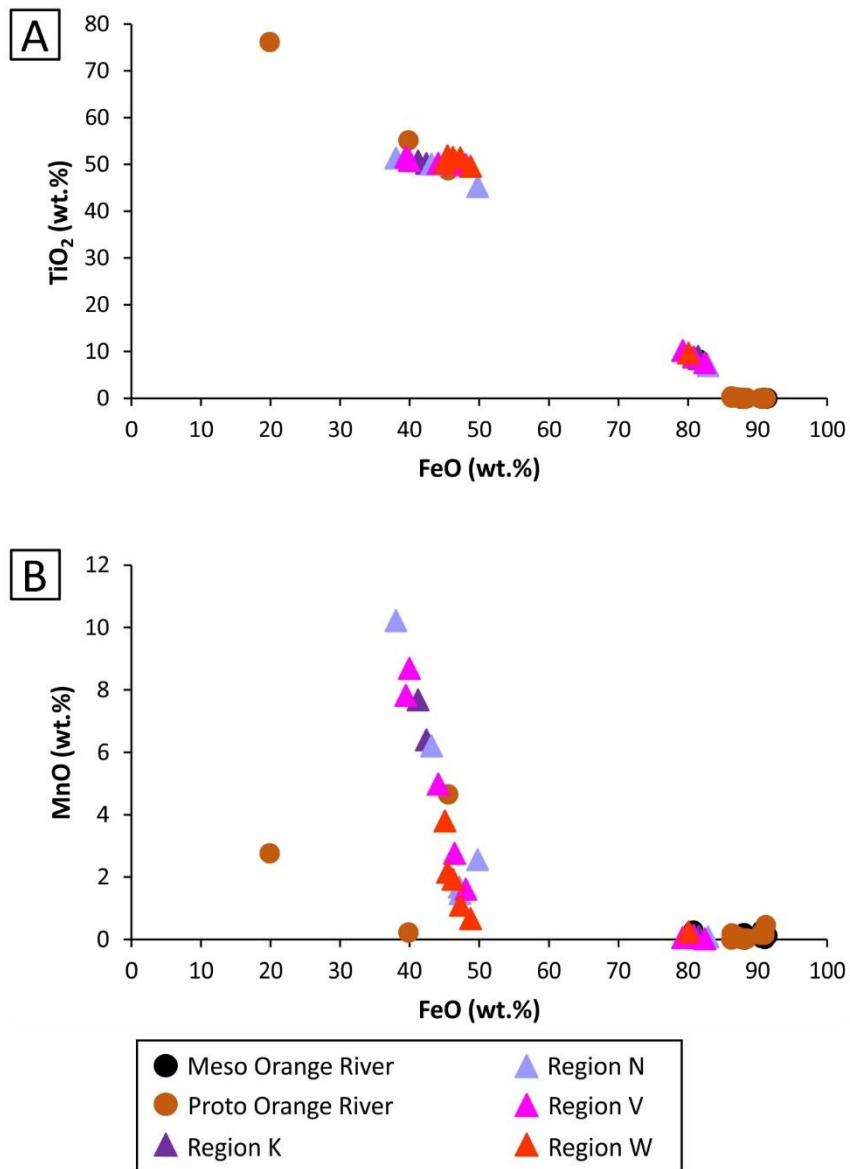


Figure 6.24 Magnetite composition from Proto Orange River deposits, Meso Orange River deposits and Atlantic 1 deposits.

Table 6.3 Diamond grade and stone size for Atlantic samples. Panel size is 625 m².

Region	Panel	Sample Name	Grade (cts/m ²)	Stone size (cts/stn)
Region K	K11/15	Region K-S1	0.079	0.578
		Region K-S2	0.079	0.578
	K26/16	Region K-S3	0.074	0.637
	K30/16	Region K-S4	0.055	0.630
		Region K-S5	0.055	0.630
		Region K-S6	0.055	0.630
		Region K-S7	0.055	0.630
Region N	N07/16	Region N-S1	0.051	0.606
		Region N-S2	0.051	0.606
		Region N-S3	0.051	0.606
		Region N-S4	0.051	0.606
		Region N-S5	0.051	0.606
		Region N-S6	0.051	0.606
Region V	V39/15	Region V-S1	0.106	0.633
		Region V-S2	0.106	0.633
		Region V-S3	0.106	0.633
	V57/15	Region V-S4	0.078	0.622
		Region V-S5	0.078	0.622
		Region V-S6	0.078	0.622
		Region V-S7	0.078	0.622
	V30/16	Region V-S8	0.054	0.721
		Region V-S9	0.054	0.721
Region W	W11/16	Region W-S1	0.077	0.649
		Region W-S2	0.077	0.649
	W08/16	Region W-S3	0.059	0.477
		Region W-S4	0.059	0.477
		Region W-S5	0.059	0.477
		Region W-S6	0.059	0.477

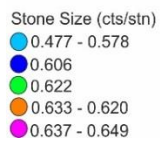
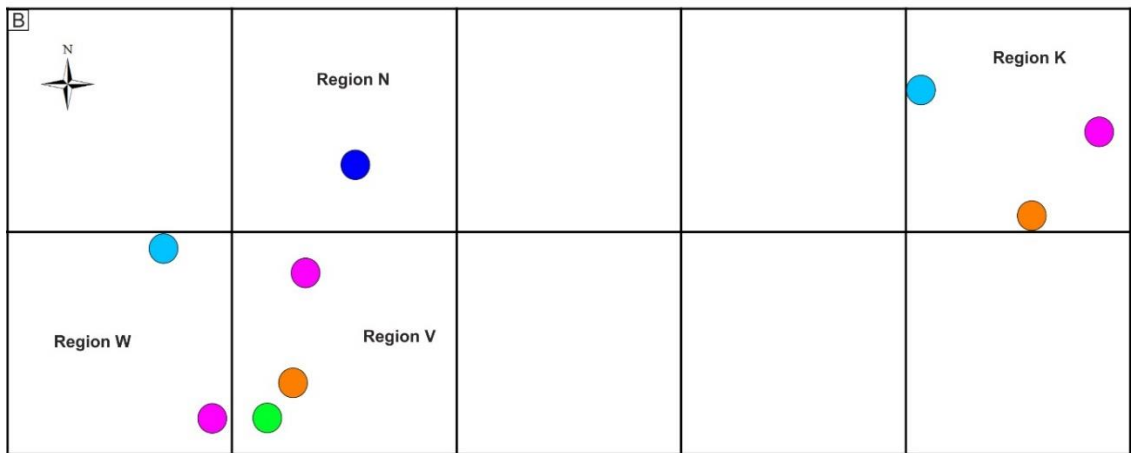
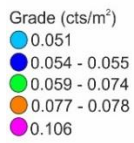
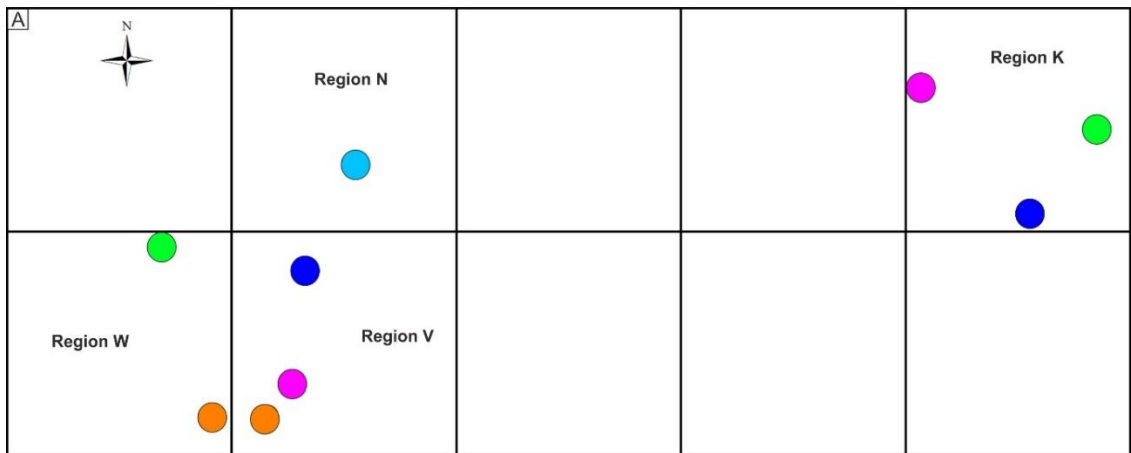


Figure 6.25 Variation of diamond grade (A) and stone size (B) in Region K, Region N, Region V and Region W.

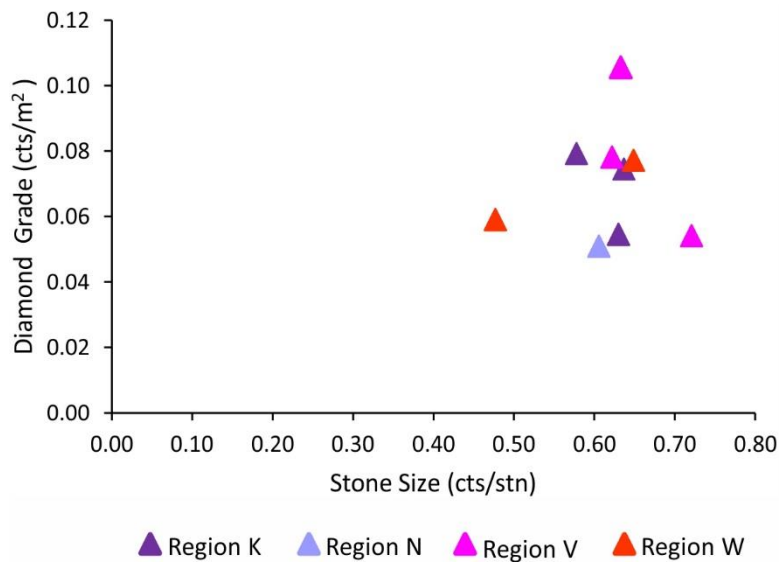


Figure 6.26 Covariation of diamond stone size and grade in Atlantic 1.

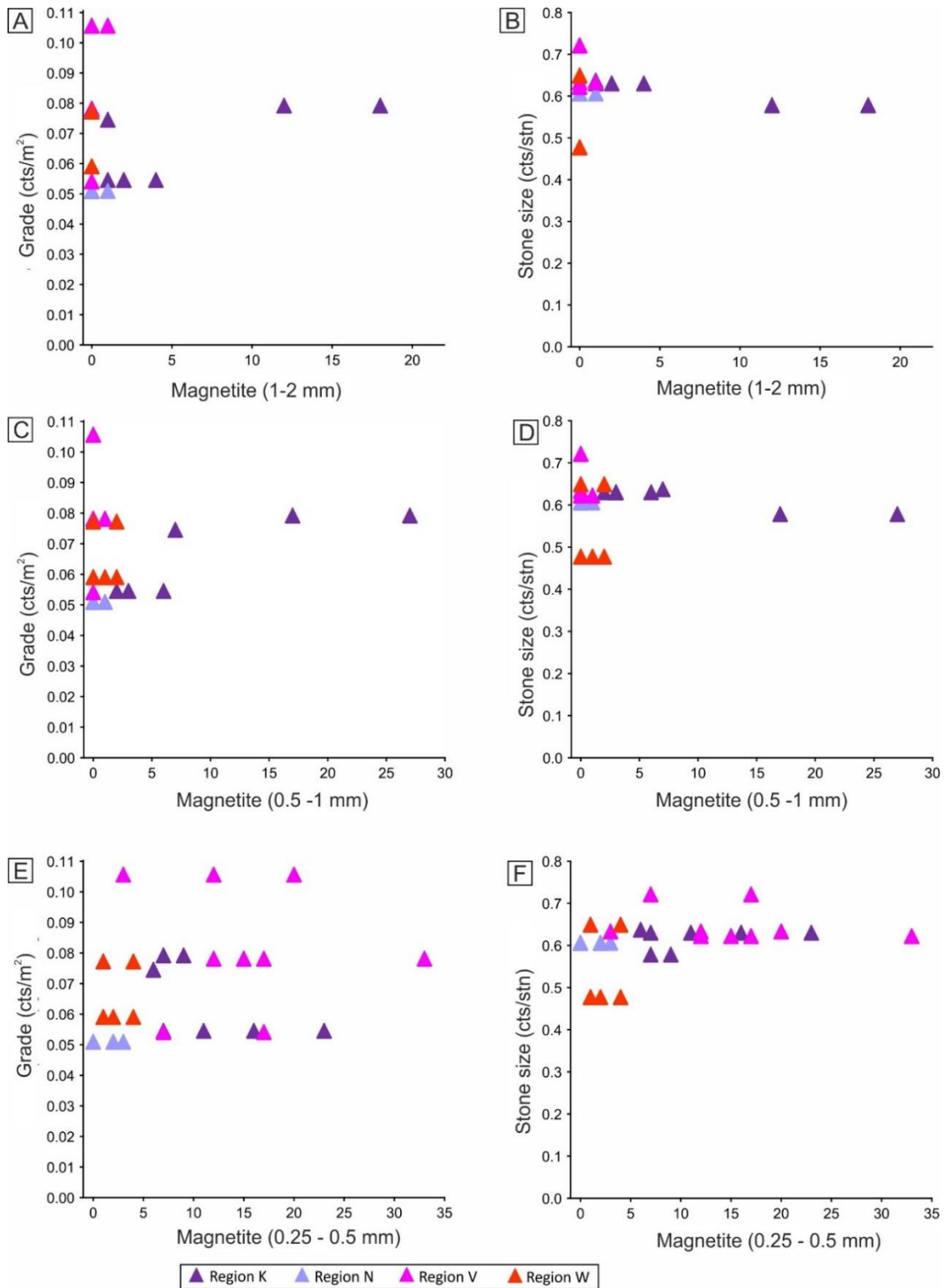


Figure 6.27 Variation of diamond grade and stone size with magnetite proportions for the Atlantic 1 gravels.

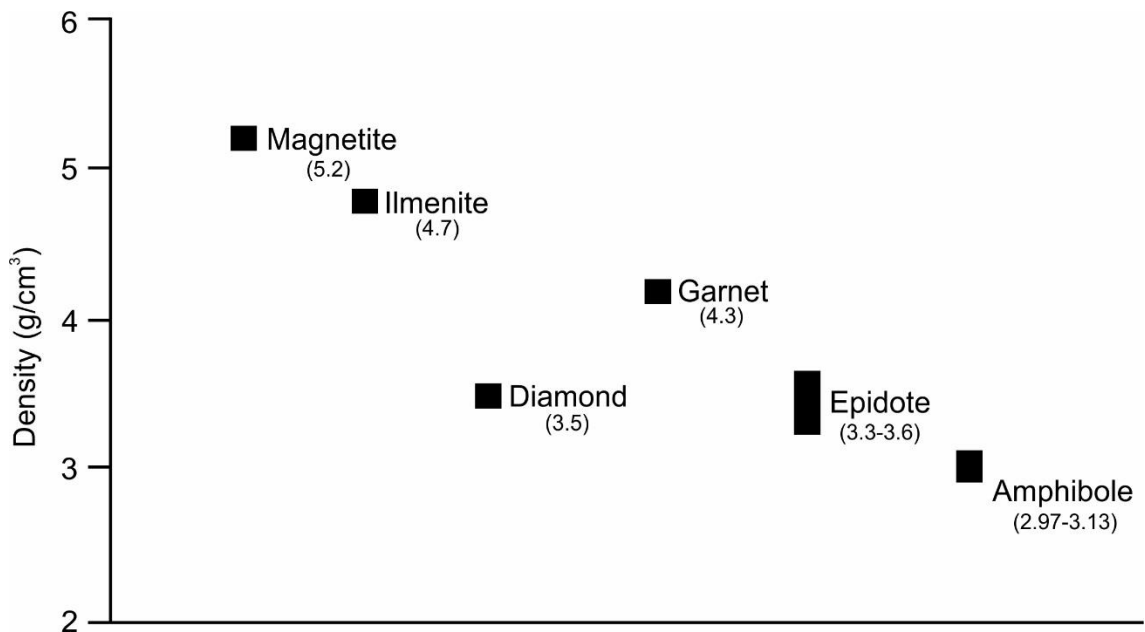


Figure 6.29 Comparison of relative density of Atlantic 1 heavy minerals and diamonds. Numbers in brackets are density values. No values are plotted on the x-axis.

6.7.2 Controls on variations of mineral surface textures

Grain surface textures of heavy minerals in sediments can be inherited from the crystalline parent rock or formed during sediment transport, deposition, diagenesis and weathering (Turner and Morton, 2007; Velbel et al., 2007) by mechanical and chemical processes (Mahaney, 2002). Preservation of inherited grain surface textures depends on the energy of the transport system. Conchoidal fractures (Figs. 6.13A, 6.13B, 6.14B) are formed by mechanical processes (Velbel et al., 2007) whereas etch pits (e.g., Fig. 6.13B, 6.13D, 6.14D) are formed by chemical dissolution as a result of reaction between mineral grain surfaces and solutions (Velbel, 1984). Morton and Hallsworth (2007) reported that the type of dissolution surface textures formed on a given mineral is influenced by its composition and crystal structure.

In the Orange River gravels, the etch pits on garnets are likely to have been formed post deposition because some etch pits are superimposed on conchoidal fracture surfaces (Figs. 6.13A, 6.13B, 6.14B). The fact that mineral surface textures are similar in both Proto Orange River and Meso Orange River gravels

(e.g., Fig. 6.14A, B) suggest minimal recycling of the Proto Orange River deposits during the depositional phase of the younger Meso Orange River gravel. Extensive reworking and recycling of the older Proto Orange River deposits would have produced a clear difference in the surface textures between the two sets of gravels as some surface textures might have been overprinted during reworking. For example, etch pits superimposed on conchoidal fractures observed on garnets (Fig. 6.14B) may not have been preserved in the Meso Orange River gravels had the gravel gone through multiple phases of reworking and inheritance from the older Proto Orange River gravels. The limited signal of reworking of older Proto Orange River gravels is also evident from both clast assemblage and heavy mineral assemblages as discussed in Chapter 4.

The process of how imbricate wedge marks (Figs. 6.18E, F) form has been widely debated with some workers suggesting origin by overgrowth (e.g., Simpson, 1976) and others by dissolution (e.g., Salvino and Velbel, 1989; Hansley and Briggs, 1994; Morton et al., 2003; Turner and Morton, 2007). Based on experimental and field data, Morton et al. (2003) confirmed that imbricate wedge marks represent advanced stages of garnet dissolution. Velbel et al. (2007) argue for formation of imbricate wedge marks by merging of large dodecahedral etch pits. Imbricate wedge marks are absent on the garnets from the Proto and Meso Orange River deposits. In Atlantic 1, imbricate wedge marks are only recorded on a single garnet grain from Region W (Figs. 6.18E, F). Therefore, the gravel in Region W had a prolonged degree of stability to allow for advanced stages of garnet dissolution and support an interpreted older age of the Region W (and by inference Region V) gravel than the Proto Orange River gravel. The prolonged period of stability is in agreement with the relative higher amount of authigenic apatite, a mineral whose formation requires extended periods in deep water (Filippelli, 2011), in Region W (and Region V) compared to the eastern regions (Region K and Region N) (Fig. 5.15, Chapter 5). Although the type of dissolution texture on garnets is sensitive to the geochemical conditions of environment of alteration (Salvino and Velbel, 1989), imbricate wedge marks have been reported on detrital garnets from both onshore sediments (Hansley, 1987; Velbel et al., 2007) and sea sediments (Turner and Morton, 2007).

The absence of euhedral triangular etch pits on the Atlantic 1 garnets (Fig. 6.18D) either means (i) the etch pits were removed by mechanical breakdown post primary deposition because the Atlantic 1 garnets have abundant conchoidal fractures or (ii) the geochemical conditions of the marine environment is not conducive for their formation. The formation of large etch pits (1- 10 μm) occurs on a decades to centuries timescale (Velbel et al., 2007). The relative smaller size of the etch pits on Atlantic 1 garnets (Fig. 6.18D) compared to the Proto Orange River and Meso Orange River garnets (Figs. 6.13C, 6.13D, 6.14A, 6.14D) either imply that the marine gravel has undergone some degree of relocation by subaqueous currents given the dynamic nature of the marine environment, or the marine environment is not favourable for the formation of large etch pits on garnets since garnet is sensitive to geochemical conditions in which dissolution takes place (Salvino and Velbel, 1989). On the basis of presence of imbricate wedge marks on garnet from Region W and associated higher apatite content that also requires extended periods of stability (Morton et al., 2003; Filippelli, 2011), the absence of large etch pits on the Atlantic 1 garnets can be attributed to differences in geochemical conditions between the river environment (Orange River) and marine environment (Atlantic 1) as opposed to gravel erosion and displacement.

While Berner et al. (1980) suggest that saw tooth terminations on epidote (Figs. 6.16, 6.20) are destroyed during transport owing to their delicate nature, Velbel et al. (2007) believe that it is possible for them to survive transport although this is largely influenced by the energy of the system. However, the abundance of conchoidal fractures on garnets from the Orange River deposits (e.g., Figs. 6.13A, 6.13B, 6.14B) and Atlantic 1 deposits (Figs. 6.18A, B, C) suggest a high energy transport system (Velbel et al., 2007) in which the saw tooth textures would be destroyed. Therefore, the saw tooth textures on epidote from the Meso Orange River gravels (Fig. 6.16) and the Atlantic 1 gravels (Fig. 6.20) were likely formed post deposition. It is striking that saw tooth terminations are present on epidotes from both the river and marine gravels whereas euhedral etch pits on garnets are only present on garnets from the Orange River gravels (Figs. 6.13D, 6.14A, D) and they are absent in the marine environment. Perhaps the absence of euhedral etch pits on garnets in Atlantic 1 gravels is because the type of grain

surface textures formed on garnets are very sensitive to the geochemistry of the environment in which they are formed compared to other silicate minerals as documented by Salvino and Velbel (1989).

Epidote is diagenetically less stable than garnet and magnetite (Morton, 1986; Morton and Hallsworth, 2007) and shows a higher degree of dissolution, in both fluvial samples (Figs. 6.15, 6.16) and marine samples (Figs. 6.19, 6.20). This suggests that there was no inheritance of minerals from older sediments through reworking. Inheritance of minerals from older sediments through recycling would produce a set of surface textures where the most stable minerals (garnet and magnetite) show the highest degree of dissolution textures than the least stable mineral (epidote). Therefore the mineral surface texture data show that the Atlantic 1 gravel have not been extensively recycled.

Magnetite grains from the marine samples have suffered much more extensive dissolution (Fig. 6.21) compared to the magnetite from river samples (Fig. 6.17). This can be explained by preferential dissolution of magnetite in the relatively reducing marine environment where hydrogen sulphide responsible for magnetite dissolution is generated by decay of organic matter (Kasten and Jørgensen, 2000; Brüchert et al., 2003). The Namibian continental shelf is enriched in organic matter as a result of the upwelling Benguela current (Diester-Haass et al., 2002; Monteiro et al., 2005; Edelman-Furstenberg, 2014; Nagel et al., 2016) making it a favourable environment for magnetite dissolution. In addition to being sequestered in the Orange River deposits, dissolution of magnetite may in part have contributed to the lower magnetite content in the marine gravels relative to the river gravels.

6.7.3 Controls on mineralogy of heavy mineral assemblage

The strong correlation in major element chemistry between garnets derived from the Namaqua Metamorphic Complex and those from Orange River and Atlantic 1 sediments (Fig. 6.22) both indicates the source of the garnet assemblage and suggests that the Namaqua Metamorphic Complex is a major contributor of other minerals to the heavy mineral inventory. There are, however, the few low-FeO, high-MnO (up to 25 wt.% MnO, Fig. 6.22) garnets recorded in both the river and

marine deposits that are consistent with known composition of garnets from the Gariep Belt, particularly with respect to their MnO content. The fact that only a few garnets from the Orange River deposits and Atlantic 1 deposits are derived from the Gariep Belt either suggest that the Orange River drained only a small percentage of the Gariep Belt rocks or the Gariep Belt rocks contain a low proportion of garnet. The similarities in garnet, epidote and magnetite compositions between the Orange River deposits and Atlantic 1 deposits (Figs. 6.22, 6.23, 6.24) further strengthen arguments for a common provenance of the heavy minerals in the Orange River gravels and the Atlantic 1 terrigenous marine gravels. There are two compositional groups of magnetite from the Orange River and the Atlantic 1 deposits, namely the low TiO₂ group and high TiO₂ group (Fig. 6.24A). As described in Chapter 3, Section 3.3.5, magnetite grains in this study were selected by using a hand held magnet and any mineral that was picked up by the magnet was classified as magnetite. The high TiO₂ minerals (Fig. 6.24A) are possibly magnetic ilmenites.

The proportion of garnet in the samples from the Atlantic 1 deposits is higher than in the Proto samples and Meso Orange River samples in the finer size fractions (0.5-1 mm and 0.25-0.50 mm) (Figs. 6.2, 6.3, 6.4). This could be a function of sediment bypass where garnet being more mobile (as a consequence of density) than magnetite, is transported longer distance to the continental shelf from the Namaqua Metamorphic Complex and Gariep Belt source rocks. Proto Orange River gravel has the highest number of coarse garnets (1-2 mm) (Fig. 6.4A) and the lowest number of fine grained garnets (0.5-1 mm and 0.25-0.50 mm) (Fig. 6.4B, C). The Atlantic 1 gravel follows an opposite trend to the Proto Orange River gravel where it has the lowest number of coarse garnets and the highest number of fine grained garnets (Fig. 6.4). Most of the fine grained garnets in the Atlantic 1 gravels are possibly those that have been bypassed through the Orange River and a higher proportion of coarser garnets remained in the river deposits. Alternatively, the Atlantic 1 garnets may have been further reduced in size through abrasion in the marine environment given the higher abundance of conchoidal fractures in the marine environment than the river environment or transport distance threshold (Table 6.2). Cascalho and Fradique (2007) reported a similar trend on the Portuguese shelf where the proportion of garnets (among

biotite, andalusite, tourmaline, amphibole, staurolite, zircon and apatite) is higher in the shelf sediments than in the coeval river sediments.

On the basis that the proportion of fine grained garnet (0.25-0.5 mm and 0.5-1 mm) increases from the river deposits to the marine deposits, the lower amount of magnetite in the marine deposits can be explained as a function of relative density. Magnetite is denser than garnet, and could be sequestered in the Proto Orange River and Meso Orange River deposits because they are closer to the magnetite source rocks (Namaqua Metamorphic Complex rocks) than Atlantic 1. In Atlantic 1, magnetite is higher in Region K, but decreases away from the Orange River mouth, and is rare to absent in Regions N and W (Figs. 6.6, 6.7, 6.8, 6.9). In Region V, magnetite is present in the fine size fraction (0.25-0.50 mm). This could be a function of density as magnetite (5.2 g/cm^3) (Pellant, 2000) is the densest among the Atlantic 1 heavy minerals and therefore will not travel far from the input point. Frihy (2007) observed a similar pattern on the continental shelf, along the Nile Delta, where magnetite is deposited close to the Nile River mouth and its abundance decreases offshore. However, the amount of magnetite in Region V is similar to that of Region K for the 0.25-0.50 mm size fraction (Fig. 6.6D) despite Region V being located seaward of Region N. A plausible explanation for the higher amount of magnetite in Region V could be that Region V was located close to the palaeo-Orange River mouth, which is believed to have been 10 km north of the modern Orange River mouth. Evidence for the palaeo-Orange River mouth is cited to be the fluvial sandstone footwall on which some raised beach gravels were deposited (Fig. 2.6A, Chapter 2).

The Atlantic 1 sedimentary deposits are the offshore depositional record of periods of incision and sediment bypass prior to accumulation of the Proto Orange River deposits, Meso Orange River deposits, and modern gravel terrace deposits of the lower Orange River. The thick nature of the Proto Orange River deposits, up to 50 m, (Early to Middle Miocene; Corvinus, 1978; Corvinus and Hendey, 1978; Hendey, 1978; Pickford, 1987; Pickford and Senut, 2002) and Meso Orange River deposits, 6-23 m, (Plio-Pleistocene; Pether, 1986) suggest that their accumulation was coeval with a marked decrease of sediment flux to

the offshore at the time of their respective aggradation and a reduced gravel accumulation in Atlantic 1. The inferred Plio-Pleistocene age of the Meso Orange River gravel (Pether, 1986) is a time of global sea level fall after a late Miocene high stand (Miller et al., 2005). In contrast the age of the Meso Orange River gravels suggest that they were deposited during a low stand after the late Miocene high stand, with the implication that the timing of incision and aggradation of the Orange River was not controlled only by base-level changes. Conventionally, conditions that drive sediment deposition by rivers on continents are high sea levels during which sediment flux to the oceans is low, whereas during low sea level rivers are in incision mode and most sediments are transferred to the oceans (Leeder, 1999; Bridgland and Westaway, 2008). Similarly, if denudation in the catchment area is reduced, rivers tend to incise their floodplains (Métivier and Gaudemer, 1999). However, the timing of sediment generation, and the capacity of the rivers to transport and bypass sediment is also controlled by climate (Charlton, 2008; Hidy et al., 2014). The duration of the two periods of high sediment flux to the offshore via the Orange River, before aggradation of the Proto Orange River gravel deposits and the Meso Orange River deposits is poorly constrained. Similarly, the change in sediment flux to the coast in response to the aggradation events on the lower Orange River is not possible to quantify.

The basement geology of Atlantic 1 is dominantly sedimentary made up of clay, sandstone and conglomerate. On the basis that crystalline rock (Gariiep Belt) is only known to occur along the coastline, (its western boundary is located 4 -12 km from the coastline (Dingle, 1973), the heavy minerals in Atlantic 1 can be assumed to be primarily derived from onshore via the Orange River. Similarly, only a small number of Orange River garnets and Atlantic 1 garnets are similar in composition to the Gariiep Belt garnets with the majority showing compositions of Namaqua Metamorphic Complex garnets (Fig. 6.22B, D). Basei et al. (2005) correlated the Gariiep Belt to the Dom Feliciano Belt of Brazil and Uruguay, which represent the western extension of the Gariiep rift basin. The Gariiep Belt may therefore extend further offshore below Region V and W. However, even if the Gariiep Belt extends further offshore below the Cretaceous clay, the thick (> 8 m) clay would effectively form a barrier to erosional products from the supposedly

deep-seated Gariep Belt rocks. On this basis, heavy minerals can be used to link the Proto and Meso Orange River gravels with the Atlantic 1 gravels.

Gravel in Region V and Region W has low amphibole-epidote content that is characteristic of the Proto Orange River gravel (Figs. 6.6, 6.7) whereas Region K and Region N have amphibole-epidote content similar to that of the Meso Orange River gravel (Figs. 6.8, 6.9). Based on these observations, the majority of the Atlantic 1 gravels in Region V and Region W were primarily deposited before the main aggradational phase of the Early to Middle Miocene Proto Orange River gravels. By contrast, the main gravel deposition in Region K and Region N were possibly deposited prior to the aggradation event that led to the deposition of the Meso Orange River gravels when sediment flux to the offshore was still high. By this logic, the Region V and Region W gravel is possibly Oligocene whereas the Region K and Region N gravels are likely to be late Middle Miocene to early Late Miocene. However, there is still a possibility of sediment mixing and processes that move sediment seaward, landward (wave action) and northward (longshore drift).

In Atlantic 1, the proportion of amphibole-epidote decreases away from the river mouth (Region K and Region N) to the offshore regions (Region V and Region W) (Fig. 6.6). Compared to garnet and magnetite, amphibole-epidote are highly mobile (Frihy, 2007; Garzanti et al., 2015), so if the amount of amphibole-epidote supplied to the coast remained the same through time then amphibole-epidote would be expected to have been moved northward by longshore drift and other littoral currents. However, this is not the case. Similarly, Garzanti et al. (2015), through the study of heavy minerals in beach sands along the coast, northward of Orange River mouth have reported that amphibole proportion decreases northward between the Orange River mouth and Lüderitz (300 km stretch). The fact that amphibole-epidote is higher in Atlantic 1 regions that are closer to the river mouth could suggest that Region K and Region N gravels underwent minimal erosion and redistribution of amphibole-epidote. Factors that could have prevented extensive erosion include rapid burial of the gravels in Region K and Region N. Therefore, on the basis of northward decreasing amphibole-epidote content, the gravels in Region K and Region N did not undergo extensive erosion

that could have removed mobile amphibole and epidote. Instead, amphibole-epidote minerals decrease from the Orange River mouth to the offshore regions due to the increase of Namaqua Metamorphic Complex sediments, the dominant source of the heavy minerals, to the coast through time. On the basis of positive correlation between the amphibole-epidote content and Namaqua Metamorphic Complex clasts in the Proto and Meso Orange River gravels, and increase of amphibole-epidote through time in the Orange River gravels, the amount of amphibole-epidote can be used as an indicator of the relative age of gravel (Figure 4.13, Chapter 4). However among the heavy minerals present amphibole and epidote are the least stable heavy minerals both in terms of mechanical and chemical stability (Morton and Hallsworth, 2007). Like amphibole and epidote the rest of the heavy minerals (garnet, magnetite and ilmenite) are also dominantly sourced from the Namaqua Metamorphic Complex. Jacob (2005) noted that clasts of Namaqua Metamorphic Complex increased from the older Proto Orange River gravels to the younger Meso Orange River gravels through to the modern Orange River gravels. The fact that garnet, magnetite and ilmenite do not show a marked difference between the Proto Orange River deposits and Meso Orange River deposits suggest that the increase of amphibole-epidote from older gravels to the younger gravels is related to a combination of two factors; (i) increase of Namaqua Metamorphic Complex sediments to the Orange River through time and (ii) mechanical degradation of amphibole-epidote over time.

In summary, the decrease of amphibole-epidote content from Region K towards the offshore is interpreted to be due to the increase in the supply of Namaqua Metamorphic Complex-derived sediments to the coast through time and that Region K gravel is younger for most of the amphibole-epidote to have been preserved. The northward decrease of magnetite from Region K and Region V is due to the relative density of magnetite where magnetite remained closer to the input point, the Orange River mouth, which migrated southward through time.

6.7.4 Controls on the relationship between heavy mineral assemblage and diamond grade

Garnet and ilmenite associated with diamondiferous kimberlites have characteristic Mg and Na compositions relative to those from non-diamond bearing kimberlites or any other rock types (McCandless and Gurney, 1989; Wyatt et al., 2004). McCandless and Gurney (1989) advocates that eclogitic garnets associated with diamondiferous kimberlites have elevated trace values of Na ($\text{Na}_2\text{O} > 0.07$ wt.%). Within the Orange River drainage basin, diamondiferous kimberlites, the source of diamonds in the Orange River and Atlantic 1 deposits (Phillips and Harris, 2009), are located about 2600 km from the Orange River mouth (Jacob, 2005). It seems unlikely that these sand sized mineral particles would survive such long fluvial transport to the study area. In addition, the results presented in Chapter 5 show that garnet compositions in Atlantic 1 gravels correspond to those present in the Namaqua Metamorphic Complex and Gariiep Belt, which crop out in lower Orange River area. Therefore, the garnets are locally derived. In this way the clast assemblage differs from the heavy mineral suite, as exotic clasts (BIF, Karoo shales and sandstone, Karoo Supergroup basalts, and agates) in the Atlantic 1 gravels are derived from the upstream catchment area (Jacob, 2005). In the absence of kimberlite-derived diamond indicator minerals, the relationship of the detrital heavy minerals proportions and diamond grade in the Atlantic 1 gravels is explored in this section.

The diamonds recovered by mining are confined to the > 3 mm size range. The largest size range of heavy minerals studied during this project is 1-2 mm. However, as the range of specific gravity of the heavy minerals encompasses that of diamond (Fig. 6.29) particles of specific heavy minerals may behave in a similar way in sedimentary settings. The relative hydrodynamic behaviour of a given particle is influenced by particle shape (Komar, 2007). The majority of diamonds from Atlantic 1 are equant, whereas heavy mineral particles are mostly of irregular shape. These morphological differences further increase differences in hydrodynamic behaviour.

Consideration of the degree of variation in hydrodynamic equivalence of diamond and other minerals provides a context to interpret the results presented in Figures

6.27 and 6.28. The weak diamond and magnetite relationship suggested in Figure 6.27 may be explained in these terms, as may the lack of correlation between diamond abundance and other less dense minerals in the heavy mineral assemblage, particularly as size ranges diverge.

In summary, this study has demonstrated that heavy minerals can be used to link gravel deposits above bedrock fluvial terrace surfaces with marine clastic gravels. The older gravels of both the Orange River (Proto Orange River gravels) and Atlantic 1 gravels (western offshore regions) are correlated by the similar heavy mineral signature of lower amphibole-epidote content, whereas the younger gravels (Meso Orange River gravels) and the eastern regions of Atlantic 1 show similar elevated amphibole-epidote content. However, in the future independent absolute chronological control is needed to confirm these compositional correlations.

6.8 Conclusions

Major element composition of garnets from the Orange River deposits and Atlantic 1 deposits indicate that the heavy mineral suite, except apatite, in the two sets of deposits is derived from the Namaqua Metamorphic Complex. Few heavy minerals were derived from the Gariep Belt. The garnet proportion of Atlantic 1 gravels is higher than in the fluvial samples, although the particle size is lower, whereas magnetite is far more common onshore. The decrease of magnetite from the river to the marine environment is ascribed to the relative density of magnetite, where magnetite is sequestered in the Proto and Meso Orange River deposits, whereas the majority of garnets (< 1 mm) are bypassed through the river system and delivered to the marine environment. The offshore decreasing trend in amphibole-epidote proportion in Atlantic 1 is a result of increase of Namaqua Metamorphic Complex sediments through time where the majority of the gravels in Region V and Region W were deposited at a time when sediments delivered to the coast by the Orange River were largely from the upstream

catchment area and much less from the local rocks of the lower Orange River. Time controlled decay of the amphibole-epidote group remains a possibility. As the amount of sediments supplied from the catchment area decreased through time, the lower Orange River increased its incision in the local lithology Namaqua Metamorphic Complex rocks and perhaps Gariep Belt rocks. The southward shift of the Orange River mouth through time is reflected in the northward decrease of magnetite proportion in Atlantic 1 both in the western regions (from Region V to Region W) and eastern regions (from Region K to Region N).

Euhedral etch pits are common on the Proto and Meso Orange River garnets and their absence on garnets from Atlantic 1 gravels is due to the geochemical conditions in the marine environment. Imbricate wedge marks are absent on the garnets from the Orange River deposits but their occurrence on garnet from Region W suggest a prolonged period of sediment stability in this region that is also supported by the relative high amount of apatite in the same region because apatite also requires deep water that have a prolonged period of stability. Both the Orange River deposits and Atlantic 1 deposits show a limited signature of reworking because the most stable minerals (magnetite and garnet) show a lower degree of dissolution textures than the least stable mineral epidote.

On the basis that the heavy minerals of the Orange River deposits and Atlantic 1 deposits share the same provenance, the amphibole-epidote proportion of gravel in the western Atlantic 1 regions (Region V and Region W) is similar to that of the Proto Orange River gravel whereas the eastern regions (Region K and Region N) display amphibole-epidote content characteristic of the Meso Orange River gravels. Therefore Region V and Region W gravel is possibly Oligocene whereas the Region K and Region N gravels are likely to be late Middle Miocene to early Late Miocene. The accumulation of Proto Orange River deposits and Meso Orange River deposits accumulation was coeval with a marked decrease of sediment flux to the offshore at the time of their respective aggradation and a reduced gravel accumulation in Atlantic 1.

Diamond indicator minerals derived from kimberlites do not persist into the heavy mineral assemblage of the study area. The diamond and heavy mineral relationships are confined to their co-transport in local fluvial and marine settings. A weak positive correlation of coarse magnetite with diamond grade in Region K

could be explained by their hydrodynamic similarities. Hydrodynamic differences between diamonds and other less dense heavy minerals explain the overall lack of correlation.

Chapter 7 Discussion

In this chapter the results from chapters 4, 5, 6 and 7 are synthesised to answer each of the research question described in the introduction chapter (Chapter 1).

7.1 What factors control heavy mineral and clast assemblages in gravel terrace deposits of continental-scale bedrock rivers, and do terraces of different ages have distinct assemblages?

Gravel terrace deposits of bedrock rivers provide a fragmented record of the evolution of drainage basins (e.g., Bridgland and Westaway, 2008; Wegmann and Pazzaglia, 2009; Foster et al., 2017) that can be used to understand sediment production, transport and depositional histories between continents (source) and oceans (sink) (Fig. 8.1) (Romans et al., 2016). Bedrock rivers have a wide range of physiographic and tectonic configurations, and range widely in their latitudinal and climatic position, the hinterland geology they pass over, their tectonic setting, the distance from the end of bedrock confinement to the coastline, and the nature of the receiving basin. However, modern continental-scale rivers such as the Nile (Egypt), the Mississippi (USA), the Amazon (Brazil), and the Yangtze and Yellow Rivers (China) have long tracts that pass over alluvial substrates and are very low gradient with long backwater lengths (Frihy, 2007; Rittenour et al., 2007; do Nascimento et al., 2015). However, most studies of controls on bedrock river deposits have focussed on relatively small and steep rivers (Merritts et al., 1994; Montgomery, 2004; Maher et al., 2007; Cunha et al., 2008; Finnegan and Dietrich, 2011), and rarely assess the heavy mineral or clast assemblages to elucidate factors controlling such assemblages. Therefore,

detailed analysis of terrace gravels in the bedrock-confined tracts of continental-scale rivers is rare (e.g., Whetten et al., 1969).

The Orange River is an unusual continental-scale river as it is bedrock-confined in its lower reaches. With its headwaters in high relief eastern southern Africa, the lower Orange River has thick gravel terrace deposits (up to 50 m thick), namely the early to middle Miocene Proto Orange River deposits (Corvinus and Hendey, 1978; Pickford, 1987) and Plio-Pleistocene Meso Orange River deposits (Pether, 1986). These two deposits have distinct clast assemblages. Proto Orange River deposits are characterised by a dominance of Karoo Supergroup shale and sandstone clasts whereas the younger Meso Orange River deposits are characterised by dominance of BIF and prominent amount of Karoo Supergroup basalt clasts (Jacob, 2005) (Fig. 8.2). These key clasts are sourced from the Orange River catchment area (Jacob, 2005). Not only do the Proto and Meso Orange River deposits have distinct clast assemblage signatures but each deposit type has characteristic heavy mineral assemblage, with the younger Meso Orange River deposits showing higher amphibole-epidote proportion than the older Proto Orange River deposits (Fig. 8.2). The key difference in both the clast assemblage and heavy mineral assemblage between the two gravel deposits is the relative abundance, and not absence or presence of specific clasts or minerals, which suggests that there has not been a change in provenance of the Orange River deposits through drainage reorganisation. Instead the clast proportions indicate that there has been a change in the availability of different lithologies to the Orange River through landscape evolution of the catchment area. For example, the decrease of the Karoo Supergroup shale and sandstone from the Proto Orange River deposits to the Meso Orange River deposits (Fig. 8.2) suggest that most of the Karoo Supergroup was eroded by the end of the Proto-Orange River times and were less available to be exploited by the Meso-Orange River (Fig. 8.3). However, Karoo Supergroup basalt increases from the older deposits to the younger deposits, showing the opposite trend to that displayed by the Karoo Supergroup shale and sandstone. Because basalt clasts are sourced from the same unit (Karoo Supergroup) together with the shale and sandstones, the basalts are expected to have decreased through time as well especially that they are sourced from the topmost, and youngest unit, of the Karoo

Supergroup, the Drakensberg flood basalts. Basalts are prone to chemical weathering particularly under wet and humid climate (Amiotte Suchet and Probst, 1993; Louvat and Allègre, 1997; Dessert et al., 2001; Malvoisin et al., 2012; Cox et al., 2016) and could have been lost from the Proto Orange River deposits through chemical degradation. The onset of arid conditions in the study area is contentious with Pether et al. (2000) arguing for a late Middle Miocene while Siesser and Salmon (1979) and Miller (2008) suggest an Eocene onset. However, the presence of clasts of unweathered feldspar, which is chemically unstable in humid wet climate (Nesbitt et al., 1980; Komar and Wang, 1984; Nesbitt et al., 1997; Liu et al., 2016), in the Proto and Meso Orange River deposits suggests that both deposits were deposited under similar arid climate that enhanced the preservation of feldspar. The similarity in surface textures suggest that epidote from the two sets of gravels has undergone a similar degree of alteration. Therefore, the lower abundance of the Karoo basalts clasts in the Proto Orange River deposits can be attributed to mechanical degradation as opposed to chemical degradation. Thicker gravel terraces and coarser gravel matrix compared to the Meso Orange River deposits together with imbricated clasts all suggest that the Proto-Orange River system was a powerful river during its incisional phase when basalt clasts were mechanically broken down. Therefore, the clast assemblage of the Orange River deposits was controlled by availability of Karoo Supergroup sediments and BIF through landscape evolution and mechanical breakdown of softer Karoo basalt. This scenario is likely to be similar to other continental scale bedrock rivers most especially in similar tectonically inert areas. Another primary control on sediment production is tectonic uplift (Selby, 1985; Romans et al., 2016) that could have influenced the clast assemblage of the Proto and Meso Orange River deposits.

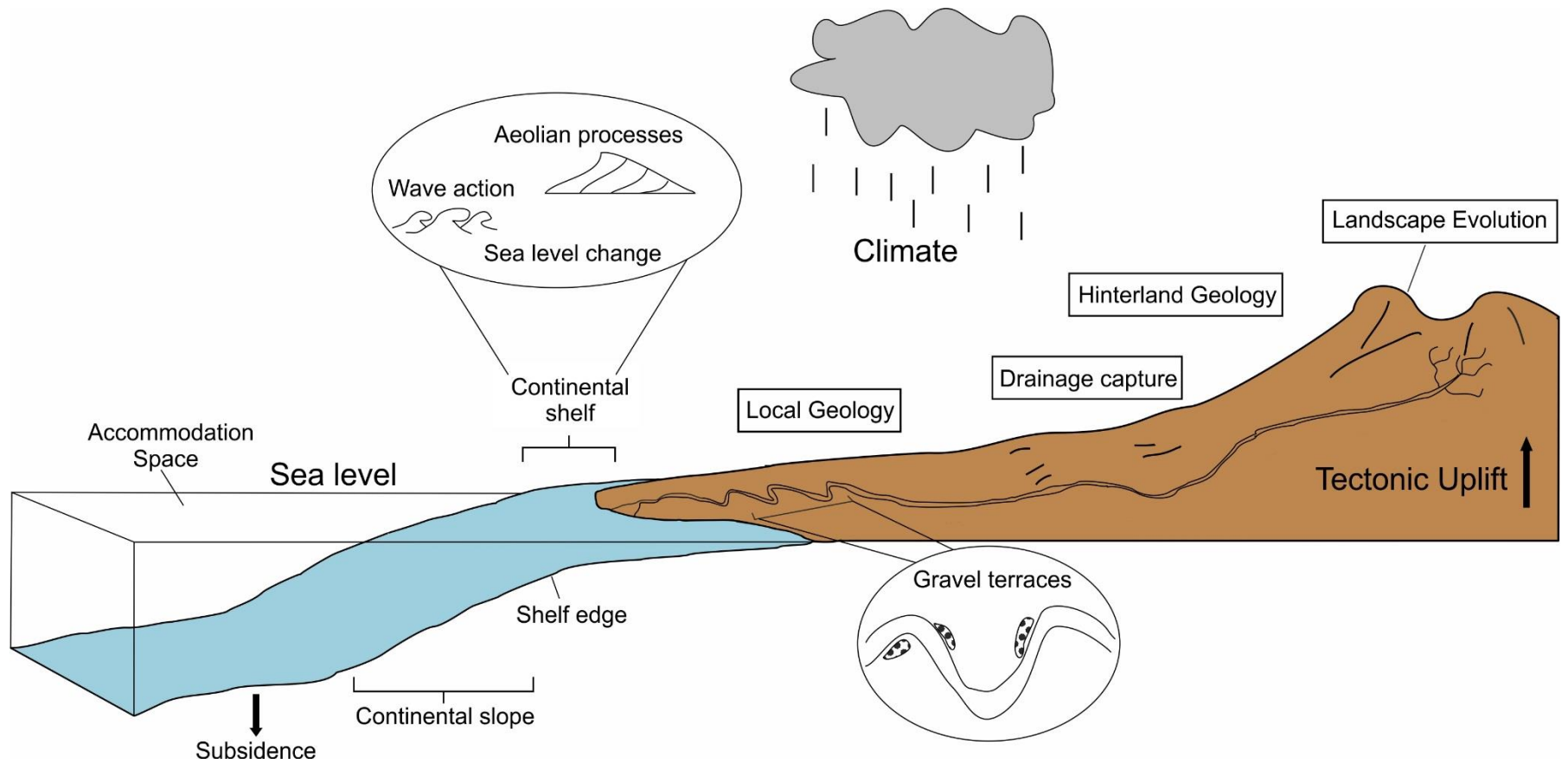


Figure 7.1 Generalised diagram of sedimentary system profile between continents (source) and oceans (sink). Modified from Romans and Graham (2013).

Tectonic uplift events that resulted in increased erosion in southern Africa are the Cretaceous (de Wit, 1999; Stevenson and McMillan, 2004), the Miocene and the Pliocene (Partridge and Maud, 2000). Although the erosion rates, and associated sedimentation rates, of the southern African landscape remain highly debated (Hawthorne, 1975; Brown et al., 1999; Gallagher and Brown, 1999; Tinker et al., 2008b; Hanson et al., 2009), the sedimentation rates in the offshore Orange Basin (Rust and Summerfield, 1990; Aizawa et al., 2000; Rouby et al., 2009) and Outeniqua Basin offshore South Africa (Tinker et al., 2008a) suggest that sediment production and deposition continued to decrease after the Cretaceous uplift event. The Proto and Meso Orange River deposits are younger than the Cretaceous, therefore tectonic uplift may have not directly influenced the clast assemblage between the two sets of deposits. However, tectonic uplift may have influenced the rate at which Karoo sediments were eroded such that most of the Karoo shales and sandstone were eroded during the Proto Orange River period and were less available in the Meso Orange River period.

Amphibole and epidote, together with the rest of the heavy minerals, are sourced from the Namaqua Metamorphic Complex rocks and Gariep Belt Rocks that crops out in the vicinity of, and forms the basement to, the lower Orange River as evidenced by the positive correlation between the Namaqua Metamorphic Complex clasts and amphibole-epidote content (Fig. 8.2). Also detrital garnet compositions of the Orange River deposits are similar to those of the Namaqua Metamorphic Complex, although a few garnets have compositions similar to that of the Gariep Belt rocks as discussed in Chapter 6. The increase of amphibole-epidote through time from the Proto Orange River deposits to the Meso Orange River deposits is ascribed to increase in the availability of Namaqua Metamorphic Complex rocks (and Gariep Belt rocks) to the Orange River (Fig. 8.3). The presence of fresh feldspar clasts in the Proto Orange River deposits rules out loss of amphibole-epidote in the Proto Orange River deposits through chemical weathering, as the dominant process, because feldspar is also prone to chemical weathering as reported by Nesbitt et al. (1997). In contrast, feldspar clasts are fresh with limited evidence of weathering. There is also a possibility that some amphibole-epidote in the Proto Orange River deposits were lost through

mechanical breakdown either during transport because garnets show conchoidal fractures that are produced by mechanical processes (Velbel et al., 2007) in light of the Proto Orange River being a more powerful river system. However, conchoidal fractures are also present on garnets from the Meso Orange River deposits which suggest that these gravels were also subjected to mechanical processes.

Sediment reworking and recycling is another mechanism that can alter the original clast and heavy mineral assemblages. In this study, the clast assemblage and heavy mineral assemblage data does not show evidence of reworking of the older Proto Orange River deposits by the Meso-Orange River. The only exception is at the Auchas Major Deposit where the Meso Orange River gravels at this location exhibit high amount of Karoo Supergroup shale and sandstone clasts and low amount of amphibole-epidote proportion, features that are characteristic of Proto Orange River gravels (Fig. 8.2). It is interesting to note that the lack of reworking of the Proto Orange River deposits is also evident in mineral surface textures because the magnitude of chemical dissolution (e.g. etch pits) increases with decreasing mineral stability from magnetite and garnet to epidote. This trend is also observed in the Meso Orange River deposits. The lack of reworking of the older gravels is ascribed to a changing river course where the Orange River evolved to a straighter course in the Meso period (Jacob, 2005) such that the older Proto Orange River deposits were out of influence of the Meso-Orange River (Fig. 8.3).

In summary, this study has shown that gravel terrace deposits of the continental-scale Orange River have distinctive clast assemblages and heavy mineral assemblage that are controlled by different factors. The clast assemblage of the Proto and Meso Orange River gravel terrace deposits is controlled by catchment-scale processes marked by decrease in the availability of Karoo sediments and increase in the availability of BIF through time in response to changing drainage basin geomorphology (Fig. 8.3). In contrast, the difference in heavy mineral assemblage between the two gravels is influenced by local controls, i.e. availability of Namaqua Metamorphic Complex rocks to the Orange River and the preservation potential of amphibole and epidote (Fig. 8.3). The matrix (heavy

minerals) is not simply a finer scale reflection of the clast assemblage and cautions against using only one technique. Furthermore, this result is somewhat counter intuitive, in that the key diagnostic minerals in the matrix is ascribed to local/intrinsic factors and short transport distances, whereas the key lithologies in clast composition is due to far field controls over long transport distances. This implies that extrinsic controls on clast assemblage and intrinsic controls on heavy mineral assemblage of the Orange River gravels need to be considered in evaluation of terrace deposits of other bedrock river systems globally. The sand size fraction and the coarse clasts can be derived from different sources such that they carry different provenance signatures and reflect different transport histories. This is likely to be a similar scenario in other continental-scale bedrock rivers. Therefore, prediction of the nature of the fine size fraction on the basis of clasts alone is problematic. Mechanically (and chemically) weaker rocks such as basalt may be lost. For example in this study, basalt was mechanically degraded in the Proto Orange River deposits. Therefore using clast assemblage to reconstruct the drainage history of high energy river systems should take into account the possibility of loss of mechanically weaker clasts. However, despite the different factors controlling the clast assemblage and heavy mineral contents of the lower Orange River gravels, the Proto and Meso Orange River deposits differ in terms of both clasts and heavy minerals. This suggests that understanding the intrinsic controls on heavy mineral assemblages can be used in isolation to predict the distribution of Proto and Meso Orange River gravels in coeval offshore gravels derived from the Orange River.

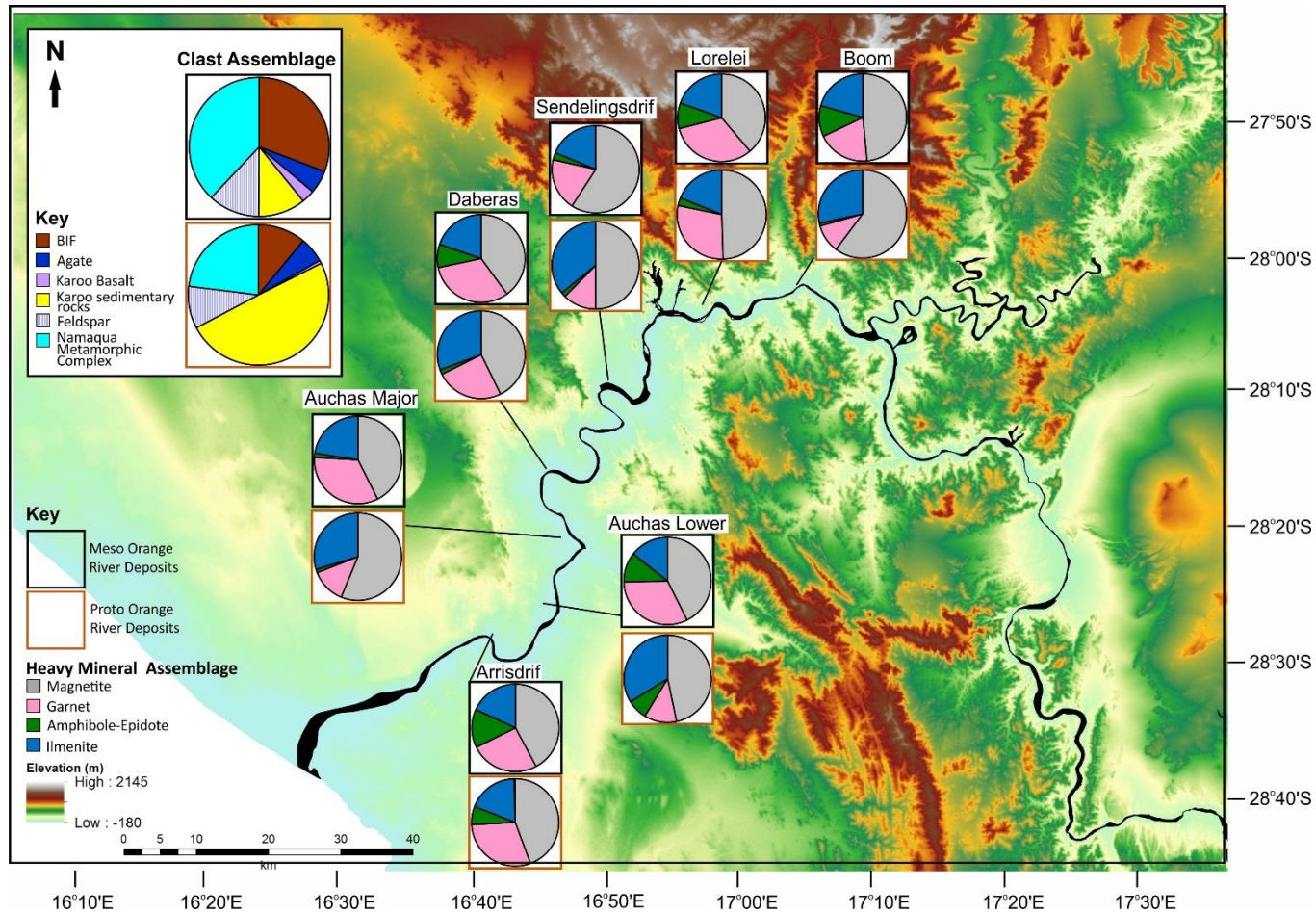


Figure 7.2 Clast assemblage (inset) and heavy mineral assemblage of Proto and Meso Orange River deposits. Size fractions are 3-25 mm and 0.25-0.50 mm for clast and heavy mineral assemblage data, respectively. Clast assemblage data for Proto and Meso Orange River gravels represent average of sampled deposits. Clast assemblage and elevation data after Jacob (2005) and Jarvis et al. (2008), respectively.

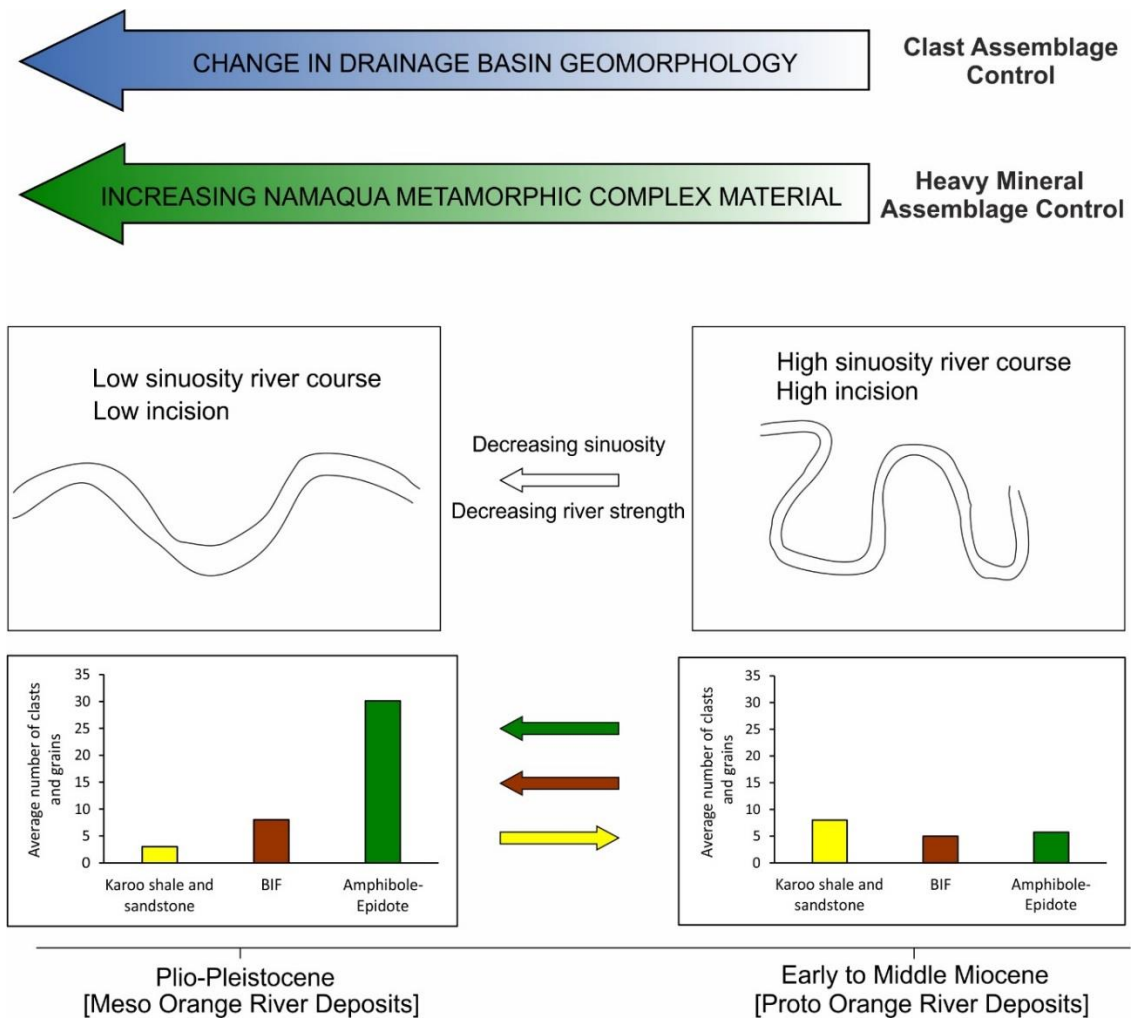


Figure 7.3 Synthesis on major changes in clast and heavy mineral assemblage of the Orange River deposits, and the interpreted controls. Yellow, brown and green arrows point in the direction of increase.

7.2 How can heavy mineral assemblages be used to characterise seabed marine gravels on passive continental margins?

Sediments on continental margins, whether on the seabed or buried, are dominated by clastic continent derived sediments (Romans and Graham, 2013). Continental shelves are the first receptors of terrigenous material (Covault and Fildani, 2014) and are therefore important in linking controls on the transfer of sediment from continents to oceans. The residence time of sediments on

continental shelves is variable. In some cases the sediments are directly bypassed, or reworked and later transferred to the deep sea by sediment gravity flows (e.g., Tinker et al., 2008a; Covault and Fildani, 2014), or deposited on the shelf in a range of depositional environments (e.g., Swift, 1974; Lacombe, 2007).

The application of heavy minerals to offshore settings is synonymous with the oil and gas industry where it is primarily applied to deducing sediment provenance (e.g., Pujos et al., 1990; Morton et al., 2005; Cascalho and Fradique, 2007; Hallsworth and Chisholm, 2008; Tsikouras et al., 2011; Cao et al., 2015) and correlation of sedimentary units for hydrocarbon reservoir evaluation (Morton, 2007; Poulsen et al., 2007). Most offshore hydrocarbon resources are hosted in deeply buried sandstone and fine grained sedimentary successions in sedimentary basin-fills and rarely in unconsolidated gravel. Characterisation of seabed unconsolidated marine gravels using heavy minerals is rarely performed, possibly due to lack of economic interest. However, the offshore Orange River derived Atlantic 1 gravels host economic diamond resources although the timing of the deposition and evolution of these clastic gravels across Atlantic 1 is poorly constrained. The Namibian continental shelf is unusual in that there have been little net subsidence, meaning that a thin and patchy sedimentary record is preserved, forming a complicated palimpsest to interpret, similar to the English channel/La Manche (Mellett et al., 2013). On the lower Orange River, coeval gravel terrace deposits are well understood in terms of their depositional age with respect to the aggradation and incision cycles of the Orange River as deduced from clast assemblage analysis by Jacob (2005). In addition, Chapter 4 has characterised and discussed the heavy mineral signatures of the Proto and Meso Orange River deposits and established that the two gravel deposits also have distinct heavy mineral assemblages with the proportion of amphibole-epidote increasing from the older Proto Orange River deposits to the younger Meso Orange River deposits.

With the exception of apatite and clinopyroxene, the heavy minerals present in Atlantic 1 gravels (magnetite, garnet, amphibole, epidote and ilmenite) are the same as those recorded in the fluvial gravel terrace deposits of the lower Orange River (Proto and Meso Orange River deposits). Importantly, the composition of

garnet from the Orange River deposits and Atlantic 1 deposits indicate derivation from the Namaqua Metamorphic Complex rocks (and few from Gariep Belt rocks) on the basis that they share similar compositions. Apatite is absent in all the Orange River deposits including the modern Orange River gravel terrace deposits suggesting that apatite was formed *in situ*. Among the Orange River deposits, clinopyroxene was only recorded in the modern Orange River deposits. In Atlantic 1, magnetite shows a northward decreasing trend both in the western regions (from Region V to Region W) and in the eastern regions (from Region K to Region N) (Fig. 8.4). Amphibole-epidote proportion decreases offshore from the eastern regions to the western regions (Fig. 8.4). Within the eastern regions, amphibole-epidote shows a northward decreasing trend from Region K to Region N. Systematically, Atlantic 1 gravels can be grouped into high magnetite gravels proximal to the palaeo-Orange River mouth (Region V) and modern Orange River mouth (Region K) and low magnetite gravels (Region N and Region W). These heavy mineral trends in the Atlantic 1 could have been influenced by sediment supply, relative sea level, ocean currents, seabed morphology, sea water chemistry and post depositional process (e.g., Romans and Graham, 2013).

Since the majority of sediments on continental margins are derived from continents, the composition of sediments on continental shelves is a reflection of evolving geology and geomorphology of the drainage basin at any given time. For example, Diester-Haass et al. (1988) and Holtar and Forsberg (2000) have linked the Cretaceous mudstone underlying the gravels in Atlantic 1 to an Orange River origin. Therefore, the composition of heavy minerals can be related to the landscape evolution of the drainage basin. For most continental shelves (and deep sea areas), sediment flux can be directly correlated to how much sediment is produced in the drainage basin. However, for the southern Namibian continental shelf, sediment supply was influenced by i) how much sediment was produced in the Orange River drainage basin, ii) how much sediment is locked up in the thick gravel terrace deposits (up to 50 m) along the lower Orange River, and iii) how much was redistributed northward by a combination of oceanic currents during highstand, and aeolian processes during lowstand. A similar scenario on a passive continental margin is the continental shelf offshore Texas that is fed by Colorado, Brazos and Trinity Rivers. These rivers also have terrace

deposits within their respective coastal plain (Phillips, 2011; Hidy et al., 2014). Similarly, in the Amazon drainage basin, some of the sediments generated from the Andes does not end up in the ocean because it is sequestered in basins at the foothills of the Bolivian Andes (Guyot et al., 1993).

Relative sea level change controls initial sedimentation patterns. Post deposition relative sea level fall (forced regression) exposes sediments to subaerial conditions where they may be reworked basinward by fluvial or coast parallel by aeolian processes (e.g., Pether et al., 2000; Stevenson and McMillan, 2004). During relative sea level rise (transgression) ocean currents may redistribute sediments sub-parallel to the coastline (e.g., Covault et al., 2007). In the case of heavy mineral assemblage, post depositional processes such as chemical and physical weathering may alter the mineralogy of heavy minerals. Formation of authigenic minerals in the environment of deposition should also be considered. Therefore, characterisation of seabed sediments based on heavy minerals should take into account the above mentioned factors, each of which is discussed below.

7.2.1 Sediment supply

Sediment supply from the drainage basin influences the composition of sediments on the continental shelf. The compositions of garnet, magnetite and epidote from Atlantic 1 deposits are similar to that of the Proto and Meso Orange River deposits. Therefore, the Atlantic 1 gravels can be linked to the aggradation and incision cycles of the lower Orange River. On the Orange River deposits, the decreasing amphibole-epidote trend from older to younger deposits coincides with increasing supply of Namaqua Metamorphic Complex derived sediments through time (Fig. 8.2). This increase in the amount of Namaqua Metamorphic Complex sediments to the lower Orange River through time is ascribed to the decrease in the volume of sediments from the catchment area as noted by Jacob (2005) where the modern Orange River gravels (younger than Meso Orange River gravels) have relatively lower amounts of exotic clasts and a higher amount of locally derived clasts. Therefore the decrease of amphibole-epidote in Atlantic 1 from the younger gravels (proximal to the modern Orange River mouth) to the

older gravels in the western regions of Atlantic 1 (Fig. 8.4) can be explained by the same phenomena on the river where higher Namaqua Metamorphic Complex sediments coincides with high amphibole-epidote proportion. On the basis that the amount of Namaqua Metamorphic Complex derived sediments increased through time, the amount of amphibole-epidote content can be used to estimate the relative age of the gravel deposits of both the lower Orange River and the marine gravels offshore southern Namibia where amphibole-epidote proportion is inversely proportional to the gravel age.

7.2.2 Effect of Sea Level

Relative sea level change affects where sediments are initially deposited. Post deposition relative sea level fall exposes sediments to subaerial conditions, where they may be reworked by fluvial processes or aeolian processes. During the last glacial maximum (~21 kyr) the eastern regions were completely exposed, and this coincides with the lower authigenic apatite proportion in the eastern regions. The proportion of authigenic apatite is higher in the western regions compared to the eastern regions (Fig. 8.4). Formation of authigenic apatite requires prolonged periods of stable deep water (Filippelli, 2011). During the Pleistocene lowstands, mobile minerals such as amphibole and epidote could have been carried northward by strong aeolian processes, which have been in operation along the Namibian coast since the Eocene (Siesser and Salmon, 1979; Miller, 2008). However, this is not the case as amphibole-epidote shows a northward decreasing trend in the eastern regions. Therefore, sea level affected the distribution of apatite but not amphibole-epidote.

7.2.3 Effect of Sea Currents

Shallow marine currents that operate along the Namibian coast include northward longshore drift (Pether et al., 2000; Bluck et al., 2007) and Benguela current (Diester-Haass et al., 2002; Mohrholz et al., 2014; Nagel et al., 2016). Amphibole-epidote, which shows a northward decreasing trend in the eastern regions, are mobile (Cascalho and Fradique, 2007; Frihy, 2007; Garzanti et al., 2015) and can

easily be transported by waves and currents (Fig. 8.4). If amphibole-epidote were carried northward by longshore drift, the most southern region, Region K will be expected to show a lower amount of amphibole-epidote which is not the case (Fig. 8.4). Therefore, ocean currents did not influence the distribution of amphibole-epidote in Atlantic 1 but rather the higher amount of amphibole-epidote in Region K is interpreted to be due to the increasing supply of Namaqua Metamorphic Complex derived sediments through time. In addition, clinopyroxene derived from the Namaqua Metamorphic Complex rocks, which is present in Region K, the most southern region, is absent in the Proto and the Meso Orange River samples but abundant in the modern Orange River gravels that are characterised by high amount of Namaqua Metamorphic Complex clasts (Jacob, 2005) in strong support for the increase of Namaqua Metamorphic Complex derived sediments over time.

7.2.4 Post Depositional Processes

In a marine environment, sea water chemistry has a large influence on post depositional sediment modification because it affects the chemical alteration of certain minerals such as magnetite. The preservation potential of detrital magnetite is influenced by the Eh (reducing and oxidising conditions) of the depositional environment (Weibel and Friis, 2007). The northward decreasing trend displayed by magnetite in both the western regions (from Region V to Region W) and eastern regions (from Region K to Region N) could indicate that magnetite was preferentially dissolved in Region N and Region W (Fig. 8.4). However, loss of magnetite through dissolution alone is unlikely because Region K, which is closer to the Orange River mouth, has the highest proportion of magnetite implying that most of the magnetite is due to its relative high density and it was retained closer to the input point. Region V, which also has a relative high amount of magnetite, is distal from the modern Orange River mouth. However, the paleo-Orange River mouth is believed to have been 10 km north of the modern Orange River mouth. Therefore, at some time Region V was closer to the palaeo-Orange River mouth producing a northward decreasing trend in magnetite proportion from Region V to Region W (Fig. 8.4). In comparison to the lower Orange River deposits, magnetite decreases from the lower Orange River

deposits to the marine deposits highlighting a function of relative density of magnetite. Garnet, which is less dense than magnetite, shows an opposite trend where it increases from the river environment to the marine environment in the fine size fractions (0.5-1 mm and 0.25-0.50 mm).

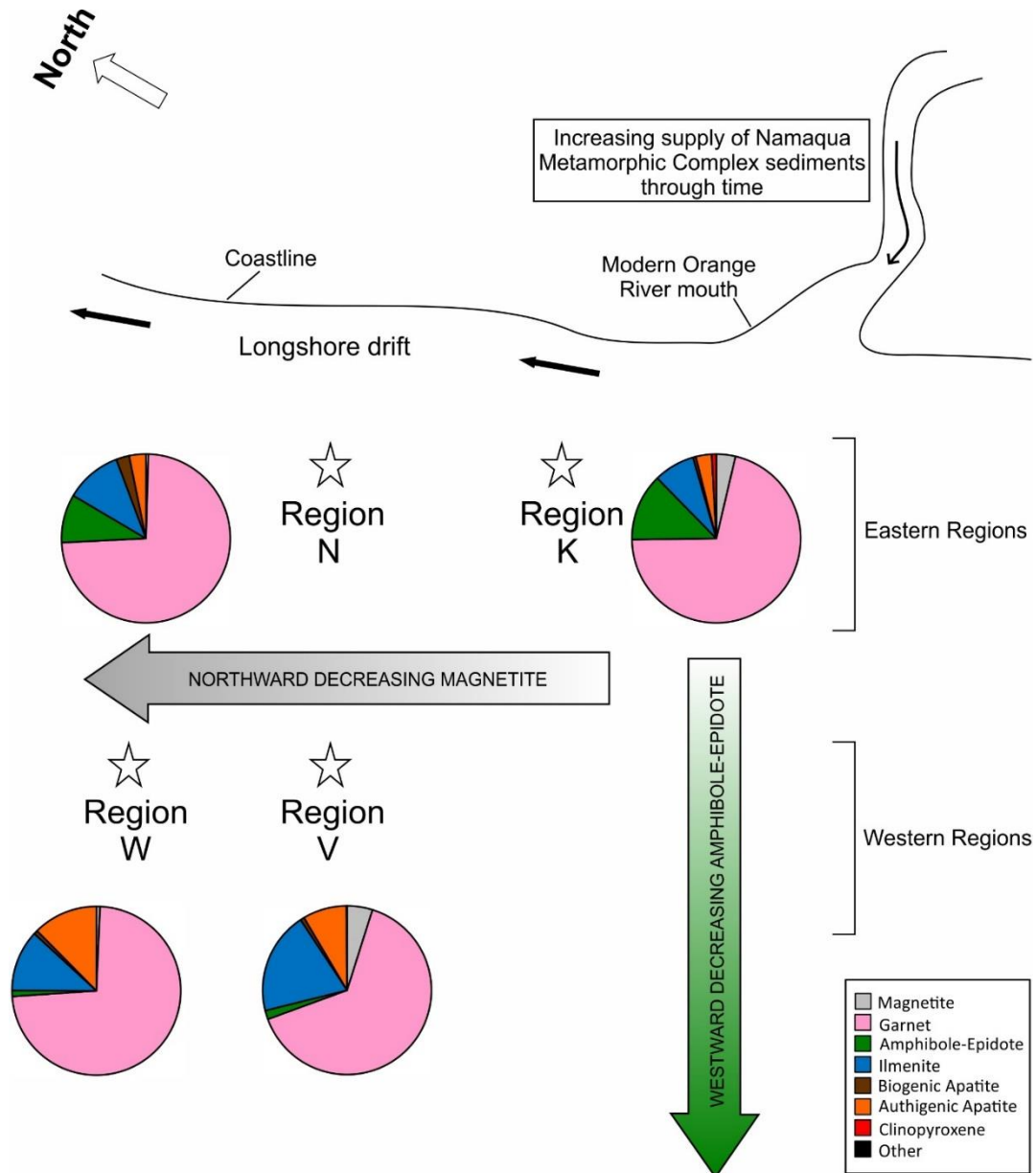


Figure 7.4 Heavy mineral proportion trends in Atlantic 1 for 0.25-0.50 mm size fraction.

In summary, this study has shown that heavy minerals can be used to characterise seabed deposits and also be used to deduce factors that influence the distribution of sediments on continental shelf from passive continental margin. Heavy minerals of marine gravels in conjunction with coeval fluvial gravels can also be used to link phases of degradation and incision of continental scale bedrock rivers. The offshore decrease of amphibole-epidote proportion in Atlantic 1 is related to the relative amount of Namaqua Metamorphic Complex sediments that increased through time, whereas the northward decrease in magnetite content in both the western and eastern regions is due to the relative higher density of magnetite resulting in preferential accumulation of magnetite closer to the input point, the Orange River mouth, that has shifted southward through time. Therefore, the heavy mineral data suggest that the spatial distribution of sediments in Atlantic 1 in terms of the composition of gravel was largely controlled by the composition of sediments supplied by the Orange River. It appears that beach erosion or sea cliff erosion by waves is limited on the Namibian coast but rather the exposed sand on the beach is transported northward by wind in mobile sand dunes before it is carried offshore to form part of the continental shelf sediments resulting in continental shelf sediments whose composition is dominantly terrigenous. An example of continental shelf sediments that have been derived from sea cliff erosion during transgression is offshore California (Covault et al., 2011), however, the California setting is on an active continental margin.

This study has demonstrated that when characterising sea bed sediments using heavy minerals the relative distance to the sediment input point (river mouth) needs to be considered because sediments of similar age can show differences in the amount of high density heavy minerals like magnetite. Such high density heavy minerals tend to concentrate close to the river mouth. In Atlantic 1 for example, magnetite content is higher in gravels that are closer to the river mouth irrespective of the gravel age.

7.3 How can onshore and offshore heavy mineral assemblages be correlated?

In the last decade, a number of studies have attempted to link the amount of sediment eroded from continents (source) to the amount of sediments deposited offshore (sink) (e.g., Tinker et al., 2008a; Marsaglia et al., 2010; Covault et al., 2011; Covault and Fildani, 2014; Anderson et al., 2016; Kuehl et al., 2016; Richardson et al., 2017). The production and transfer of sediments from source areas to sedimentary sinks is controlled by climate and tectonics (Fig. 8.1) (Romans and Graham, 2013). Secondary factors include sea level, shelf physiography, geology and geomorphology of the drainage basin and river aggradation on the coastal plain. On continental shelves, sea level fluctuations further affects sedimentation together with interplay of waves, ocean currents and aeolian processes (Fig. 8.1). Since most of sediments on continental shelves is derived from continents (Romans and Graham, 2013), the offshore stratigraphic record can reveal changes in landscape evolution and regional climate (Kuehl et al., 2016). The depth configuration of continental shelves also has influence on the distribution of sediments (Paris et al., 2016). For example, the shallow nature of continental shelves on active margins may make it easier for shelf sediment remobilisation and transfer to the deep sea by interplay of waves and currents (Wiberg et al., 1996). In comparison to the average global continental shelf depth (~258 m) (Paris et al., 2016), the Namibian continental shelf is deep (up to 400 m) (Compton and Bergh, 2016), which may have enhanced a prolonged residence time of sediment on the shelf instead of being transported to the deep sea. The depth profile on the continental shelf (Fig. 8.5) is steeper than the onshore Orange River profile (Fig. 8.6). This indicates the unusual deep and steep nature of the Namibian shelf. Upstream between Arrisdrif and Boom, the Proto Orange River and Meso Orange River gradient is 0.69 m/km and 0.60 m/km, respectively (Fig. 8.6). Jacob (2005) reported a few bedrock scours in the Meso Orange River deposits that are at mean sea level although the time during which the scours were cut remains unknown.

Studies that have correlated heavy minerals assemblage of river and continental shelf sediments are primarily focused on deducing sediment provenance (Cascalho and Fradique, 2007). On the basis that the sediments on the continental shelf in Atlantic 1 are dominantly of siliciclastic origin, the gravels can be linked to the incisional and aggradation phases of the lower Orange River, although sediments in the marine environment may be further affected by an interplay of tidal, aeolian and ocean currents. Garnet, magnetite and epidote compositions of the Orange River deposits are similar to those of the Atlantic 1 deposits suggesting that the two deposits are coeval as discussed earlier in this chapter. On the basis that detrital garnet composition from the Orange River deposits and Atlantic 1 deposits matches that of the Namaqua Metamorphic Complex and Gariep Belt rocks suggest that the heavy minerals were derived from the local rocks in the lower Orange River.

The Atlantic 1 western regions (Region V and Region W) show amphibole-epidote content similar to that of the Proto Orange River deposits whereas the eastern regions (Region K and Region N) have amphibole-epidote content characteristic of the Meso Orange River deposits. Amphibole-epidote indicates that the western regions are similar in age to the Proto Orange River deposits (Fig. 8.7). Accumulation of the Proto Orange River deposits would have resulted in a marked decrease in sediment flux to the Atlantic Ocean given the thick nature of the Proto Orange River deposits (up to 50 m) (Jacob, 2005) suggesting that the majority of the gravels in the western Atlantic 1 regions were either deposited before or after the accumulation of the Proto Orange River deposits. Formation of imbricate wedge marks recorded on garnet from one of the western regions (Region W) requires extended period of stability (Morton et al., 2003) but their absence in the Orange River deposits supports an older age for the western Atlantic 1 regions gravel deposits. Similarly, the relative higher amount of apatite in the western Atlantic 1 regions relative to the eastern regions (Fig. 8.4) supports an age older than the Proto Orange River deposits because a high amount of apatite is suggestive of deep water that had a prolonged period of stability (Morton et al., 2003; Filippelli, 2011). On the basis that amphibole-epidote decreases from the older gravel deposits, both in the river and marine

environment, suggest that the amount of Namaqua Metamorphic Complex rocks has increased through time. However, it is difficult to constrain if some of the amphibole-epidote has been mechanically degraded in the older deposits (i.e. western Atlantic 1 regions and Proto Orange River deposits). Amphibole-epidote does not show any preferential size distribution between the younger and older gravel in Atlantic 1, suggesting that lower amount of amphibole-epidote in the older gravels is not due to loss by mechanical breakdown. Loss by mechanical degradation would have produced relative enrichment of finer grained amphibole-epidote in the older gravels, which is not the case as discussed in Chapter 5. Also loss of amphibole-epidote by chemical degradation alone in the older Atlantic 1 gravels can be ruled out because amphibole-epidote from both the older gravels (Regions V and W) and younger gravels (Regions K and N) display saw tooth termination textures produced by coalescence of lenticular etch pits (Berner et al., 1980; Lång, 2000). These features are associated with advanced stages of weathering (Velbel, 1989; Mikesell et al., 2004) suggesting that amphibole-epidote from older and younger gravels has suffered similar degree of alteration. Therefore the amount of amphibole-epidote content can be related to the relative age of Orange River deposits and Atlantic 1 deposits where amphibole-epidote content decreases with increasing gravel deposit age. Similarly, Mikesell et al. (2004) have used the degree of amphibole etching (that has similar chemical stability to epidote) as a relative age indicator of Michigan soils. Earlier studies of Locke (1986) and Hall and Michaud (1988) have also used the same approach in deducing the relative age of sediments.

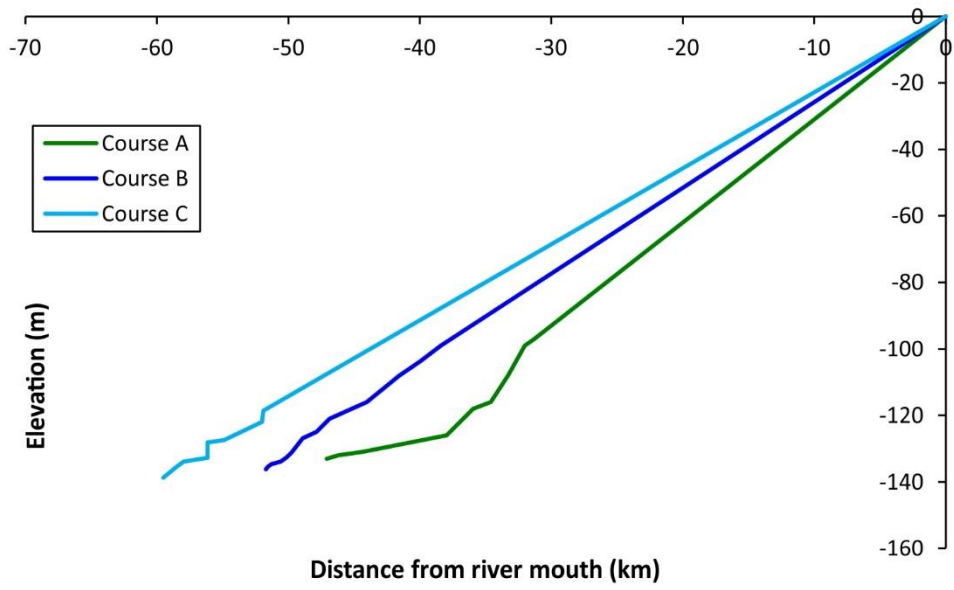


Figure 7.5 Offshore Orange River profile constructed from bathymetry data across Region L to Region T (Course A), Region M to Region U (Course B) and Region N to Region V (Course C).

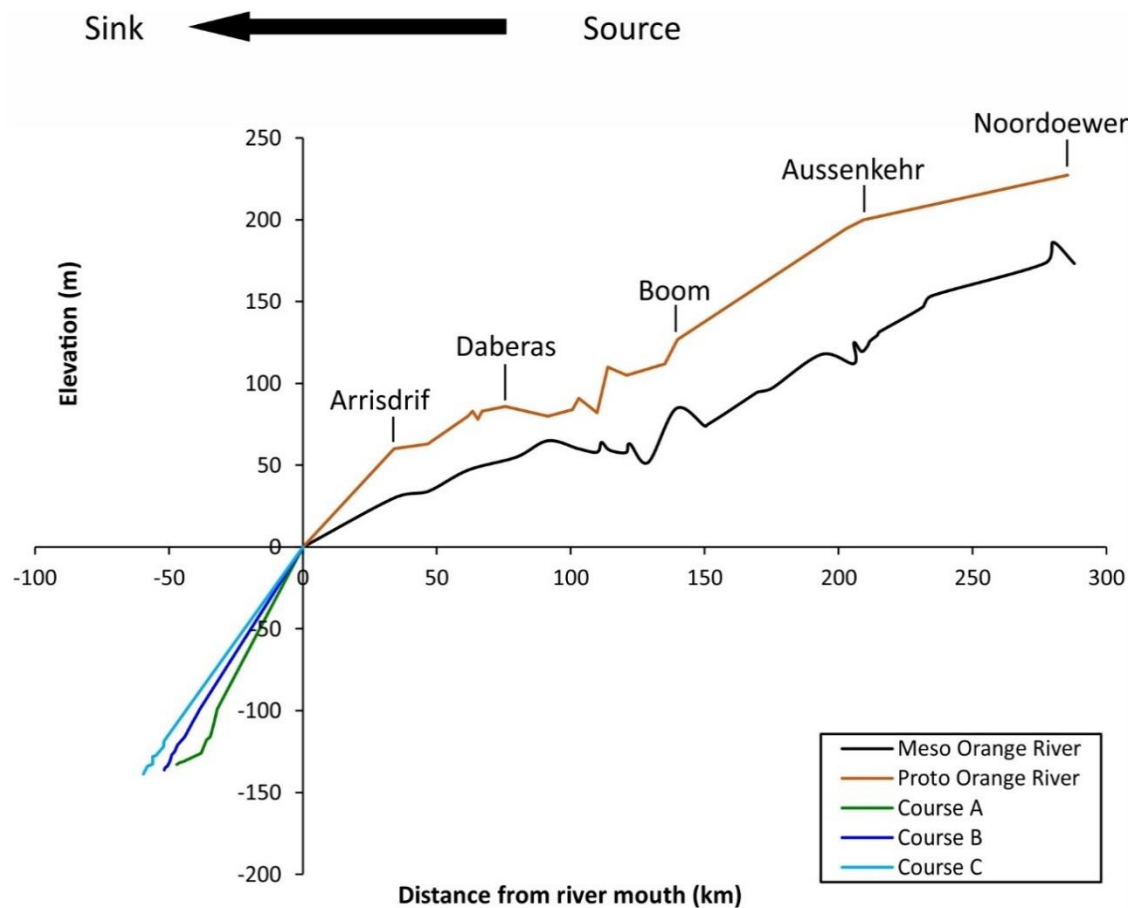


Figure 7.6 Longitudinal profile of the Proto Orange River and Meso Orange River. Onshore river profiles constructed using data from Jacob (2005). Offshore river profile constructed from bathymetry data across Region L to Region T (Course A), Region M to Region U (Course B) and Region N to Region V (Course C).

The concentration of magnetite decreases from the Orange River deposits to the Atlantic 1 deposits irrespective of grain size (1-2 mm, 0.5-1 mm and 0.25-0.50 mm) whereas garnet abundance is much higher and finer in Atlantic 1 gravels. These trends can be related to the respective relative density of magnetite where magnetite being denser is retained in the lower Orange River deposits whereas the majority of finer garnets being lighter are bypassed through the river system and were delivered to the coast. Conventionally, conditions that drive sediment deposition by rivers on continents are high sea levels during which sediment flux to the oceans is low, whereas during low sea level, rivers are in incision mode and most sediments are transferred to the deep oceans (Leeder, 1999; Bridgland and Westaway, 2008; Anderson et al., 2016). On the basis that the majority of the sediments in Region V and Region W are older than the Proto Orange River

deposits, based on the higher abundance of apatite and imbricate wedge marks on garnet that all require extended period of stability (Filippelli, 2011), the majority of the gravel in the western Atlantic 1 regions was deposited before the accumulation of the Proto Orange River deposits when sediment flux to the Atlantic Ocean was high. The age of the Proto Orange River deposits is early to middle Miocene (Corvinus, 1978; Corvinus and Hendey, 1978; Hendey, 1978; Pickford, 1987; Pickford and Senut, 2002). Therefore, some of the Atlantic 1 gravel deposits in the western regions are possibly Oligocene (Fig. 8.7). However, the climate in southern Africa during the Oligocene is reported to have been dry (Dingle et al., 1983) with a marked decrease in sediment flux to the offshore during this period (Séranne and Anka, 2005). In contrast in West Africa, the Oligocene climate was wet on the basis of high sedimentation rate recorded for the deep sea Congo fan during this period (Séranne and Anka, 2005). The deposition of the Proto Orange River deposits in the early to middle Miocene resulted in a decrease of sediment supply to the coast on the basis of their thickness of up to 50 m. However, it is difficult to quantify the magnitude of the sediment decrease given the fact that most of the sand delivered to the coast is carried northward in mobile sand dunes becoming part of the Namib Sand sea. Equally important, the Namibian continental shelf has limited subsidence (Dingle, 1973). After the deposition of the Proto Orange River deposits sediment flux to the sea possibly increased again but this time accompanied by an increase in the amount of Namaqua Metamorphic Complex sediments and a relative decrease in the catchment area derived sediments as well as decrease in the Karoo Supergroup sediments and increase in BIF as revealed by clast assemblage data of the fluvial river terraces (Fig. 8.2). The renewed increase in sediment flux saw the deposition of the gravels in the eastern Atlantic 1 regions possibly during the middle to late Miocene characterised by high proportions of amphibole-epidote.

After the deposition of the Meso Orange River gravel deposits upstream catchment area sediments continued to decrease producing modern Orange River gravel terrace deposits with a low number of exotic clasts and high amount of Namaqua Metamorphic Complex sediments (Jacob, 2005) and high proportion of amphibole-epidote (Fig. 8.7). It was not possible to undertake clast assemblage analysis on the Atlantic 1 deposits. However, the clast assemblage-

heavy mineral assemblage correlation established in this study on the Proto and Meso Orange River deposits can be used to predict the offshore clast assemblages. Onshore, high proportions of Karoo shales and sandstones clasts are associated with relative low proportion of amphibole-epidote, whereas BIF dominance is associated with high amphibole-epidote. Therefore, exotic clast assemblage of the Atlantic 1 gravels may be deduced from the heavy mineral assemblage. A working hypothesis follows that the clast assemblage of the western regions is likely to be characterised by dominance of Karoo shales and sandstones and the eastern regions by dominance of BIF among the exotic upstream catchment area derived sediments.

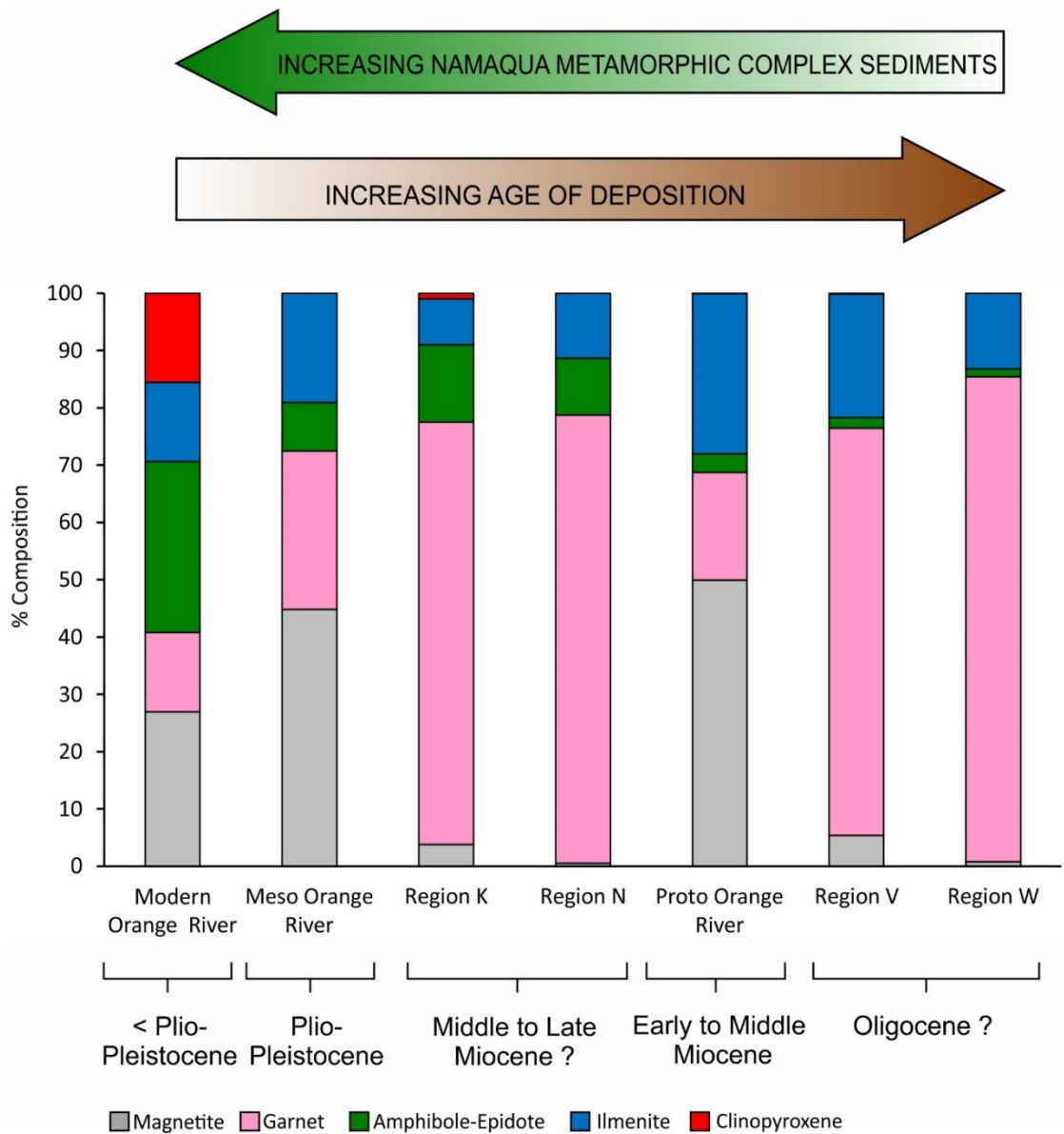


Figure 7.7 Depositional sequence of Orange River and Atlantic 1 gravel deposits.

7.4 How can a better understanding of long-term relationships between river catchment dynamics and offshore sedimentation patterns be used to improve predictions and reduce uncertainties in exploration for offshore diamondiferous deposits in Atlantic 1?

The improved prediction of detrital diamonds using heavy mineral fraction of sand size sediment can be achieved when either specific minerals share a common provenance with the diamonds, or the minerals have a separate origin from the diamonds but act as a diamondiferous facies marker.

The term diamond indicator minerals is commonly used to describe heavy minerals that have characteristic compositions relative to the same mineral types from non-diamondiferous rocks (McCandless and Gurney, 1989; Wyatt et al., 2004). Such minerals have been applied to exploration of alluvial diamond deposits (Marshall and Baxter-Brown, 1995). Diamond indicator minerals that occur in both the Atlantic 1 gravels as well as the Proto and Meso Orange River gravel terrace deposits are garnet and ilmenite. The discussion in Chapter 6 showed that the heavy mineral assemblage in both the Proto and Meso Orange River deposits and the Atlantic 1 gravels are derived from the Namaqua Metamorphic Complex rocks and Gariep Belt rocks, which crop out in the lower Orange River. Therefore, the original diamond indicator minerals, sourced from the diamondiferous kimberlites in the hinterland, do not persist downstream into the study area. Consideration of the potential use of the heavy mineral suite as a marker for diamonds in the lower Orange River and Atlantic 1 is confined to the timing of their release from local lithologies into the sediment load with respect to conveyance of diamonds from upstream.

The discussion in Chapter 6 evaluated the relationship between specific heavy minerals and age of sediment. The proportion of amphibole-epidote in the heavy mineral fraction provided the best indication of relative gravel age in the lower Orange River and marine sediments. The Proto Orange River gravels (characterised by lower amphibole-epidote) have a higher diamond grade than

the younger Meso Orange River gravels (characterised by higher amphibole-epidote) (Jacob et al., 1999). Therefore, the abundance of amphibole-epidote provides a potential marker for the diamond grade of sediments offshore.

Diamonds have been recovered from marine and shoreline sediments in Namibia much further north than the northerly extent of Atlantic 1. Although there is an overall northward decrease in stone size as discussed in Chapter 2, this systematic change is not clear over the geographical range of Atlantic 1 (Fig. 6.25B, Chapter 6). In contrast, there is a pronounced variation in the assemblage of heavy minerals across Atlantic 1 (Fig. 5.16, Chapter 5). It is this change in the relationship between the abundance of individual heavy minerals and diamonds which is of interest in the context of investigating the potential of heavy minerals as diamond grade indicator minerals.

Despite their different source and size, the fact that the diamonds (> 3 mm) and heavy minerals (< 3 mm) are found in the same terrace deposits of the lower Orange River suggests that they were transported into the Atlantic 1 area at similar times. This provides a starting point from which to evaluate subsequent differences in mineral transport and longevity with a view to determining the fate of diamondiferous gravels introduced into the marine environment.

From the limited amount of data available, the only correlation between diamond grade and heavy mineral is that of the association with coarse grained magnetite in Region K. This relationship, and the lack of other such correlations, have been explained in terms of the hydrodynamic equivalence of diamonds and other heavy minerals in their respective size ranges (Chapter 6). It is possible that coarse magnetite and diamonds responded in a similar way to the various influences responsible for sediment redistribution on the continental shelf, whereas the size and density of the other heavy minerals resulted in different hydrodynamic behaviour.

The amphibole-epidote signature of the Meso age gravel deposits established onshore is evident in the marine sediments closest to the river mouth. The scarcity of amphibole-epidote in more distal offshore localities indicates that either there has been limited redistribution by longshore drift, or that the longevity is limited for chemical and physical reasons. The chemical stability of amphibole-

epidote has been discussed in Chapter 5, which concluded that dissolution could have contributed to lower concentration of the these two minerals. Similarly, the chemical and physical durability of magnetite would result in both size reduction and chemical degradation with increasing residence in the marine environment.

On the lower Orange River deposits, diamond grades are known to be positively correlated with trap sites such as bedrock potholes and scours even in areas of generally low grades (Jacob et al., 1999). Such localised zones of diamond enrichment in trap sites of competent bedrock have also been observed in other fluvial deposits such as the deposits of the lower Caroni River, Venezuela (Marshall and Baxter-Brown, 1995), the Birim River, Ghana (Hall et al., 1985) and the Vaal Valley, South Africa (Spaggiari et al., 1999). In the Orange River deposits, diamond grades are high in trapsites due to high turbulence created during flow where the light material is removed leaving behind diamonds and other dense pebbles. For the raised beach gravel deposits described in Chapter 2, the diamond grades are also high in areas of high turbulence such as bedrock potholes and gullies (Spaggiari et al., 2006). Also in these raised beach deposits, the diamond grade is highest in gravels that were deposited in the intertidal zone compared to the sub-tidal zone and back barrier beaches because the intertidal zone is subject to higher wave energy conducive for gravel sorting thus concentrating diamonds together with dense pebbles (Spaggiari et al., 2006). Therefore as reported by Jacob et al. (1999) and Spaggiari et al. (2006) turbulence was an important control on the accumulation of diamonds (and subsequently diamond grade) in sub-environments and this is likely to apply to the marine environments in Atlantic 1.

Chapter 8 Conclusions and Future Work

8.1 Conclusions

Terrace deposits in bedrock rivers provide an important but enigmatic record of landscape evolution, and can help in understanding of links to sedimentary basin-fills downstream. This study has integrated clast assemblage and heavy mineral assemblages to investigate the character and controls in a series of bedrock confined river terrace deposits formed during degradation and aggradation cycles by the palaeo-Orange River, a continental-scale river system. The analysis of onshore deposits have been augmented with analysis of offshore samples from the Namibian continental shelf.

The Proto and Meso Orange River deposits show distinct clast and heavy mineral assemblage signatures. These differences in clast character and type can be ascribed to a more powerful river system during Proto times driven by a changing drainage basin geomorphology, rather than reworking of older deposits or changes in provenance. The decrease in incision depths, and sediment transport from Proto to Meso Orange River deposits was accompanied by an increase in the proportion of sediments supplied to the river from local lithologies, including Namaqua Metamorphic Complex and Gariep Belt rocks. This change is reflected by the increase of amphibole-epidote in the heavy mineral assemblages, which was derived from the erosion of Namaqua Metamorphic Complex and Gariep Belt rocks, from Proto to Meso Orange River times.

The Proto Orange River gravel deposit shows limited reworking by the younger Meso Orange River system. Only at Auchas Major Deposit is the Proto Orange River gravel reworked as seen in both the clast assemblage and heavy mineral assemblage. The limited reworking of the Proto Orange River gravel deposits is attributed to an evolving river course where the Proto-Orange River had a higher sinuosity than the Meso-Orange River.

This study indicates that clast assemblage analysis should not be used as a proxy for the character of the sand sized matrix and vice versa, and that an integrated

approach is needed to improve the prediction of heavy minerals, including placer minerals, in ancient river terrace deposits and their offshore time equivalent deposits.

In Atlantic 1, an offshore mining area, the heavy mineral suite of gravels in the eastern regions is distinguished by higher amphibole-epidote, whilst authigenic apatite is more prevalent in the western regions. The higher concentration of apatite in the western regions can be attributed to the fact that the eastern regions have been exposed to subaerial conditions during Pleistocene sea level lowstand. The northward decreasing trend of amphibole-epidote in the eastern regions is neither a function of northward longshore drift nor the geomorphology of the seabed. Sea level fluctuations also did not influence the distribution of amphibole-epidote in Atlantic 1 gravels but instead amphibole-epidote distribution is a result of the relative amount of Namaqua Metamorphic Complex derived sediments and disintegration of the amphibole-epidote over time. The southward shift of the Orange River mouth through time is reflected in the northward decrease of magnetite proportion in Atlantic 1 both in the western regions (from Region V to Region W) and eastern regions (from Region K to Region N).

In comparison, the garnet proportion of Atlantic 1 gravels is higher than in the Orange River gravels, although the particle size is lower, whereas magnetite is far more common onshore. The decrease of magnetite from the river to the marine environment is ascribed to the relative density of magnetite, where magnetite is sequestered in the Proto and Meso Orange River deposits, whereas the majority of garnets (< 1 mm) are bypassed through the river system and delivered to the marine environment. Both the Orange River deposits and Atlantic 1 deposits show limited evidence of reworking because the most stable minerals (magnetite and garnet) show a lower degree of dissolution textures than the least stable minerals amphibole and epidote.

On the basis that the heavy minerals of the Orange River deposits and Atlantic 1 deposits share the same provenance (as evidenced by similar garnet, magnetite and epidote compositions), the amphibole-epidote proportion of gravel in the western Atlantic 1 regions (Region V and Region W) is similar to that of the Proto Orange River gravel whereas the eastern regions (Region K and Region N) display amphibole-epidote content characteristic of the Meso Orange River

gravels. The accumulation of Proto Orange River deposits and Meso Orange River deposits was coeval with a marked decrease of sediment flux to the offshore at the time of their respective aggradation and a reduced gravel accumulation in Atlantic 1.

This study has demonstrated that when characterising seabed sediments using heavy minerals the relative distance to the sediment input point (river mouth) needs to be considered because sediments of similar age can show differences in the amount of high density heavy minerals such as magnetite, which tend to concentrate close to the river mouth. Additionally, chemical and physical attrition influences both concentration and particle size range of specific heavy minerals to different degrees.

The suite of minerals collectively known as diamond indicator minerals co-derived from kimberlites have not been recorded in the heavy mineral suite in the lower Orange River or marine sediments. In Atlantic 1, there is no correlation between the concentrations of heavy minerals (garnet, ilmenite and amphibole-epidote) and diamond grade, most probably as a consequence of large differences in hydrodynamic behaviour between sand sized heavy minerals and clast sized diamonds.

In addressing the objectives of this study, the drainage history of the lower Orange River has been reconstructed by using the relative dominance in marker clasts from Proto to Meso Orange River gravels which is interpreted to reflect changes in the availability of specific lithologies. The extrinsic and intrinsic controls on the clast assemblage and heavy minerals assemblage of the lower Orange River gravels have been assessed by considering the different provenance between the exotic clasts and the heavy minerals. This study has shown that the exotic clasts and heavy minerals of the lower Orange River gravels have different provenances thus reflecting different transport histories and controls. In this study, the value of an integrated clast assemblage and heavy mineral assemblage method to understanding continental-scale bedrock river evolution has been evaluated and given the differences in provenances and

transport histories between the clasts and the heavy minerals, an integrated approach is recommended to improve the prediction of placer minerals.

In Atlantic 1, the sediment distribution patterns were investigated by assessing the distribution patterns of heavy minerals. However, the heavy minerals patterns may only reflect the distribution pattern of sand sized sediments (< 3 mm) and cannot be used as a guide for the clasts because the heavy minerals are sourced from local rocks in the lower Orange River area, whereas the exotic clasts that make up the large proportion of the gravels are from the upstream part of the Orange River catchment area, which is located about 2600 km from the Orange River mouth. The assessment of the influence of marine processes suggests that the distribution of heavy minerals in Atlantic 1 are not influenced by changes in sea level, or northward longshore drift or aeolian currents. The clast assemblage of Atlantic 1 gravels has been inferred from the amphibole-epidote content based on the integrated clast assemblage and heavy mineral assemblage established for Proto and Meso Orange River gravels. The depositional sequence of the Atlantic 1 gravels has been established on the basis of their similarities in amphibole-epidote content to the Proto Orange River gravels (western Atlantic 1 regions) and the Meso Orange River gravels (eastern Atlantic 1 gravels).

8.2 Future Work

This study has correlated the clast assemblage and heavy mineral assemblage of the fluvial Orange River terrace deposits. The Atlantic 1 marine gravels have been linked to the fluvial gravel using heavy mineral assemblage. In the future, clast assemblage analysis of the marine gravels would enable better constraints to be placed on the landscape evolution in the Orange River drainage basin by correlating clast assemblage and heavy mineral assemblage of the Atlantic 1 gravels. Absolute chronological dating of the terrace deposits and the marine gravels will be an important test of the current compositionally-driven correlations between phases of fluvial incision and aggradation and offshore deposition, and test the composite nature of the marine record.

In Atlantic 1, amphibole-epidote shows a northward decreasing trend in the eastern sampled regions (Chapter 5). In the future, more sampling could investigate whether this trend continues further north of Region N, the most northern region sampled in this study. This study would have benefited from a widespread sample coverage across the Atlantic 1 region to better constrain the regional sediment distribution patterns.

The provenance of the heavy minerals in the fluvial and marine gravel deposits is the Namaqua Metamorphic Complex rocks, and to a lesser extent the Gariiep Belt rocks. In this study, this provenance was constrained by comparing the composition of the detrital fluvial and marine garnets from the gravels with the Namaqua Metamorphic Complex and Gariiep Belt garnet composition obtained from the literature (Chapter 6). Detrital magnetite and epidote compositions were also analysed in this study. However, these could not be compared to Namaqua Metamorphic Complex or Gariiep Belt compositions as none are available in literature. In the future, sampling the Namaqua Metamorphic Complex rocks and Gariiep Belt protolith in the lower Orange River area, and analysing them for both mineral compositions that are present in the fluvial and marine gravel deposits, i.e. garnet, magnetite, amphibole, epidote and ilmenite, will help support correlations between terraces, and from onshore to offshore.

Modern river terrace and marine sediment analysis (river mouth and alongshore) as an analogue for older situations to test suitability and risks. This would be as a test of the links over a shorter period with more defined set of controls (and their interplay).

References

- Aalto, R., Lauer, J., Dietrich, W.E., 2008. Spatial and temporal dynamics of sediment accumulation and exchange along Strickland River floodplains (Papua New Guinea) over decadal-to-centennial timescales. *Journal of Geophysical Research* 113, F01S04, doi:10.1029/2006JF000627.
- Aizawa, M., Bluck, B.J., Cartwright, J., Milner, S., Swart, R., Ward, J.D., 2000. Constraints on the geomorphological evolution of Namibia from the offshore stratigraphic record. *Communications of the Geological Survey of Namibia* 12, 337-346.
- Allen, P.A., 2008. From landscapes into geological history. *Nature* 451, 274-276.
- Amiotte Suchet, P., Probst, J.L., 1993. Modelling of atmospheric CO₂ consumption by chemical weathering of rocks: Application to the Garonne, Congo and Amazon basins. *Chemical Geology* 107, 205-210.
- Anderson, J.B., Wallace, D.J., Simms, A.R., Rodriguez, A.B., Weight, R.W.R., Taha, Z.P., 2016. Recycling sediments between source and sink during a eustatic cycle: Systems of late Quaternary northwestern Gulf of Mexico Basin. *Earth-Science Reviews* 153, 111-138.
- Andò, S., Garzanti, E., Padoan, M., Limonta, M., 2012. Corrosion of heavy minerals during weathering and diagenesis: A catalog for optical analysis. *Sedimentary Geology* 280, 165-178.
- Ashley, G.M., Renwick, W.H., Haag, G.H., 1988. Channel form and processes in bedrock and alluvial reaches of the Raritan River, New Jersey. *Geology* 16, 436-439.
- Bagguley, J., Prosser, S., 1999. The Interpretation of passive margin depositional processes using seismic stratigraphy: examples from offshore Namibia. In: Cameron, N.R., Bate, R.H., Clure, V.S. (Eds.), *The Oil and Gas Habitats of the South Atlantic*, Geological Society of London, Special Publications 153. pp. 321-344.

- Ballarini, M., Wallinga, J., Wintle, A.G., Bos, A.J.J., 2007. A modified SAR protocol for optical dating of individual grains from young quartz samples. *Radiation Measurements* 42, 360-369.
- Bangert, B., Stollhofen, H., Lorenz, V., Armstrong, R., 1999. The geochronology and significance of ash-fall tuffs in the glaciogenic Carboniferous-Permian Dwyka Group of Namibia and South Africa. *Journal of African Earth Sciences* 29, 33-49.
- Barbarand, J., Quesnel, F., Pagel, M., 2013. Lower Paleogene denudation of Upper Cretaceous cover of the Morvan Massif and southeastern Paris Basin (France) revealed by AFT thermochronology and constrained by stratigraphy and paleosurfaces. *Tectonophysics* 608, 1310-1327.
- Basei, M.A.S., Frimmel, H.E., Nutman, A.P., Preciozzi, F., Jacob, J., 2005. A connection between the Neoproterozoic Dom Feliciano (Brazil/Uruguay) and Gariep (Namibia/South Africa) orogenic belts - evidence from a reconnaissance provenance study. *Precambrian Research* 139, 195-221.
- Bateman, R.M., Catt, J.A., 2007. Provenance and palaeoenvironmental interpretation of superficial deposits, with particular reference to post depositional modification of heavy mineral assemblages. In: Mange, M.A., Wright, D.T. (Eds.), *Heavy Minerals in Use, Developments in Sedimentology* 58. Elsevier, Oxford, pp. 151-188.
- Berner, R.A., Sjöberg, E.L., Velbel, M.A., Krom, M.D., 1980. Dissolution of pyroxenes and amphiboles during weathering. *Science* 207, 1205-1206.
- Bhattacharya, J.P., Copeland, P., Lawton, T.F., Holbrook, J., 2016. Estimation of source area, river paleo-discharge, paleoslope, and sediment budgets of linked deep-time depositional systems and implications for hydrocarbon potential. *Earth-Science Reviews* 153, 77-110.
- Bial, J., Büttner, S.H., Schenk, V., Appel, P., 2015. The long-term high-temperature history of the central Namaqua Metamorphic Complex: Evidence for a Mesoproterozoic continental back-arc in southern Africa. *Precambrian Research* 268, 243-278.
- Bierman, P.R., Coppersmith, R., Hanson, K., Neveling, J., Portenga, E.W., Rood, D.H., 2014. A cosmogenic view of erosion, relief generation, and the age of faulting in southern Africa. *GSA Today* 24, 4-11.

- Bluck, B.J., Ward, J.D., Cartwright, J., Swart, R., 2007. The Orange River, southern Africa: an extreme example of a wave-dominated sediment dispersal system in the South Atlantic Ocean. *Journal of the Geological Society, London* 164, 341-351.
- Bluck, B.J., Ward, J.D., de Wit, M.C.J., 2005. Diamond mega-placers: southern Africa and the Kaapvaal craton in a global context. *Mineral Deposits and Earth Evolution: Geological Society of London Special Publication* 248, 213-245.
- Böhn, J., 1926. Über tertiäre Versteinerungen von den Bogenfelsen Diamantfeldern. In: E., K. (Ed.), *Die Diamantenwüste Südwest-Afrikas*, 2. D, Reimer, Berlin, pp. 55-106.
- Bosman, D.E., Jourbert, J.R., 2008. Report on wave, wind and water level conditions at Walvis Bay. Namibian Port Authority, Walvis Bay,
- Botha, B.J.V., Grobler, N.J., 1979. Models for the geotectonic evolution of the middle to late Precambrian Namaqua mobile belt in eastern Namaqualand, South Africa. *Precambrian Research* 10, 21-41.
- Bremner, J.M., 1981. Shelf Morphology and surficial sediment off central and northern South West Africa (Namibia). *Geo-Marine Letters* 1, 91-96.
- Bremner, J.M., Willis, J.P., 1993. Mineralogy and geochemistry of the clay fraction of sediments from the Namibian continental margin and the adjacent hinterland. *Marine Geology* 115, 85-116.
- Bridgland, D., Westaway, R., 2008. Climatically controlled river terrace staircases: A worldwide Quaternary phenomenon. *Geomorphology* 98, 285-315.
- Bridgland, D.R., 1999. 'Wealden rivers' north of the Thames: a provenance study based on gravel clast analysis. *Proceedings of the Geologists' Association* 110, 133-148.
- Bristow, J.W., Smith, C.B., Brown, R., Gleadow, A.J.W., Kramers, J.D., Garvie, O.G., 1989. A summary of radiometric dating methods applicable to kimberlites and related rocks. In: *Geological Society of Australia Special Publication*, 14. Perth, 343-357.

- Brown, L.F., Benson, J.M., Brink, G.J., Doherty, S., Jollands, A., Jungslage, E.H.A., Keenan, J.H.G., Muntingh, A., Van Wyk, N.J.S., 1995. Sequence stratigraphy in offshore South African divergent basins. An Atlas on exploration for Cretaceous lowstand traps by Soekor (Pty) Ltd. AAPG, Studies in Geology 41, 139-184.
- Brown, R.W., Gallagher, K., Griffin, W.L., Ryan, C.G., De Wit, M.C.J., Belton, D.X., Harman, R., 1999. Kimberlites, accelerated erosion and evolution of the lithospheric mantle beneath the Kaapvaal Craton during the mid-Cretaceous, In: Gurney, J.J., Dawson, J.B., Nixon, P.H. (Eds.), 7th International Kimberlite Conference - Extended Abstracts. Cape Town, pp. 105-107.
- Brüchert, V., Jørgensen, B.B., Neumann, K., Riechmann, D., Schlösser, M., Schulz, H., 2003. Regulation of bacterial sulfate reduction and hydrogen sulfide fluxes in the central namibian coastal upwelling zone. *Geochimica et Cosmochimica Acta* 67, 4505-4518.
- Bull, W.B., 1979. Threshold of critical power in streams. *GSA Bulletin* 90, 453-464.
- Bynum, G.L., 2007. Heavy mineral provenance in an estuarine environment, Willapa Bay, Washington, USA: palaeogeographic implications and estuarine evolution. In: Mange, M.A., Wright, D.T. (Eds.), *Heavy Minerals in Use, Developments in Sedimentology* 58. Elsevier, Oxford, pp. 587-605.
- Canfield, D.E., Berner, R.A., 1987. Dissolution and pyritization of magnetite in anoxic marine sediments *Geochimica et Cosmochimica Acta* 51, 645-659.
- Cao, L., Jiang, T., Wang, Z., Zhang, Y., Sun, H., 2015. Provenance of Upper Miocene sediments in the Yinggehai and Qiongdongnan basins, northwestern South China Sea: Evidence from REE, heavy minerals and zircon U–Pb ages. *Marine Geology* 361, 136-146.
- Caracciolo, L., Orlando, A., Marchev, P., Critelli, S., Manetti, P., Raycheva, R., Riley, D., 2016. Provenance of Tertiary volcanoclastic sediment in NW Thrace (Bulgaria): Evidence from detrital amphibole and pyroxene geochemistry. *Sedimentary Geology* 336, 120-137.

- Carmody, L., Taylor, L.A., Thaisen, K.G., Tychkov, N., Bodnar, R.J., Sobolev, N.V., Pokhilenko, L.N., Pokhilenko, N.P., 2014. Imenite as a diamond indicator mineral in the Siberian craton: a tool to predict diamond potential. *Economic Geology* 109, 775-783.
- Cascalho, J., Fradique, C., 2007. The sources and hydraulic sorting of heavy minerals on the northern Portuguese continental margin. In: Mange, M.A., Wright, D.T. (Eds.), *Heavy Minerals in Use, Developments in Sedimentology* 58. Elsevier, Oxford, pp. 75-110.
- Catuneanu, O., Hancox, P.J., Rubidge, B.S., 1998. Reciprocal flexural behavior and contrasting stratigraphies: a new basin development model for the Karoo retroarc foreland system, South Africa. *Basin Research* 10, 417-439.
- Catuneanu, O., Wopfner, H., Eriksson, P.G., Cairncross, B., Rubidge, B.S., Smith, R.M.H., Hancox, P.J., 2005. The Karoo basins of south-central Africa. *Journal of African Earth Sciences* 43, 211-253.
- Chamberlain, E.L., Wallinga, J., Reimann, T., Goodbred, S.L., Steckler, M.S., Shen, Z., Sincavage, R., 2017. Luminescence dating of delta sediments: Novel approaches explored for the Ganges-Brahmaputra-Meghna Delta. *Quaternary Geochronology* 41, 97-111.
- Charlton, R., 2008. *Fundamentals of Fluvial Geomorphology*. Routledge, New York, 234 pp.
- Chen, J., Wang, Z., Chen, Z., Wei, Z., Wei, T., Wei, W., 2009. Diagnostic heavy minerals in Plio–Pleistocene sediments of the Yangtze Coast, China with special reference to the Yangtze River connection into the sea. *Geomorphology* 113, 129-136.
- Claude, A., Akçar, N., Ivy-Ochs, S., Schlunegger, F., Kubik, W.P., Dehnert, A., Kuhlemann, J., Rahn, M., Schlüchter, C., 2017. Timing of early Quaternary gravel accumulation in the Swiss Alpine Foreland. *Geomorphology* 276, 71-85.
- Clift, P.D., Giosan, L., Henstock, T.J., Tabrez, A.R., 2014. Sediment storage and reworking on the shelf and in the Canyon of the Indus River-Fan System since the last glacial maximum. *Basin Research* 26, 183-202.

- Cockburn, H.A.P., Brown, R.W., Summerfield, M.A., Seidl, M.A., 2000. Quantifying passive margin denudation and landscape development using a combined fission-track thermochronology and cosmogenic isotope analysis approach. *Earth and Planetary Science Letters* 179, 429-435.
- Compton, J.S., 2006. The mid-Holocene sea-level highstand at Bogenfels Pan on the southwest coast of Namibia. *Quaternary Research* 66, 303-310.
- Compton, J.S., Bergh, E.W., 2016. Phosphorite deposits on the Namibian shelf. *Marine Geology* 380, 290-314.
- Corbett, I.B., 1993. The Modern and ancient pattern of sand flow through the southern Namib deflation basin. In: Pye, K., Lancaster, N. (Eds.), *Aeolian Sediments: Ancient and Modern*, International Association of Sedimentologists Special Publications 14. Blackwell Scientific Publications, Oxford, 45-60.
- Corbett, I.B., 1996. A review of diamondiferous marine deposits of western southern Africa. *Africa Science Review* 3, 157-174.
- Cornell, D.H., Humphreys, H., Theart, H.F.J., Scheepers, D.J., 1992. A collision-related pressure-temperature-time path for Prieska copper mine, namaqua-natal tectonic province, South Africa. *Precambrian Research* 59, 43-71.
- Corvinus, G., 1978. Palaeontological and archaeological investigations in the Lower Orange River Valley from Arrisdrif to Obib (in the concession area of the Consolidated Diamond Mines of South West Africa (Proprietary) Limited). In: Coetzee, J.A. (Ed.), *Palaeoecology of Africa and the surrounding islands* 10. Balkema, Rotterdam.
- Corvinus, G., Hendey, Q.B., 1978. A new Miocene vertebrate locality at Arrisdrif in SWA (Namibia). *Neues Jahrbuch fur Geologie und Palaontologie* 4, 193-205.
- Counts, R.C., Murari, M.K., Owen, L.A., Mahan, S.A., Greenan, M., 2015. Late Quaternary chronostratigraphic framework of terraces and alluvium along the lower Ohio River, southwestern Indiana and western Kentucky, USA. *Quaternary Science Reviews* 110, 72-91.

- Covault, J.A., Fildani, A., 2014. Continental shelves as sediment capacitors or conveyors: Source-to-sink insights from the tectonically active Oceanside shelf, southern California, USA. In: Chiocci, F.L., Chivas, A.R. (Eds.), *Geological Society London Memoirs*, 41. 315-326.
- Covault, J.A., Normark, W.R., Romans, B.W., Graham, S.A., 2007. Highstand fans in the California borderland: the overlooked deep-water depositional systems. *Geology* 35, 783-786.
- Covault, J.A., Romans, B.W., Graham, S.A., Fildani, A., Hilley, G.E., 2011. Terrestrial source to deep-sea sink sediment budgets at high and low sea levels: Insights from tectonically active Southern California. *Geology* 39, 619-622.
- Cox, G.M., Halverson, G.P., Stevenson, R.K., Vokaty, M., Poirier, A., Kunzmann, M., Li, Z.-X., Denyszyn, S.W., Strauss, J.V., Macdonald, F.A., 2016. Continental flood basalt weathering as a trigger for Neoproterozoic Snowball Earth. *Earth and Planetary Science Letters* 446, 89-99.
- Cunha, P.P., Martins, A.A., Huot, S., Murray, A., Raposo, L., 2008. Dating the Tejo river lower terraces in the Ródão area (Portugal) to assess the role of tectonics and uplift. *Geomorphology* 102, 43-54.
- Day, R.W., Franzsen, A.J., Rogers, J., 1992. Coast-parallel palaeochannels off southern Namibia. *Marine Geology* 105, 299-304.
- de Vera, J., Granado, P., McClay, K., 2010. Structural evolution of the Orange Basin gravity-driven system, offshore Namibia. *Marine and Petroleum Geology* 27, 223-237.
- de Villiers, J., Sohnge, P.G., 1959. The Geology of the Richtersveld. In: *Memoir of the Geological Survey of South Africa*, 48. Government Printer, pp. 295.
- de Wit, M.C.J., 1999. Post-Gondwana drainage and the development of diamond placers in western South Africa. *Economic Geology* 94, 721-270.
- de Wit, M.C.J., Marshall, T.R., Partridge, T.C., 2000. Fluvial deposits and drainage evolution. In: Partridge, T.C., Maud, R.R. (Eds.), *The*

Cenozoic of Southern Africa, Oxford Monographs on Geology and Geophysics 40. Oxford University Press, New York, pp. 55-72.

de Wit, M.J., de Ronde, C.E.J., Tredoux, M., Roering, C., Hart, R.J., Armstrong, R.A., Green, R.W.E., Peberdy, E., Hart, R.A., 1992. Formation of an Archaean continent. *Nature* 357, 553-562.

Decker, D., 1988. The wave regime on the inner shelf south of the Orange River and its implications for sediment transport. *South African Journal of Geology* 91, 358-371.

Decker, J.E., Niedermann, S., de Wit, M.J., 2011. Soil erosion rates in South Africa compared with cosmogenic ^3He -based rates of soil production. *South African Journal of Geology* 114, 475-488.

Decker, J.E., Niedermann, S., de Wit, M.J., 2013. Climatically influenced denudation rates of the southern African plateau: Clues to solving a geomorphic paradox. *Geomorphology* 190, 48-60.

Deer, W.A., Howie, R.A., Zussman, J., 1992. An introduction to the rock forming minerals Longman Group (FE) Limited, Hong Kong 696 pp.

Deer, W.A., Howie, R.A., Zussman, J., 2001. Rock Forming Minerals: Framework Silicates, Feldspars. The Geological Society London, Bath, 972 pp.

Dessert, C., Dupré, B., François, L.M., Schott, J., Gaillardet, J., Chakrapani, G., Bajpai, S., 2001. Erosion of Deccan Traps determined by river geochemistry: impact on the global climate and the $^{87}\text{Sr}/^{86}\text{Sr}$ ratio of seawater. *Earth and Planetary Science Letters* 188, 459-474.

DiBenedetto, S., Grotzinger, J., 2005. Geomorphic evolution of a storm-dominated carbonate ramp. *Geological Magazine* 142, 583-604.

Dickinson, W.R., Gehrels, G.E., 2003. U–Pb ages of detrital zircons from Permian and Jurassic eolian sandstones of the Colorado Plateau, USA: paleogeographic implications. *Sedimentary Geology* 163, 29-66.

Diener, J.F.A., Thomas, R.J., Macey, P.H., 2017. Pan-African accretionary metamorphism in the Sperrgebiet Domain, Gariep Belt, SW Namibia. *Precambrian Research* 292, 152-162.

- Diener, J.F.A., White, R.W., Link, K., Dreyer, T.S., Moodley, A., 2013. Clockwise, low-P metamorphism of the Aus granulite terrain, southern Namibia during the Mesoproterozoic Namaqua Orogeny. *Precambrian Research* 224, 629-652.
- Diester-Haass, L., Heine, K., Rothe, P., Schrader, H., 1988. Late Quaternary history of continental climate and the Benguela Current off South West Africa. *Palaeogeography, Palaeoclimatology, Palaeoecology* 65, 81-91.
- Diester-Haass, L., Meyers, P.A., Vidal, L., 2002. The late Miocene onset of high productivity in the Benguela Current upwelling system as part of a global pattern. *Marine Geology* 180, 87-103.
- Diester-Haass, L., Meyers, P.A., Rothe, P., 1990. Miocene history of the Benguela Current and Antarctic ice volumes: Evidence from rhythmic sedimentation and current growth across the Walvis Ridge (Deep Sea Drilling Project Sites 362 and 532). *Paleoceanography* 5, 685-707.
- Dill, H.G., 1994. Can REE patterns and U-Th variations be used as a tool to determine the origin of apatite in clastic rocks? *Sedimentary Geology* 92, 175-196.
- Dill, H.G., 1995. Heavy mineral response to the progradation of an alluvial fan: implications concerning unroofing of source area, chemical weathering and palaeo-relief (Upper Cretaceous Parkstein fan complex, SE Germany). *Sedimentary Geology* 95, 39-56.
- Dill, H.G., 1998. A review of heavy minerals in clastic sediments with case studies from the alluvial-fan through the nearshore-marine environments. *Earth-Science Reviews* 45, 103-132.
- Dill, H.G., 2007. Grain morphology of heavy minerals from marine and continental placer deposits, with special reference to Fe–Ti oxides. *Sedimentary Geology* 198, 1-27.
- Dingle, R.V., 1971. Tertiary sedimentary history of the continental shelf off Southern Cape Province, South Africa. *Transactions of the Geological Society of South Africa* 74, 173-186.

- Dingle, R.V., 1973. The geology of the continental shelf between Luderitz and Cape Town (Southwest Africa), with special reference to Tertiary strata. *Journal of the Geological Society* 129, 337-362.
- Dingle, R.V., Hendey, Q.B., 1984. Late Mesozoic and Tertiary sediment supply to the Eastern Cape basins (SE Atlantic) and the palaeo-drainage systems in southwestern Africa. *Marine Geology* 56, 13-26.
- Dingle, R.V., Siesser, W.G., Newton, A.R., 1983. *Mesozoic and Tertiary Geology of Southern Africa*. Balkema, Rotterdam, 375 pp.
- do Nascimento, D.R., Sawakuchi, A.O., Guedes, C.C.F., Giannini, P.C.F., Grohmann, C.H., Ferreira, M.P., 2015. Provenance of sands from the confluence of the Amazon and Madeira rivers based on detrital heavy minerals and luminescence of quartz and feldspar. *Sedimentary Geology* 316, 1-12.
- Dott, R.H., Bourgeois, J., 1982. Hummocky stratification: significance of its variable bedding sequences. *Geological Society of America Bulletin* 93, 663-680.
- Dowdeswell, J.A., Hambrey, M.J., Ruitang, W., 1985. A Comparison of Clast Fabric and Shape in Late Precambrian and Modern Glacigenic Sediments. *Journal of Sedimentary Petrology* 55, 691-704.
- Duncan, R.A., Hooper, P.R., Rehacek, J., Marsh, J.S., Duncan, A.R., 1997. The timing and duration of the Karoo igneous event, southern Gondwana. *Journal of Geophysical Research* 102, 18127-18138.
- Dunlevey, J.N., August, R.B., 2010. Radiometric ages of monazite from the Kwabonambi and Sibaya Formations (Maputaland Group) of northern Kwazul-Natal, South Africa and the provenance implications. *Journal of African Earth Sciences* 58 585 - 594.
- Durn, G., Aljinović, D., Crnjaković, M., Lugović, B., 2007. Heavy and light mineral fractions indicate polygenesis of extensive Terra Rossa soils in Istria, Croatia. In: Mange, M.A., Wright, D.T. (Eds.), *Heavy Minerals in Use, Developments in Sedimentology* 58. Elsevier, Oxford, pp. 701-737.
- Dutton, A., Carlson, A.E., Long, A.J., Milne, G.A., Clark, P.U., DeConto, R., Horton, B.P., Rahmstorf, S., Raymo, M.E., 2015. Sea-level rise due to

polar ice-sheet mass loss during past warm periods. *Science* 349, DOI: 10.1126/science.aaa4019.

Edelman-Furstenberg, Y., 2014. Distribution and paleoecology of molluscan skeletal remains along an upwelling tract: Benguela system, Namibian shelf. *Marine Geology* 353, 153-162.

Eglington, B.M., 2006. Evolution of the Namaqua-Natal belt, southern Africa - A geochronological and isotope geochemical review. *Journal of African Earth Sciences* 46, 93-111.

Faupl, P., Pavlopoulos, A., Migiros, G., 2007. Provenance of flysch sediments and the Palaeogene-Early Miocene geodynamic evolution of the Hellenides: a contribution from heavy mineral investigations. In: Mange, M.A., Wright, D.T. (Eds.), *Heavy Minerals in Use, Developments in Sedimentology* 58. Elsevier, Oxford, pp. 765-788.

Filippelli, G.M., 2011. Phosphate rock formation and marine phosphorus geochemistry: The deep time perspective. *Chemosphere* 84, 759-766.

Finnegan, N.J., Dietrich, W.E., 2011. Episodic bedrock strath terrace formation due to meander migration and cutoff. *Geology* 39, 143-146.

Fleming, A., Summerfield, M.A., Stone, J.O., Fifield, L.K., Cresswell, R.G., 1999. Denudation rates for the southern Drakensberg escarpment, SE Africa, derived from in-situ-produced cosmogenic ^{36}Cl : initial results. *Journal of the Geological Society, London* 156, 209-212.

Fleming, E.J., Flowerdew, M.J., Smyth, H.R., Scott, R.A., Morton, A.C., Omma, J.E., Frei, D., Whitehouse, M.J., 2016. Provenance of Triassic sandstones on the southwest Barents Shelf and the implication for sediment dispersal patterns in northwest Pangaea. *Marine and Petroleum Geology* 78, 516-535.

Forbes, D.L., Tayloer, R.B., Frobels, D., 1982. Barrier overwash and washover sedimentation Aspy Bay, Cape Breton Island. *Atlantic Geology* 18, 43-44.

Foster, M.A., Anderson, R.S., Gray, H.J., Mahan, S.A., 2017. Dating of river terraces along Lefthand Creek, western High Plains, Colorado, reveals punctuated incision. *Geomorphology* 295, 176-190.

- Frihy, O.E., 2007. The Nile Delta: processes of heavy mineral sorting and depositional patterns. In: Mange, M.A., Wright, D.T. (Eds.), *Heavy Minerals in Use, Developments in Sedimentology* 58. Elsevier, Oxford, pp. 49-74.
- Frihy, O.E., Dewidar, K.M., 2003. Patterns of erosion/sedimentation, heavy mineral concentration and grain size to interpret boundaries of littoral sub-cells of the Nile Delta, Egypt. *Marine Geology* 199, 27-43.
- Frimmel, H.E., Frank, W., 1998. Neoproterozoic tectono-thermal evolution of the Gariep Belt and its basement, Namibia and South Africa. *Precambrian Research* 90, 1-28.
- Frimmel, H.E., Hartnady, C.J.H., Koller, F., 1996. Geochemistry and tectonic setting of magmatic units in the Pan-African Gariep Belt, Namibia. *Chemical Geology* 130, 101-121.
- Frimmel, H.E., Johansson, I.R., Mubita, P., 2004. An Eburnean base metal source for sediment-hosted zinc-lead deposits in Neoproterozoic units of Namibia: Lead isotopic and geochemical evidence. *Mineralium Deposita* 39, 328-343.
- Gallagher, K., Brown, R., 1999. Denudation and uplift at passive margins: the record on the Atlantic Margin of southern Africa. *Philosophical Transactions of the Royal Society of London. Series A: Mathematical, Physical and Engineering Sciences* 357, 835-859.
- Garzanti, E., 2016. From static to dynamic provenance analysis—Sedimentary petrology upgraded. *Sedimentary Geology* 336, 3-13.
- Garzanti, E., Resentini, A., Ando, S., Vezzoli, G., Pereira, A., Vermeesch, P., 2015. Physical controls on sand deposition and relative durability of detrital minerals during ultra-long distance littoral and aeolian transport (Namibia and southern Angola). *Sedimentology* 62, 971-996.
- Garzanti, E., Vermeesch, P., Andò, S., Lustrino, M., Padoan, M., Vezzoli, G., 2014. Ultra-long distance littoral transport of Orange sand and provenance of the Skeleton Coast Erg (Namibia). *Marine Geology* 357, 25-36.
- Gibbard, P.L., 1979. Middle Pleistocene drainage in the Thames Valley. *Geological Magazine* 116, 35-44.

- Goodbred, J.S.L., Paolo, P.M., Ullah, M.S., Pate, R.D., Khan, S.R., Kuehl, S.A., Singh, S.K., Rahaman, W., 2014. Piecing together the Ganges-Brahmaputra-Meghna River delta: Use of sediment provenance to reconstruct the history and interaction of multiple fluvial systems during Holocene delta evolution. *GSA Bulletin* 126, 1495-1510.
- Goudie, A., Viles, H., 2015. *Landscapes and landforms of Namibia*. Springer, New York, 173 pp.
- Green, C.P., Hey, R.W., McGregor, D.F.M., 1980. Volcanic pebbles in Pleistocene gravels of the Thames in Buckinghamshire and Hertfordshire. *Geological Magazine* 117, 59-64.
- Green, C.P., McGregor, D.F.M., Evans, A.H., 1982. Development of the Thames drainage system in the early and middle Pleistocene times. *Geological Magazine* 119, 281-290.
- Green, P.F., Duddy, I.R., Japsen, P., Bonow, J.M., Malan, J.A., 2017. Post-breakup burial and exhumation of the southern margin of Africa. *Basin Research* 29, 96-127.
- Grotzinger, J., Adams, E.W., Schroder, S., 2005. Microbial-metazoan reefs of the terminal Proterozoic Nama Group (c. 550-543 Ma), Namibia. *Geological Magazine* 142, 499-517.
- Grotzinger, J.P., Miller, R.M., 2008. Nama Group. In: Miller, R.M. (Ed.), *The Geology of Namibia*, Ministry of Mines and Energy Geological Survey, Windhoek, pp. 229-272.
- Guillocheau, F., Rouby, D., Robin, C., Helm, C., Rolland, N., de Veslud, C.L., Braun, J., 2012. Quantification and causes of the terrigenous sediment budget at the scale of a continental margin: a new method applied to the Namibia-South Africa margin. *Basin Research* 24, 3-30.
- Gurney, J.J., Helmstaedt, H., Moore, R.O., 1993. A review of the use and application of mantle mineral geochemistry in diamond exploration. *Pure and Applied Chemistry* 65, 2423-2442.
- Gurney, J.J., Zweistra, P., 1995. The interpretation of major element compositions of mantle minerals in diamond exploration. *Journal of Geochemical Exploration* 53, 293-309.

- Guyot, J.-L., Jouanneau, J.-M., Quintanilla, J., Wasson, J.-G., 1993. Dissolved and suspended sediment loads exported from the Andes by the Beni river (Bolivian Amazonia), during a Flood. *Geodinamica Acta* 6, 233-241.
- Hall, A.M., Thomas, M.F., Thorp, M.B., 1985. Late Quaternary alluvial placer development in the humid tropics: the case of the Birim diamond placer, Ghana. *Journal of the Geological Society London* 142, 777-787.
- Hall, R.D., Michaud, D., 1988. The use of hornblende etching, clast weathering, and soils to date alpine glacial and periglacial deposits: A study from southwestern Montana. *GSA Bulletin* 100, 458-467.
- Hallsworth, C.R., Chisholm, J.I., 2008. Provenance of late Carboniferous sandstones in the Pennine Basin (UK) from combined heavy mineral, garnet geochemistry and palaeocurrent studies. *Sedimentary Geology* 203, 196-212.
- Hamers, T., Kamstra, J.H., van Gils, J., Kotte, M.C., van Hattum, A.G.M., 2015. The influence of extreme river discharge conditions on the quality of suspended particulate matter in Rivers Meuse and Rhine (The Netherlands). *Environmental Research* 143, 241-255.
- Hansley, P.L., 1987. Petrologic and experimental evidence for the etching of garnets by organic acids in the Upper Jurassic Morrison Formation, northwestern New Mexico. *Journal of Sedimentary Petrology* 57, 666-681.
- Hansley, P.L., Briggs, P.H., 1994. Garnet dissolution in oxalic acid; a possible analog for natural etching of garnet by dissolved organic matter. *U.S. Geological Survey Bulletin* 2106, 1-14.
- Hanson, E.K., Moore, J.M., Bordy, E.M., Marsh, J.S., Howarth, G., Robey, J.V.A., 2009. Cretaceous erosion in central South Africa: evidence from upper-crustal xenoliths in kimberlite diatremes. *South African Journal of Geology* 112, 125-140.
- Haq, B.U., Hardenbol, J., Vail, P.R., 1987. Chronology of Fluctuating Sea Levels since the Triassic. *Science* 235, 1156-1167.

- Hassan, F.A., 1976. Heavy minerals and the evolution of the modern Nile. *Quaternary Research* 6, 425-444.
- Hawthorne, J.B., 1975. Model of a kimberlite pipe. *Physics and Chemistry of the Earth* 9, 1-15.
- Hendey, Q.B., 1978. Preliminary report on the Miocene vertebrates from Arrisdrift, South West Africa. *Annals of the South African Museum* 76, 1-41.
- Hidy, A.J., Gosse, J.C., Blum, M.D., Gibling, M.R., 2014. Glacial-interglacial variation in denudation rates from interior Texas, USA, established with cosmogenic nuclides. *Earth and Planetary Science Letters* 390, 209-221.
- Hirsch, K.K., Scheck-Wenderoth, M., van Wees, J.-D., Kuhlmann, G., Paton, D.A., 2010. Tectonic subsidence history and thermal evolution of the Orange Basin. *Marine and Petroleum Geology* 27, 565-584.
- Holtar, E., Forsberg, A.W., 2000. Postrift development of the Walvis Basin, Namibia: results from the exploration campaign in Quadrant 1911. In: Mello, M.R., Katz, B.J. (Eds.), *Petroleum Systems of the South Atlantic Margins*, American Association of Geologists, Memoirs 73. pp. 429-446.
- Howarth, J.D., Fitzsimons, S.J., Jacobsen, G.E., Vandergoes, M.J., Norris, R.J., 2013. Identifying a reliable target fraction for radiocarbon dating sedimentary records from lakes. *Quaternary Geochronology* 17, 68-80.
- Humphreys, H.C., Van Bever Donker, J.M., 1990. Early Namaqua low-pressure metamorphism: deformation and porphyroblast growth in the Zoovorby staurolite schist, South Africa. *Journal of Metamorphic Geology* 8, 159-170.
- Jacob, J., Ward, J.D., Bluck, B.J., Scholtz, R.A., Frimmel, H.E., 2006. Some observations on diamondiferous bedrock gully trapsites on late Cainozoic marine cut platforms of the Sperrgebiet, Namibia *Ore Geology Reviews* 28, 493-506.
- Jacob, R.J., 2005. The Erosional and Cainozoic Depositional History of the Lower Orange River, southwestern Africa. PhD Thesis, University of Glasgow, UK, 354 pp.

- Jacob, R.J. (2007) Base Booklet for Sam Nuyoma's Visit - September 2007,
- Jacob, R.J., Bluck, B.J., Ward, J.D., 1999. Tertiary-age diamondiferous fluvial deposits of the lower Orange River valley, southwestern Africa. *Economic Geology* 94, 749-758.
- Jacobs, J., Pisarevsky, S., Thomas, R.J., Becker, T., 2008. The Kalahari Craton during assembly and dispersal of Rodinia. *Precambrian Research* 160, 142-158.
- Jarvis, A., Reuter, H.I., Nelson, A., Guevara, E., 2008. Hole-filled seamless SRTM data V4. International Centre for Tropical Agriculture (CIAT) [online], available: <http://srtm.csi.cgiar.org> [accessed June 2017].
- Jerolmack, D.J., Paola, C., 2010. Shredding of environmental signals by sediment transport. *Geophysical Research Letters* 37, L19401, doi: 10.1029/2010GL044638.
- Jiang, T., Cao, L., Xie, X., Wang, Z., Li, X., Zhang, Y., Zhang, D., Sun, H., 2015. Insights from heavy minerals and zircon U–Pb ages into the middle Miocene–Pliocene provenance evolution of the Yinggehai Basin, northwestern South China Sea. *Sedimentary Geology* 327, 32-42.
- Johnson, M.R., van Vuuren, C.J., Visser, J.N.J., Cole, D.J., Wickens, H.d., Christie, A.D.M., Roberts, D.I., 1997. The foreland Karoo Basin, South Africa. In: Selley, R.C. (Ed.), *African Basins, Sedimentary Basins of the World* 3. Elsevier, Amsterdam, pp. 269-317.
- Jones, A.P., 2000. Late Quaternary sediment sources, storage and transfers within mountain basins using clast lithological analysis: Pineta Basin, central Pyrenees, Spain. *Geomorphology* 34, 145-161.
- Jourdan, F., Feraud, G., Bertrand, H., Watkeys, M.K., Renne, P.R., 2007. Distinct brief major events in the Karoo large igneous province clarified by new $^{40}\text{Ar}/^{39}\text{Ar}$ ages on Lesotho basalts. *Lithos* 98, 195-209.
- Jubb, R.A., 1964. Fresh water fishes and drainage basins in southern Africa. *South African Journal of Science* 60, 17-21.

- Kadereit, A., DeWitt, R., Johnson, T.C., 2012. Luminescence properties and optically (post-IR blue-light) stimulated luminescence dating of limnic sediments from northern Lake Malawi – Chances and limitations. *Quaternary Geochronology* 10, 160-166.
- Kasten, S., Jørgensen, B.B., 2000. Sulfate reduction in marine sediments. In: Schulz, H.D., Zabel, M. (Eds.), *Marine Geochemistry*, Springer pp. 263-282.
- Key, R.M., Tidi, J., McGeorge, I., Aitken, G., Cadman, A., Anscombe, J., 1998. The Lower Karoo Supergroup geology of the southeastern part of the Gembok Sub-basin of the Kalahari Basin, Botswana. *South African Journal of Geology* 101, 225-236.
- Knight, J., Grab, S.W., 2016a. A continental scale perspective on landscape evolution in southern Africa during the Cenozoic. In: Knight, J., Grab, S.W. (Eds.), *Quaternary environmental change in southern Africa: physical and human dimensions*, Cambridge University Press, Cambridge, pp. 30-46.
- Knight, J., Grab, S.W., 2016b. The context of Quaternary environmental change in southern Africa. In: Knight, J., Grab, S.W. (Eds.), *Quaternary Environmental Change in Southern Africa: Physical and Human Dimensions*, Cambridge University Press, Cambridge, pp. 1-17.
- Komar, P.D., 2007. The entrainment, transport and sorting of heavy minerals by waves and currents. In: Mange, M.A., Wright, D.T. (Eds.), *Heavy Minerals in Use, Developments in Sedimentology* 58. Elsevier, Oxford, pp. 3-48.
- Komar, P.D., Wang, C., 1984. Processes of selective grain transport and formation of placers on beaches. *Journal of Geology* 92, 637-655.
- Krippner, A., Meinhold, G., Morton, A.C., Schöning, J., von Eynatten, H., 2016. Heavy minerals and garnet geochemistry of stream sediments and bedrocks from the Almklovdalen area, Western Gneiss Region, SW Norway: Implications for provenance analysis. *Sedimentary Geology* 336, 96-105.
- Kristmannsson, S.S., 1999. Dissolved oxygen conditions on the shelf off Namibia in 1994. *Rit Fiskideildar* 16, 89-95.

- Kuehl, S.A., Alexander, C.R., Blair, N.E., Harris, C.K., Marsaglia, K.M., Ogston, A.S., Orpin, A.R., Roering, J.J., Bever, A.J., Bilderback, E.L., Carter, L., Cerovski-Darriau, C., Childress, L.B., Reide Corbett, D., Hale, R.P., Leithold, E.L., Litchfield, N., Moriarty, J.M., Page, M.J., Pierce, L.E.R., Upton, P., Walsh, J.P., 2016. A source-to-sink perspective of the Waipaoa River margin. *Earth-Science Reviews* 153, 301-334.
- Kuhlmann, G., Adams, S., Campher, C., van der Spuy, D., di Primio, R., Horsfield, B., 2010. Passive margin evolution and its controls on natural gas leakage in the southern Orange Basin, blocks 3/4, offshore South Africa. *Marine and Petroleum Geology* 27, 973-992.
- Lambeck, K., Rouby, H., Purcell, A., Sun, Y., Sambridge, M., 2014. Sea level and global ice volumes from the Last Glacial Maximum to the Holocene. *Proceedings of the National Academy of Sciences* 111, 15296-15303.
- Lancaster, N., 1981. Grain size characteristics of Namib Desert linear dunes. *Sedimentology* 28, 115-122.
- Lancaster, N., 1985. Winds and sand movements in the Namib Sand Sea. *Earth Surface Processes and Landforms* 10, 607-619.
- Lång, L.-O., 2000. Heavy mineral weathering under acidic soil conditions. *Applied Geochemistry* 15, 415-423.
- Larcombe, P., 2007. Continental shelf environments. In: Perry, C., Taylor, K. (Eds.), *Environmental Sedimentology*, Blackwell Publishing Oxford, pp. 351-388.
- Laudien, J., Brey, T., Arntz, W.E., 2003. Population structure, growth and production of the surf clam *Donax serra* (Bivalvia, Donacidae) on two Namibian sandy beaches. *Estuarine, Coastal and Shelf Science* 58, Supplement, 105-115.
- Leeder, M., 1999. *Sedimentology and Sedimentary Basins: From Turbulence to Tectonics*. Blackwell Science Ltd, Oxford, 592 pp.
- Lewis, C.J., Sancho, C., McDonald, E.V., Peña-Monné, J.L., Pueyo, E.L., Rhodes, E., Calle, M., Soto, R., 2017. Post-tectonic landscape evolution in NE Iberia using staircase terraces: Combined effects of uplift and climate. *Geomorphology* 292, 85-103.

- Lindsey, D.A., Langer, W.H., Van Gosen, B.S., 2007. Using pebble lithology and roundness to interpret gravel provenance in piedmont fluvial systems of the Rocky Mountains, USA. *Sedimentary Geology* 199, 223-232.
- Liu, W., Liu, C., Brantley, S.L., Xu, Z., Zhao, T., Liu, T., Yu, C., Xue, D., Zhao, Z., Cui, L., Zhang, Z., Fan, B., Gu, X., 2016. Deep weathering along a granite ridgeline in a subtropical climate. *Chemical Geology* 427, 17-34.
- Locke, W.W., 1986. Rates of hornblende etching in soils on glacial deposits, Baffin Island, Canada. In: Coleman, S.M., Dethier, D.P. (Eds.), *Rates of Chemical Weathering of Rocks and Minerals*, Academic Press, New York, pp. 129-145.
- Louvat, P., Allègre, C.J., 1997. Present denudation rates on the island of Réunion determined by river geochemistry: Basalt weathering and mass budget between chemical and mechanical erosions. *Geochimica et Cosmochimica Acta* 61, 3645-3669.
- Maddy, D., Veldkamp, A., Jongmans, A.G., Candy, I., Demir, T., Schoorl, J.M., van der Schriek, T., Stemerding, C., Scaife, R.G., van Gorp, W., 2012. Volcanic disruption and drainage diversion of the palaeo-Hudut River, a tributary of the Early Pleistocene Gediz River, Western Turkey. *Geomorphology* 165–166, 62-77.
- Mahaney, W.C., 2002. *Atlas of Sand Grain Surface Textures and Applications*. Oxford University Press, Oxford, 246 pp.
- Maher, E., Harvey, A.M., France, D., 2007. The impact of a major Quaternary river capture on the alluvial sediments of a beheaded river system, the Rio Alias SE Spain. *Geomorphology* 84, 344-356.
- Malvoisin, B., Austrheim, H., Malthe-Sørensen, A., Glodny, J., 2012. Deformation-related alteration of basaltic clasts during deep burial in sedimentary basins. *Chemical Geology* 322–323, 47-67.
- Mange, M.A., Morton, A.C., 2007. Geochemistry of Heavy Minerals. In: Mange, M.A., Wright, D.T. (Eds.), *Heavy Minerals in Use, Developments in Sedimentology* 58. Elsevier, Oxford, pp. 345-391.

- Mange, M.A., Otvos, E.G., 2005. Gulf coastal plain evolution in West Louisiana: Heavy mineral provenance and Pleistocene alluvial chronology. *Sedimentary Geology* 182, 29-57.
- Marsaglia, K.M., DeVaughn, A.M., James, D.E., Marden, M., 2010. Provenance of fluvial terrace sediments within the Waipaoa sedimentary system and their importance to New Zealand source-to-sink studies. *Marine Geology* 270, 84-93.
- Marsh, J.S., Hooper, P.R., Rehacek, J., Duncan, R.A., Duncan, A.R., 1997. Stratigraphy and age of Karoo basalts of Lesotho and implications for correlations within the Karoo igneous province. In: Mahoney, J.J., Coffin, M.F. (Eds.), *Large Igneous Provinces: Continental, Oceanic, and Planetary Flood Volcanism*, Geophysical Monograph 100. American Geophysical Union, pp. 247-271.
- Marshall, T.R., Baxter-Brown, R., 1995. Basic principles of alluvial diamond exploration. *Journal of Geochemical Exploration* 53, 277-292.
- Mather, A.E., 2000. Adjustment of a drainage network to capture induced base-level change: an example from the Sorbas Basin, SE Spain. *Geomorphology* 34, 271-289.
- McCandless, T.E., Gurney, J.J., 1989. Sodium in garnet and potassium in clinopyroxene: criteria for classifying mantle xenoliths. In: Ross, J. (Ed.), *Kimberlites and Related rocks* Geological Society of Australia Special Publication 14. Blackwell Scientific Publications, Perth, 827-832.
- McClenaghan, M.B., 2011. Overview of common processing methods for recovery of indicator minerals from sediment and bedrock in mineral exploration *Geochemistry: Exploration, Environment, Analysis* 11 265-278.
- Mellett, C.L., Hodgson, D.M., Plater, A.J., Mauz, B., Selby, I., Lang, A., 2013. Denudation of the continental shelf between Britain and France at the glacial–interglacial timescale. *Geomorphology* 203, 79-96.
- Merritts, D.J., Vincent, K.R., Wohl, E.E., 1994. Long river profiles, tectonism, and eustasy: A guide to interpreting fluvial terraces. *Journal of Geophysical Research: Solid Earth* 99, 14031-14050.

- Métivier, F., Gaudemer, Y., 1999. Stability of output fluxes of large rivers in south and east Asia during the last 2 million years: Implications on floodplain processes. *Basin Research* 11, 293-303.
- Miao, X., Lindsey, D.A., Lai, Z., Liu, X., 2010. Contingency table analysis of pebble lithology and roundness: A case study of Huangshui River, China and comparison to rivers in the Rocky Mountains, USA. *Sedimentary Geology* 224, 49-53.
- Mikesell, L.R., Schaetzl, R.J., Velbel, M.A., 2004. Hornblende etching and quartz/feldspar ratios as weathering and soil development indicators in some Michigan soils. *Quaternary Research* 62, 162-171.
- Mikesell, L.R., Weissmann, G.S., Karachewski, J.A., 2010. Stream capture and piracy recorded by provenance in fluvial fan strata. *Geomorphology* 115, 267-277.
- Millad, M.G., 2004. The Depositional History and Evaluation of Two Late Quaternary, Diamondiferous Pocket Beaches, South-Western Namibia. Masters Thesis, Rhodes University, South Africa (137 pp.).
- Miller, K.G., Fairbanks, R.G., Mountain, G.S., 1991a. Tertiary oxygen isotope synthesis, sea level history, and continental margin erosion. *Paleoceanography* 2, 1-19.
- Miller, K.G., Kominz, M.A., Browning, J.V., Wright, J.D., Mountain, G.S., Katz, M.E., Sugarman, P.J., Cramer, B.S., Christie-Blick, N., Pekar, S.F., 2005. The Phanerozoic record of global sea-level change. *Science* 310, 1293-1298.
- Miller, K.G., Mountain, G.S., Browning, J.V., Kominz, M., Sugarman, P.J., Christie-Blick, N., Katz, M.E., Wright, J.D., 1998. Cenozoic global sea level, sequences, and the New Jersey Transect: Results From coastal plain and continental slope drilling *Reviews of Geophysics* 36, 569-601.
- Miller, K.G., Sugarman, P.J., Browning, J.V., Kominz, M.A., Olsson, R.K., Feigenson, M.D., Hernandez, J.C., 2004. Upper Cretaceous sequences and sea-level history, New Jersey Coastal Plain. *Geological Society of America Bulletin* 116, 368-393.

- Miller, K.G., Wright, J.D., Fairbanks, R.G., 1991b. Unlocking the Ice House: Oligocene-Miocene oxygen isotopes, eustasy, and margin erosion. *Journal of Geophysical Research: Solid Earth* 96, 6829-6848.
- Miller, R.M., 2008. *The Geology of Namibia*. Ministry of Mines and Energy, Geological Survey, Windhoek, 1506 pp.
- Mischke, S., Lai, Z., Aichner, B., Heinecke, L., Mahmoudov, Z., Kuessner, M., Herzschuh, U., 2017. Radiocarbon and optically stimulated luminescence dating of sediments from Lake Karakul, Tajikistan. *Quaternary Geochronology* 41, 51-61.
- Mohrholz, V., Eggert, A., Junker, T., Nausch, G., Ohde, T., Schmidt, M., 2014. Cross shelf hydrographic and hydrochemical conditions and their short term variability at the northern Benguela during a normal upwelling season. *Journal of Marine Systems* 140, Part B, 92-110.
- Monteiro, P.M.S., Nelson, G., van der Plas, A., Mabilhe, E., Bailey, G.W., Klingelhoeffer, E., 2005. Internal tide—shelf topography interactions as a forcing factor governing the large-scale distribution and burial fluxes of particulate organic matter (POM) in the Benguela upwelling system. *Continental Shelf Research* 25, 1864-1876.
- Montgomery, D.R., 2004. Observations on the role of lithology in strath terrace formation and bedrock channel width. *American Journal of Science* 304, 454-476.
- Moore, J.M., Moore, A.E., 2004. The roles of primary kimberlitic and secondary Dwyka glacial sources in the development of alluvial and marine diamond deposits in southern Africa. *Journal of African Earth Sciences* 38, 115-134.
- Morton, A., Knox, R., Frei, D., 2016. Heavy mineral and zircon age constraints on provenance of the Sherwood Sandstone Group (Triassic) in the eastern Wessex Basin, UK. *Proceedings of the Geologists' Association* 127, 514-526.
- Morton, A.C., 1984. Stability of detrital heavy minerals in Tertiary sandstones from the North Sea Basin. *Clay Minerals* 19, 287-308.

- Morton, A.C., 1986. Dissolution of apatite in North Sea Jurassic sandstone: implications for the generation of secondary porosity. *Clay Minerals* 21, 711-733.
- Morton, A.C., 1991. Geochemical studies of detrital heavy minerals and their application to provenance research. In: Morton, A.C., Todd, S.P., Haughton, P.D.W. (Eds.), *Developments in Sedimentary Provenance Studies*, Geological Society London Special Publications 57. Blackwell Scientific Publications, London, pp. 31-45.
- Morton, A.C., 2007. The role of heavy mineral analysis as a geosteering tool during drilling of high-angle wells. In: Mange, M.A., Wright, D.T. (Eds.), *Heavy Minerals in Use*, *Developments in Sedimentology* 58. Elsevier, Oxford, pp. 1123-1142.
- Morton, A.C., Borg, G., Hansley, P.L., Haughton, P.D.W., Krinsley, D.H., Trusty, P., 2003. The origin of faceted garnets in sandstones: dissolution or overgrowth? In: Burley, S.D., Worden, R.H. (Eds.), *Sandstone Diagenesis: Recent and Ancient*, Blackwell Publishing Ltd, Oxford, pp. 507-522.
- Morton, A.C., Hallsworth, C.R., 1999. Processes controlling the composition of heavy mineral assemblages in sandstones. *Sedimentary Geology* 124, 3-29.
- Morton, A.C., Hallsworth, C.R., 2007. Stability of detrital heavy minerals during burial diagenesis. In: Mange, M.A., Wright, D.T. (Eds.), *Heavy Minerals in Use*, *Developments in Sedimentology* 58. Elsevier, Oxford, pp. 215-245.
- Morton, A.C., Meinhold, G., Howard, J.P., Phillips, R.J., Strogon, D., Abutarruma, Y., Algadry, M., Thusu, B., Whitham, A.G., 2011. A heavy mineral study of sandstones from the eastern Murzuq basin, Libya: constraints on provenance and stratigraphic correlation *Journal of African Earth Sciences* 61, 308-330.
- Morton, A.C., Whitham, A.G., Fanning, C.M., 2005. Provenance of Late Cretaceous to Paleocene submarine fan sandstones in the Norwegian Sea: Integration of heavy mineral, mineral chemical and zircon age data. *Sedimentary Geology* 182, 3-28.
- Mubita, P., Mwet, A., Apollus, L. (2015). *Atlantic 1 Geozones Legend Update*, De Beers Marine Namibia (Pty) Limited. 145.

- Nagel, B., Gaye, B., Lahajnar, N., Struck, U., Emeis, K.-C., 2016. Effects of current regimes and oxygenation on particulate matter preservation on the Namibian shelf: Insights from amino acid biogeochemistry. *Marine Chemistry* 186, 121-132.
- Nelson, D.R., 2001. An assessment of the determination of depositional ages for precambrian clastic sedimentary rocks by U–Pb dating of detrital zircons. *Sedimentary Geology* 141-142, 37-60.
- Nesbitt, H.W., Fedo, C.M., Young, G.M., 1997. Quartz and feldspar stability, steady and non- steady-state weathering, and petrogenesis of siliciclastic sands and muds. *Journal of Geology* 105, 173-191.
- Nesbitt, H.W., Markowics, G., Price, R.C., 1980. Chemical processes affecting alkalis and alkaline earths during continental weathering. *Geochimica et Cosmochimica Acta* 44, 1659-1666.
- Nowicki, T.E., Moore, R.O., Gurney, J.J., Baumgartner, M.C., 2007. Diamonds and associated heavy minerals in kimberlite: a review of key concepts and applications. In: Mange, M.A., Wright, D.T. (Eds.), *Heavy Minerals in Use, Developments in Sedimentology* 58. Elsevier, Oxford, pp. 1235-1267.
- Olivarius, M., Rasmussen, E.S., Siersma, V., Knudsen, C., Pedersen, G.K., 2011. Distinguishing fluvio-deltaic facies by bulk geochemistry and heavy minerals: an example from the Miocene of Denmark. *Sedimentology* 58, 1155-1179.
- Paris, P.J., Walsh, J.P., Corbett, D.R., 2016. Where the continent ends. *Geophysical Research Letters* 43, 12208-12216.
- Partridge, T.C., Dollar, E.S.J., Moolman, J., Dollar, L.H., 2010. The geomorphic provinces of South Africa, Lesotho and Swaziland: A physiographic subdivision for earth and environmental scientists. *Transactions of the Royal Society of South Africa* 65, 1-47.
- Partridge, T.C., Maud, R.R., 1987. Geomorphological evolution of southern Africa since the Mesozoic. *South African Journal of Geology* 90, 179-208.

- Partridge, T.C., Maud, R.R., 2000. Macro-scale geomorphic evolution of southern Africa. In: Partridge, T.C., Maud, R.R. (Eds.), *The Cenozoic of southern Africa*, Oxford Monographs on Geology and Geophysics 40. Oxford University Press, New York, pp. 3-18.
- Passchier, S., 2007. The use of heavy minerals in the reconstruction of ice-sheet drainage patterns: an example from the edge of the East Antarctic Ice Sheet. In: Mange, M.A., Wright, D.T. (Eds.), *Heavy Minerals in Use, Developments in Sedimentology* 58. Elsevier, Oxford, pp. 677-699.
- Pazzaglia, F.J., Gardner, T.W., 1993. Fluvial terraces of the lower Susquehanna River. *Geomorphology* 8, 83-113.
- Pellant, C., 2000. *Rocks and Minerals*. Dorling Kindersley, London, 254 pp.
- Pether, J., 1986. Late Tertiary and early Quaternary marine deposits of the Namaqualand coast, Cape Province: New perspectives. *South African Journal of Geology* 82, 464-470.
- Pether, J., Roberts, D.L., Ward, J.D., 2000. Deposits of the West Coast. In: Partridge, T.C., Maud, R.R. (Eds.), *The Cenozoic of southern Africa*, Oxford Monographs on Geology and Geophysics 40. Oxford University Press, New York, 33-54.
- Phillips, D., Harris, J.W., 2009. Diamond provenance studies from dating of clinopyroxene inclusions: An example from the west coast of Namibia. *Lithos* 112 793-805.
- Phillips, J.D., 2011. Drainage area and incised valley fills in Texas rivers: A potential explanation. *Sedimentary Geology* 242, 65-70.
- Pickford, M., 1987. Miocene Suidae from Arrisdrift, South West Africa - Namibia. *Annals of the South African Museum* 97, 283-295.
- Pickford, M., Senut, B., 2002. *The fossil record of Namibia*. Geological Survey of Namibia, Windhoek, 39 pp.
- Pirazzoli, P.A., 1996. *Sea-Level Changes: The Last 20 000 Years*. John Wiley and Sons, Chichester, UK, 211 pp.

- Poulsen, M.L.K., Friis, H., Svendsen, H.B., Jensen, C.B., Bruhn, R., 2007. The application of bulk rock geochemistry to reveal heavy mineral sorting and flow units in thick, massive gravity flow deposits, Siri Canyon Palaeocene sandstones, Danish North Sea. In: Mange, M.A., Wright, D.T. (Eds.), *Heavy Minerals in Use, Developments in Sedimentology* Elsevier, Oxford, pp. 1099-121.
- Powers, M.C., 1953. A new roundness scale for sedimentary particles. *Journal of Sedimentary Petrology* 23, 117-119.
- Pujos, M., Bouysse, P., Pons, J.-C., 1990. Sources and distribution of heavy minerals in late quaternary sediments of the French Guiana continental shelf. *Continental Shelf Research* 10, 59-79.
- Ramsay, P.J., 1995. 9000 Years of sea-level change along the southern African coastline. *Quaternary International* 31, 71-75.
- Ramsay, P.J., Cooper, J.A.G., 2002. Late Quaternary Sea-Level Change in South Africa. *Quaternary Research* 57, 82-90.
- Rhodes, E.J., 2015. Dating sediments using potassium feldspar single-grain IRSL: Initial methodological considerations. *Quaternary International* 362, 14-22.
- Richardson, J.C., Hodgson, D.M., Paton, D., Craven, B., Rawcliffe, A., Lang, A., 2017. Where is my sink? Reconstruction of landscape development in southwestern Africa since the Late Jurassic. *Gondwana Research* 45, 43-64.
- Richardson, J.C., Hodgson, D.M., Wilson, A., Carrivick, J.L., Lang, A., 2016. Testing the applicability of morphometric characterisation in discordant catchments to ancient landscapes: a case study from southern Africa. *Geomorphology* 261, 162-176.
- Rittenour, T.M., Blum, M.D., Goble, R.J., 2007. Fluvial evolution of the lower Mississippi River valley during the last 100 k.y. glacial cycle: Response to glaciation and sea-level change. *GSA Bulletin* 119, 586-608.
- Robb, L.J., Armstrong, R.A., Waters, D.J., 1999. The History of Granulite-Facies Metamorphism and Crustal Growth from Single Zircon U–Pb Geochronology: Namaqualand, South Africa. *Journal of Petrology* 40, 1747-1770.

- Robb, L.J., Davis, D.W., Kamo, S.L., 1990. U-Pb ages on single detrital zircon grains from the Witwatersrand basin, South Africa: constraints on the age of sedimentation and on the evolution of granites adjacent to the basin. *Journal of Geology* 98, 311-328.
- Roberts, G.G., White, N., 2010. Estimating uplift rate histories from river profiles using African examples. *Journal of Geophysical Research* 115, B02406, doi: 10.1029/2009JB006692.
- Roberts, S.J., Hodgson, D.A., Bentley, M.J., Smith, J.A., Millar, I.L., Olive, V., Sugden, D.E., 2008. The Holocene history of George VI Ice Shelf, Antarctic Peninsula from clast-provenance analysis of epishelf lake sediments. *Palaeogeography, Palaeoclimatology, Palaeoecology* 259, 258-283.
- Rogers, J., Li, X.C., 2002. Environmental impact of diamond mining on continental shelf sediments off southern Namibia. *Quaternary International* 92, 101-112.
- Romans, B.W., Castelltort, S., Covault, J.A., Fildani, A., Walsh, J.P., 2016. Environmental signal propagation in sedimentary systems across timescales. *Earth-Science Reviews* 153, 7-29.
- Romans, B.W., Graham, S.A., 2013. A deep-time perspective of land-ocean linkages in the sedimentary record. *Annual Review of Marine Science*, 69-94.
- Roskosch, J., Tsukamoto, S., Meinsen, J., Frechen, M., Winsemann, J., 2012. Luminescence dating of an Upper Pleistocene alluvial fan and aeolian sandsheet complex: The Senne in the Münsterland Embayment, NW Germany. *Quaternary Geochronology* 10, 94-101.
- Rossouw, J. (1984). *Review of Existing Wave Data, Wave Climate and Design Waves for South African and South West African (Namibian) Coastal Waters*, Stellenbosch. 1-66.
- Rouby, D., Bonnet, S., Guillocheau, F., Gallagher, K., Robin, C., Biancotto, F., Dauteuil, O., Braun, J., 2009. Sediment supply to the Orange sedimentary system over the last 150 My: An evaluation from sedimentation/denudation balance. *Marine and Petroleum Geology* 26, 782-794.

- Rowan, C.J., Roberts, A.P., Broadbent, T., 2009. Reductive diagenesis, magnetite dissolution, greigite growth and paleomagnetic smoothing in marine sediments: A new view. *Earth and Planetary Science Letters* 277, 223-235.
- Rust, D.J., Summerfield, M.A., 1990. Isopach and borehole data as indicators of rifted margin evolution in southwestern Africa. *Marine and Petroleum Geology* 7, 277-287.
- Salvino, J.F., Velbel, M.A., 1989. Faceted garnets from sandstones of the Munising Formation (Cambrian), northern Michigan: petrographic evidence for their origin by intrastratal dissolution. *Sedimentology* 36, 371-379.
- Schneiderman, J.S., Chen, Z., 2007. Interpretation of Quaternary tectonic and environmental change using heavy minerals of the Yangtze Delta plain. In: Mange, M.A., Wright, D.T. (Eds.), *Heavy Minerals in Use, Developments in Sedimentology* 58. Elsevier, Oxford, pp. 607-620.
- Schumm, S.A., Licity, R.W., 1965. Time, space, and causality in geomorphology. *American Journal of Science* 263, 110-119.
- Seggie, A.G., Hannweg, G.W., Colgan, E.A., Smith, C.B., 1999. The geology and geochemistry of the Venetia kimberlite cluster, Northern Province, South Africa, In: Gurney, J.J., Gurney, J.L., Pascoe, M.D., Richardson, S.H. (Eds.), *VIIIth International Kimberlite Conference Cape Town*, pp. 750-756.
- Selby, M.J., 1985. *Earth's changing surface: An introduction to geomorphology*. Oxford, 602 pp.
- Séranne, M., Anka, Z., 2005. South Atlantic continental margins of Africa: A comparison of the tectonic vs climate interplay on the evolution of equatorial west Africa and SW Africa margins. *Journal of African Earth Sciences* 43, 283-300.
- Shirey, S.B., Carlson, R.W., Richardson, S.H., Menzies, A., Gurney, J.J., Pearson, D.G., Harris, J.W., Wiechert, U., 2001. Archean emplacement of eclogitic components into the lithospheric mantle during formation of the Kaapvaal Craton. *Geophysical Research Letters* 28, 2509-2512.

- Siesser, W., Dingle, R.V., 1981. Tertiary Sea-level Movements around southern Africa. *The Journal of Geology* 89, 83-96.
- Siesser, W.G., Salmon, D., 1979. Eocene marine sediments in the Sperrgebiet, South West Africa. *Annals of the South African Museum* 79, 9-34.
- Simpson, G.S., 1976. Evidence of overgrowths on, and solution of, detrital garnets. *Journal of Sedimentary Research* 46, 689-693.
- Skelton, P.H., 1986. Fish from the Orange-Vaal system. In: Davies, B.R., Walker, K.F. (Eds.), *The Ecology of River Systems*, Springer Science and Business Media, Dordrecht, pp. 143-161.
- Smale, D., Morton, A.C., 1987. Heavy mineral suites of core samples from McKee Formation (Eocene-Lower Oligocene), Taranaki: implications for provenance and diagenesis. *New Zealand Journal of Geology and Geophysics* 30, 299-306.
- Sonibare, W.A., Sippel, J., Scheck-Wenderoth, M., Mikeš, D., 2015. Crust-scale 3D model of the Western Bredasdorp Basin (Southern South Africa): data-based insights from combined isostatic and 3D gravity modelling. *Basin Research* 27, 125-151.
- Spaggiari, R.I., Bluck, B.J., Ward, J.D., 2006. Characteristics of diamondiferous Plio-Pleistocene littoral deposits within the palaeo-Orange River mouth, Namibia. *Ore Geology Reviews* 28, 475-492.
- Spaggiari, R.I., Ward, J.D., de Wit, M.C.J., 1999. Fluid characteristics of the diamondiferous Droogeveldt Gravels, Vaal Valley, South Africa. *Economic Geology* 94, 741-747.
- Stevenson, I.R., McMillan, I.K., 2004. Incised valley fill stratigraphy of the Upper Cretaceous succession, proximal Orange Basin, Atlantic margin of southern Africa. *Journal of the Geological Society* 161, 185-208.
- Stocken, C.G., 1978. A Review of Cenozoic Climatic and Geological Events in the Sperrgebiet. *Consolidated Diamond Mines, Oranjemund*, 38 pp.

- Stollhofen, H., Stanistreet, I.G., von Hagke, C., Nguno, A., 2014. Pliocene–Pleistocene climate change, sea level and uplift history recorded by the Horingbaai fan-delta, NW Namibia. *Sedimentary Geology* 309, 15-32.
- Sutherland, D.G., 1982. The transport and sorting of diamonds by fluvial and marine processes. *Economic Geology* 77, 1613-1620.
- Swift, D.J., 1974. Continental shelf sedimentation. In: Burk, C.A., Drake, C.L. (Eds.), *The geology of continental margins*, Springer, Berlin Heidelberg, pp. 117-135.
- Tan, P., Oberhardt, N., Dypvik, H., Riber, L., Ferrell Jr, R.E., 2017. Weathering profiles and clay mineralogical developments, Bornholm, Denmark. *Marine and Petroleum Geology* 80, 32-48.
- Thomas, R.J., Agenbacht, A.L.D., Cornell, D.H., Moore, J.M., 1994. The Kibaran of southern Africa: tectonic evolution and metallogeny. *Ore Geology Reviews* 9, 131-160.
- Tinker, J., de Wit, M., Brown, R., 2008a. Linking source and sink: Evaluating the balance between onshore erosion and offshore sediment accumulation since Gondwana break-up, South Africa. *Tectonophysics* 455, 94-103.
- Tinker, J., de Wit, M., Brown, R., 2008b. Mesozoic exhumation of the southern Cape, South Africa, quantified using apatite fission track thermochronology. *Tectonophysics* 455, 77-93.
- Tsikouras, B., Pe-Piper, G., Piper, D.J.W., Schaffer, M., 2011. Varietal heavy mineral analysis of sediment provenance, Lower Cretaceous Scotian Basin, eastern Canada. *Sedimentary Geology* 237, 150-165.
- Turner, G., Morton, A.C., 2007. The effects of burial diagenesis on detrital heavy mineral grain surface textures. In: Mange, M.A., Wright, D.T. (Eds.), *Heavy Minerals in Use, Developments in Sedimentology* Elsevier, Oxford, pp. 393-412.
- Uddin, A., Kumar, P., Sarma, J.N., Akhter, S.H., 2007. Heavy mineral constraints on the provenance of Cenozoic sediments from the foreland basins of Assam and Bangladesh: erosional history of the eastern Himalayas and the Indo-Burman Ranges. In: Mange, M.A., Wright, D.T.

(Eds.), *Heavy Minerals in Use, Developments in Sedimentology* 58. Elsevier, Oxford, pp. 823-847.

Vail, P.R., Mitchum, R.M., Thompson, S., 1977. Seismic stratigraphy and global changes of sea level, Part 4: Global cycles of relative changes of sea level. In: Payton, C.E. (Ed.), *Seismic Stratigraphy-Applications to Hydrocarbon Exploration*, American Association of Petroleum Geologists 26. 83-97.

van der Beek, P., Summerfield, M.A., Braun, J., Brown, R.W., A., F., 2002. Modeling postbreakup landscape development and denudational history a cross the southeast African (Drakensberg Escarpment) margin. *Journal of Geophysical Research* 107, B12, doi:10.1029/2001JB000744.

Van Wyk, J.P., Pienaar, L.F., 1986. Diamondiferous gravels of the lower Orange River. In: Anhaeusser, C.R., Maske, S. (Eds.), *Mineral Deposits of South Africa*, 2. Geological Society of South Africa, Pretoria, 2309-2321.

Velbel, M.A., 1984. Natural weathering mechanisms of almandine garnet. *Geology* 12, 631-634.

Velbel, M.A., 1989. Weathering of Hornblende to Ferruginous Products by a Dissolution-Reprecipitation Mechanism: Petrography and Stoichiometry. *Clays and Clay Minerals* 37, 515-524.

Velbel, M.A., Mcguire, J.T., Madden, A.S., 2007. Scanning Electron Microscopy of Garnet from Southern Michigan Soils: Etching Rates and Inheritance of Pre-Glacial and Pre-Pedogenic Grain-Surface Textures. In: Mange, M.A., Wright, D.T. (Eds.), *Heavy Minerals in Use, Developments in Sedimentology* 58. Elsevier, Oxford, pp. 413-432.

Visser, J.N.J., 1993. Sea-level changes in a back-arc-foreland transition: the late Carboniferous-Permian Karoo Basin of South Africa. *Sedimentary Geology* 83, 115-131.

von Eynatten, H., Gaupp, R., 1999. Provenance of Cretaceous synorogenic sandstones in the Eastern Alps: constraints from framework petrography, heavy mineral analysis and mineral chemistry. *Sedimentary Geology* 124, 81-111.

- Watanuki, T., Murray, A.S., Tsukamoto, S., 2005. Quartz and polymineral luminescence dating of Japanese loess over the last 0.6 Ma: Comparison with an independent chronology. *Earth and Planetary Science Letters* 240, 774-789.
- Waters, D.J., 1989. Metamorphic evidence for the heating and cooling path of Namaqualand granulites. In: Daly, J.S., Cliff, R.A., Yardley, B.W.D. (Eds.), *Evolution of Metamorphic Belts*, Geological Society London Special Publications 43. Blackwell Scientific Publications, London, pp. 357-363.
- Webster, J.R., Kight, R.P., Winburn, R.S., Cool, C.A., 2003. Heavy mineral analysis of sandstones by Rietveld analysis. *Advances in X-Ray Analysis* 46, 198-203.
- Wegmann, K.W., Pazzaglia, F.J., 2009. Late Quaternary fluvial terraces of the Romagna and Marche Apennines, Italy: Climatic, lithologic, and tectonic controls on terrace genesis in an active orogen. *Quaternary Science Reviews* 28, 137-165.
- Weibel, R., Friis, H., 2007. Alteration of opaque minerals as a reflection of the geochemical conditions in depositional and diagenetic environments. In: Mange, M.A., Wright, D.T. (Eds.), *Heavy Minerals in Use, Developments in Sedimentology* Elsevier, Oxford, pp. 277-303.
- Whetten, J.T., Kelley, J.C., Hanson, L.G., 1969. Characteristics of Columbia River sediment and sediment transport. *Journal of Sedimentary Research* 39, 1149-1166.
- Wiberg, P.L., Cacchione, D.A., Sternberg, R.W., Wright, L.D., 1996. Linking sediment transport and stratigraphy on the continental shelf. *Oceanography* 9, 153-157.
- Wickens, H.d., MacLachlan, I.R., 1990. The stratigraphy and sedimentology of the reservoir interval of the Kudu 9A-2 and 9A-3 boreholes. *Communications of the Geological Society of Namibia* 6, 9-22.
- Wildman, M., Brown, R., Watkins, R., Carter, A., Gleadow, A., Summerfield, M., 2015. Post break-up tectonic inversion across the southwestern cape of South Africa: New insights from apatite and zircon fission track thermochronometry. *Tectonophysics* 654, 30-55.

- Wittenberg, L., 2002. Structural patterns in coarse gravelriver beds: typology, survey and assessment of the roles of grain size and river regime. *Geografiska Annaler: Series A, Physical Geography* 84, 25-37.
- Wong, F.L., Woodrow, D.L., McGann, M., 2013. Heavy mineral analysis for assessing the provenance of sandy sediment in the San Francisco Bay Coastal System. *Marine Geology* 345, 170-180.
- Wright, J.A., 1964. Gully pattern and development in wave-cut bedrock shelves north of the Orange River mouth, South West Africa. *Transactions of the Geological Society of South Africa* 67, 163-171.
- Wyatt, B.A., Baumgartner, M., Anckar, E., Grutter, H., 2004. Compositional classification of "kimberlitic" and "non-kimberlitic" ilmenite. *Lithos* 77, 819-840.
- Yue, W., Jin, B., Zhao, B., 2018. Transparent heavy minerals and magnetite geochemical composition of the Yangtze River sediments: Implication for provenance evolution of the Yangtze Delta. *Sedimentary Geology* 364, 42-52.
- Zimmermann, S., Hall, R., 2016. Provenance of Triassic and Jurassic sandstones in the Banda Arc: Petrography, heavy minerals and zircon geochronology. *Gondwana Research* 37, 1-19.

Appendix A: Heavy Mineral Assemblage Data

Table A.1 Heavy mineral assemblage data of Proto Orange River samples for 1-2 mm size fraction.

Deposit Name	Sample Name	Size Fraction	Magnetite	Garnet	Epidote	Amphibole	Imenite	Zircon	Titanite	Other	Total
Arrisdrif	Arrisdrif Proto Lower	1-2 mm	3	116	2	0	8	0	0	0	131
	Arrisdrif Proto Upper	1-2 mm	19	227	4	1	11	0	0	0	267
Auchas Lower	Auchas Lower Proto Lower	1-2 mm	4	19	0	0	9	0	0	0	32
	Auchas Lower Proto Upper	1-2 mm	40	221	3	0	39	0	0	0	303
Auchas Major	AM11 Upper	1-2 mm	0	29	0	0	0	0	0	0	29
	AM59 Lower	1-2 mm	22	65	2	0	15	0	0	0	104
	AM59 Upper	1-2 mm	3	18	3	0	0	0	0	0	24
Daberas	Daberas Sample 4 Lower	1-2 mm	41	217	0	0	59	0	0	0	317
	Daberas Sample 4 Upper	1-2 mm	29	259	3	0	19	1	0	0	311
Sendelingsdrif	Sendelingsdrif Sample 7 Lower	1-2 mm	40	44	0	0	30	0	0	0	114
	Sendelingsdrif Sample 8 Upper	1-2 mm	4	6	1	0	7	0	0	0	18
Lorelei	Lorelei West Proto	1-2 mm	97	187	2	9	31	0	0	0	326
Boom	Boom Proto Lower	1-2 mm	124	143	2	0	60	0	0	0	329
	Boom Proto Upper	1-2 mm	71	184	1	0	46	0	0	0	302

Table A.2 Heavy mineral assemblage data of Proto Orange River samples for 0.5-1 mm and 0.25-0.50 mm size fractions.

Deposit Name	Sample Name	Size Fraction	Magnetite	Garnet	Epidote	Amphibole	Imenite	Zircon	Titanite	Other	Total
Arrisdrif	Arrisdrif Proto Lower	0.5-1 mm	49	198	3	0	70	1	0	0	324
	Arrisdrif Proto Upper	0.5-1 mm	41	227	11	0	44	0	1	2	338
Auchas Lower	Auchas Lower Proto Lower	0.5-1 mm	84	87	6	0	132	0	0	0	309
	Auchas Lower Proto Upper	0.5-1 mm	99	102	0	0	115	0	0	0	316
Auchas Major	AM11 Upper	0.5-1 mm	114	98	11	0	86	0	0	0	309
	AM59 Lower	0.5-1 mm	103	158	3	0	84	0	0	0	348
	AM59 Upper	0.5-1 mm	139	99	4	0	79	0	0	0	321
Daberas	Daberas Sample 4 Lower	0.5-1 mm	131	150	0	0	73	0	0	0	354
	Daberas Sample 4 Upper	0.5-1 mm	80	138	2	1	85	0	0	0	306
Sendelingsdrif	Sendelingsdrif Sample 7 Lower	0.5-1 mm	175	43	1	0	133	0	0	0	352
	Sendelingsdrif Sample 8 Upper	0.5-1 mm	161	45	2	0	124	0	0	0	332
Lorelei	Lorelei West Proto	0.5-1 mm	95	183	5	2	38	0	0	0	323
Boom	Boom Proto Lower	0.5-1 mm	153	87	9	0	63	0	0	0	312
	Boom Proto Upper	0.5-1 mm	121	71	2	0	106	0	0	0	300
Arrisdrif	Arrisdrif Proto Lower	0.25-0.50 mm	170	65	33	3	73	0	0	0	380
	Arrisdrif Proto Upper	0.25-0.50 mm	130	135	9	1	53	0	3	0	341
Auchas Lower	Auchas Lower Proto Lower	0.25-0.50 mm	131	30	45	0	95	0	0	0	301
	Auchas Lower Proto Upper	0.25-0.50 mm	163	46	0	0	118	0	0	0	327
Auchas Major	AM11 Upper	0.25-0.50 mm	223	15	8	0	111	0	0	0	357
	AM59 Lower	0.25-0.50 mm	200	65	1	0	83	0	0	0	349
	AM59 Upper	0.25-0.50 mm	159	51	4	0	111	0	0	0	325
Daberas	Daberas Sample 4 Lower	0.25-0.50 mm	156	53	10	0	88	0	0	0	307
	Daberas Sample 4 Upper	0.25-0.50 mm	115	108	1	0	108	0	0	0	332
Sendelingsdrif	Sendelingsdrif Sample 7 Lower	0.25-0.50 mm	161	65	10	0	148	0	0	0	384
	Sendelingsdrif Sample 8 Upper	0.25-0.50 mm	206	28	3	0	118	0	0	0	355
Lorelei	Lorelei West Proto	0.25-0.50 mm	155	90	7	2	59	0	0	0	313
Boom	Boom Proto Lower	0.25-0.50 mm	198	42	5	0	93	0	0	0	338
	Boom Proto Upper	0.25-0.50 mm	193	26	2	0	91	0	0	0	312

Table A.3 Heavy mineral assemblage data of Meso Orange River samples for 1-2 mm size fraction.

Deposit Name	Sample Name	Size Fraction	Magnetite	Garnet	Epidote	Amphibole	Imenite	Zircon	Titanite	Other	Total
Arrisdrif	Arrisdrif Meso	1-2 mm	33	15	17	0	6	0	0	0	71
	Arrisdrif Young Terrace	1-2 mm	87	119	12	3	29	0	0	2	252
Auchas Lower	Auchas Lower Meso	1-2 mm	175	137	42	0	23	0	0	0	377
Auchas Major	Auchas Outlet Meso Trench	1-2 mm	63	281	3	1	27	0	0	0	375
Daberas	Daberas Meso Lower	1-2 mm	95	87	17	10	17	0	0	0	226
	Daberas Meso Upper	1-2 mm	48	15	4	5	7	0	0	0	79
Sendelingsdrif	Sendelingsdrif Zone 7 Meso	1-2 mm	49	126	7	6	29	0	0	0	217
Lorelei	Lorelei West Meso	1-2 mm	52	246	12	1	31	0	0	0	342
	Lorelei East Meso Lower	1-2 mm	37	60	8	11	2	0	0	1	119
	Lorelei East Meso Upper	1-2 mm	23	38	5	14	8	0	0	0	88
Boom	Boom Meso Lower	1-2 mm	135	110	2	7	62	0	0	0	316
	Boom Meso Upper	1-2 mm	35	23	9	18	7	0	0	0	92

Table A.4 Heavy mineral assemblage data of Meso Orange River samples for 0.5-1 mm and 0.25-0.50 mm size fractions.

Deposit Name	Sample Name	Size Fraction	Magnetite	Garnet	Epidote	Amphibole	Imenite	Zircon	Titanite	Other	Total
Arrisdrif	Arrisdrif Meso	0.5-1 mm	64	170	63	5	34	0	0	1	337
	Arrisdrif Young Terrace	0.5-1 mm	88	159	68	4	44	0	0	0	363
Auchas Lower	Auchas Lower Meso	0.5-1 mm	37	261	53	0	20	0	0	0	371
Auchas Major	Auchas Outlet Meso Trench	0.5-1 mm	58	184	1	2	57	0	1	0	303
Daberas	Daberas Meso Lower	0.5-1 mm	35	203	7	6	52	0	0	0	303
	Daberas Meso Upper	0.5-1 mm	67	140	37	12	46	0	0	0	302
Sendelingsdrif	Sendelingsdrif Zone 7 Meso	0.5-1 mm	64	178	9	1	76	0	0	0	328
Lorelei	Lorelei West Meso	0.5-1 mm	31	231	11	0	32	0	0	0	305
	Lorelei East Meso Lower	0.5-1 mm	59	194	16	18	45	0	0	0	332
	Lorelei East Meso Upper	0.5-1 mm	43	150	24	60	31	0	0	0	308
Boom	Boom Meso Lower	0.5-1 mm	149	108	10	1	68	0	0	0	336
	Boom Meso Upper	0.5-1 mm	108	77	51	12	67	0	0	0	315
Arrisdrif	Arrisdrif Meso	0.25-0.50 mm	175	141	65	2	115	0	0	0	498
	Arrisdrif Young Terrace	0.25-0.50 mm	161	74	49	0	43	0	0	0	327
Auchas Lower	Auchas Lower Meso	0.25-0.50 mm	190	143	49	0	64	0	0	0	446
Auchas Major	Auchas Outlet Meso Trench	0.25-0.50 mm	161	126	4	2	85	0	0	0	378
Daberas	Daberas Meso Lower	0.25-0.50 mm	128	101	14	2	71	0	0	0	316
	Daberas Meso Upper	0.25-0.50 mm	127	101	32	7	55	0	0	0	322
Sendelingsdrif	Sendelingsdrif Zone 7 Meso	0.25-0.50 mm	226	74	10	0	72	0	0	0	382
Lorelei	Lorelei West Meso	0.25-0.50 mm	113	121	16	1	71	0	0	0	322
	Lorelei East Meso Lower	0.25-0.50 mm	214	142	10	6	67	0	0	0	439
	Lorelei East Meso Upper	0.25-0.50 mm	107	88	35	29	70	0	0	0	329
Boom	Boom Meso Lower	0.25-0.50 mm	155	81	6	4	67	0	0	0	313
	Boom Meso Upper	0.25-0.50 mm	145	40	43	17	61	0	0	0	306

Table A.5 Heavy mineral assemblage data of modern Orange River samples for 1-2 mm, 0.5-1 mm and 0.25-0.50 m size fractions.

Deposit Name	Sample Name	Size Fraction	Magnetite	Garnet	Epidote	Amphibole	Imenite	Titanite	Clinopyroxene	Total
Auchas Major	Auchas Modern	1-2 mm	152	19	8	0	20	0	5	204
Sendelingsdrif	Sendelingsdrif Modern	1-2 mm	233	42	21	0	26	0	18	340
Auchas Major	Auchas Modern	0.5-1 mm	81	26	43	0	19	0	141	310
Sendelingsdrif	Sendelingsdrif Modern	0.5-1 mm	93	65	54	0	20	0	146	378
Auchas Major	Auchas Modern	0.25-0.50 mm	80	43	97	0	47	0	48	315
Sendelingsdrif	Sendelingsdrif Modern	0.25-0.50 mm	88	43	89	0	39	0	49	308

Table A.6 Heavy mineral assemblage data of Atlantic 1 samples for 1-2 mm size fraction.

Region	Sample Name	Size Fraction	Magnetite	Garnet	Epidote	Amphibole	Imenite	Biogenic Apatite	Authigenic Apatite	Clinopyroxene	Other	Total
Region K	Region K-S1	1-2 mm	18	47	4	1	0	1	2	0	0	73
	Region K-S2	1-2 mm	12	48	3	0	0	4	1	0	0	68
	Region K-S3	1-2 mm	1	3	0	0	0	5	0	0	0	9
	Region K-S4	1-2 mm	2	21	0	2	0	16	1	0	0	42
	Region K-S5	1-2 mm	1	7	0	2	0	3	0	0	0	13
	Region K-S6	1-2 mm	4	116	1	9	0	4	2	0	0	136
	Region K-S7	1-2 mm	2	276	7	18	0	8	1	0	0	312
Region N	Region N-S1	1-2 mm	0	63	0	1	0	9	0	0	0	73
	Region N-S2	1-2 mm	0	36	1	0	0	7	0	0	0	44
	Region N-S3	1-2 mm	0	35	0	0	0	7	0	0	0	42
	Region N-S4	1-2 mm	0	39	0	1	4	10	0	0	0	54
	Region N-S5	1-2 mm	0	93	1	0	0	8	0	0	0	102
	Region N-S6	1-2 mm	1	91	0	0	0	8	0	0	0	100
Region V	Region V-S1	1-2 mm	0	297	1	0	0	3	0	0	0	301
	Region V-S2	1-2 mm	1	271	0	0	0	6	0	0	0	278
	Region V-S3	1-2 mm	0	295	0	0	0	8	0	0	0	303
	Region V-S4	1-2 mm	0	104	0	0	0	0	0	0	0	104
	Region V-S5	1-2 mm	0	298	0	0	0	2	0	0	0	300
	Region V-S6	1-2 mm	0	17	0	0	0	1	0	0	0	18
	Region V-S7	1-2 mm	0	36	0	0	0	0	0	0	0	36
	Region V-S8	1-2 mm	0	39	0	0	0	0	0	0	0	39
	Region V-S9	1-2 mm	0	4	0	0	0	1	0	0	0	5
Region W	Region W-S1	1-2 mm	0	292	3	0	0	5	2	0	0	302
	Region W-S2	1-2 mm	0	49	0	0	2	2	0	0	0	53
	Region W-S3	1-2 mm	0	1	0	0	0	0	0	0	0	1
	Region W-S4	1-2 mm	0	0	0	0	0	0	0	0	0	0
	Region W-S5	1-2 mm	0	62	0	0	0	1	0	0	0	63
	Region W-S6	1-2 mm	0	86	0	0	0	2	0	0	0	88

Table A.7. Heavy mineral assemblage data for Atlantic 1 samples for 0.5-1 mm size fraction.

Region	Sample Name	Size Fraction	Magnetite	Garnet	Epidote	Amphibole	Imenite	Biogenic Apatite	Authigenic Apatite	Clinopyroxene	Other	Total
Region K	Region K-S1	0.5-1 mm	17	237	23	10	3	11	0	22	0	323
	Region K-S2	0.5-1 mm	27	208	13	8	8	25	0	12	0	301
	Region K-S3	0.5-1 mm	7	287	2	1	0	12	1	0	1	311
	Region K-S4	0.5-1 mm	3	249	7	14	6	11	1	12	0	303
	Region K-S5	0.5-1 mm	6	248	18	16	10	2	0	0	0	300
	Region K-S6	0.5-1 mm	2	273	9	14	9	0	0	0	0	307
	Region K-S7	0.5-1 mm	3	278	6	12	9	0	0	0	0	308
Region N	Region N-S1	0.5-1 mm	1	271	2	0	1	31	0	0	0	306
	Region N-S2	0.5-1 mm	0	284	1	0	2	18	0	0	0	305
	Region N-S3	0.5-1 mm	0	282	3	0	3	18	0	0	0	306
	Region N-S4	0.5-1 mm	0	280	4	0	2	16	0	0	0	302
	Region N-S5	0.5-1 mm	0	258	1	0	1	43	0	0	0	303
	Region N-S6	0.5-1 mm	0	278	0	1	1	21	0	0	0	301
Region V	Region V-S1	0.5-1 mm	0	301	1	4	0	2	3	0	0	311
	Region V-S2	0.5-1 mm	0	292	0	0	0	3	7	0	0	302
	Region V-S3	0.5-1 mm	0	295	2	2	3	6	3	0	0	311
	Region V-S4	0.5-1 mm	0	288	0	0	5	0	8	0	0	301
	Region V-S5	0.5-1 mm	0	290	1	4	2	4	5	0	0	306
	Region V-S6	0.5-1 mm	1	291	6	0	1	8	7	0	0	314
	Region V-S7	0.5-1 mm	1	296	2	3	2	10	14	0	0	328
	Region V-S8	0.5-1 mm	0	284	0	0	1	12	6	0	0	303
	Region V-S9	0.5-1 mm	0	286	2	1	2	10	9	0	0	310
Region W	Region W-S1	0.5-1 mm	0	286	1	0	5	0	10	0	0	302
	Region W-S2	0.5-1 mm	2	274	1	0	3	8	13	0	0	301
	Region W-S3	0.5-1 mm	2	258	2	0	6	9	32	0	0	309
	Region W-S4	0.5-1 mm	1	284	0	0	0	10	7	0	0	302
	Region W-S5	0.5-1 mm	0	310	0	0	3	4	7	0	0	324
	Region W-S6	0.5-1 mm	0	293	2	1	1	4	2	0	0	303

Table A.8. Heavy mineral assemblage data of Atlantic 1 samples, 0.25-0.50 mm size fraction.

Region	Sample Name	Size Fraction	Magnetite	Garnet	Epidote	Amphibole	Imenite	Biogenic Apatite	Authigenic Apatite	Clinopyroxene	Other	Total
Region K	Region K-S1	0.25-0.50 mm	7	209	36	8	9	0	26	11	0	306
	Region K-S2	0.25-0.50 mm	9	194	46	6	14	0	25	8	0	302
	Region K-S3	0.25-0.50 mm	6	272	9	1	16	1	0	0	0	305
	Region K-S4	0.25-0.50 mm	16	215	35	6	25	7	7	0	0	311
	Region K-S5	0.25-0.50 mm	23	197	43	13	24	2	2	0	0	304
	Region K-S6	0.25-0.50 mm	11	232	28	2	40	1	4	0	0	318
	Region K-S7	0.25-0.50 mm	7	210	33	11	41	1	1	0	0	304
Region N	Region N-S1	0.25-0.50 mm	0	221	22	2	32	21	2	0	0	300
	Region N-S2	0.25-0.50 mm	0	312	25	7	54	5	0	0	0	403
	Region N-S3	0.25-0.50 mm	2	236	29	2	28	6	0	0	0	303
	Region N-S4	0.25-0.50 mm	2	228	17	7	39	6	3	0	0	302
	Region N-S5	0.25-0.50 mm	2	226	32	11	26	3	30	0	0	330
	Region N-S6	0.25-0.50 mm	3	210	24	2	31	8	27	0	0	305
Region V	Region V-S1	0.25-0.50 mm	3	202	5	0	73	7	14	0	0	304
	Region V-S2	0.25-0.50 mm	12	207	8	0	67	0	13	0	0	307
	Region V-S3	0.25-0.50 mm	20	202	2	1	60	1	18	0	0	304
	Region V-S4	0.25-0.50 mm	12	185	7	0	70	3	30	0	0	307
	Region V-S5	0.25-0.50 mm	15	200	4	0	73	1	27	0	0	320
	Region V-S6	0.25-0.50 mm	33	179	1	0	62	1	34	0	0	310
	Region V-S7	0.25-0.50 mm	17	223	4	0	53	2	26	0	0	325
	Region V-S8	0.25-0.50 mm	17	184	8	3	35	6	46	4	0	303
	Region V-S9	0.25-0.50 mm	7	218	4	0	54	0	26	0	0	309
Region W	Region W-S1	0.25-0.50 mm	1	254	2	0	61	0	9	0	0	327
	Region W-S2	0.25-0.50 mm	4	217	2	0	57	4	31	0	0	315
	Region W-S3	0.25-0.50 mm	1	241	6	0	24	1	30	0	0	303
	Region W-S4	0.25-0.50 mm	2	204	5	1	23	3	62	0	0	300
	Region W-S5	0.25-0.50 mm	1	220	3	0	25	5	51	0	0	305
	Region W-S6	0.25-0.50 mm	4	221	2	0	28	1	47	0	0	303

Appendix B: Bulk Sediment geochemistry data

Table B.1 Geochemistry data of Proto Orange River sand samples (K, Ca, Ti, V, Cr, Mn, Fe, Co, Cu) for 0.25-0.50 mm size fraction.

Deposit Name	Sample Name	K	Ca	Ti	V	Cr	Mn	Fe	Co	Cu
Arrisdrijf	Arrisdrijf Proto Lower	7713	11225	3630	128	98	1637	44747	0	19
	Arrisdrijf Proto Upper	7791	106185	4325	66	259	914	45176	0	25
Auchas Lower	Auchas Lower Proto Lower	6212	11026	4078	90	167	772	51703	0	27
	Auchas Lower Proto Upper	3018	27372	4661	111	233	1307	63839	234	37
Auchas Major	AM11 Upper	8291	8186	2889	0	0	523	37902	0	23
	AM59 Lower	6513	16532	4626	87	164	726	65710	0	29
	AM59 Upper	8697	13630	3572	99	179	580	58384	171	46
Daberas	Daberas Sample 4 Lower	6837	12187	3042	87	158	603	49954	0	40
	Daberas Sample 4 Upper	7014	20432	4462	174	159	327	51578	0	23
Sendelingsdrif	Sendelingsdrif Sample 7 Lower	6199	11859	3561	93	211	726	97897	198	43
	Sendelingsdrif Sample 8 Upper	4732	48963	4600	115	247	396	64595	0	26
Lorelei	Lorelei West Proto	6714	31906	3706	192	132	1517	77408	0	74
Boom	Boom Proto Lower	11007	24777	3544	109	169	631	50385	0	35
Boom	Boom Proto Upper	8455	24826	4209	91	0	333	42648	0	27

Table B.2 Geochemistry data of Proto Orange River sand samples (Cl, S, Zn, As, Rb, Sr, Y, Zr, Pb) for 0.25-0.50 mm size fraction.

Deposit Name	Sample Name	Cl	S	Zn	As	Rb	Sr	Y	Zr	Pb
Arrisdrijf	Arrisdrijf Proto Lower	1363	2070	36	7.2	57.4	211	16.9	237	10.2
	Arrisdrijf Proto Upper	5569	25933	33	0	52.7	182	23.4	142	6.7
Auchas Lower	Auchas Lower Proto Lower	3731	2475	46	7.2	42.9	121	15.4	272	15.7
	Auchas Lower Proto Upper	7034	27068	46	0	25.6	137	29.1	161	19
Auchas Major	AM11 Upper	0	0	27	9.8	56.6	164	15.7	201	12
	AM59 Lower	1613	684	48	0	40.4	178	24.2	206	22
	AM59 Upper	7145	1207	48	8.8	49.8	146	22.5	225	18
Daberas	Daberas Sample 4 Lower	3581	2364	39	5.3	58.5	128	18.4	174	21
	Daberas Sample 4 Upper	3757	12485	35	19.3	56.3	231	14.4	271	8.8
Sendelingsdrif	Sendelingsdrif Sample 7 Lower	2563	964	61	23.3	35.3	193	20.3	176	0
	Sendelingsdrif Sample 8 Upper	9490	15776	44	11	41.3	233	8.8	188	10
Lorelei	Lorelei West Proto	19603	3847	58	10.7	53.7	229	22.7	125	28
Boom	Boom Proto Lower	5037	1272	41	8.7	73.3	120	17.4	122	12
Boom	Boom Proto Upper	6079	0	33	6.4	55.6	119	15.7	224	12

Table B.3 Geochemistry data of Meso Orange River sand samples (K, Ca, Ti, V, Cr, Mn, Fe, Co, Cu) for 0.25-0.50 mm size fraction.

Deposit Name	Sample Name	K	Ca	Ti	V	Cr	Mn	Fe	Co	Cu
Arrisdrijf	Arrisdrijf Meso	10569	14091	1968	43.9	115	328	25531	110	32
	Arrisdrijf Young Terrace	11341	32294	3506	167	0	485	34372	0	20
Auchas Lower	Auchas Lower Meso	12441	35568	4468	85	171	1013	72270	0	21
	Auchas Outlet Meso Trench	8488	9681	4511	81	95	391	50409	0	14
Daberas	Daberas Meso Lower	10043	10189	2785	64	101	682	41015	136	62
	Daberas Meso Upper	6774	24374	3543	56	200	806	44557	180	52
Sendelingsdrif	Sendelingsdrif Zone 7 Meso	6962	35693	3501	105	247	998	47540	0	26
Lorelei	Lorelei West Meso	11959	18336	6048	128	138	566	60079	0	38
	Lorelei East Meso Lower	4768	20631	3126	0	132	261	37561	0	53
	Lorelei East Meso Upper	6808	80752	3033	87	107	349	33189	0	556
Boom	Boom Meso Lower	4171	14637	3427	72	175	1359	49158	0	61
	Boom Meso Upper	6536	270531	1124	68	0	171	12999	0	12

Table B.4 Geochemistry data of Meso Orange River sand samples (Cl, S, Zn, As, Rb, Sr, Y, Zr, Pb) for 0.25-0.50 mm size fraction.

Deposit Name	Sample Name	Cl	S	Zn	As	Rb	Sr	Y	Zr	Pb
Arrisdrijf	Arrisdrijf Meso	2743	1810	19.5	4.2	67	155	13.6	153	11.2
	Arrisdrijf Young Terrace	11616	19594	31	31	69.7	197	18	249	10
Auchas Lower	Auchas Lower Meso	8196	7333	41	11	57.3	207	56	137	10
	Auchas Outlet Meso Trench	11058	1724	28	10	63.8	130	15.4	234	8.2
Daberas	Daberas Meso Lower	8657	3364	47	9	79.3	133	16.8	207	7
	Daberas Meso Upper	4047	12081	32	9.7	48	178	21	157	0
Sendelingsdrijf	Sendelingsdrijf Zone 7 Meso	0	15523	48	0	65.7	162	13.9	229	9
Lorelei	Lorelei West Meso	0	783	50	26	70.7	121	32.5	859	12
	Lorelei East Meso Lower	3552	0	39	6.6	46.9	182	12.3	135	11
	Lorelei East Meso Upper	245	51800	373	12.6	43.2	191	12.5	256	14.9
Boom	Boom Meso Lower	1664	1809	45	13.1	43.4	313	16.2	111	0
	Boom Meso Upper	16230	142636	0	12.1	35.1	202	13.8	135	0

Table B.5 Geochemistry data of modern Orange River sand samples for 0.25-0.50 mm size fraction.

Deposit Name	Sample Name	K	Ca	Ti	V	Cr	Mn	Fe	Co	Cu
Auchas Major	Auchas Modern	18634	18252	3296	65	68	439	32151	0	0
Sendelingsdrijf	Sendelingsdrijf Modern	18860	22736	4116	90	99	626	47810	0	15
Deposit Name	Sample Name	Cl	S	Zn	As	Rb	Sr	Y	Zr	Pb
Auchas Major	Auchas Modern	0	0	22	7.2	80.5	150	27	155	11.2
Sendelingsdrijf	Sendelingsdrijf Modern	0	796	39	7.3	93.6	139	34	175	14

Table B.6 Geochemistry data of Atlantic 1 sand samples (K, Ca, Ti, V, Cr, Mn, Fe, P) for 0.25-0.50 mm size fraction.

Deposit Name	Sample Name	K	Ca	Ti	V	Cr	Mn	Fe	P
Region K	Region K-S1	16640	83857	705	43	43.3	197	12605	0
	Region K-S2	18883	85989	1140	42.8	48.3	157	11974	0
	Region K-S3	13453	89323	2789	84	44	2716	385860	0
	Region K-S4	21166	166715	1684	38.1	30.9	239	11073	0
	Region K-S5	22773	68278	1057	47.4	68	260	16798	0
	Region K-S6	18463	52453	1005	39.6	63.3	203	13233	0
	Region K-S7	18455	57143	2080	48.6	54.1	271	15639	0
Region N	Region N-S1	13423	359162	600	26	27	79	8268	25679
	Region N-S2	11163	372088	953	30.6	40	190	11436	40877
	Region N-S3	18219	162796	507	58.8	66	219	10498	78650
	Region N-S4	17701	175615	1696	76.7	88	350	13529	105334
	Region N-S5	12212	151067	640	77.3	84	455	12539	109497
	Region N-S6	18285	131649	672	80.5	63.4	216	9414	72718
Region V	Region V-S1	9454	477200	595	15.7	27.7	175	9193	27423
	Region V-S2	9760	432171	837	19	32	438	15777	0
	Region V-S3	7815	502597	1048	16.6	30	305	13503	0
	Region V-S4	7637	547917	548	11.9	22.3	227	10285	0
	Region V-S5	8840	518229	725	20.1	38	310	12058	23818
	Region V-S6	8937	518804	509	13.5	30	335	12416	19101
	Region V-S7	7197	584600	618	10.2	23	140	11866	0
	Region V-S8	16234	266099	691	35.7	39	498	20535	45703
	Region V-S9	5421	591612	219	6.3	17.9	161	7855	0
Region W	Region W-S1	10211	510453	518	17.4	34	345	13962	18463
	Region W-S2	7862	537419	435	11	22.8	312	10056	0
	Region W-S3	11326	462927	551	24	29	655	17665	22245
	Region W-S4	11625	469026	542	24.8	33	810	18884	20842
	Region W-S5	11512	469225	549	18.2	46	731	23865	32757
	Region W-S6	13739	439272	682	30.1	34	1006	25829	25093

Table B.7 Geochemistry data of Atlantic 1 sand samples (Cl, S, Zn, As, Rb, Sr, Y, Zr, Mo, Pb) 0.25-0.50 mm size fraction.

Deposit Name	Sample Name	Cl	S	Zn	As	Rb	Sr	Y	Zr	Mo	Pb
Region K	Region K-S1	6988	4368	12.4	6.5	87	292	21.7	66	4.1	10.8
	Region K-S2	7683	4428	16.5	0	87.5	284	17.2	64	0	14.1
	Region K-S3	18594	9247	82	74	23	169	28	70	0	0
	Region K-S4	7883	4844	16.2	5.8	102.7	353	22.5	55	4	13.2
	Region K-S5	3514	2944	10.7	7.2	104.4	262	17.5	94	0	14.7
	Region K-S6	6134	3744	13.7	4.3	93	236	15.3	81	4	9.7
	Region K-S7	3906	2858	16.9	5	91.8	242	23	84	0	14.9
Region N	Region N-S1	13803	12215	0	17.7	63.4	922	39.7	64	7.4	8.7
	Region N-S2	9012	10741	0	21.2	50.8	965	64	107	9.4	0
	Region N-S3	8022	9976	13	20	77	819	109	123	5.8	14.8
	Region N-S4	6415	13394	17	18.1	78.8	903	131	126	9.2	18
	Region N-S5	2799	9445	7.8	23.8	55.3	739	118	57	8	8.4
	Region N-S6	5122	7955	8.9	18	72.2	673	93	54	5.1	13.7
Region V	Region V-S1	30505	10312	6.1	10.7	39.1	773	38.7	44	8.2	7.7
	Region V-S2	32234	13019	19	17.9	37.7	660	23.2	61	7.1	0
	Region V-S3	24260	14411	14	14.6	32.7	746	20.9	161	7.9	0
	Region V-S4	21260	9741	13	11.1	32.3	770	16	48	5.3	0
	Region V-S5	11033	9460	7	10.6	30.4	819	24.5	140	9	0
	Region V-S6	17189	8766	7	8.1	30.9	777	19.6	56	7.1	0
	Region V-S7	11954	5547	12	6.8	29.1	821	17.8	52	5.3	5.6
	Region V-S8	7431	12814	17	20.2	67.6	710	56	42	12.8	6.3
	Region V-S9	16931	13737	0	9.3	23.7	1432	15.8	0	12.5	6.2
Region W	Region W-S1	17252	8901	8	12.8	35.6	997	33.4	34	8.5	5.8
	Region W-S2	15336	6720	0	8.3	26.8	892	26.2	37	7.5	6.9
	Region W-S3	15565	13246	18	21.9	43.7	801	31.8	69	8.4	11
	Region W-S4	9683	10765	15	18.4	39.5	721	31.3	50	6.1	7.2
	Region W-S5	14803	22400	14	26.9	35.5	836	28.9	58	8.7	0
	Region W-S6	9756	17162	18	25.7	43.8	767	31.1	191	14	0

Appendix C: Mineral Composition Data

Table C.1 Garnet composition from Proto Orange River deposits.

Sample Name	Boom Proto Upper			Boom Proto Lower			Sendelingsdrif
SiO ₂	37.02	38.14	38.68	37.68	38.21	38.75	38.17
TiO ₂	0.11	0.02	0.01	0.01	0.01	0.01	0.01
Al ₂ O ₃	19.82	21.18	21.41	20.18	20.84	21.40	21.23
FeO	15.79	34.15	34.31	19.62	34.91	32.07	35.92
MnO	26.25	1.19	1.09	20.70	1.34	0.86	0.59
MgO	0.82	4.90	5.95	1.87	4.47	6.30	4.22
CaO	0.61	0.91	0.84	0.64	0.99	1.55	1.19
Total	100.41	100.49	102.29	100.69	100.77	100.94	101.33
Sample Name	Sendelingsdrif			Auchas Major Lower			
SiO ₂	37.38	38.31	38.42	39.52	37.79	38.58	37.75
TiO ₂	0.01	0.01	0.01	0.00	0.02	0.01	0.00
Al ₂ O ₃	20.60	21.40	21.52	21.39	20.85	21.32	20.71
FeO	33.44	34.02	33.58	27.22	35.88	32.28	35.15
MnO	7.34	0.90	0.67	2.59	0.68	0.49	2.96
MgO	1.60	5.25	5.77	8.65	3.61	6.90	2.82
CaO	0.62	1.02	0.95	1.26	1.33	0.74	1.02
Total	100.98	100.91	100.92	100.64	100.16	100.33	100.40
Sample Name	Arrisdrif Proto Upper			Arrisdrif Proto Lower			
SiO ₂	37.98	37.80	37.47	38.27	37.31	38.68	
TiO ₂	0.01	0.01	0.01	0.04	0.01	0.03	
Al ₂ O ₃	20.95	20.75	20.79	21.01	20.41	20.89	
FeO	34.67	36.51	35.80	32.32	29.30	33.40	
MnO	2.81	1.42	2.44	2.50	9.45	0.58	
MgO	3.28	2.91	2.83	4.90	2.35	5.78	
CaO	1.08	1.08	0.75	1.52	1.30	1.04	
Total	100.79	100.48	100.09	100.56	100.15	100.41	

Table C.2 Garnet composition from Meso Orange River deposits.

Sample Name	Boom Meso Upper			Boom Meso Lower			Sendelingsdrif
SiO ₂	38.60	37.93	38.53	37.70	38.42	37.49	37.95
TiO ₂	0.02	0.02	0.04	0.02	0.04	0.01	0.01
Al ₂ O ₃	21.19	20.90	21.08	20.64	21.36	20.89	20.89
FeO	32.59	34.92	33.03	36.28	31.60	36.25	35.54
MnO	0.90	0.79	0.82	1.49	0.61	1.47	0.62
MgO	6.00	4.41	5.82	3.22	7.07	3.26	4.14
CaO	1.16	1.03	1.17	1.01	0.96	1.01	1.21
Total	100.45	100.00	100.48	100.36	100.05	100.39	100.37

Sample Name	Sendelingsdrif			Auchas Major			
SiO ₂	38.16	37.79	38.86	37.90	38.10	37.44	37.23
TiO ₂	0.05	0.00	0.01	0.01	0.02	0.00	0.00
Al ₂ O ₃	20.87	20.95	21.06	20.75	20.92	20.55	20.79
FeO	34.92	35.11	33.70	33.86	34.85	32.16	37.40
MnO	1.66	1.26	0.72	2.06	0.71	6.50	1.36
MgO	3.97	4.12	5.60	4.52	4.15	2.46	2.52
CaO	1.28	1.05	0.88	1.11	1.76	1.04	0.81
Total	100.91	100.29	100.84	100.22	100.52	100.14	100.13

Sample Name	Arrisdrijf Meso			Arrisdrijf Young Terrace		
SiO ₂	37.68	38.12	37.62	37.80	38.20	38.66
TiO ₂	0.01	0.01	0.02	0.03	0.02	0.03
Al ₂ O ₃	20.72	20.94	20.89	20.13	21.29	21.43
FeO	34.59	34.82	35.54	24.36	32.11	31.58
MnO	2.31	0.80	0.51	10.46	0.75	0.72
MgO	3.19	4.61	3.89	2.36	6.55	6.81
CaO	1.32	0.95	1.37	5.05	0.90	1.02
Total	99.81	100.25	99.83	100.20	99.81	100.26

Table C.3 Garnet composition from Atlantic 1 deposits.

Sample Name	K-S1				K-S5			
SiO ₂	36.55	37.38	37.64	35.27	37.98	36.89	37.74	36.80
TiO ₂	0.00	0.03	0.04	0.02	0.06	0.00	0.03	0.02
Al ₂ O ₃	20.97	21.33	21.81	20.48	21.09	21.03	21.71	21.34
FeO	20.70	29.78	32.89	24.61	24.36	34.64	32.58	36.26
MnO	17.88	0.97	0.48	0.44	1.13	1.36	1.29	1.83
MgO	1.95	1.68	6.19	5.99	3.46	3.05	6.24	3.05
CaO	1.87	9.18	1.09	0.82	11.89	2.63	0.62	0.85
Total	99.92	100.35	100.13	87.63	99.96	99.60	100.21	100.16
Sample Name	N-S4				N-S6			
SiO ₂	37.47	36.92	37.22	37.48	36.41	37.74	37.42	36.57
TiO ₂	0.05	0.01	0.02	0.02	0.08	0.03	0.01	0.03
Al ₂ O ₃	21.77	21.70	21.33	21.59	20.32	21.79	21.37	21.17
FeO	31.62	33.78	35.55	32.82	20.78	31.64	33.22	37.43
MnO	0.87	3.29	0.94	0.72	19.88	0.79	1.14	1.57
MgO	6.96	3.32	4.01	6.23	1.70	7.06	5.21	2.37
CaO	0.99	1.52	1.08	0.88	1.11	1.14	1.45	0.81
Total	99.72	100.54	100.14	99.74	100.29	100.20	99.82	99.95
Sample Name	V-S7				V-S9			W-S1
SiO ₂	37.63	38.23	36.93	37.38	37.44	37.17	37.54	36.69
TiO ₂	0.03	0.01	0.04	0.03	0.00	0.00	0.03	0.02
Al ₂ O ₃	21.68	21.94	21.43	21.60	21.64	21.28	21.98	21.33
FeO	31.59	26.58	33.70	34.95	31.38	34.65	31.74	33.48
MnO	0.68	2.06	0.64	0.78	2.04	1.84	0.83	1.63
MgO	6.78	9.53	5.58	4.84	6.01	3.78	6.76	3.93
CaO	1.37	1.55	0.97	0.81	1.32	1.49	1.25	2.58
Total	99.76	99.90	99.28	100.39	99.84	100.22	100.14	99.65
Sample Name	W-S1				W-S6			
SiO ₂	36.66	36.62	36.81	36.60	36.65	37.39	37.22	
TiO ₂	0.00	0.01	0.01	0.00	0.02	0.01	0.03	
Al ₂ O ₃	21.02	21.02	21.40	20.96	21.34	21.74	21.62	
FeO	29.46	35.07	34.18	21.87	32.59	31.61	33.61	
MnO	9.77	2.35	1.41	17.11	3.05	0.67	0.64	
MgO	1.91	2.78	4.10	1.96	4.36	6.26	5.38	
CaO	1.17	1.57	1.55	1.56	1.34	1.99	1.01	
Total	99.99	99.42	99.46	100.06	99.34	99.67	99.52	

Table C.4 Epidote composition from Proto Orange River deposits.

Sample Name	Boom Proto Upper			Boom Proto Lower			Sendelingsdrif
SiO ₂	28.43	36.36	36.46	36.52	43.90	36.36	36.30
TiO ₂	0.03	0.10	0.07	0.05	0.16	0.06	0.59
Al ₂ O ₃	17.36	20.33	21.19	22.04	31.89	23.05	19.70
Cr ₂ O ₃	0.27	0.00	0.00	0.00	0.03	0.01	0.03
FeO	10.87	13.97	12.91	11.66	2.79	10.15	13.66
MnO	0.25	0.06	0.25	0.12	0.00	0.34	0.12
MgO	24.76	0.00	0.02	-0.02	0.58	0.01	-0.02
CaO	0.05	22.87	22.78	22.79	0.00	22.77	22.86
Na ₂ O	-0.02	0.00	-0.01	-0.03	0.87	0.00	-0.02
K ₂ O	0.01	0.00	0.00	0.00	10.51	0.00	0.01
TOTAL	82.00	93.69	93.68	93.15	90.72	92.75	93.21
Sample Name	Sendelingsdrif			Auchas Major			
SiO ₂	36.52	36.47	36.85	36.40	36.21	36.32	36.37
TiO ₂	0.02	0.06	0.04	0.12	0.19	0.05	0.02
Al ₂ O ₃	20.42	20.69	23.58	21.62	19.18	21.46	19.19
Cr ₂ O ₃	0.01	0.01	-0.01	0.01	0.01	-0.01	0.00
FeO	13.59	13.12	9.70	11.95	14.75	12.71	15.05
MnO	0.12	0.28	0.17	0.03	0.07	0.20	0.08
MgO	0.01	0.00	0.00	0.00	0.01	0.01	0.01
CaO	22.22	22.45	22.99	22.61	22.66	22.69	22.43
Na ₂ O	-0.01	-0.02	-0.02	-0.01	0.01	0.00	-0.01
K ₂ O	0.00	0.00	0.00	0.00	0.00	0.00	0.00
TOTAL	92.90	93.07	93.31	92.73	93.09	93.43	93.13
Sample Name	Arrisdrif Proto Upper			Arrisdrif Proto Lower			
SiO ₂	51.90	36.04	51.69	35.66	36.38	36.80	
TiO ₂	0.32	0.02	0.44	0.14	0.16	0.07	
Al ₂ O ₃	1.44	19.45	1.63	17.33	21.21	21.56	
Cr ₂ O ₃	0.22	0.02	0.21	0.01	0.02	0.03	
FeO	7.39	14.45	7.81	16.83	12.69	12.34	
MnO	0.20	0.10	0.24	0.15	0.03	0.19	
MgO	16.68	0.11	16.18	0.03	0.03	-0.01	
CaO	19.00	22.38	18.71	22.42	22.78	22.99	
Na ₂ O	0.20	-0.04	0.22	-0.01	0.01	-0.01	
K ₂ O	0.00	0.00	0.00	0.00	-0.01	0.00	
TOTAL	97.34	92.54	97.13	92.57	93.30	93.96	

Table C.5 Epidote composition from Meso Orange River deposits.

Sample Name	Boom Meso Upper			Boom Meso Lower			Sendelingsdrif
SiO ₂	50.96	64.99	36.20	36.86	36.55	36.50	99.80
TiO ₂	0.59	0.01	0.05	0.10	0.03	0.07	0.00
Al ₂ O ₃	2.16	18.94	20.71	22.52	20.71	22.75	0.44
Cr ₂ O ₃	0.07	0.00	0.01	0.19	0.00	0.04	-0.01
FeO	8.54	0.06	13.43	10.52	13.16	11.00	0.24
MnO	0.22	0.01	0.08	0.21	0.10	0.20	0.01
MgO	15.43	-0.01	0.03	0.00	0.03	0.02	-0.02
CaO	19.26	1.18	22.84	22.82	22.24	23.14	0.00
Na ₂ O	0.26	11.86	0.00	0.02	-0.03	-0.01	-0.02
K ₂ O	0.00	0.10	0.00	0.00	0.00	0.00	0.01
TOTAL	97.49	97.13	93.35	93.24	92.80	93.71	100.43
Sample Name	Sendelingsdrif			Auchas Major			
SiO ₂	99.76	50.38	66.32	50.85	36.24	35.83	35.62
TiO ₂	0.00	0.10	0.00	0.48	0.14	0.03	0.05
Al ₂ O ₃	-0.02	25.94	18.03	1.72	22.80	22.13	20.61
Cr ₂ O ₃	-0.01	0.00	0.01	0.15	-0.02	0.00	0.00
FeO	0.18	3.61	0.20	7.68	10.91	11.91	13.52
MnO	0.00	0.06	0.00	0.23	0.25	0.05	0.26
MgO	-0.05	1.59	-0.04	16.36	-0.02	0.01	0.01
CaO	0.02	0.11	0.13	19.00	22.90	23.11	22.84
Na ₂ O	-0.05	0.37	12.59	0.19	0.03	-0.03	-0.01
K ₂ O	0.00	11.75	0.05	-0.01	0.00	0.00	0.01
TOTAL	99.82	93.91	97.30	96.65	93.21	93.04	92.90
Sample Name	Arrisdrijf Meso			Arrisdrijf Young Terrace			
SiO ₂	35.80	50.98	50.79	50.11	51.48	51.73	
TiO ₂	0.04	0.28	0.35	0.55	0.32	0.29	
Al ₂ O ₃	21.04	2.05	1.96	1.92	1.44	1.45	
Cr ₂ O ₃	0.01	0.77	0.80	0.07	0.61	0.69	
FeO	12.99	5.89	6.34	7.74	6.24	6.40	
MnO	0.21	0.17	0.18	0.19	0.19	0.18	
MgO	0.06	17.19	16.87	15.40	16.84	17.75	
CaO	22.97	19.32	19.42	20.21	19.59	18.47	
Na ₂ O	-0.01	0.23	0.24	0.26	0.24	0.22	
K ₂ O	0.00	0.00	0.01	0.00	0.00	-0.01	
TOTAL	93.10	96.87	96.94	96.45	96.95	97.16	

Table C.6 Epidote composition from Atlantic 1 deposits (Region K, Region N, and Region V).

Sample Name	K-S1				K-S5			
SiO ₂	52.93	36.96	36.79	36.22	36.92	35.73	37.18	53.13
TiO ₂	0.30	0.07	0.23	0.07	0.25	0.10	1.00	0.31
Al ₂ O ₃	1.46	22.14	22.11	21.30	22.01	22.86	19.84	1.42
Cr ₂ O ₃	0.22	-0.02	0.00	0.00	0.01	0.01	0.00	0.39
FeO	8.07	12.89	13.86	14.36	12.01	11.44	2.92	6.70
MnO	0.25	0.15	0.19	0.39	0.76	0.31	0.59	0.20
MgO	17.41	0.18	0.05	0.06	0.04	-0.01	0.51	17.31
CaO	18.59	23.51	23.38	23.08	22.88	22.80	35.33	20.07
Na ₂ O	0.04	0.01	-0.08	-0.05	-0.09	-0.02	-0.01	0.24
K ₂ O	0.00	0.01	0.01	0.02	0.00	0.00	0.00	-0.01
TOTAL	99.27	95.90	96.55	95.45	94.79	93.22	97.37	99.76
Sample Name	N-S4				N-S6			
SiO ₂	37.49	36.61	56.95	36.60	36.77	37.28	45.14	55.01
TiO ₂	0.03	0.12	0.04	0.06	0.02	0.06	0.65	0.16
Al ₂ O ₃	27.22	21.84	17.41	22.16	19.89	21.58	30.01	0.93
Cr ₂ O ₃	0.01	-0.03	-0.02	0.00	0.03	0.08	0.03	0.23
FeO	7.92	13.47	2.94	13.68	15.65	13.87	3.85	12.20
MnO	0.16	0.04	0.11	0.01	0.14	0.21	0.05	0.24
MgO	0.00	0.02	2.90	0.01	0.03	-0.01	1.86	28.25
CaO	23.91	23.77	0.55	23.72	23.25	23.18	0.02	2.38
Na ₂ O	-0.08	-0.03	0.27	0.05	-0.02	-0.03	0.10	-0.04
K ₂ O	0.00	-0.02	13.18	0.00	0.00	0.01	10.99	0.00
TOTAL	96.67	95.78	94.34	96.28	95.77	96.22	92.70	99.37
Sample Name	V-S7				V-S9			
SiO ₂	37.24	37.56	52.06	36.29	37.35	68.80	37.96	37.70
TiO ₂	0.00	0.10	0.32	0.11	0.05	0.01	0.12	0.12
Al ₂ O ₃	22.82	25.25	2.24	19.38	20.91	18.21	24.84	22.51
Cr ₂ O ₃	0.04	0.00	0.95	0.04	0.00	-0.02	-0.01	0.02
FeO	12.66	10.27	6.25	16.49	13.95	0.06	10.20	12.80
MnO	0.22	0.25	0.21	0.06	0.30	-0.02	0.18	0.24
MgO	0.27	0.07	17.87	-0.02	-0.04	-0.12	0.00	0.06
CaO	23.15	23.56	18.88	23.58	23.02	0.18	23.60	23.32
Na ₂ O	0.09	-0.01	0.10	0.04	-0.07	11.95	-0.08	-0.01
K ₂ O	-0.01	-0.01	0.01	0.01	0.03	0.07	0.01	0.01
TOTAL	96.48	97.05	98.88	95.97	95.50	99.12	96.82	96.76

Table C.7 Epidote composition from Atlantic 1 deposit (Region W).

Sample Name	W-S1				W-S6			
	SiO ₂	37.83	37.79	37.30	38.29	37.46	37.79	37.64
TiO ₂	0.05	0.05	0.03	0.10	0.06	0.03	0.09	0.00
Al ₂ O ₃	23.94	23.17	20.42	25.30	19.86	22.27	22.56	0.29
Cr ₂ O ₃	0.00	-0.02	0.00	-0.01	-0.02	-0.04	-0.03	-0.01
FeO	10.74	11.70	14.87	9.53	15.34	12.83	12.19	6.35
MnO	0.57	0.27	0.23	0.15	0.12	0.09	0.35	0.54
MgO	-0.04	0.07	0.08	0.00	0.10	0.00	-0.08	13.34
CaO	23.31	23.36	23.10	23.98	23.40	23.60	23.18	32.54
Na ₂ O	0.00	-0.01	-0.01	0.00	-0.07	-0.06	0.01	0.00
K ₂ O	0.01	0.00	0.00	0.00	0.00	0.00	-0.01	0.10
TOTAL	96.41	96.39	96.00	97.33	96.27	96.51	95.92	53.99

Table C.8 Magnetite composition from Proto Orange River deposits.

Sample Name	Boom Proto Upper			Boom Proto Lower			Sendelingsdrif
SiO ₂	-0.20	-0.15	-0.11	-0.22	-0.07	-0.15	0.21
TiO ₂	0.01	0.02	0.07	0.01	55.13	0.06	0.17
Al ₂ O ₃	-0.17	-0.16	0.00	-0.19	-0.07	0.07	-0.04
Cr ₂ O ₃	0.02	0.01	0.07	0.00	0.02	0.02	0.03
V ₂ O ₃	0.27	0.41	0.41	0.10	0.07	0.21	0.34
FeO	88.32	87.92	87.96	91.20	39.83	87.63	86.30
MnO	0.00	0.01	0.03	0.47	0.23	0.02	0.20
MgO	-0.16	-0.07	-0.11	-0.12	-0.13	-0.04	-0.06
CaO	-0.01	0.00	0.00	-0.01	0.04	0.00	0.03
NiO	0.05	-0.02	0.00	0.01	-0.02	-0.01	-0.01
TOTAL	88.12	87.98	88.32	91.23	95.02	87.81	87.17

Sample Name	Sendelingsdrif			Auchas Major			
SiO ₂	0.15	-0.13	-0.24	-0.15	-0.15	-0.12	-0.21
TiO ₂	0.21	0.03	0.41	0.01	48.75	0.01	8.46
Al ₂ O ₃	-0.08	-0.08	-0.10	-0.10	-0.16	-0.07	-0.06
Cr ₂ O ₃	0.09	0.05	0.07	0.02	0.01	0.04	0.78
V ₂ O ₃	0.22	0.28	1.86	0.40	0.01	0.21	0.39
FeO	87.14	88.47	86.29	90.87	45.56	90.44	80.42
MnO	0.09	0.03	0.00	0.16	4.65	0.15	0.02
MgO	-0.09	-0.10	-0.11	-0.08	-0.10	-0.08	-0.07
CaO	0.03	0.00	-0.01	-0.01	0.00	0.02	-0.01
NiO	-0.02	0.03	-0.01	-0.01	-0.03	-0.01	0.01
TOTAL	87.74	88.58	88.17	91.11	98.54	90.60	89.73

Sample Name	Arrisdrijf Proto Upper			Arrisdrijf Proto Lower		
SiO ₂	-0.16	-0.19	-0.18	0.09	-0.12	-0.19
TiO ₂	0.05	0.03	0.02	76.17	0.02	0.00
Al ₂ O ₃	-0.13	-0.08	-0.10	-0.01	-0.10	-0.09
Cr ₂ O ₃	0.07	0.03	0.11	0.04	0.05	0.00
V ₂ O ₃	0.15	0.30	0.26	0.12	0.29	-0.01
FeO	88.46	91.01	87.53	19.88	87.86	88.11
MnO	0.03	0.15	0.04	2.76	0.04	0.02
MgO	-0.14	-0.08	-0.09	0.01	-0.14	-0.18
CaO	0.00	-0.01	-0.01	0.01	-0.01	-0.01
NiO	0.00	-0.02	-0.01	-0.02	0.01	-0.02
TOTAL	88.32	91.15	87.58	99.04	87.89	87.64

Table C.9 Magnetite composition from Meso Orange River deposits.

Sample Name	Boom Meso Upper			Boom Meso Lower			Sendelingsdrif
SiO ₂	-0.21	-0.19	-0.17	-0.21	-0.16	-0.20	-0.21
TiO ₂	0.04	0.03	8.79	0.03	0.01	0.03	0.01
Al ₂ O ₃	-0.06	-0.11	-0.03	-0.16	-0.09	-0.15	-0.02
Cr ₂ O ₃	0.02	0.03	0.12	0.00	0.12	0.08	0.06
V ₂ O ₃	0.13	0.24	0.24	0.19	0.23	0.32	0.32
FeO	90.91	90.80	80.47	91.44	90.99	91.14	87.66
MnO	0.15	0.07	0.05	0.12	0.15	0.12	0.03
MgO	-0.11	-0.08	-0.03	-0.13	-0.08	-0.06	-0.04
CaO	0.00	0.00	-0.01	0.00	0.00	0.00	0.00
NiO	0.00	-0.02	-0.02	-0.01	-0.01	-0.02	-0.02
TOTAL	90.86	90.77	89.42	91.27	91.17	91.26	87.78
Sample Name	Sendelingsdrif			Auchas Major			
SiO ₂	-0.22	-0.23	-0.21	-0.15	-0.21	-0.16	-0.22
TiO ₂	0.02	0.01	0.02	8.25	0.01	0.04	0.03
Al ₂ O ₃	-0.14	-0.14	-0.16	-0.09	-0.10	-0.08	-0.11
Cr ₂ O ₃	0.05	0.03	0.02	0.13	0.01	0.07	0.03
V ₂ O ₃	0.37	0.38	0.11	0.19	0.20	0.21	0.17
FeO	91.13	91.06	90.66	81.67	87.56	87.57	88.14
MnO	-0.01	0.02	0.30	0.01	0.05	0.05	0.00
MgO	-0.06	-0.05	-0.22	-0.05	-0.10	-0.11	-0.17
CaO	0.00	0.00	-0.01	0.01	-0.01	0.00	0.00
NiO	-0.02	0.02	-0.03	-0.03	-0.02	-0.01	0.00
TOTAL	91.12	91.10	90.50	89.95	87.38	87.58	87.88
Sample Name	Arrisdrif Meso			Arrisdrif Young Terrace			
SiO ₂	-0.16	-0.15	-0.17	-0.19	-0.15	-0.13	
TiO ₂	0.03	8.72	0.01	8.37	0.01	8.58	
Al ₂ O ₃	-0.16	0.03	-0.12	-0.06	-0.11	-0.06	
Cr ₂ O ₃	0.03	0.03	0.17	0.01	0.06	0.01	
V ₂ O ₃	0.21	0.10	0.26	0.05	0.33	0.26	
FeO	88.06	80.81	87.85	81.11	90.66	81.12	
MnO	0.20	0.28	0.04	0.03	0.06	0.11	
MgO	-0.10	0.15	-0.15	-0.10	-0.15	-0.05	
CaO	0.00	0.00	0.01	0.01	0.00	0.00	
NiO	-0.03	0.00	-0.03	-0.02	-0.01	0.01	
TOTAL	88.09	89.96	87.88	89.20	90.70	89.85	

Table C.10 Magnetite composition from Atlantic 1 deposits.

Sample Name	K-S5				N-S4				
SiO ₂	-0.15	-0.18	-0.17	-0.17	-0.19	-0.17	-0.18	-0.16	
TiO ₂	50.74	8.99	50.21	8.52	50.60	51.26	45.26	50.05	
Al ₂ O ₃	-0.13	-0.04	-0.06	-0.09	-0.08	-0.12	-0.06	-0.11	
Cr ₂ O ₃	0.01	0.05	0.01	0.02	0.02	0.00	0.01	0.00	
V ₂ O ₃	0.04	0.22	0.00	0.14	0.26	0.08	0.08	0.10	
FeO	41.25	81.50	42.41	81.62	47.19	47.27	49.81	43.17	
MnO	7.68	0.07	6.40	0.12	1.69	1.47	2.55	6.21	
MgO	-0.04	-0.12	0.10	-0.08	0.09	-0.03	0.46	-0.02	
CaO	0.00	-0.01	0.14	0.03	-0.01	0.00	0.00	0.00	
NiO	-0.02	-0.04	-0.02	0.01	-0.02	0.00	-0.02	0.01	
TOTAL	99.38	90.46	99.03	90.11	99.54	99.77	97.92	99.25	
Sample Name	N-S6		V-S7			V-S9			
SiO ₂	-0.21	-0.14	-0.18	-0.20	-0.18	-0.14	-0.18	-0.13	
TiO ₂	6.96	51.36	51.55	8.84	10.24	50.17	7.61	50.84	
Al ₂ O ₃	-0.04	-0.10	-0.11	-0.06	-0.07	-0.15	-0.09	-0.11	
Cr ₂ O ₃	0.11	0.02	0.00	0.02	0.14	-0.01	0.15	0.00	
V ₂ O ₃	0.28	0.02	0.01	0.22	0.22	0.02	0.27	0.07	
FeO	82.91	38.05	39.49	80.83	79.27	46.48	82.45	39.97	
MnO	0.09	10.22	7.83	0.14	0.06	2.76	0.02	8.69	
MgO	-0.10	-0.10	-0.10	-0.09	-0.16	-0.11	-0.15	-0.06	
CaO	0.00	0.11	0.00	-0.01	-0.01	0.04	0.00	0.22	
NiO	-0.03	0.01	-0.02	0.00	-0.05	-0.01	-0.03	-0.01	
TOTAL	89.97	99.46	98.49	89.68	89.44	99.06	90.04	99.49	
Sample Name	V-S9		W-S1			W-S6			
SiO ₂	-0.18	-0.14	-0.10	-0.15	-0.14	-0.15	-0.19	-0.16	
TiO ₂	49.91	50.17	51.87	51.36	51.53	50.35	9.67	49.55	
Al ₂ O ₃	-0.14	-0.11	-0.13	-0.09	-0.12	-0.14	-0.02	-0.13	
Cr ₂ O ₃	0.02	-0.01	0.06	0.00	0.02	0.00	0.01	0.01	
V ₂ O ₃	0.12	0.03	0.21	0.10	0.06	0.08	0.11	0.14	
FeO	48.11	44.13	45.46	47.30	46.26	45.12	80.11	48.79	
MnO	1.61	4.98	2.15	1.10	1.93	3.80	0.25	0.66	
MgO	-0.06	-0.06	-0.02	0.00	-0.07	-0.05	-0.01	0.32	
CaO	0.00	0.00	0.11	-0.01	0.01	0.00	0.00	0.00	
NiO	0.00	0.01	-0.01	0.01	-0.02	-0.02	-0.01	0.00	
TOTAL	99.39	99.00	99.61	99.62	99.44	98.97	89.92	99.17	